Some Metal-Organic Framework Compounds: Synthesis, Structure and Studies on Physico-chemical Property

A Thesis

Submitted for the Degree of

Doctor of Philosophy (Science)

By

Saikat Gayen

Department of Chemistry

JADAVPUR UNIVERSITY

JADAVPUR, KOLKATA - 700032

INDIA

May, 2022

Dedicated
to
my parents and my beloved wife

CERTIFICATE FROM THE SUPERVISOR

This is to certify that thesis entitled **"Some Metal-Organic Framework Compounds: Synthesis, Structure and Studies on Physico-chemical Property"** submitted by Sri Saikat Gayen, who got his name registered on 13/02/2015 for the award of Ph.D. (Science) degree of Jadavpur University, is absolutely based upon his own work under my supervision and that neither this thesis nor any part of it has been submitted for either any degree/diploma or any other academic award anywhere before.

Subrata nath Koner 25/05/2022

(Signature of the Supervisor, date with official seal)

Dr. Subratanath Koner
Professor of Chemistry
Jadavpur University
Kolkata – 700 032

<u>Acknowledgements</u>

Saikat Gayen

25|05|2022

(Saikat Gayen)

(Senior Research Fellow)

Department of Chemistry,

Inorganic Chemistry Section,

Jadavpur University,

Kolkata – 700032,

India,

May, 2022.

Table of Contents

List of Abbreviations

0D	Zero- dimensional
1D	One- dimensional
2D	Two- dimensional
3D	Three- dimensional
MOF	Metal-organic framework
PCPs	Porous coordination polymers
LMOFs	Luminescent MOFs
SBUs	Secondary building units
MOMs	Metal-organic materials
IRMOFs	Isoreticular metal-organic frameworks
MIL	Materials of Institute Lavoisier
HKUST	Hong Kong University of Science and Technology
BDC	1,4-benzenedicarboxylate
$H_2Sp5-BF_4$	1,3-bis(4-carboxyphenyl)-4,5-dihydro-1H-imidazol-3-iumtetrafluoroborate
IAST	Ideal Adsorbed Solution Theory
H_4PDBAD	5,5′-(pyridine-3,5-dicarbonyl)bis(azanediyl)di- isophthalic acid
TDC	Thiophene-2,5-dicarboxylate
DABCO	1,4-diazabicyclo-[2.2.2]octane
bpy	4,4′-bipyridine
bpp	1,3-bis(4-pyridyl)propane
pdc	Pyridine-2,5-dicarboxylate
BTC	Benzene-1,3,5-tricarboxylate
TBHP	Tertiary butyl-hydroperoxide
TCBPA	Tris(4′-carboxybiphenyl)amine
DMA	N,N-Dimethylacetamide
ZIF	Zeolitic imidazolate framework
TCPP	Tetrakis(4-carboxyphenyl)porphyrin
BTEC	1,2,4,5-benzene tetracarboxylate
bipy	2,2′-bipyridine
pypz	Bis[3,5-dimethyl-4-(4′-pyridyl)pyrazol-1-yl]methane
NPDC	2,6-napthalenedicarboxylate
NHPI	N-hydroxyphthalimide

ILCT	Intra-ligand charge transfer
MLCT	Metal-to-ligand charge transfer
LMCT	Ligand-to-metal charge transfer
LLCT	Ligand-to-ligand charge transfer
H_4tptc	1,1′:4′,1′′-terphenyl]-2′,3,3′′,5′-tetracarboxylic acid
TPE	Tetraphenylethene
NUS	National University of Singapore
TCPE	Tetrakis(4-carboxyphenyl)ethylene
$DHBDC^{2-}$	2,5-dihydroxybenzene-1,4-dicarboxylate
bmtdc	2′,5′-bis(methoxymethyl)-[1,1′:4′,1′′-terphenyl]-4,4′′-dicarboxylate
tcpa	Tris((4-carboxyl)-phenyl)amine
DMF	Dimethylformamide
VOCs	Volatile organic compounds
msitpa	5,5′,5′′-(methylsilanetriyl)triisophthalic acid
abb	3,3′-azobis(benzoate)
mqc	4-methoxy-2-quinolinecarboxylate
im	Imidazole
Hnic	Isonicotinic acid
azpy	4,4′-azopyridine
pzdc	Pyrazole-3,5-dicarboxylate
pzedc	Pyrazolate-3,5-dicarboxylate
BASF	Baden Aniline and Soda Factory
BET	Brunauer- Emmett-Teller
DTA	Differential thermal analysis
TGA	Thermogravimetric analysis
DMSO	Dimethylsulfoxide
THF	Tetrahydrofuran
TOF	Turn over frequency
TON	Turn over number
UV−vis	Ultraviolet–visible
XRD	X-ray diffraction
PXRD	Powder X-ray diffraction
NMR	Nuclear magnetic resonance
PSM	Post-synthetic modification

HRMS	High resolution mass spectrometer
IR	Infrared
MeCN	Acetonitrile
MeOH	Methanol
EtOH	Ethanol
FTIR	Fourier transform infrared
GC	Gas chromatography
DSB	Distyrylbenzene
CVBA	(E)-4-(2-carboxyvinyl)-benzoic acid
H_6hcpo	Hexa[4-(carboxyphenyl)oxamethyl]-3-oxapentane acid
CP/MAS NMR	Cross-polarization magic angle spinning nuclear magnetic resonance
CCDC	Cambridge crystallographic data centre
DFT	Density functional theory
NLDFT	Non-local density functional theory
CCS	Carbon capture and sequestration
MD	Molecular dynamics
MC	Monte Carlo
AAS	Atomic absorption spectrometer

Chapter 1

General introduction
and
brief review

1.1 General

Metal-organic frameworks (MOFs) or porous coordination polymers (PCPs) are widely attracting attention in recent time because of their fascinating and tunable porosity and molecular topologies as functional materials for gas adsorption and storage, luminescent sensing, catalysis and many other applications. MOFs have been rapidly emerging as a new type of functional material for selective CO_2 adsorption due to the presence of highly ordered adjustable pore shape and size, large surface areas with controllable pore surface properties, and high thermal/solution stability. Selectivity of CO_2 over CH_4 which can be utilized in betterment of energy content of natural gases and separation of CO_2 from binary gas mixtures in various industrial processes [1-5]. Last few years witnessed a great evolution towards configuring of catalytic schemes which cover the entire applicable range of distinctive methods, in heterogeneous catalysis (zeolites, nanocrystallites etc.), homogeneous catalysis (well-defined local environment of the active center) and engineering (reactor internals, structured catalyst bodies, microreactors etc.). Metal incorporated micro/meso-porous solids bear prospects for designing of new heterogeneous catalysts that are spatially accessible for directing the reactions to the site-isolated and structurally well-defined active centers like enzymatic catalysts [6]. Metal inorganic/organic framework compounds being porous play key role in the same way like zeolites or aluminosilicate-based catalysts.

In recent studies, luminescent MOFs (LMOFs) have attracted significant attention as a brilliant candidate for sensor applications. The attention towards MOFs in field of chemical sensing is being increased not only for its integral or activated luminescent properties but also because of their low framework density, interactions due to open metal sites, customizable pore size and immediate response with high sensitivity and selectivity. Studies on LMOFs to sense metal ions are exponentially progressing and a huge number of MOF-based fluorescent sensors have been reported [7-12]. Though, maximum reported work on sensing metal ions is principally related to lanthanide-based LMOFs and comparatively limited LMOFs reported based on transition metals. In case of transition metal based LMOFs, generally Zn^{2+}, Cd^{2+} and Cu^{2+} cations are used which have fully-filled d-orbitals where d–d transition is not possible [13].

1.2 Metal-organic frameworks

Metal-organic frameworks (MOFs, also known as porous coordination polymers or PCPs) are an emerging class of porous materials constructed from metal-containing nodes (also known as secondary building units, or SBUs) and organic linkers. Due to their structural and functional tunability, the area of MOFs has become one of the fastest growing fields in chemistry. This is demonstrated through the ever-increasing number of structures, publications, and citations, as well as by the continuous expansion of

research scope and researcher engagements. There is an unprecedented surge in MOF research that can be ascribed to the following five developments: (1) advances in cluster chemistry, (2) maturation of organic synthesis pertinent to ligand preparation and post-synthetic modification, (3) improvement in structure determination, particularly through X-ray crystallography and progress of hardware and software for characterization of sorption properties, (4) interdisciplinary evolution of research on MOF and related fields, and (5) the ever-expanding potential in several applications. The desirability of MOFs is not only restricted in the field of crystal engineering and molecular topologies but also covers extensive research owing to their several applications in luminescence and sensing [13-22], magnetism [23-25], drug delivery [26-27], gas storage and separation [28-31], catalysis [32-38] and proton conductance [39-41] (Scheme 1.1).
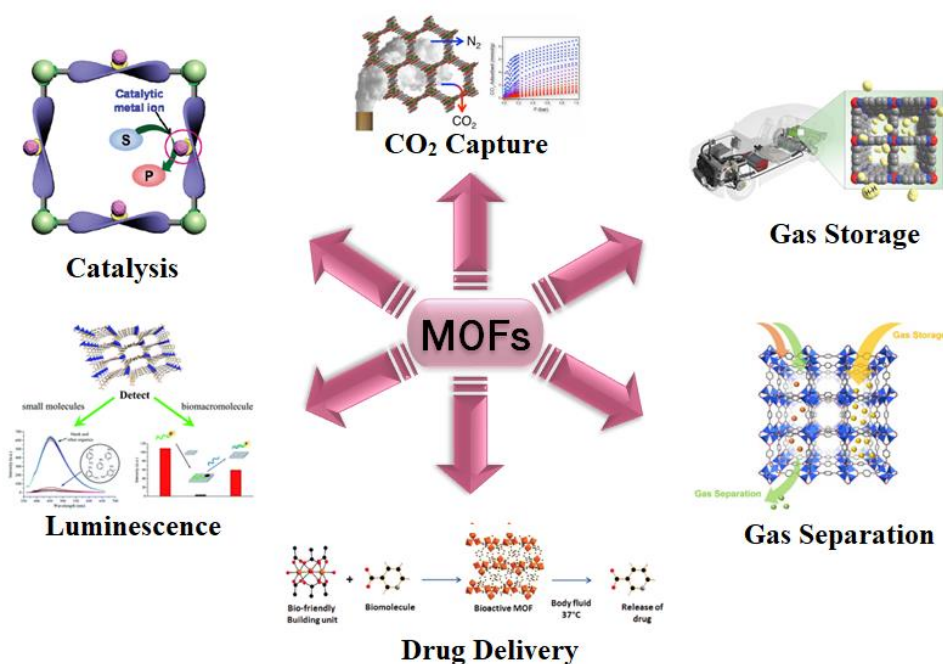
Scheme 1.1. Schematic representation of several applications of MOFs

Research group of O. M. Yaghi first reported "MOF" material, which is designated as MOF-5 [42]. However, the term "coordination polymer" was first introduced in a publication in 1916 [43], but there was no means to show infinite frameworks deprived of single-crystal-X-ray-crystallography. Later in 1936, the well-known Prussian Blue compounds, based on Fe-CN-Fe linkages, were presented which had a three-dimensional coordination framework [44]. But it was not till the early 1990 that research into materials with polymeric, occasionally porous, structures based on metal ions and organic bridging linkers improved immensely [45]. Initial publications by Robson [46], Moore [47], Yaghi [48], and Zawarotko [49] contributed to the field of MOFs, which currently witnesses of an exponential development as can be seen

from literature. The basis for present development in metal-organic materials, namely MOMs, resides with the seminal work of A. F. Wells who pioneered the simple and practically suitable ''node and spacer'' understanding of inorganic crystal structures. Inorganic crystal structures thus can be defined as metal ions (nodes) connected together through bonds (spacer or edge) [50].

MOFs, all together, define the formation of extended structures constructed by metals and organic linkers. The building blocks of MOFs, metals and organic linkers, are linked via coordination bonds and other weak chemical bonds like van der Waals and hydrogen bonding interactions. The metal ions designed as 'nodes' and the organic ligands as the 'linkers'. Variability of coordination numbers may be attained depending upon the metal ion. Prediction of the network topology, even though not the determination of the cell parameters, and the dimensionality of these compounds may be accomplished by the selection of metal ion and organic linker, and also by more indirect circumstances such as selection of solvent and counterions involved in a synthesis [51]. Additional components, for example, counter ions, template molecules and non-bonding surrounded guest molecules can also arrange part of coordination polymers. Counter ions are required in a synthesis while using neutral ligands to facilitate the positive charge of the metal center is balanced. Counter anions for example ClO_4^-, BF_4^-, NO_3^-, $CF_3SO_3^-$, SiF_6^{2-} and PF_6^- etc. have been availed in this manner act as free guests, hydrogen-bond acceptors or coordination units [52]. In MOF synthesis, it has been revealed that subtle change in reaction conditions, like change of concentrations, temperature, reaction time and also change of pH, may diminish crystallinity or yielding serendipitous product. Hence, the reaction conditions perform a dynamic role in determining the formation of final structure.

Solvent molecules act as the reaction medium but it might regulate the topology of the resultant framework as they can co-crystallize into the final structure and also occupy the void space as guest molecules. These guest solvent molecules may be eliminated when the structural network has formed allowing porosity to be attained, and if the framework does not breakdown on desolvation. Consequently, the solvent can play as a template while porous phases formed [53].

It can be possible to add functional groups in MOF compounds, differ the framework forming metal cation and change the pore size although framework topology retained, demonstrated by the honeycomb-like structure of the isoreticular porous materials, STA-12(Ni) [54] and STA-16(Co) [55] (Figure 1.1). This versatility implies that the traditional materials may be limited to a definite type of interaction (e.g. porous carbons are limited to separations involving only anhydrous components), MOFs can be tuned. For example, a pore structure that is demarcated by hydrophobic organic linker could be made hydrophilic by adding of an amine group to the linker.
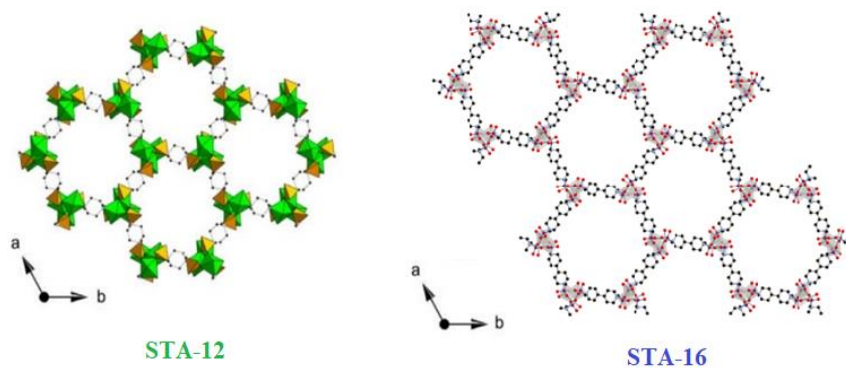
Figure 1.1. View of the hexagonal channels in the honeycomb like pore structure of metal bisphosphonates STA-12(Ni) (left) [54] and STA-16(Co) (right) [55]

Secondary building units (SBUs) are generally found to be pre-designed in a MOFs structure, and are defined as the inorganic clusters or coordination spheres formed in MOF synthesis, connected together by the organic linkers. SBUs are not supplied directly in a synthesis however these are formed *in-situ* under definite reaction conditions. Some common SBUs that are formed in MOFs are shown in Figure 1.2 [56]. Branched organic ligands, with above two coordinating functionalities, such as square tetrakis(4-carboxyphenyl)porphyrin (Figure 1.3a), tetrahedral adamantine-1,3,5,7-tetracarboxylic acid (Figure 1.3b), and trigonal 1,3,5-tris(4-carboxyphenyl)benzene (Figure 1.3c), are also recognized SBUs nevertheless they are formed before synthesis [57]. The index of SBUs which have been designed in the synthesis of MOFs permits one to guess if certain SBUs will be fastened by some specific metals and organic linkers in synthesis.
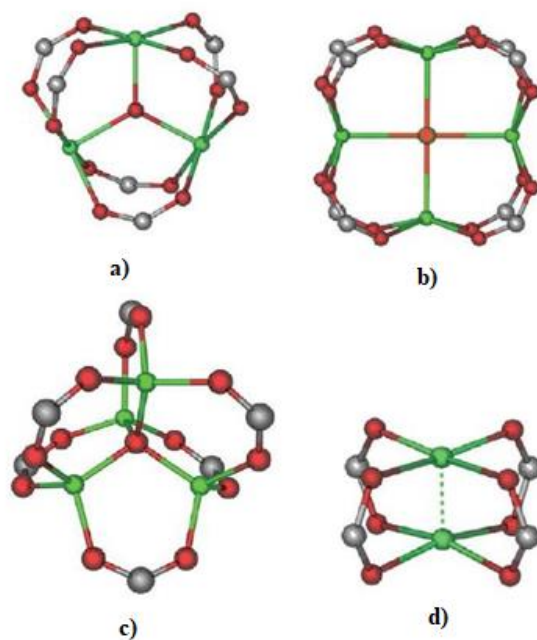
Figure 1.2. Structural representation of SBUs commonly occur in the formation of metal-organic frameworks including (a) trigonal planar, (b) square planar, (c) tetrahedral and (d) tetragonal paddlewheel [56]
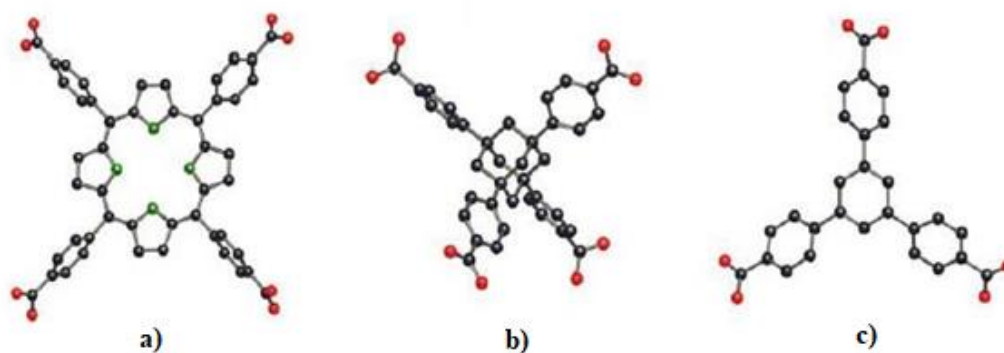
Figure 1.3. Some carboxylate SBUs which are pre-formed before synthesis of MOFs (a) square tetrakis-(4-carboxyphenyl)porphyrin, (b) tetrahedral adamantine-1,3,5,7-tetracarboxylic acid, and (c) trigonal 1,3,5-tris(4-carboxyphenyl)benzene [57]

There is an extensive range of choices for organic linkers. Rigid backbones type ligands are regularly favored, since the rigidity makes it easier to predict the structural network or geometry prior to

synthesis, and even after the removal of the guest solvents, the rigidity helps to maintain the open-pore structure of MOF compound. Basically, the linkers are anionic or cationic or electrically neutral, (Figure 1.4) [58]. The most commonly used neutral organic ligands are pyrazine and 4,4′-bipyridine (bpy) [59]. In particular, these linkers are efficient for construction of pillared-layer in 3D networks [60]. Carboxylates ligands are most commonly used anionic linkers [61], since they have the capability to accumulate metal ions into clusters and thus more stable frameworks are formed. Conversely, due to lower affinities for cationic metal ions, cationic organic ligands are comparatively less used [62]. The organic linkers also play a vital role in the construction of porous MOFs, such as long bridging ligands. This type of ligands can create some troubles within a framework like interpenetration, while large voids are created with longer ligands which permit a second polymer network to interpenetrate the first created network, consequently infusing potential cavities that led to diminished or total elimination of porosity. The proper selection of metal ion and organic linker are known to influence the topology of framework and hence, the size and shape of the pores.
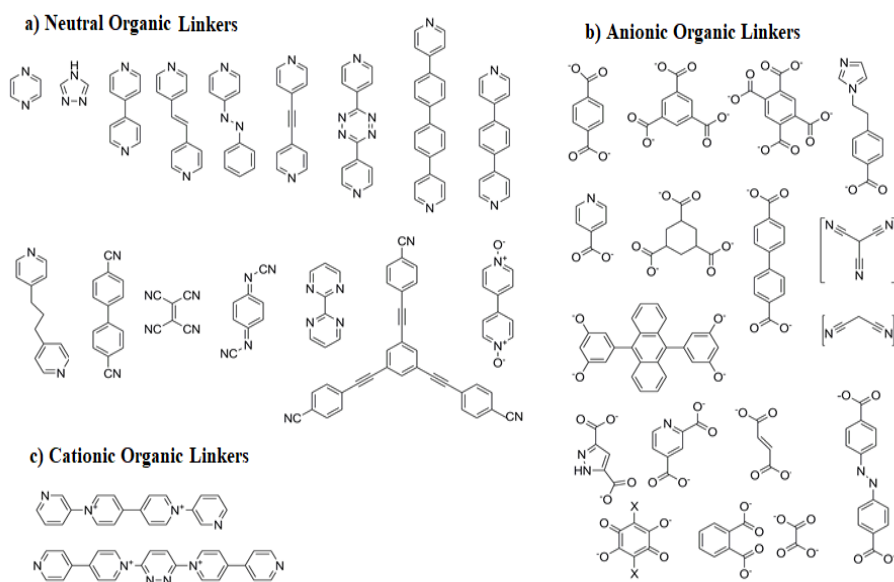
Figure 1.4. Examples of linkers used in MOFs [58]

Same functional groups containing ligands may have a different organic connectivity, such as linear dicarboxylates (like benzene-1,4-dicarboxylate, biphenyl-4,4′-dicarboxylate etc.) be able to form a series of isoreticular materials which are topologically indistinguishable however the organic linking molecule is extended [57]. This is represented by the MOF-5 [42] (also designated as IRMOF-1) and successively linked frameworks IRMOFs 2-16, where the identical $Zn_4O(COO)_6$ clusters afford the inorganic core, whereas the ligand between the carboxylate groups is diverse with maintenance of the cubic network of

channels (Figure 1.5). Reticular synthesis is a strategy which exploits previously formed SBUs [61]. In some cases, utilization of reticular synthesis encompasses the construction of carboxylate MOFs derived via MOF-5 as a prototype. These kinds of MOFs are recognized as isoreticular metal-organic frameworks (IRMOFs), wherein they are created on the same net and topology as in MOF-5 (Figure 1.5). The organic ligands employed different functionality of the pendant groups in IRMOFs 1-7, as they have the additional functional groups such as bromo (2), amino (3), n-propoxy (4), n-pentaoxy (5), cyclobutyl (6) and fused benzene functional groups (7), and in length by substituting 1,4-benzenedicarboxylate producing IRMOFs 8-16, by 2,6-naphthalenedicarboxyalate (8), biphenyl-4,4′-dicarboxylate (10), pyrene-2,7-dicarboxylate (14) and terphenyl-4″-dicarboxylate (16) (Figure 1.5) [57, 63]. Each structure comprises of the same SBUs i.e., $Zn_4O(COO)_6$ as well as in MOF-5, consequently the topology of the structure remains identical, even though the pore size and their functionalities differ.
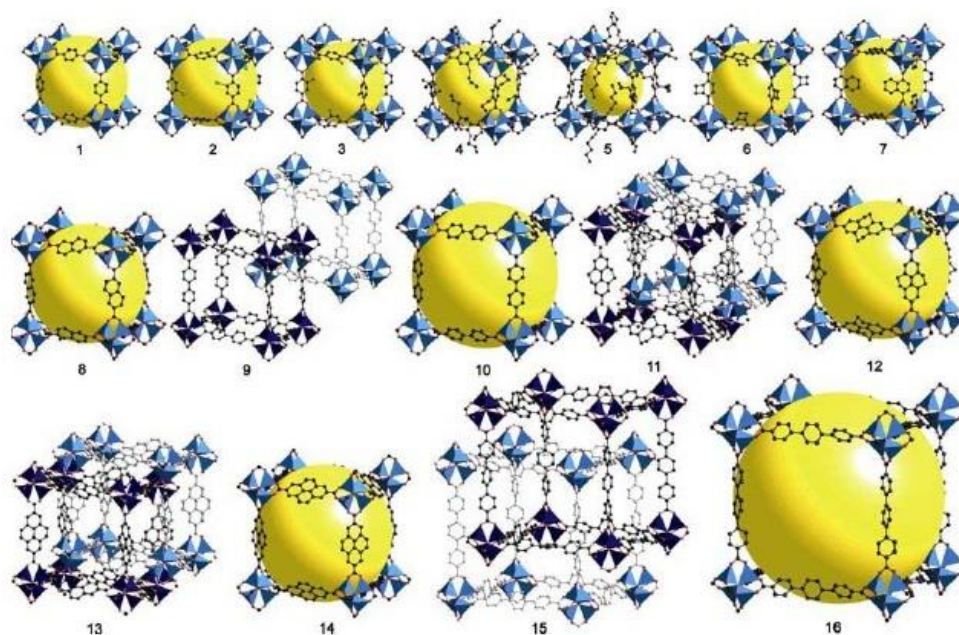
Figure 1.5. Structures of isoreticular MOFs (IRMOFs 1-16) using MOF-5 as the prototype [57]

Another important feature of porous framework compound in view of adsorption and separation is the surface area. In most cases, the interaction between the guest molecules and the surface of an adsorbent is much larger than the guest-guest interaction. MOF compounds have reported incredibly high surface areas, such as MIL-101 has showed surface area of 4230 m^2g^{-1} [64] and 4500 m^2g^{-1} for MOF-177 [57]. These were not only the materials of largest surface areas among reported MOF compounds, however, the maximum for all known porous materials as well. The pore systems are uniform all over the material due

to the crystalline structure of MOFs, that facilitate greater repeatability and consistency of sorption properties while compared with other porous materials such as amorphous carbons and silicas.

One area in which traditional materials still have advantages is the thermal stability. Zeolites can, in some cases, be heated to temperatures in excess of 1000 °C in air without degradation [65] which can allow for applications in the separation (or purification) of gases such as flue gas [66] or high temperature catalysis [67]. MOF materials tend to have significantly lower thermal stability than zeolites but some examples of MOFs with strong metal-ligand bonds and stable organic components have shown thermal stability, in air, greater than 550 °C in case of porous MOF [68] and over 600 °C in high density non-porous MOF [69].

There are several synthetic procedures employed in the formation of crystalline hybrid compounds for example diffusion-based crystallization and hydrothermal or solvothermal and ionothermal synthesis. Usually, MOFs are synthesized by using solvothermal or hydrothermal process [70], wherein the reactions are carried out with an organic solvent or in water, respectively, at high temperature under autogenous pressure. Though, these processes normally involve time-consuming reaction, from several hours up to several months, depending on the MOF of concern and the several factors such as solvent, temperature, concentrations of reactants etc. A microwave-aided method has been evolved in which synthesis of MOFs can be carried out in large scale in a few minutes or few hours [71]. This process can also control the size of crystal from near-millimeter to sub-micrometer by controlling the temperature and the concentration of reactants in solution.

To facilitate expand of an eco-friendly process; many researchers have reported the synthesis of MOFs under solvent-free condition [72]. The mechano-chemical synthesis involving application of mechanical force to afford the solvent-less reactions of metal oxides with organic linkers at room temperature. Additionally, the electrochemical synthesis of MOFs has been employed by BASF on commercial scale [73].

1.2.1 Hydrothermal synthesis of MOFs

Zeolites are naturally created in presence of rationally high temperatures (> 573 K) and pressures (> 300 MPa) originated in the Earth's upper crust as an outcome of burial metamorphism. Consequently, in beginning attempts to manufacture synthetic zeolites were carried out in similar conditions. It was not before the 1950s that zeolite chemistry later diverted towards the substitute hydrothermal synthesis route suggested by Barrer and Milton [74].

Hydrothermal synthesis depends on the principle that the precursors used in microporous framework construction are insoluble under ambient conditions, nevertheless are highly soluble at higher temperatures (100-260 °C) and pressures [75]. Most of the reported MOFs have been synthesized by solvothermal and hydrothermal synthetic methods, normally using sealed Teflon-lined stainless-steel autoclaves or reaction bombs. The design of the autoclave is a thick-walled sealed steel reaction vessel and the inner wall comprises of Teflon-lined coating wherein, the reaction temperature is able to rise above the boiling point of the solvent at high pressure. Under these circumstances autogenic pressure is established, wherein the pressure inside the reaction vessel is auto-developed and no need to apply externally, letting the formation of novel products. The pressure inside the reaction vessel rises intensely with rising temperature even if dependent on the sealing of the vessel and also depends upon the quantity of reactants used in the reaction [76]. The viscosity of water decreases under these conditions which improves the diffusion processes to facilitate growth of crystals from the solution is favored and permitting retention of the structural elements of the reactants in the ultimate product [77]. This ''soft-chemistry'' method allows the formation of polymeric units via molecular building blocks [78]. Further, solvents are used within this reaction method altering the synthesis to solvothermal synthesis. The both hydrothermal and solvothermal synthesis methods have been employed to synthesize new materials, and for the progress of new processes for the preparation of new functional materials with new shapes i.e., crystal growth [79]. In comparison to the solution phase reactions hydrothermal methods have active role in making robust and stable MOF materials [80]. The growth of crystal is not possible to watch visually, however, it is likely to get insight into the mechanism of crystalline formation through availing in-situ energy dispersive X-ray diffraction method in suitable cases [81].

1.2.2 Carboxylate based MOFs

To construct the MOFs, several types of organic linkers have been used tactically. Organic carboxylates are the most challenging candidate owing to its numerous binding modes (Figure 1.6), which helps to form several categories of framework with functional properties.
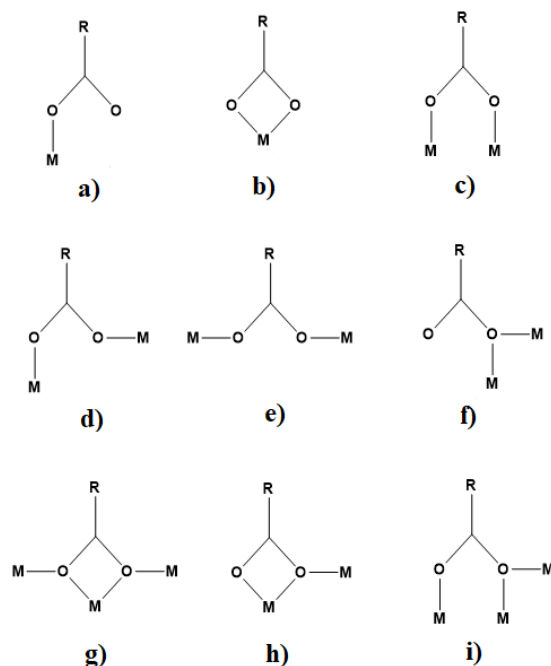
Figure 1.6. Coordination modes of carboxylate; (a) unidentate (b) chelating bidentate (c) *syn-syn* bridging (d) *syn-anti* bridging (e) *anti-anti* bridging (f) $\mu_{1,1}$-bridging (g) unidentate with $\mu_{1,1}$-bridging (h) chelation with $\mu_{1,1}$-bridging (i) chelation with $\mu_{1,2}$-bridging

Continued and targeted research has been commenced into MOF systems, that culminated in the synthesis of myriad of porous structures [82]. Most of the MOFs have been synthesized in the metal carboxylate scheme, where di- and trivalent metals are connected with di- and tricarboxylate linkers, lead to formation of high symmetry structure. The strong M-O-C bonds showing high thermal stabilities in framework, whereas the carboxylate linkers are not apt to self-condensation. A variation of metal surroundings has been reported, for example four zinc atoms cluster in MOF-5 [42]; vanadium atoms chain in MIL-47 [83] and MIL-68 [84] and clusters of three chromium atoms connecting to the identical μ_3 oxygen atom in MIL-100 [85] and MIL-101 [86]. Research group of O. M. Yaghi discovered the structure of MOF-5 in 1999, it was the first three-dimensional porous metal-organic framework structure reported in the literature, which is stable to solvent elimination, representing permanent and reversible nitrogen adsorption at 77 K and 1 atm. As described previously, a complete family of associated reticular MOF structure has been delineated with the similar primary structure as MOF-5, however, by a variety of dissimilar dicarboxylate ligands (namely IRMOF-n series) [63]. By using varieties of dicarboxylic acid linkers (Figure 1.7) the topology and features of the frameworks can be altered and improved in predictable manner.
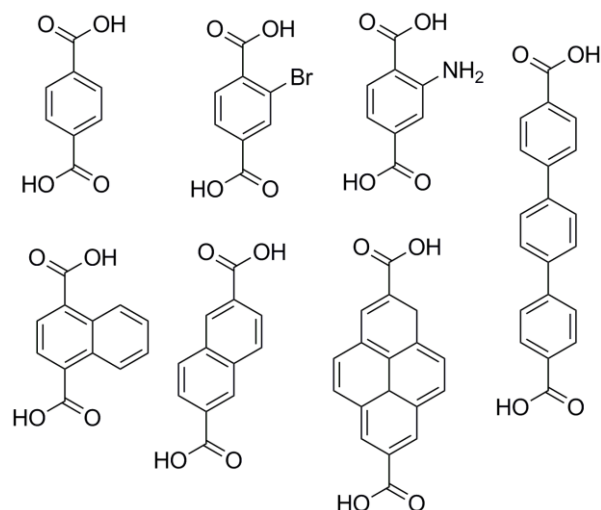
Figure 1.7. Examples of dicarboxylic acid linkers used in the IRMOF-n series of structures [57]

When MOF-5 was invented, around the same time one more interesting porous carboxylate MOF compound was synthesized, named HKUST-1 (abbreviated from Hong Kong University of Science and Technology) [87]. The MOF material was synthesized by copper nitrate salt and 1,3,5-benzenetricarboxylate (trimesic acid) linker. The structure comprises of dinuclear copper units with a short Cu-Cu distance of 2.63 Å. Viewed along the [100] plane, the structure encompasses 1-dimensional square shaped channels (diameter of *ca.* 10 Å). These 1-dimensional channels are existing in all three crystallographic planes, and the intersections create large hexagonal shaped channels (10 Å in diameter). Physically adsorbed water is occupying in the channels, and chemically adsorbed water is coordinated to the binuclear copper species. The chemically adsorbed water or metal coordinated water can be eliminated thermally, that results vacant coordination sites on the copper cations. These vacant sites or voids act as Lewis acids, ensuring adsorption of gases and catalysis.

1.3 Gas adsorption and separation studies

Metal-organic frameworks comprising of one-, two-, and three-dimensional architectures, have been emerging at an accelerating rate due to existence of their high porosity and high pore volume, particularly for the gas adsorption studies.

In 1998, Yaghi *et al.* [88] synthesized a microporous material, MOF-2, with formula $Zn(BDC)(H_2O)$ [BDC = 1,4-benzenedicarboxylate], was first report creating microporosity which was verified by surface area and pore volume measurements. Structural integrity and porosity of the structure are sustained in presence of solvent molecules or guest molecules [89-91]. The structure of MOF-2 composed of polynuclear metal cluster, $Zn_2(–COO)_4(H_2O)_2$ paddlewheel like secondary building units

(SBUs) are linked through BDC linkers (Figure 1.8a, b). A potential void space was filled with guest molecules, which can be eliminated under vacuum with heating to form the desolvated MOF-2, with formula Zn(BDC). Gas adsorption studies revealed typical reversible type-1 gas sorption isotherms, such as zeolites, indicating that MOF-2 is permanently microporous, as demonstrated by nitrogen at 77K (Figure 1.8c) or carbon dioxide at 195K as sorbate molecules. However, the Langmuir surface areas for this specific MOF were calculated to be 270 and 310 m^2g^{-1} for N_2 and CO_2, respectively, which was smaller than conventional zeolite molecules. The finding of MOF-2 was a crucial point in progress of 3D structures of MOF materials, creating a plethora of opportunities of combination of SBUs with organic linkers.
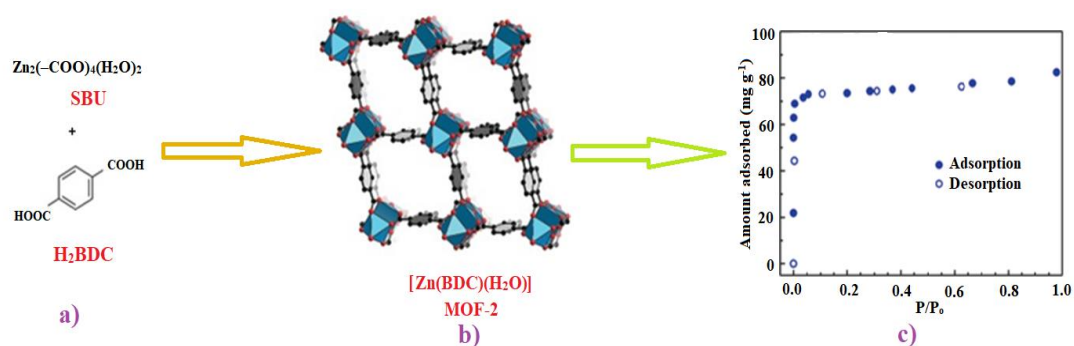
Figure 1.8. a) $Zn_2(-COO)_4(H_2O)_2$ secondary building units (SBUs) are linked through BDC linkers to form MOF-2; b) View of MOF-2 along the crystallographic [001] direction, the rectangular channels are clearly visible (hydrogen atoms are omitted for better clarity). Color encryption: black, C atoms; red, O atoms; blue polyhedra, Zn metal centers; c) N_2 sorption isotherm of MOF-2 at 77 K [88]

In 1999, Yaghi *et al.* [42] further reported synthesis of a very highly porous material, MOF-5 using octahedral basic zinc acetate building unit $Zn_4O(-COO)_6$ and BDC linkers (Figure 1.9a, b). The name, MOF-5 coined in reflection of the well-known zeolite ZSM-5. A primitive cubic (pcu) topology (single atom vertices connected by edges) displays small resistance to mechanical forces owing to practical strain upon frameworks. Conversely, the tetrahedral form of Zn_2O clusters are attached to rigid BDC linkers consequences in a 3D rigid structure having more thermodynamic stability [92-93]. Excellent rigidity was gained throughout the activation process, even though mechanical forces leading the framework, which further showing unchanged in morphology up to 400 °C temperature under vacuum. MOF-5 was prepared by solvothermal synthesis of zinc nitrate tetrahydrate and H_2BDC in a mixture of chlorobenzene and DMF solvents. The resulting framework contains voids space packed with DMF and chlorobenzene guest molecules, which can be exchanged with chloroform and that may be eliminated under vacuum at room temperature. The desolvated MOF retained their structural integrity and framework stability. The N_2

adsorption experiment was done at 77K that showed a type I adsorption isotherm with calculated Langmuir surface area of 2,900 m^2 g^{-1} and pore volume of 1.04 cm^3 g^{-1} (Figure 1.9c). These values are higher than all known usual porous materials for example silicates, zeolites or porous carbon.
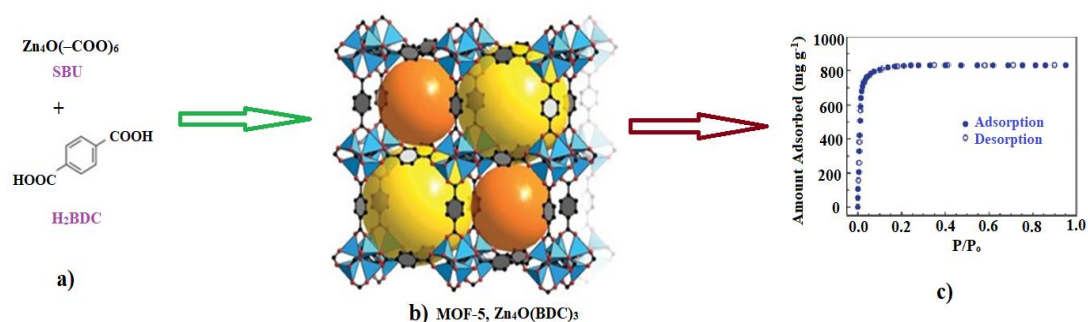
Figure 1.9. a) & b) Single-crystal-X-ray structure of MOF-5 built by $Zn_4O(-COO)_6$ SBUs, linked through BDC linkers (hydrogen atoms are omitted for clarity); Color encryption: black, C atoms; red, O atoms; light blue polyhedra, Zn metal centers; c) N_2 sorption isotherm of MOF-5 at 77 K [42]

On the other hand, hydrogen is gravimetrically energy condensed and harmless, and its oxidation product is water. Hydrogen is best fuel option not only due to massive energy content (33.3 $kWhkg^{-1}$) [94], but also for carbon-neutral energy system. Consequently, it is of importance to find substances that adsorb hydrogen with a H_2 density greater than the density of liquid H_2 [95]. Further, elimination of CO_2 from sources of anthropogenic emission is now a topmost importance, since CO_2 emission has close relevance to climate change.

Koner *et al*. reported a 2D layered alkaline earth metal based MOF compound, $\{[Mg_2(pzdc)_2(H_2O)_4]\cdot H_2O\}_n$ (pzdc = pyrazole-3,5-dicarboxylate). This MOF displayed significantly selective hydrogen (H_2) sorption (*ca.* 63 cc g^{-1}) over N_2 at 1 atm and 77K (Figure 1.10). Such a favored hydrogen uptake over nitrogen might be ascribed to the slight inter layer separations which allows only H_2 molecules to enter into the layers, hindering the entry for the N_2 molecules wherein kinetic diameters of H_2 is around 2.89 Å, smaller than the kinetic diameters of N_2 which is 3.64 Å [96].
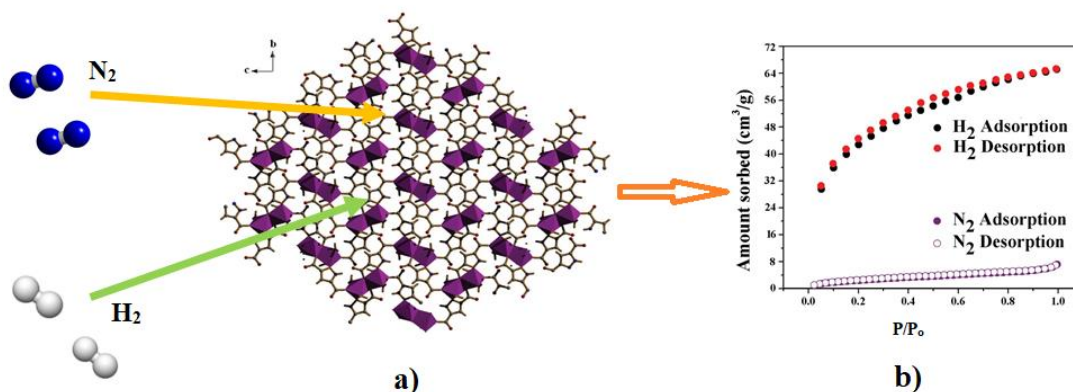
Figure 1.10. a) 2D network of compound {[Mg$_2$(pzdc)$_2$(H$_2$O)$_4$]·H$_2$O}$_n$ along to *bc* plane; b) H$_2$ and N$_2$ sorption isotherm at 77 K [96]

Bu *et al.* have reported a sixfold interpenetrated microporous Cd-based 3D MOF. The MOF has been formed by a heterometallic tetranuclear cluster. The framework comprises of two categories of 1D micro-channels along opposite directions. Besides, this compound displayed highly selective gas sorption for H$_2$ over N$_2$. The compound was immersed in pure methanol (CH$_3$OH) for 3 days to eliminate guest solvent molecules, then filtrated and activation of methanol-exchanged MOF was done at 120 °C under vacuum overnight. Gas sorption measurements showed that the activated MOF reveals very fascinating selective adsorption of H$_2$ over N$_2$. The activated MOF adsorbed a significant quantity of H$_2$ (*ca.* 64 cc g^{-1}) in comparison to amount of N$_2$ (*ca.* 15 cc g^{-1}) adsorption, around 4.3 times higher for H$_2$ than N$_2$, emphasizing the potential for selective separation of H$_2$ over N$_2$. Such favored H$_2$ uptake over N$_2$ might be ascribed to effect of pore-size-exclusive, explicitly, the micropores in activated MOF are easily reachable to H$_2$ but not to N$_2$, owing to their different kinetic diameters of 2.89 Å and 3.64 Å, correspondingly. Moreover, it could be functional in hydrogen separation of the H$_2$/N$_2$ industrial exhaust, for example, in synthesis of ammonia [97].

Immense emission of anthropogenic carbon dioxide (CO$_2$) into the atmosphere has become an utmost environmental concern since it is the main source of green-house gas causing climate change and other environmental damage [98-100]. To progress the purity of biogas separation of CO$_2$ from methane (CH$_4$) plays vital role in recent days [101]. Similarly, pre-combustion CO$_2$ capture also plays crucial role to separate it from hydrogen (H$_2$) containing mixture, which is basically formed through the reaction of primary fuel with oxygen or air [102]. Hence, selective trapping of CO$_2$ using carbon capture and sequestration (CCS) method plays an important role in all these processes [103-104]. Last few decades global warming is one of the most prominent universal ecological issues arising out owing to discharge of anthropogenic green-house gases, particularly CO$_2$. Different CO$_2$ capture technologies have been acquired

for reducing global warming in which CO_2 adsorption method plays a major part. Along with trivial CCS methods, using of MOFs have been fast developing as new functional materials for the selective CO_2 adsorption by feature of their vastly ordered adjustable pore shape and size, greater surface areas with manageable pore surface properties, and high thermal stability [105-112]. Though, it is not easy to attain the selectivity of CO_2 over N_2 and CH_4 by simply controlling the adjustable pore size, as their kinetic diameters are almost close to each other (CO_2 = 3.30 Å, CH_4 = 3.76 Å, N_2 = 3.65 Å). Mostly, pore size as well as environment both supports to attain selectivity [113-118]. Presence of unsaturated coordination of metal centers or open metal sites in the MOF enables adsorption of CO_2 on surface of framework compounds. Typically, organic linkers and coordinated solvent molecules make the metal centers coordinately saturated. However, often unsaturated metal centers are formed by the elimination of coordinated volatile solvent molecules in a controlled way without changing the structural integrity of framework. It can be possible by drying under vacuum or controlled heating or slow heating of the MOF or by applying both. Studies on synthesis and characterization of MOFs were prolific in past few years, nevertheless, porous MOF of mixed linker arrangements for selective CO_2 adsorption over N_2 or CH_4 are still rare in the literature.

Recently, Queen *et al*. reported a novel highly crystalline MOF, Cu-Sp5-EtOH has a charged framework that is likely to produce high selectivity of CO_2 over N_2. First, they synthesized a new linker, 1,3- bis(4-carboxyphenyl)-4,5-dihydro-1H-imidazol-3-ium tetrafluoroborate, (H_2Sp5-BF_4) which is later used for the construction of Cu-Sp5-EtOH. Though, the pores of primary structure might not be opened because of strongly coordinated ethanol molecules. Subsequently solvent exchange method was done with methanol to formation of Cu-Sp5-MeOH and further heating of solvent exchanged MOF under vacuum makes it easier to remove the solvent. On the other hand, small gas molecules like CO_2 easily get access into the desolvated porous structure, Cu-Sp5. The porous MOF displayed exceptionally high selectivity of CO_2 over N_2 owing to the combination of framework charge and open-metal sites. The Ideal Adsorbed Solution Theory (IAST) based calculations were performed on single-component adsorption isotherms. The CO_2/N_2 selectivity of porous material, Cu-Sp5 exhibited a value of over 200 at pressures generally found in post-combustion flue gas (0.15 bar CO_2 / 0.85 bar N_2), showing the highest value reported till date [119].

A three-dimensional highly porous MOF, PCN-124-stu(Cu), molecular formula of $[Cu_2(PDBAD)(H_2O)]_n$ (H_4PDBAD = 5,5′-(pyridine-3,5-dicarbonyl)bis(azanediyl)di- isophthalic acid) has been synthesized that demonstrates exceptional chemical and thermal stability. Furthermore, PCN-124-stu(Cu) showed brilliant result for selective adsorption of CO_2/CH_4. To analyze the surface area of activated MOF, N_2 sorption measurement has been carried out at 77K. PCN-124-stu(Cu) exhibits a type I sorption isotherm which confirms the microporous nature of PCN-124-stu(Cu). The highest uptake of N_2 was 604

cc g$^-$1. The Brunauer-Emmett-Teller (BET) and Langmuir surface areas of the activated sample were measured to be 2153 m^{2}g^{-1} and 2438 m^{2}g^{-1}, respectively. In comparison to typical PCN-124, PCN-124-stu(Cu) displayed higher surface area and larger pore size. The brilliant selective adsorption of CO_2 over CH_4 has attracted attention for application in refinement of natural gas [120-121]. The uptake capacity of CO_2 was as high as 85.8 cc g^{-1} at 298 K and 160 cc g^{-1} at 273 K, both the values are much higher than the uptake capacity of CH_4 [122].

Further, the complex [Zn$_2$(TDC)$_2$DABCO] (TDC = thiophene-2,5-dicarboxylate; DABCO = 1,4-diazabicyclooctane) displayed a significant carbon dioxide (CO_2) adsorption and CO_2/N_2 selectivity compared to the non-thiophene analogue [Zn$_2$(BDC)$_2$DABCO] (BDC = 1,4-benzenedicarboxylate). The maximum CO_2 uptake of [Zn$_2$(TDC)$_2$DABCO] is 67.4 cc g^{-1} at 298 K and 153 cc g^{-1} at 273 K and 1 bar pressure, whereas, in [Zn$_2$(BDC)$_2$DABCO], the corresponding sorption values were 46 cc g^{-1} at 298 K and 122 cc g^{-1} at 273 K, respectively (Figure 1.11). The isosteric heat of adsorption for CO_2 was low (23.65 kJ mol^{-1}), confirming superficial regeneration of the porous substance. Substitution of a phenyl group with thiophene substantially increases CO_2 adsorption as well as the CO_2/N_2 separation selectivity. The selected binding positions of adsorbed CO_2 in [Zn$_2$(TDC)$_2$DABCO] have been explicitly determined by in situ single crystal X-ray diffraction studies on CO_2-adsorbed [Zn$_2$(TDC)$_2$DABCO] [123].
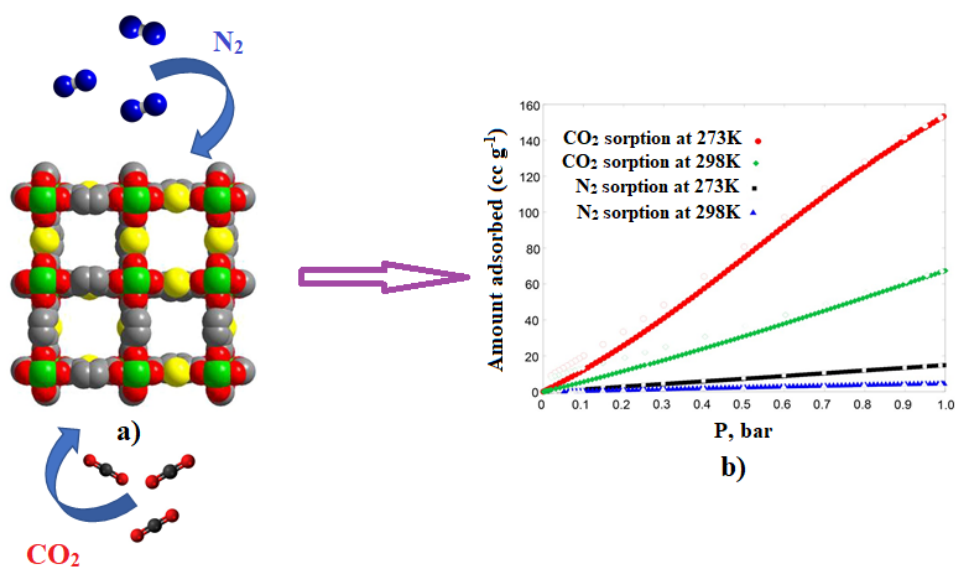
Figure 1.11. a) Van der Waals model of [Zn$_2$(TDC)$_2$DABCO] along the 4-fold axis; Color encryption: green, Zn metal centers; yellow, S atoms; red, O atoms; blue, N atoms; gray, C atoms (hydrogen atoms are omitted for clarity); b) CO_2 and N_2 sorption isotherms at 273K and 298K [123]

Due to deficiency of high internal surface area two-dimensional MOFs are thought to be incapable of adsorbing CO_2, however some recent reports revealed that 2D MOFs can accommodate CO_2 molecules [124-125]. In a previous study on 2D layered MOF, $[Cu(BF_4)_2(bpy)_2]$ (bpy = 4,4′-bipyridine) displayed expansion/shrinkage structural conversion for CO_2 gated adsorption/desorption at 273 K temperature owing to of weak interlayer interactions [125]. Even a flexible 1D MOF $[Cu(BF_4)_2(bpp)_2]$ (bpp = 1,3-bis(4-pyridyl)propane) also showed expansion/shrinkage structural conversion to adsorb gas molecules [126]. In both the cases there was no noticeable crystallographic void space.

1.4 Heterogeneous catalysis over MOFs

Among the several potential applications of MOF in field of gas storage and separation, sensing, drug delivery etc. applications in catalysis take the center stage in recent years. For obvious reasons MOFs enticed researchers to employ these porous solids in heterogeneous catalysis. MOFs have been recently played a significant role as heterogeneous catalysts in Friedel-Crafts reactions [127-131], aldol condensation [132-134], Knoevenagel condensation [135-139], oxidation [140-143], cyanosilylation [144-146], various coupling reactions [147-154], carbon dioxide fixation [155-156] etc. However, catalytic applications of MOFs are limited due to their moisture sensitivity.

1.4.1 MOFs catalyst in condensation reactions

Koner *et al*. reported hydrothermal synthesis of a new 3D alkaline-earth metal-based MOF compound, $[Ba(pdc)]_n$ (pdc = pyridine-2,5-dicarboxylate), catalyzes proficiently aldol condensation reactions of several aromatic aldehydes in presence of cyclohexanone and acetone in THF/triethylamine medium and furnished notable yields (approx. 96%) under eco-friendly heterogeneous condition with 100% selectivity in a quick reaction time of 6 h. The catalyst, $[Ba(pdc)]_n$ was recycled up to five successive runs without noteworthy loss of catalytic activity [132]. The temperature of the catalytic reaction medium was maintained in the range 5-10 °C. On increasing reaction temperature, condensation reaction occurred and benzylideneketone was formed from the *β*-aldol. The best result obtained in presence of THF medium. The decreasing order of efficiency of the catalyst followed by THF > THF-water > solvent-less medium. The catalytic reaction was not carried out in absence of triethylamine base. Further, the decreasing order of yield of the *β*-aldol followed by *p-* > *o-* > *m*-nitrobenzaldehyde.

Pathan *et al.* reported a MOF, $Cu_3(BTC)_2$ (BTC = benzene-1,3,5-tricarboxylate) that catalyzes aldol condensation reaction in presence of toluene and small amount of concentrated H_2SO_4 under mild conditions to afford pyramidine-chalcones [157]. It has recorded a maximum isolated yield of 87% for 1 mmol of substrate. When, $Cu_3(BTC)_2$ separated from the reaction mixture, the reaction stopped immediately

which evidently indicates that the reaction did not catalyze only by H_2SO_4. $Cu_3(BTC)_2$ acts as a strong Lewis acid, however in catalytic reaction, negligible conversion has been observed in absence of conc. H_2SO_4. Hence, the Lewis acidity of $Cu_3(BTC)_2$ was regulated by addition of only 2 drops of conc. H_2SO_4 to make the reaction fast. No prominent structural change was observed from PXRD pattern of the virgin and reused catalyst.

Furthermore, PCN-124 displayed exceptional catalytic efficacy in a tandem one-pot deacetalization-Knoevenagel condensation reaction as a supportive catalyst [158]. The catalytic reaction was performed with 0.5 mol% of PCN-124 as catalyst using 2 mmol substrate in d^6-DMSO for 12 h. In this reaction, benzaldehyde dimethyl acetal was formed with ~ 100% conversion towards the formation of benzaldehyde which further reacted with malonitrile leading to formation of benzylidene malononitrile with very high yield, ~100% in a single one-pot reaction (Scheme 1.2). The catalyst was used for four times and PXRD pattern of used catalyst did not demonstrate any structural change, proved the stability of MOF.
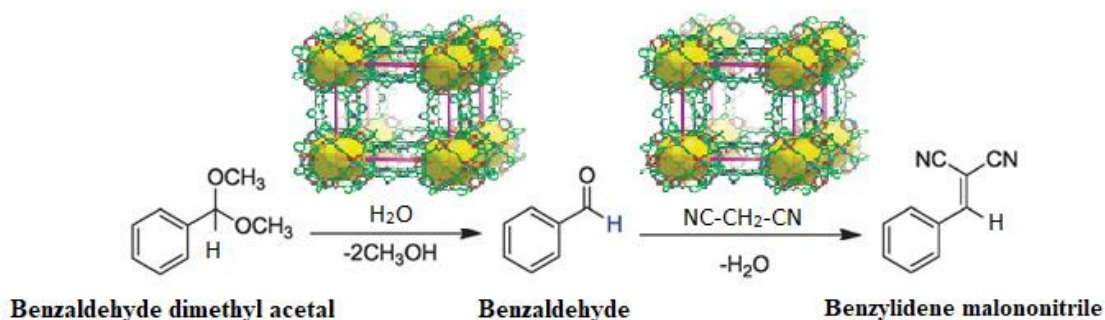
Scheme 1.2. One-pot reaction of deacetalization-Knoevenagel condensation [158]

1.4.2 MOFs catalyst in epoxidation reaction

Oxidation of C=C double bonds establish another significant role that can lead to a various range of derivatives. Epoxidation reaction is one of the vital types of oxidation reactions. Epoxides play an important role in industrial applications as feedstocks for value-added products. Generally, epoxidation reactions take place in presence of an oxidant for example TBHP (tertiary butyl-hydroperoxide), hydrogen peroxide, or peracids. Even though hydroperoxides mixed with suitable catalysts create an appropriate system from the standpoint of green chemistry, owing to their cost it would be desirable to find substitute systems. In the present section, several possibilities will be discussed wherein, MOFs can be employed as heterogeneous catalysts in addition to one of the above-mentioned oxidants. Notably selectivity of products depends on the experimental conditions applied in catalytic reaction.

Jiang *et al*. reported a three-dimensional Cu-based MOF, [Cu(TCBPA)(DMA)] (TCBPA = tris(4′-carboxybiphenyl)amine; DMA = dimethylacetamide) showing catalytic activity in olefin epoxidation reactions [159]. [Cu(TCBPA)(DMA)] was synthesized by a reaction between TCBPA and $Cu(NO_3)_2.3H_2O$ under solvothermal condition. A DMA and H_2O mixture in 3:1 (v/v) ratio was used as solvent along with 15 drops of 3 M HCl solution. The crystal structure revealed the 3D framework of compound contains one dimensional channel (9.4×9.8 Å^2). After the removal of coordinated DMA and guest molecules (H_2O), 1D channels along to crystallographic *c*-axis clearly observed. Desolvated MOF was used in heterogeneous catalytic epoxidation reactions of olefins using TBHP which acts as an oxidant and the reaction carried out at 60 ºC for 24 h (Figure 1.12). The observed results showed very high yield of epoxide products. Oxidation of cyclooctene and *cis*-stilbene, afforded 98% and 94% conversion, respectively, while epoxide yields are 91% and 82%, respectively. Notably, the reaction displayed excellent selectivity, among non-terminal olefins.
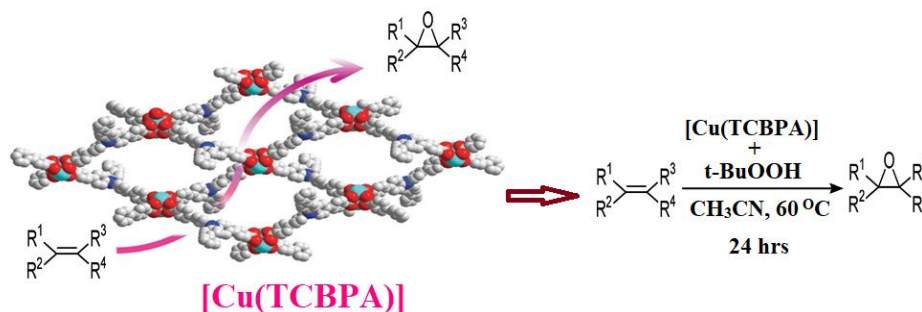
Figure 1.12. Space-filling view of compound [Cu(TCBPA)] (Cu atoms in turquoise) and its catalytic activity in olefins epoxidation reaction [159]

Huo *et al*. reported a strategy to acquire multi-component MOFs derivatives by treating the MOFs under suitable conditions [160]. They have used ZIF-67 as the template to introduce Zn and effectively synthesized the multicomponent MOFs under suitable gas atmosphere and high temperature. ZIF-67 powder was activated overnight in vacuum at around 120 °C before the carbonization step. After carbonization process, the derivatives of multicomponent MOFs (with Co and CoO nanoparticles) display higher conversion of styrene (approx 99%) as well as higher selectivity (approx 70%). These also exhibit more stability than those of other MOFs even more than the derivative of single component MOF.

Two observations were published by Wu's group about the catalytic MOFs created with metalloporphyrin [34, 161]. Porous metalloporphyric MOFs, [CH$_3$NH$_2$][M$_2$′(HCOO)$_2$(M^{III}-TCPP)](guest), (where, M = Mn^{3+} or Fe^{3+} and M′ = Zn^{2+} or Cd^{2+}; TCPP = tetrakis(4-carboxyphenyl)porphyrin), were obtained from solvothermal synthesis of M^{III}-TCPP and M′(NO$_3$)$_2$ [34]. These isomorphous frameworks

can be used as a recyclable heterogeneous catalyst in epoxidation of olefins. However, the Fe-porphyrinic MOFs were not as much of efficient. The main reason of less efficiency of Fe-porphyrinic MOFs was caused by the deactivation of this compound by self-oxidation. $[CH_3NH_2][M_2'(HCOO)_2(Mn^{III}\text{-}TCPP)]$ did not demonstrate size-selectivity in catalysis, as the inner porphyrinic Mn^{III} centers have been blocked by formate pillars and become unapproachable to the substrates. Conversely, $[CH_3NH_2][M_2'(HCOO)_2(Fe^{III}\text{-}TCPP)]$ still displayed good outcomes in intermolecular aldol reaction of carbonyl compounds (aldehydes and ketones). In both catalytic schemes, the porphyrinic MOF catalysts exhibited better activities than the corresponding homogeneous (M^{III}-TCPP) catalysts.

Brown *et al*. reported a Cu-based MOF, $[Cu(H_2BTEC)(bipy)]_n$ (BTEC = 1,2,4,5-benzene tetracarboxylate; bipy = 2,2′-bipyridine) that has been used as a heterogeneous catalyst for epoxidation reaction of cyclohexene and oxidation of styrene in presence of TBHP [162]. Oxidation of styrene resulted in 23.7% conversion with 71% styrene oxide product with a turn over number 673 and 29% of benzaldehyde product in reaction time 24 h at 75 °C. Conversely, oxidation of cyclohexene resulted in 64.5% conversion with a turn-over number of 1886 and 73.1% selectivity of cyclohexene oxide at temperature 75 °C in 24 h. Thus, it appears that the Cu-MOF displayed a high selectivity for the oxidation from the standpoint of hydroperoxide consumption, minimizing spurious decomposition of TBHP.

Example of Cu(I)-based MOF, ($\{[Cu_2Br_2(pypz)]_n \cdot nH_2O\}$ (Cu-Br-MOF) [pypz = bis[3,5-dimethyl-4-(4′-pyridyl)pyrazol-1-yl] methane] has been investigated by Konar *et al*. [163]. The structural analysis revealed pypz ligand which acts as a tritopic ligand linked through two Cu_2Br_2 dimeric units, establishing a 1D zig-zag chain, and those 1D chains further linked by a Cu_2Br_2 unit, finally formed a 2D structural framework parallel to the crystallographic *bc*-plane. The copper ions are four coordinated in a Cu_2Br_2 dimeric unit and having a tetrahedral geometry which demonstrated as an excellent heterogeneous catalyst for both aerobic homocoupling reactions and epoxidation of olefins (Figure 1.13). The aerobic homocoupling reaction requires only 3 mol% of catalyst and it did not involve any base or oxidant associated to other orthodox catalysts like Cu, Pd, Fe, and Au etc. for the conversion of arylboronic acids. The investigation of shape and size selectivity of the Cu(I)-based MOF-catalyst in the homocoupling reaction has been also performed.
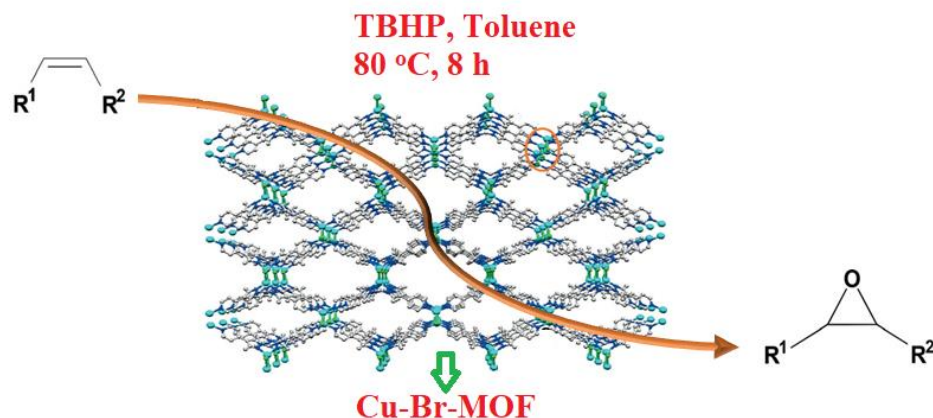
Figure 1.13. 2D framework of Cu-Br-MOF with rhomboid-shaped channels along the *a*-axis (Cu atoms in cyan) and olefins epoxidation catalyzed by Cu-Br-MOF [163]

Furthermore, vanadium-based metal-organic framework, V-MIL-47 has been reported by Leus *et al*. [164]. MIL-47 comprises of a porous terephthalate framework constructed by infinite chains of $V^{IV}O_6$ octahedra well-ordered in orthorhombic three-dimensional architecture that displays large pores. V-MIL-47 exhibited catalytic movement of oxidation of cyclohexene in heterogeneous conditions by adding of 2 equivalents of TBHP. Pores of V-MIL-47 remained blocked by organic compounds and regeneration of catalyst is achieved through activation of catalyst at 523 K for 4 h.

Liu *et al*. reported synthesis of a vanadium 2,6-naphthalenedicarboxylate MOF, $V^{III}(OH)(NPDC) \cdot H_2O$ (NPDC = 2,6-napthalenedicarboxylate). Consequently, dehydrated MOF showed comparable catalytic activity to that of above-mentioned porous V-MIL-47 [165].

Dhakshinamoorthy *et al*. reported an iron based MOF, [Fe(BTC)] (BTC = 1,3,5-benzenetricarboxylate) encumbered with N-hydroxyphthalimide (NHPI) which catalyzes the oxidation of cycloalkenes in aerobic condition depending upon the nature of the substrate to produce allylic oxidation products in variable percentages along with corresponding epoxides. In case of cyclohexene and cyclopentene, this catalyst displays their corresponding unsaturated ketone and cyclic alcohol upon aerobic oxidation with 97% selectivity of products. However, conversion was 12% and 6% for cyclohexene and cyclopentene, respectively in reaction time 5h. Under the similar conditions, cyclooctene showed 95% selectivity towards the production of cyclooctene oxide along with minor product 2% of cyclooctenol/one in 4 h [166].

Besides, Zhao *et al.* reported preparation of three novel Cu@UiO-66-(COOH)$_2$ catalysts using a solvothermal method and a post-synthetic modification thereafter to introduce three different copper salts on a Zr-based MOF, UiO-66-(COOH)$_2$. Amongst three catalysts, Cu@UiO-1 displayed excellent catalytic activity in aerobic olefin epoxidation. Cu@UiO-1 also demonstrated outstanding thermal stability and excellent recyclability [167].

1.5 MOFs in photoluminescence sensing

Induction of luminescent moieties into porous MOFs has produced numerous exceptionally functional luminescent materials. Environmental sensing and biological imaging are realized using photoluminescent MOFs as they are capable of encapsulating guest molecules. Luminescent MOFs display the following characteristics: (1) the PL features are steadily tunable by merely regulating the constituent luminescent moieties, for example metal nodes, organic linkers and encapsulated molecules into the pores; (2) the size of pores, shapes, functionality, and hydrophobic and hydrophilic pore aperture can be judiciously designed and altered to enhance the recognition capacity; (3) a small changes of the interactions between encapsulated guests and PL moieties would suggestively affect the emissions [168].

Luminescent MOFs (LMOFs) have received a great importance in last two decades in the field of metal-organic frameworks. LMOFs have been employed in variety of applications including sensory materials, optoelectronic materials etc. [169]. By definition, luminescence is spontaneous emission of light (electromagnetic waves) by a substance not resulting from heat. In addition, it can be classified into two different classes typically, *viz*., fluorescence and phosphorescence. Different categories of phenomena have been initiated to perform vital role as per source of luminescence in LMOFs (Scheme 1.3), which contains generally metal-based emission, ligand-based emission, emission owing to excimer or exciplex formation and guest attracted emission etc. These processes exhibit most crucial roles and significant contributions to the emission property of LMOFs. Mostly, aromatic conjugated organic ligands play important role for emission property in LMOFs. The π-conjugated organic ligand containing metal-organic frameworks made from d^{10} metal centers have been employed as luminescent sensing materials [170]. Luminescence properties of such MOFs have attracted attention in potential application of chemical sensing through host-guest chemistry. The π-rich conjugated organic ligands are recognized to absorb light and later radiative transition of this energy outcomes into the luminescence actions of LMOFs. Besides ligand-based luminescence, charge transfer methods (inter-ligand charge transfer (ILCT), metal-ligand charge transfer (MLCT), ligand-metal charge transfer (LMCT) etc.) relating aromatic organic linkers have also been reported and these types of luminescence in LMOFs have enormous potential to design sensory materials [169, b-e].
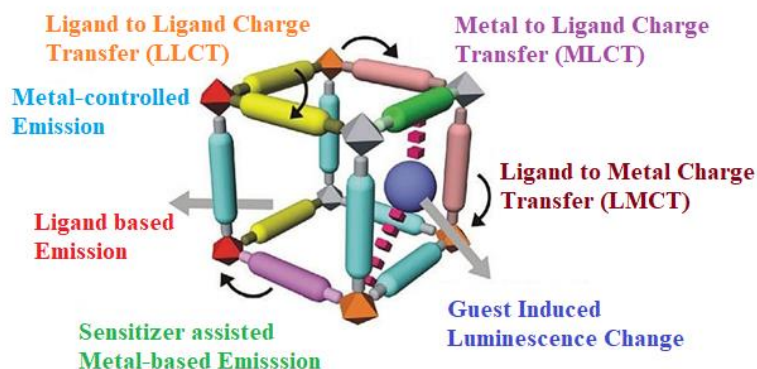
Scheme 1.3. Schematic representation of various types of processes in luminescent MOFs [169c]

Lanthanide metals are major contributor in case of metal node-based luminescence property. Due to the Laporte forbidden f-f transitions in these types of lanthanides, weak emission profiles have been observed because of inefficient absorption. On complex formation with organic linkers, those organic molecules act as light absorbers and consequently enhance emission intensity. This effect is known as "sensitization" or "antenna effect" [13; 169, b-d].

There are two basic types of luminescence, fluorescence and phosphorescence which is shown by Jablonski diagram in Figure 1.14. Generally, fluorescence is fast process with nanosecond time period and phosphorescence is slow process with longer time period which may possibly last from microseconds to minutes or even hours. Luminescence in MOFs happens when electrons in the excited singlet state (S_1) come back to the ground state (S_0) by emission of photon. This luminescence property can either be quenched or intensified upon analyte absorption and is termed as "turn-off" or "turn-on" mechanism respectively.
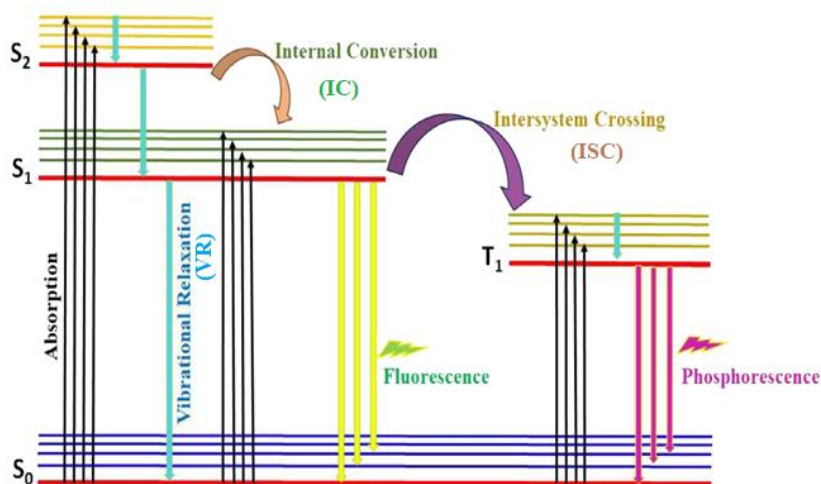
Figure 1.14. Brief representation of Jablonsky diagram

Ligand-based emission processes play a major role in luminescence of MOFs because of their highly conjugated organic structure [171]. Increasing the conjugation of ligands can result in emission dominated by linkers, and upon coordination to metals, the linkers usually turn into more rigid in this way to reduce the efficiency of non-radiative track that frequently increases the lifespan of fluorescence and quantum efficiency. This decrease in non-radiative rate which enhances the fluorescence emission as described in the various literature. There are also cases of intensity depletion [172-173]. Ligand-centered luminescence is usually found in d^{10} metal containing MOFs such as Zn^{2+} and Cd^{2+} ions since these ions having difficulty to undergo oxidation or reduction reactions owing to their core structure of d-orbitals [174]. A large number of studies have compared for ligand-based fluorescence in variety of solvent medium. For instance, three solvent-mediated Cd(II)-MOFs i.e. $[Cd(H_2tptc)(H_2O)_3]NMP$; $[Cd_3(tptc)(OH)_2(H_2O)_4]$ and $[Cd(tptc)_{0.5}(H_2O)]H_2O$ was synthesized based on multidentate tetracarboxylic acid linker, [1,1′:4′,1′′-terphenyl]-2′,3,3′′,5′-tetracarboxylic acid (H_4tptc) using different solvents. The emission spectrum of $[Cd(H_2tptc)(H_2O)_3]NMP$ and $[Cd_3(tptc)(OH)_2(H_2O)_4]$ exhibited blue shift of 378 nm peak, which excited at 300 nm in comparison to that of H_4tptc ligand which displayed emission at 414 nm, upon excitation at 280 nm. This shift may be attributed due to the ligand-metal interactions. While the emission of $[Cd(tptc)_{0.5}(H_2O)]H_2O$ ($\lambda_{ex} = 414$ nm) is found to be indistinguishable to that of H_4tptc ligand, which may take place from the linker-centered $\pi \rightarrow \pi^*$ electronic transitions as shown in Figure 1.15 [175].
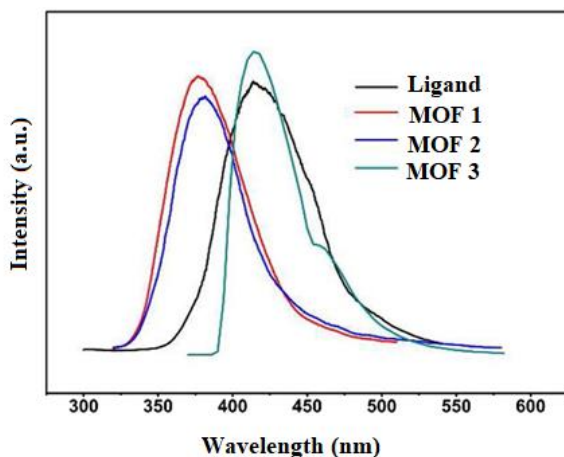
Figure 1.15. Solid state emission spectra of ligand and three MOFs [175]

In study on "turn-on" sensors, adding of targeted analyte to the probe resulted in the enhancement in the luminescence of the probe. Alternatively, quenching in the emission after addition of analyte to the MOF is named as "turn-off" sensing. It is notable that MOFs based sensors are mostly works through "turn-off" phenomenon [176]. However, it can be mentioned that "turn on" sensors have advantages over the "turn-off" sensors. Furthermore, "turn-on" sensing in biological systems is more desirable as it has been carried out mainly in dark condition where enhancement of emission is easy to display in contrast to quenching [177]. MOFs have attracted enormous attention in past few years as "turn-on" probe towards sensing applications.

Zhao *et al.* synthesized a two-dimensional MOF based on the tetraphenylethene (TPE) core ligand, 4,4´-(2,2-diphenylethene-1,1-diyl)dibenzoicacid and Zn^{2+} metal ion (namely, NUS-1a, abbreviated from National University of Singapore) [178]. The porous MOF displayed a predictable aggregation-induced emission (AIE) features due to presence of rigid angular linkers in the structural network. The quantum yield of the parent material has been enhanced significantly upon treatment of various VOCs such as benzene, toluene, xylenes and mesitylene. The parent crystals when soaked with benzene exhibited the major red shift, however, in mesitylene it displayed blue shift. Further, the shift of peak in the photoluminescence spectra was consistent with turn-on response (Figure 1.16). This was attributed to the conformational variations initiated due to the interaction of the analytes with the phenyl rings of the MOF.
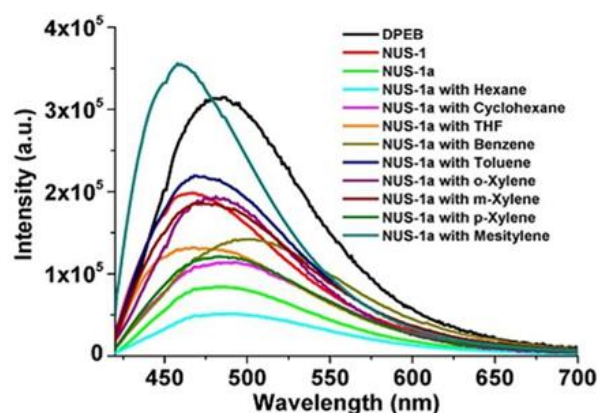
Figure 1.16. Fluorescence emission profile of the ligand and MOF in solid state and MOF in various solvent dispersed medium [178]

Dincă *et al.* reported two compounds $Zn_2(TCPE)$ (TCPE = tetrakis(4-carboxyphenyl)ethylene) and $Mg(H_2DHBDC)$ ($DHBDC^{2-}$ = 2,5-dihydroxybenzene-1,4-dicarboxylate) which are capable of sensing of NH_3 at high temperature (100 °C). The ligand-based emission was crucial for the selective and fast recognition of the analyte at such a high temperature [179]. The presence of open metal sites in the crystal structures is vital in sensing a toxic gas owing to the binding of NH_3 gas molecules towards the metal centers. At high temperature a notable shift was observed in the emission maxima while other vapors like water or methanol experienced no such changes. This is one of the first examples of exploitation of poisonous gas sensing by virtue of the presence of open metal sites in MOF.

Song *et al.* demonstrated a lanthanide based Eu-MOF with molecular formula $[Eu_2(bmtdc)_3(H_2O)_4]\cdot3DMF]$ (bmtdc = 2´,5´-bis(methoxymethyl)-[1,1´:4´,1´´-terphenyl]-4,4´´-dicarboxylate) that can be used as a selective turn-on sensor for DMF vapors [180]. The water exchanged phase of the parent MOF displayed nearly eight-fold increase in the luminescence and this was attributed to the interaction between DMF and linkers which resulted in such an effect.

Research group of C. S. Hong reported the synthesis, structure and luminescence properties of a three-dimensional metal-organic framework $[Cd_3(tcpa)_2(\mu-H_2O)(H_2O)]\cdot3DMF\cdot5H_2O$ (tcpa = tris((4-carboxyl)-phenyl)amine) containing one-dimensional hexagonal channels [181]. The fluorescence data exhibited detection of Mg^{2+} selectively in presence of other metal ions. Remarkably, the emission of MOF upon Mg^{2+} capture was 5.2 times greater than that of the linker. This type of "turn-on" sensing is exceptional and desirable as it permits detection of a target analyte on a dark background, which is not possible in case

of a "turn-off" sensor. The enhancement and recovery methods were reversible, demonstrating that MOF is recyclable, which is a useful feature for sensor applications.

Amongst various analytes, volatile organic compounds (VOCs), for example, benzene and its derivatives, aromatic compounds and common organic solvent vapors are markedly toxic and air/water pollutants. Such pollutant can cause serious environmental problems and bring about intimidation to the ecosystems [182]. As a result, useful and selective detection of VOCs, particularly in vapor phase and/or in aqueous medium, is of immense importance both in chemical assay and environmental tracking [183].

Tian *et al*. revealed solvothermal reaction of Cd^{2+} cations with a silicon-centered carboxylate linker (msitpa = 5,5′,5′′-(methylsilanetriyl)triisophthalic acid) produced a novel metal-organic framework, $[Cd_3(msitpa)_4(H_2O)_5] \cdot DMA \cdot H_2O$ [184]. It is constructed by three $\{CdO_6\}$ clusters and organosilicone linkers to form a three-dimensional porous network. The MOF of steric organosilicone ligand is rare in the literature. Incidentally, it has displayed spontaneous formations of microtubular crystals, which is rarely reported previously. Additionally, the luminescence behavior of this MOF inspected in several organic solvents in disperse medium, exhibiting turn-on and turn-off luminescence responses for *n*-butanol and acetone, respectively (Figure 1.17). Such solvent-mediated luminescence behaviors are of attention for the sensing of n-butanol and acetone solvent molecules. The interaction between open metal sites and guest solvent molecules played a major role in fluorescent sensing. In case of turn-on fluorescence effect, it is proposed that there is a weak interaction between hydroxyl and luminescent open metal sites of the activated MOF [185]. The pore captivity of the analyte in the molecular-sized channels of activated compound may enable robust interaction between n-butanol and host framework.
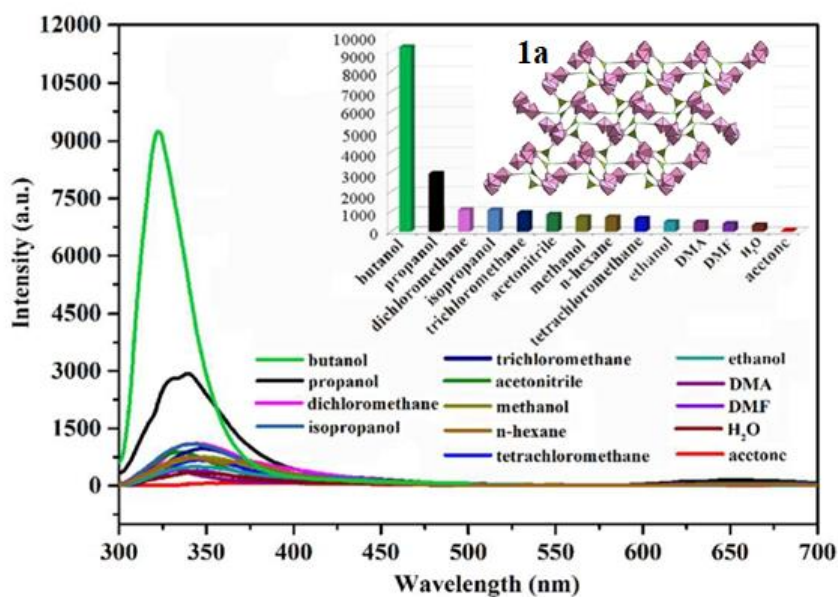
Figure 1.17. Luminescence spectra of activated MOF and the intensities (inset) including structure of activated MOF after interaction with various pure solvents (λ_{ex} = 280 nm) [184]

1.6 Scope and objective of the present thesis

The properties of metal-organic frameworks demonstrate that they have large applicability in a fundamental and industrial perspective for liquid phase heterogeneous catalysis, gas storage and separations, luminescence sensing etc. Chemical versatility of MOFs permits us to make practically infinite structures by altering the building blocks and by using the perception of isoreticularity. If we entirely employ all these properties, the approach for the preparation of the active sites might be developed adjustable fine-structure. Also, from literature survey, it is found that MOFs can be used as promising materials to perform efficient gas storage and separations, luminescent behaviors as well as potential catalysts in various organic reaction transformations, especially in epoxidation reaction. In this thesis effort was made to synthesis such microporous mixed-linker based MOFs for the study of gas sorption, especially selective CO_2 sorption also has been successfully shown in some cases. In addition, studies related to luminescence and heterogenous catalysis also undertaken using newly prepared MOFs. To complete the study following objectives were taken:

► To synthesize porous MOFs by direct hydrothermal or solvothermal synthesis method and characterize them by different physico-chemical methods such as single-crystal-X-ray diffraction, powder-X-ray diffraction, FT-IR, elemental analysis (C, H, N), UV-Vis spectral analysis, TG-DTA (Thermogravimetric analysis) etc.

► To perform gas sorption studies using activated MOFs (after elimination of guest solvent molecules); especially selective CO_2 trapping and theoretical interpretations of its behavior also attempted in this study. The separation of CO_2 from mixture of gases containing methane (CH_4) is very vital for the advancement and the treatment of biogas to improve purity of fuel.

► To examine photoluminescence behavior of MOFs in the solid state as well as in solvent dispersed medium. The π-conjugated organic linkers and coordination polymers with d^{10} metal centers (Cd, Zn etc.) have been used as luminescent materials with fascinating photoluminescent properties.

► To evaluate the catalytic activity of MOF in epoxidation reactions. The effect of different reaction parameters such as temperature, solvent, base effect etc. on the catalytic reaction was also studied to optimize the reaction condition and finally to examine the recyclability and heterogeneity nature of the catalyst.

Consequently, it is convincing that research on MOFs continues to become more interdisciplinary, and the goal in the upcoming years will be to convert the acquired knowledge into technical applications.

1.7 Summary

The thesis contains of seven (7) chapters as follows:

Chapter 1 introduces the general discussion on the multiple features of metal-organic frameworks (MOFs), numerous practices to design diverse functional MOFs, key role of the various carboxylate linkers in the adaptability of MOFs, involvement of transition metals to design carboxylate based and mixed-linker based MOFs while a variety of spacer has been used, application of MOFs in heterogeneous catalysis and the role of MOF solids in heterogeneous catalytic condensation reactions and epoxidation reactions; selective gas adsorption studies, luminescence properties etc. Scope of the current research and the summary of the research works have also been presented.

Chapter 2 accounts synthesis of a hydrogen-bonded 3D supramolecular network constructed by two-dimensional cadmium(II) layer. Two-dimensional cadmium(II) based coordination polymer [Cd(abb)H$_2$O]$_n$ (**1**) [abb = 3,3′-azobis(benzoate)] has been synthesized by hydrothermal method. Notably, [Cd(abb)H$_2$O]$_n$ exhibits unprecedented high uptake of hydrogen and also displayed moderate uptake capacity of other small gas molecules like CO_2, N_2 etc. In addition, photoluminescence property of [Cd(abb)H$_2$O]$_n$ also has been explored.

Chapter 3 discloses synthesis of quinoline derivative containing monomeric and polymeric metal carboxylates that displayed gas sorption over a 2D layered framework. Supramolecular metal-carboxylate

framework $[Co(mqc)_2]_n$ **(2)**, and another monomeric compound $[Zn(mqc)_2(H_2O)]$ **(3)** (mqc = 4-methoxy-2-quinolinecarboxylate) have been synthesized solvothermally and characterized by single crystal X-ray diffraction. Compound **2** is a 2D coordination polymer, further extended to a 3D porous supramolecular network having void space in between each 2D layers. Compound **2** displayed noticeable gas uptake capacity of both CO_2 and H_2 compared to other gas molecules. While compound **3** is a simple monomer, extended to a one-dimensional chain like structure through strong intermolecular hydrogen-bonding.

Chapter 4 deals with the structural diversity and inter-conversion among four hydrothermally synthesized metal carboxylate compounds, $\{[Mg(H_2O)_6][Cu(pdc)_2]\cdot 2H_2O\}_n$ **(4)**, $\{[CuMg(pdc)_2(H_2O)_4]\cdot 2H_2O\}_n$ **(5)**, $\{2(Him)\cdot[Cu(pdc)_2]\}_n$ **(6)**, and $\{[Cu(pdc)(im)_2]\cdot 2H_2O\}_n$ **(7)** (pdc = pyridine-2,5-dicarboxylate and im = imidazole). Compounds **4**-**7** were synthesized respectively from 1, 2, 3 and 4 mmol of imidazole. Compound **6** revealed a polymeric ribbon like 1D chain structure and catalyzes olefin epoxidation reaction in heterogeneous condition. In catalytic study, H_2O_2 acts as an oxidizing agent. Notably, cyclooctene was effectively converted to epoxy-cyclooctane with *ca.* 100% selectivity and conversion.

Chapter 5 reports a three-dimensional mixed-linker zinc-based porous MOF, $[Zn_2(H_2O)(nic)(pzdc)]_n\cdot nH_2O$ **(8)**, (pzdc = pyrazole-3,5-dicarboxylate and Hnic = isonicotinic acid) which has been synthesized by availing hydrothermal route. The as-synthesized MOF has large solvent accessible void space ($\sim 15.9\%$) which is enhanced to $\sim 34.1\%$ upon dehydration. The framework compound and its dehydrated product both displayed highly selective CO_2 adsorption over other small gas molecules at low partial pressure. The selectivity of CO_2 adsorption is well interpreted by computational methods, molecular dynamics and grand canonical Monte Carlo simulations. The adsorption capacity of MOF has been calculated theoretically that follows the order: $MOF-CO_2 > MOF-CH_4 > MOF-N_2 > MOF-H_2$.

Chapter 6 describes the synthesis of two structurally diverse 3D mixed-linker cadmium-based metal-organic frameworks (MOFs), $[Cd_2(pzdc)_2(azpy)_{0.5}(H_2O)]_n$ **(9)** and $\{[Cd_3(pzedc)_2(azpy)_2]\cdot H_2O\}_n$ **(10)** (pzdc = pyrazole-3,5-dicarboxylate, pzedc = pyrazolate-3,5-dicarboxylate and azpy = 4,4′-azopyridine) through solvothermal method. Both the frameworks **9** and **10** showed a pillared-layer structure. Photoluminescence properties of both the MOFs have been investigated in solid state as well as in different solvent medium and both displayed "turn on" and turn off" type of responses in specific solvent with selectivity.

Chapter 7 reports the noteworthy attainments of the effort embodied in the present thesis.

1.8 References:

[1] Z. Zhang, Z.-Z. Yao, S. Xiang, B. Chen, Energy Environ. Sci. 2014, **7**, 2868.

[2] X. Lin, N. R. Champness, M. Schröder, Top. Curr. Chem. 2009, **293**, 35.

[3] K. Sumida, D. L. Rogow, J. A. Mason, T. M. McDonald, E. D. Bloch, Z. R. Herm, T.-H. Bae, J. R. Long, Chem. Rev. 2012, **112**, 724.

[4] D. Andirova, C. F. Cogswell, Y. Lei, S. Choi, Microporous Mesoporous Mater. 2016, **219**, 276.

[5] J. Yu, L.-H. Xie, J.-R. Li, Y. Ma, J. M. Seminario, P. B. Balbuena, Chem. Rev. 2017, **117**, 9674.

[6] K. K. Sharma, A. Anan, R. P. Buckley, W. Ouellette, T. Asefa, J. Am. Chem. Soc. 2008, **130**, 218.

[7] Z. Hao, X. Song, M. Zhu, X. Meng, S. Zhao, S. Su, W. Yang, S. Song, H. Zhang, J. Mater. Chem. A, 2013, **1**, 11043.

[8] Q. Wang, C. Tan, Anal. Chim. Acta, 2011, **708**, 111.

[9] J. Rocha, L. D. Carlos, F.A.A. Paz, D. Ananias, Chem. Soc. Rev. 2011, **40**, 926.

[10] L. X. You, B. B. Zhao, H. J. Liu, S. J. Wang, G. Xiong, Y. K. He, F. Ding, J. J. Joos, P. F. Smet, Y. G. Sun, Cryst. Eng. Comm. 2018, **20**, 615.

[11] H. H. Wang, L. J. Zhou, Y. L. Wang, Q. Y. Liu, Inorg. Chem. Commun. 2016, **73,** 94.

[12] J. Wang, M. Jiang, L. Yan, R. Peng, M. Huangfu, X. Guo, Y. Li, P. Wu, Inorg. Chem. 2016, **55**, 12660.

[13] M. D. Allendorf, C. A. Bauer, R. K. Bhakta, R. J. T. Houk, Chem. Soc. Rev. 2009, **38,** 1330.

[14] K. A. Cychosz, A. G. Wong-Foy, A. J. Matzger, J. Am. Chem. Soc. 2009, **131**, 14538.

[15] W. P. Lustig, S. Mukherjee, N. D. Rudd, A. V. Desai, J. Li, S. K. Ghosh, Chem. Soc. Rev. 2017, **46**, 3242.

[16] M. Cametti, K. Rissanen, Chem. Commun. 2009, 2809.

[17] M. R. Tchalala, P. M. Bhatt, K. N. Chappanda, S. R. Tavares, K. Adil, Y. Belmabkhout, A. Shkurenko, A. Cadiau, N. Heymans, G. De Weireld, G. Maurin, K. N. Salama, M. Eddaoudi, Nat. Commun. 2019, **10**, 1328.

[18] H. Wang, W.P. Lustig, J. Li, Chem. Soc. Rev. 2018, **47,** 4729.

[19] A. Kobayashi, H. Hara, S. Noro, M. Kato, Dalton Trans. 2010, **39**, 3400.

[20] B. L. Chen, L. B. Wang, F. Zapata, G. D. Qian, E. B. Lobkovsky, J. Am. Chem. Soc. 2008, **130**, 6718.

[21] Z. G. Xie, L. Q. Ma, K. E. de Krafft, A. Jin, W. B. Lin, J. Am. Chem. Soc. 2010, **132,** 922.

[22] B. Gole, A. K. Bar, P. S. Mukherjee, Chem. Eur. J. 2014, **20**, 2276.

[23] W. Zhang, R.-G. Xiong, Chem. Rev. 2012, **112**, 1163.

[24] M. Kurmoo, Chem. Soc. Rev. 2009, **38**, 1353.

[25] W. J. Zhuang, H. L. Sun, H. B. Xu, Z. M. Wang, S. Gao, L. P. Jin, Chem. Commun. 2010, **46,** 4339.

[26] P. Horcajada, C. Serre, M. Vallet-Regí, M. Sebban, F. Taulelle, G. Férey, Angew. Chem. Int. Ed. 2006, **45**, 5974.

[27] P. Horcajada, R. Gref, T. Baati, P. K. Allan, G. Maurin, P. Couvreur, G. Férey, R. E. Morris, C. Serre, Chem. Rev. 2012, **112**, 1232.

[28] G. Li, H. Kobayashi, J. M. Taylor, R. Ikeda, Y. Kubota, K. Kato, M. Takata, T. Yamamoto, S. Toh, S. Matsumura, H. Kitagawa, Nat. Mater. 2014, **13,** 802.

[29] J.-R. Li, J. Sculley, H.-C. Zhou, Chem. Rev. 2012, **112**, 869.

[30] H. Sato, W. Kosaka, R. Matsuda, A. Hori, Y. Hijikata, R.V. Belosludov, S. Sakaki, M. Takata, S. Kitagawa, Science 2014, **343**, 167.

[31] P. Nugent, Y. Belmabkhout, S. D. Burd, A. J. Cairns, R. Luebke, K. Forrest, T. Pham, S. Ma, B. Space, L. Wojtas, M. Eddaoudi, M. J. Zaworotko, Nature 2013, **495**, 80.

[32] J. Liu, L. Chen, H. Cui, J. Zhang, L. Zhang, C.-Y. Su, Chem. Soc. Rev. 2014, **43**, 6011.

[33] W.-Y. Gao, M. Chrzanowski, S. Ma, Chem. Soc. Rev. 2014, **43**, 5841.

[34] M. Zhao, S. Ou, C.-D. Wu, Acc. Chem. Res. 2014, **47**, 1199.

[35] J. Lee, O. K. Farha, J. Roberts, K. A. Scheidt, S. T. Nguyen, J. T. Hupp, Chem. Soc. Rev. 2009, **38,** 1450.

[36] M. Yoon, R. Srirambalaji, K. Kim, Chem. Rev. 2012, **112,** 1196.

[37] D. Saha, T. Maity, S. Koner, Dalton Trans. 2014, **43**, 13006.

[38] R. Sen, D. Saha, S. Koner, P. Brandao, Z. Lin, ChemPlusChem 2015, **80,** 591.

[39] P. Ramaswamy, N. E. Wong, G. K. H. Shimizu, Chem. Soc. Rev. 2014, **43,** 5913.

[40] T. Yamada, K. Otsubo, R. Makiura, H. Kitagawa, Chem. Soc. Rev. 2013, **42**, 6655.

[41] D. Lim, H. Kitagawa, Chem. Rev. 2020, **120**, 8416.

[42] H. Li, M. Eddaoudi, M. O'Keeffe, O. M. Yaghi, Nature 1999, **402**, 276.

[43] Y. Shibata, Journal of the College of Science, Imperial University of Tokyo, 1916, **37,** 1.

[44] J. F. Keggin, F. D. Miles, Nature 1936, **137**, 577.

[45] S. L. James, Chem. Soc. Rev. 2003, **32,** 276.

[46] a) B. F. Hoskins, R. Robson, J. Am. Chem. Soc. 1989, **111,** 5962; b) B. F. Hoskins, R. Robson, J. Am. Chem. Soc. 1990, **112,** 1546; c) B. F. Abrahams, B. F. Hoskins, D. M. Michail, R. Robson, Nature 1994, **369,** 727.

[47] a) D. Venkataraman, G. B. Gardner, S. Lee, J. S. Moore, J. Am. Chem. Soc. 1995, **117**, 11600; b) G. B. Gardner, D. Venkataraman, J. S. Moore, S. Lee, Nature 1995, **374**, 792.

[48] O. M. Yaghi, G. M. Li, H. L. Li, Nature 1995, **378**, 703.

[49] S. Subramanian, M. J. Zaworotko, Angew. Chem. Int. Ed. 1995, **34**, 2127.

[50] a) A. F. Wells, Acta Crystallogr. 1954, **7**, 535; b) A. F. Wells, Acta Crystallogr. 1954, **7**, 545; c) A. F. Wells, Three dimensional Nets and Polyhedra, Wiley, New York, 1977; d) A. F. Wells, Structural Inorganic Chemistry, Oxford University Press, London, 5th edn, 1984.

[51] A. Y. Robin, K. M. Fromm, Coord. Chem. Rev. 2006, **250**, 2127.

[52] S. Noro, S. Kitagawa, T. Akutagawa, T. Nakamura, Prog. Polym. Sci. 2009, **34**, 240.

[53] M. J. Rosseinsky, Microporous Mesoporous Mat. 2004, **73**, 15.

[54] J. A. Groves, S. R. Miller, S. J. Warrender, C. Mellot-Draznieks, P. Lightfoot, P. A. Wright, Chem. Commun. 2006, 3305.

[55] M. T. Wharmby, J. P. S. Mowat, S. P. Thompson, P. A. Wright, J. Am. Chem. Soc. 2011, **133**, 1266.

[56] S. L. James, Chem. Soc. Rev. 2003, **32**, 276.

[57] J. L. C. Rowsell, O. M. Yaghi, Microporous Mesoporous Mat. 2004, **73**, 3.

[58] S. Kitagawa, R. Kitaura, S. Noro, Angew. Chem. Int. Ed. Eng. 2004, **43**, 2334.

[59] B. Moulton, M. J. Zaworotko, Chem. Rev. 2001, **101**, 1629.

[60] P. Pachfule, T. Panda, C. Dey, R. Banerjee, CrystEngComm 2010, **12**, 2381.

[61] J. J. Perry IV, J. A. Perman, M. J. Zaworotko, Chem. Soc. Rev. 2009, **38**, 1400.

[62] a) J. Zhang, M. M. Matsushita, X. X. Kong, J. Abe, T. Iyoda, J. Am. Chem. Soc. 2001, **123**, 12105; b) G. J. E. Davidson, S. J. Loeb, Angew. Chem. Int. Ed. 2003, **42**, 74; c) E. S. Lee, J. S. Heo, K. Kim, Angew. Chem. Int. Ed. 2000, **39**, 2699.

[63] M. Eddaoudi, J. Kim, N. Rosi, D. Vodak, J. Wachter, M. O'Keeffe, O. M. Yaghi, Science 2002, **295**, 469.

[64] P. L. Llewellyn, S. Bourrelly, C. Serre, A. Vimont, M. Daturi, L. Hamon, G. De Weireld, J. S. Chang, D. Y. Hong, Y. K. Hwang, S. H. Jhung, G. Férey, Langmuir 2008, **24**, 7245.

[65] M. M. Mohamed, F. I. Zidan, M. H. Fodail, J. Mater. Sci. 2007, **42**, 4066.

[66] R. W. van den Brink, S. Booneveld, J. R. Pels, D. F. Bakker, M. Verhaak, Appl. Catal. B 2001, **32**, 73.

[67] K. Tanabe, W. F. Hölderich, Appl. Cata. A 1999, **181**, 399.

[68] S. R. Miller, P. A. Wright, C. Serre, T. Loiseau, J. Marrot, G. Férey, Chem. Commun. 2005, 3850.

[69] D. T. de Lill, C. L. Cahill, Chem. Commun. 2006, 4946.

[70] A. Qiu, G. Zhu, Coord. Chem. Rev. 2009, **253**, 2891.

[71] T. Chalati, P. Horcajada, R. Gref, P. Couvreur, C. Serre, J. Mater. Chem. 2011, **21**, 2220.

[72] C. Janiak, J. K. Vieth, New. J. Chem. 2010, **34**, 2366.

[73] U. Mueller, H. Puetter, M. Hesse, H. Wessel, Patent, WO2005/049892.

[74] a) R. M. Barrer, J. Chem. Soc. 1948, 2158; b) D. W. Breck, W. G. Eversole, R. M. Milton, T. B. Reed, T. L. Thomas, J. Am. Chem. Soc. 1956, **78**, 5968; c) R. M. Barrer, L. Hinds, E. A. White, J. Am. Chem. Soc. 1952, 1561.

[75] Z. F. Bian, J. Zhu, F. L. Cao, Y. F. Lu, H. X. Li, Chem. Commun. 2009, 3789.

[76] R. I. Walton, Chem. Soc. Rev. 2002, **31**, 230.

[77] P. J. Hagrman, D. Hagrman, J. Zubieta, Angew. Chem. Int. Ed. 1999, **38,** 2639.

[78] T. Jiang, A. Lough, G. A. Ozin, R. L. Bedard, J. Mater. Chem. 1998, **8**, 733.

[79] G. J. Demazeau, Mater. Chem. 1999, **9,** 15.

[80] X. X. Zhao, J. P. Ma, Y. B. Dong, R. Q. Huang, Cryst. Growth Des. 2007, **7**, 1058.

[81] J. S. O. Evans, R. J. Francis, D. Ohare, S. J. Price, S. M. Clark, J. Flaherty, J. Gordon, A. Nield, C. C. Tang, Rev. Sci. Instrum. 1995, **66,** 2442.

[82] S. Kaskel, Handbook of Porous Solids, Wiley, New York, 2002, **2**.

[83] K. Barthelet, J. Marrot, D. Riou, G. Férey, Angew. Chem. Int. Ed. 2006, **41**, 281.

[84] K. Barthelet, J. Marrot, G. Férey, D. Riou, Chem. Commun. 2004, 520.

[85] G. Férey, C. Serre, C. Mellot-Draznieks, F. Millange, S. Surble, J. Dutour, I. Margiolaki, Angew. Chem. Int. Ed. 2004, **43**, 6296.

[86] G. Férey, C. Mellot-Draznieks, C. Serre, F. Millange, J. Dutour, S. Surble, I. Margiolaki, Science 2005, **309**, 2040.

[87] S. S. Y. Chui, S. M. F. Lo, J. P. H. Charmant, A. G. Orpen, I. D. Williams, Science 1999, **283**, 1148.

[88] H. Li, M. Eddaoudi, T. L. Groy, O. M. Yaghi, J. Am. Chem. Soc. 1998, **120,** 8571.

[89] O. M. Yaghi, H. Li, J. Am. Chem. Soc. 1996, **118,** 295.

[90] O. M. Yaghi, C. E. Davis, G. Li, H. Li, J. Am. Chem. Soc. 1997, **119,** 2861.

[91] H. Li, C. E. Davis, T. L. Groy, D. G. Kelley, O. M. Yaghi, J. Am. Chem. Soc. 1998, **120**, 2186.

[92] O. M. Yaghi, M. J. Kalmutzki, C. S. Diercks, Angew. Chem. Int. Ed. 2019, **58**, 14024.

[93] J. Jiang, Y. Zhao, O. M. Yaghi, J. Am. Chem. Soc. 2016, **138**, 3255.

[94] L. Schlapbach, A. Zuttel, Nature 2001, **414,** 353.

[95] M. P. Suh, H. J. Park, T. K. Prasad, D.-W. Lim, Chem. Rev. 2012, **112**, 782.

[96] D. Saha, T. Maity, S. Das, S. Koner, Dalton Trans. 2013, **42,** 13912.

[97] Y.-W. Li, L.-F. Wang, K.-H. He, Q. Chen, X.-H. Bu, Dalton Trans. 2011, **40**, 10319.

[98] M. Z. Jacobson, Energy Environ. Sci. 2009, **2**, 148.

[99] K. S. Lackner, S. Brennan, J. M. Matter, A. -H. A. Park, A. Wright, B. van der Zwaan, Proc. Natl. Acad. Sci. U. S. A. 2012, **109,** 13156.

[100] M. R. Allen, D. J. Frame, C. Huntingford, C. D. Jones, J. A. Lowe, M. Meinshausen, N. Meinshausen, Nature 2009, **458**, 1163.

[101] S. Chaemchuen, N. A. Kabir, K. Zhou, F. Verpoort, Chem. Soc. Rev. 2013, **42**, 9304.

[102] J.-R. Li, Y. Ma, M. C. McCarthy, J. Sculley, J. Yu, H.-K. Jeong, P. B. Balbuena, H.-C. Zhou, Coord. Chem. Rev. 2011, **255**, 1791.

[103] M. G. Plaza, C. Pevida, B. Arias, M. D. Casal, C. F. Martin, J. Fermoso, F. Rubiera, J. J. Pis, J. Environ. Eng. 2009, **135**, 426.

[104] IPCC, IPCC Special Report on Carbon Dioxide Capture and Storage, Cambridge University Press, 2005.

[105] B. Zheng, J. Bai, J. Duan, L. Wojtas, M. J. Zaworotko, J. Am. Chem. Soc. 2011, **133**, 748.

[106] L. Du, Z. Lu, K. Zheng, J. Wang, X. Zheng, Y. Pan, X. You, J. Bai, J. Am. Chem. Soc. 2013, **135***, 562.

[107] J. Liu, P. K. Thallapally, B. P. McGrail, D. R. Brown, J. Liu, Chem. Soc. Rev. 2012, **41**, 2308.

[108] S. Kitagawa, S.-I. Noro, R. Kitaura, Angew. Chem. Int. Ed. 2004, **43**, 2334.

[109] R. Banerjee, A. Phan, B. Wang, C. Knobler, H. Furukawa, M. O'Keeffe, O. M. Yaghi, Science 2008, **319,** 939.

[110] R. Haldar, R. Matsuda, S. Kitagawa, S. J. George, T. K. Maji, Angew. Chem. Int. Ed. 2014, **53,** 11772.

[111] S. Yuan, W. Lu, Y.-P. Chen, Q. Zhang, T.-F. Liu, D. Feng, X. Wang, J. Qin, H.-C. Zhou, J. Am. Chem. Soc. 2015, **137**, 3177.

[112] Y.-B. Zhang, H. Furukawa, N. Ko, W. Nie, H. J. Park, S. Okajima, K. E. Cordova, H. Deng, J. Kim, O. M. Yaghi, J. Am. Chem. Soc. 2015, **137**, 2641.

[113] Z. Hulvey, D. A. Sava, J. Eckert, A. K. Cheetham, Inorg. Chem. 2011**, 50,** 403.

[114] J. L. C. Rowsell, O. M. Yaghi, J. Am. Chem. Soc. 2006, **128,** 1304.

[115] M. Dincă, A. Dailly, C. Tsay, J. R. Long, Inorg. Chem. 2008, **47**, 11.

[116] R. Vaidhyanathan, S. S. Iremonger, G. K. H. Shimizu, P. G. Boyd, S. Alavi, T. K. Woo, Science 2010, **330**, 650.

[117] A. Demessence, D. M. D'Alessandro, M. L. Foo, J. R. Long, J. Am. Chem. Soc. 2009, **131**, 8784.

[118] J. An, N. L. Rosi, J. Am. Chem. Soc. 2010, **132**, 5578.

[119] I. Kochetygov, S. Bulut, M. Asgari, W. L. Queen, Dalton Trans. 2018, **47**, 10527.

[120] J. Liu, P. K. Thallapally, B. P. McGrail, D. R. Brown, J. Liu, Chem. Soc. Rev. 2012, **41**, 2308.

[121] B. Wang, X. L. Lv, D. Feng, L. H. Xie, J. Zhang, M. Li, Y. Xie, J. R. Li, H. C. Zhou, J. Am. Chem. Soc. 2016, **138**, 6204.

[122] W.-G. Jin, W. Chen, P.-H. Xu, X.-W. Lin, X.-C. Huang, G.-H. Chen, F. Lu, X.-M. Chen, Chemistry - A European Journal, 2017, **23**, 13058.

[123] V. A. Bolotov, K. A. Kovalenko, D. G. Samsonenko, X. Han, X. Zhang, G. L. Smith, L. J. Mc Cormick, S. J. Teat, S. Yang, M. J. Lennox, A. Henley, E. Besley, V. P. Fedin, D. N. Dybtsev, M. Schröder, Inorg. Chem. 2018, **57,** 5074.

[124] L.-W. Lee, T.-T. Luo, S.-H. Lo, G.-H. Lee, S.-M. Peng, Y.-H. Liu, S.-L. Lee, K.-L. Lu, CrystEngComm 2015, **17**, 6320.

[125] A. Kondo, H. Noguchi, S. Ohnishi, H. Kajiro, A. Tohdoh, Y. Hattori, W.-C. Xu, H. Tanaka, H. Kanoh, K. Kaneko, Nano Lett. 2006, **6,** 2581.

[126] T. Suzuki, R. Kotani, A. Kondo, K. Maeda, J. Phys. Chem. C 2016, **120**, 21571.

[127] C. Zhu, Q. Mao, D. Li, C. Li, Y. Zhou, X. Wu, Y. Luo, Y. Li, Catal. Commun. 2018, **104,** 123.

[128] G. Calleja, R. Sanz, G. Orcajo, D. Briones, P. Leo, F. Martínez, Catal. Today, 2014, **227,** 130.

[129] N. Anbu, A. Dhakshinamoorthy, J. Colloid Interface Sci. 2017, **494**, 282.

[130] N.T.S. Phan, K.K.A. Le, T. D. Phan, Appl. Catal. A Gen. 2010, **382**, 246.

[131] L.T.L. Nguyen, C. V. Nguyen, G. H. Dang, K.K.A. Le, N.T.S. Phan, J. Mol. Catal. A Chem. 2011, **349**, 28.

[132] D. Saha, T. Maity, R. Sen, S. Koner, Polyhedron 2012, **43**, 63.

[133] N. B. Pathan, A. M. Rahatgaonkar, M. S. Chorghade, Catal. Commun. 2011, **12**, 1170.

[134] O. Kikhtyanin, D. Kubicka, J. Cejk, Catal. Today, 2015, **243**, 158.

[135] J. Gascon, U. Aktay, M. D. Hernandez-Alonso, G.P.M. van Klink, F. Kapteijn, J. Catal. 2009, **261,** 75.

[136] M. Hartmann, M. Fischer, Microporous Mesoporous Mater. 2012, **164,** 38.

[137] Y. Yang, H. Yao, F. Xi, E. Gao, J. Mol. Catal. A Chem. 2014, **390**, 198.

[138] F. X. Llabrés i Xamena, F. G. Cirujano, A. Corma, Microporous Mesoporous Mater. 2012, **157,** 112.

[139] F. Martínez, G. Orcajo, D. Briones, P. Leo, G. Calleja, Microporous Mesoporous Mater. 2017, **246,** 43.

[140] N. Anbu, A. Dhakshinamoorthy, Appl. Catal. A Gen. 2017, **544**, 145.

[141] O. A. Kholdeeva, I. Y. Skobelev, I. D. Ivanchikova, K. A. Kovalenkob, V. P. Fedin, A.R.B. Sorokin, Catal. Today, 2014, **238,** 54.

[142] I. Y. Skobelev, A. B. Sorokin, K. A. Kovalenko, V. P. Fedin, O. A. Kholdeeva, J. Catal. 2013, **298,** 61.

[143] V. V. Torbina, I. D. Ivanchikova, O. A. Kholdeeva, I. Y. Skobelev, O. V. Vodyankina, Catal. Today, 2016, **278**, 97.

[144] Y. Li, L. Zhang, W. Ji, J. Mol. Struct. 2017, **1133,** 607.

[145] S. Neogi, M. K. Sharma, P. K. Bharadwaj, J. Mol. Catal. A Chem. 2009, **299**, 1.

[146] A. Bhunia, S. Dey, J. M. Moreno, U. Diaz, P. Concepcion, K. Van Hecke, C. Janiak, P. Van Der Voort, Chem. Commun. 2016, **52,** 1401.

[147] N.T.S. Phan, T. T. Nguyen, C. V. Nguyen, T. T. Nguyen, Appl. Catal. A Gen. 2013, **457**, 69.

[148] L. Chen, Z. Gao, Y. Li, Catal. Today, 2015, **245**, 122.

[149] K. D. Nguyen, S. H. Doan, A.N.V. Ngo, T. T. Nguyen, N.T.S. Phan, J. Ind. Eng. Chem. 2016, **44**, 136.

[150] N. Anbu, A. Dhakshinamoorthy, J. Colloid Interface Sci. 2017, **490**, 430.

[151] J. W. Brown, N. N. Jarenwattananon, T. Otto, J. L. Wang, S. Glöggler, L. S. Bouchard, Catal. Commun. 2015, **65,** 105.

[152] F. X. Luz, L. Xamena, A. Corma, J. Catal. 2012, **285**, 285.

[153] G. H. Dang, H. Q. Lam, A. T. Nguyen, D. T. Le, T. Truong, N.T.S. Phan, J. Catal. 2016, **337**, 167.

[154] L. Zhang, Z. Su, F. Jiang, Y. Zhou, W. Xu, M. Hong, Tetrahedron 2013, **69,** 9237.

[155] R. Babu, R. Roshan, Y. Gim, Y. H. Jang, J. F. Kurisingal, D. W. Kim, D. Park, J. Mater. Chem. A 2017, **5**, 15961.

[156] R. Babu, R. Roshan, A. C. Kathalikkattil, D. W. Kim, D.-W. Park, ACS Appl. Mater. Interfaces. 2016, **8**, 33723.

[157] N. B. Pathan, A. M. Rahatgaonkar, M. S. Chorghade, Catal. Commun. 2011, **12**, 1170.

[158] J. Park, J.-R. Li, Y.-P. Chen, J. Yu, A. A. Yakovenko, Z. U. Wang, L.-B. Sun, P. B. Balbuena, H.-C. Zhou, Chem. Commun. 2012, **48**, 9995.

[159] D. Shi, Y. Ren, H. Jiang, B. Cai. J. Lu, Inorg. Chem. 2012, **51**, 6498.

[160] J. Huia, H. Chua, W. Zhangc, Y. Shenb, W. Chenb, Y. Hub, W. Liua, C. Gaob, S. Guob, G. Xiaob, S. Lib, Y. Fuc, D. Fana, W. Zhangb, F. Huo, Nanoscale, 2018, **10**, 8772.

[161] M.-H. Xie, X.-L. Yang, Y. He, J. Zhang, B. Chen, C.-D. Wu, Chem. Eur. J. 2013.

[162] K. Brown, S. Zolezzi, P. Aguirre, D. Venegas-Yazigi, V. Paredes-Garcia, R. Baggio, M. A. Novak, E. Spodine, Dalton Trans. 2009, 1422.

[163] S. Parshamoni, J. Telangae, S. Sanda, S. Konar, Chem. Asian J. 2016, **11**, 540.

[164] a) K. Leus, M. Vandichel, Y. Y. Liu, I. Muylaert, J. Musschoot, S. Pyl, H. Vrielinck, F. Callens, G. B. Marin, C. Detavernier, P. V. Wiper, Y. Z. Khimyak, M. Waroquier, V. Van Speybroeck, P. Van Der Voort, J. Catal. 2012, **285**, 196; b) K. Leus, I. Muylaert, M. Vandichel, G. B. Marin, M. Waroquier, V. Van Speybroeck, P. Van Der Voort, Chem. Commun. 2010, **46**, 5085.

[165] Y.-Y. Liu, K. Leus, M. Grzywa, D. Weinberger, K. Strubbe, H. Vrielinck, R. V. Deun, D. Volkmer, V. Van Speybroeck, P. V. Der Voort, Eur. J. Inorg. Chem. 2012, 2819.

[166] A. Dhakshinamoorthy, M. Alvaro, H. Garcia, J. Catal. 2012, **289**, 259.

[167] J. Zhao, W. Wang, H. Tang, D. Ramella, Y. Luan, Mol. Catal. 2018, **456**, 57.

[168] K. Chen, C. Wu, Chin. Chem. Lett. 2018, **29**, 823.

[169] a) L. E. Kreno, K. Leong, O. K. Farha, M. Allendorf, R. P. Van Duyne, J. T. Hupp, Chem. Rev. 2012, **112**, 1105; b) Z. Hu, B. J. Deibert, J. Li, Chem. Soc. Rev. 2014, **43**, 5815 ; c) W. P. Lustig, S. Mukherjee, N. D. Rudd, A. V. Desai, J. Li, S. K. Ghosh, Chem. Soc. Rev. 2017, **46**, 3242; d) Y. Cui, Y. Yue, G. Qian, B. Chen, Chem. Rev. 2012, **112**, 1126; e) L. V. Meyer, F. Schönfeld, K. Müller-Buschbaum, Chem. Commun. 2014, **50**, 8093.

[170] a) S. S. Nagarkar, B. Joarder, A. K. Chaudhari, S. Mukherjee, S. K. Ghosh, Angew. Chem. Int. Ed. 2013, 2881; b) V. Stavila, A. A. Talin, M. D. Allendorf, Chem. Soc. Rev. 2014, **43**, 5994; c) J. Zhang, Y. Huang, D. Yue, Y. Cui, Y. Yang, G. Qian, J. Mater. Chem. B, 2018, **6**, 5174.

[171] J. Heine, K. Müller-Buschbaum, Chem. Soc. Rev. 2013, **42**, 9232.

[172] C. Jiang, Z. Yu, C. Jiao, S. Wang, J. Li, Z. Wang, Y. Cui, Eur. J. Inorg. Chem. 2004, 4669.

[173] F. Jin, H.-P. Zhou, X.-C. Wang, Z.-J. Hu, J.-Y. Wu, Y.-P. Tian, M.-H. Jiang, Polyhedron 2007, **26,** 1338.

[174] J. J. Perry Iv, P. L. Feng, S. T. Meek, K. Leong, F. P. Doty, M. D. Allendorf, J. Mater. Chem. 2012, **22**, 10235.

[175] Y. Wu, G. P. Yang, Y. Zhao, W. P. Wu, B. Liu, Y. Y. Wang, Dalton Trans. 2015, **44,** 3271.

[176] J. Zhang, Y. Huang, D. Yue, Y. Cui, Y. Yang, G. Qian, J. Mater. Chem. B, 2018, **6,** 5174.

[177] S. Sharma, S. K. Ghosh, ACS Omega, 2018, **3**, 254.

[178] M. Zhang, G. Feng, Z. Song, Y. P. Zhou, H. Y. Chao, D. Yuan, T. T. Y. Tan, Z. Guo, Z. Hu, B. Z. Tang, B. Liu, D. Zhao, J. Am. Chem. Soc. 2014, **136**, 7241.

[179] N. B. Shustova, A. F. Cozzolino, S. Reineke, M. Baldo, M. Dincă, J. Am. Chem. Soc. 2013, **135**, 13326.

[180] Y. Li, S. Zhang, D. Song, Angew. Chem. Int. Ed. 2013, **52**, 710; Angew. Chem. 2013, **52**, 710.

[181] S. Eom, S. Park, J. H. Song, W. R. Lee, H. G. Lee, D. W. Kang, J. F. Joung, S. Park, D. Moon, C. S. Hong, Eur. J. Inorg. Chem. 2019, 330.

[182] L. Mølhave, B. Bach, O. F. Pedersen, Environ. Int. 1986, **12**, 167.

[183] H. Zhang, D. Chen, H. Ma, P. Cheng, Chem. – Eur. J. 2015, **21**, 15854.

[184] H.-R. Tian, C.-Y. Gao, Y. Yang, J. Ai, C. Liu, Z.-G. Xu, Z.-M. Sun, New J. Chem. 2017, **41**, 1137.

[185] B. Chen, Y. Yang, F. Zapata, G. Lin, G. Qian, E. B. Lobkovsy, Adv. Mater. 2007, **19**, 1693.

Chapter 2
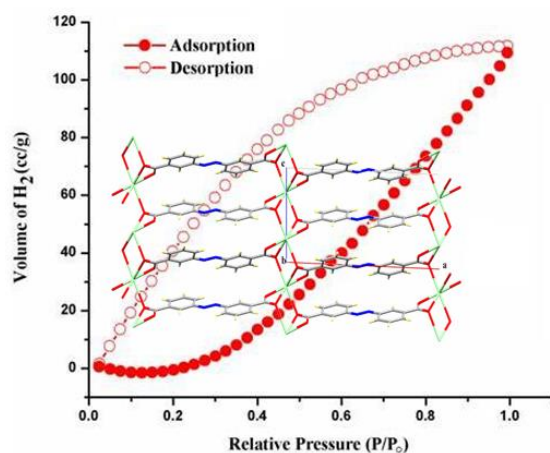
H-bonded 3D supramolecular network constructed by 2D cadmium(II) layer: synthesis, crystal structure and gas adsorption

2.1 Introduction

In this study, solvents and the ligand modification for synthesis of MOF compounds have been emphasized. Azodibenzoates were used in this study to design functional MOFs, however, most of the previously reported compounds are of 4,4′-azodibenzoate variety. Only a small number of compounds are reported containing 3,3′-azodibenzoate [1, 2]. The linker displayed a variety of coordination modes (Scheme 2.1) as described by Zhang *et al.* [3]. But cadmium(II) containing 3,3′-azodibenzoate-based MOF compounds are still limited according to reported literatures [4, 5] and all of them are synthesized by solvothermal process only.

Hence, hydrothermal process has been employed to synthesize novel cadmium(II) containing 2D metal-organic framework compound, $[Cd(abb)H_2O]_n$ (abb=3,3′-azobis(benzoate)) that adsorbs small gas molecules like CO_2, H_2, N_2 etc. Notably, example of 2D MOF network system that adsorbs CO_2, or H_2 is scarce in the literature [6-11].
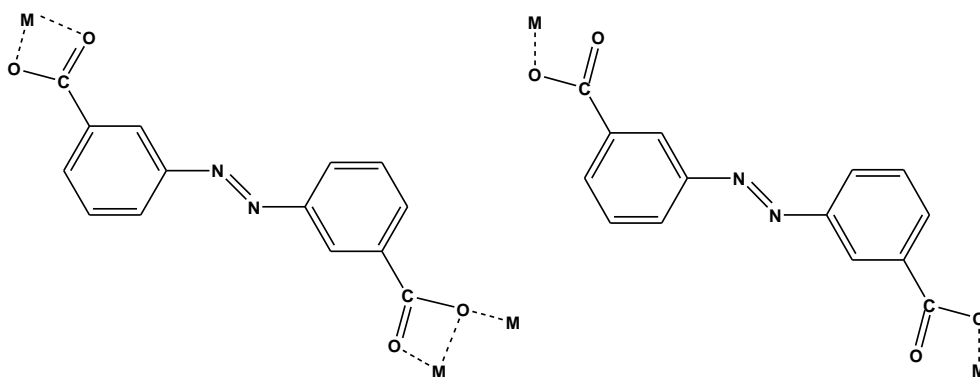
Scheme 2.1. Several coordination modes of [abb]$^{2-}$

2.2 Experimental Section

2.2.1 Materials

3-nitrobenzoic acid and dextrose monohydrate were purchased from Sigma-Aldrich and were of reagent grade. They were used without further purification. Cadmium nitrate tetrahydrate, sodium hydroxide and other chemicals were purchased from Merck (India).

2.2.2 Synthesis of compound [Cd(abb)H₂O]ₙ (1)

The organic linker (H₂abb) was prepared according to the literature methods [12]. H₂abb (67.6 mg, 0.25mmol) and $Cd(NO_3)_2 \cdot 4H_2O$ (77.1mg, 0.25mmol) were dissolved in water (3 mL) and the resulting solution was taken in a 20 mL capacity teflon-lined acid digestion bomb and treated hydrothermally. The compounds were collected as orange colored block crystals from bomb, which was heated at 140 °C for 3 days followed by slow cooling to room temperature.

Yield *ca.* 0.065 g, 65% (approx.)

Anal. for $C_{14}H_{10}N_2O_5Cd$ (M. W. = 398.65): C 42.18, H 2.53, N 7.03. Found: C 42.3, H 2.5, N7.1. IR (KBr): $\nu(COO^-) = 1546$ cm^{-1}and 1390 cm^{-1}, $\nu(N=N) = 1437$ cm^{-1}, $\nu(O-H) = 3360$ cm^{-1} (Figure 2.1).
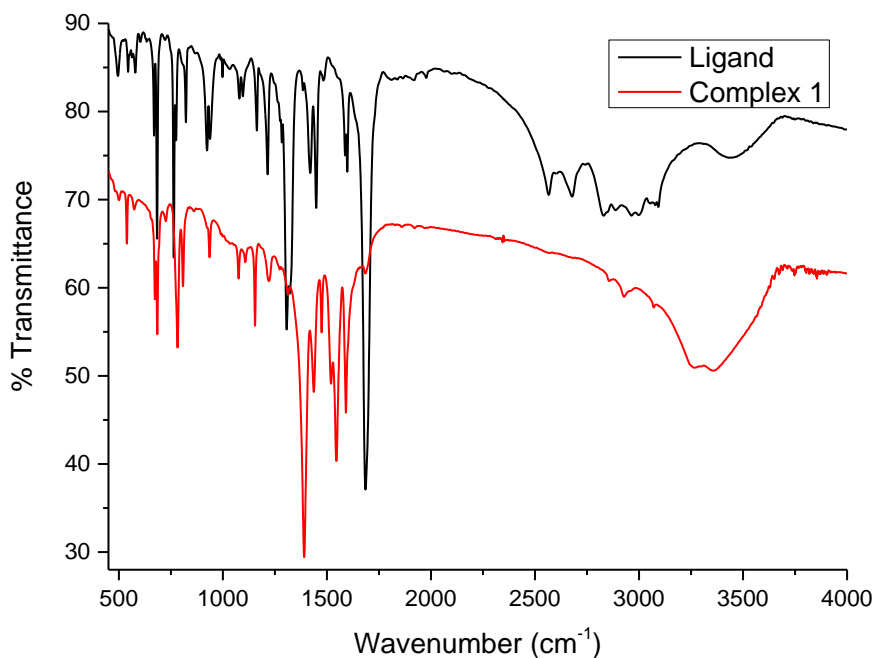
Figure 2.1. FT-IR spectra of the ligand and the compound 1

2.2.3 Physical measurements

Elemental analyses (C, H and N) were performed using a Perkin-Elmer 2400 series II CHN analyzer. IR spectra in KBr pellets (4000-500 cm^{-1}) were recorded on a Perkin-Elmer RXI FTIR spectrophotometer. Solid state electronic spectra were recorded using Shimadzu UV/VIS 1700 spectrophotometer. Luminescence spectra were recorded on a FluoroMax-P (Horiba Jobin Yvon)

luminescence spectrophotometer. Thermogravimetric analysis was performed with a Perkin-Elmer (Singapore) Pyris Diamond TG-DTA instrument. Single-crystal-X-ray diffraction was performed with a Bruker-AXS SMART APEX CCD diffractometer equipped with a graphite monochromator and Mo-Kα (λ = 0.71073 Å) radiation (Figure 2.2a). Powder X-ray diffraction (PXRD) was recorded with a Bruker D8 Advance X-ray powder diffractometer equipped with Cu-Kα radiation (λ = 1.54 Å). Gas adsorption study was carried out on Quantachrome Autosorb iQ(model no. ASIQM0000-1) instrument (Figure 2.2b).

a)   b)
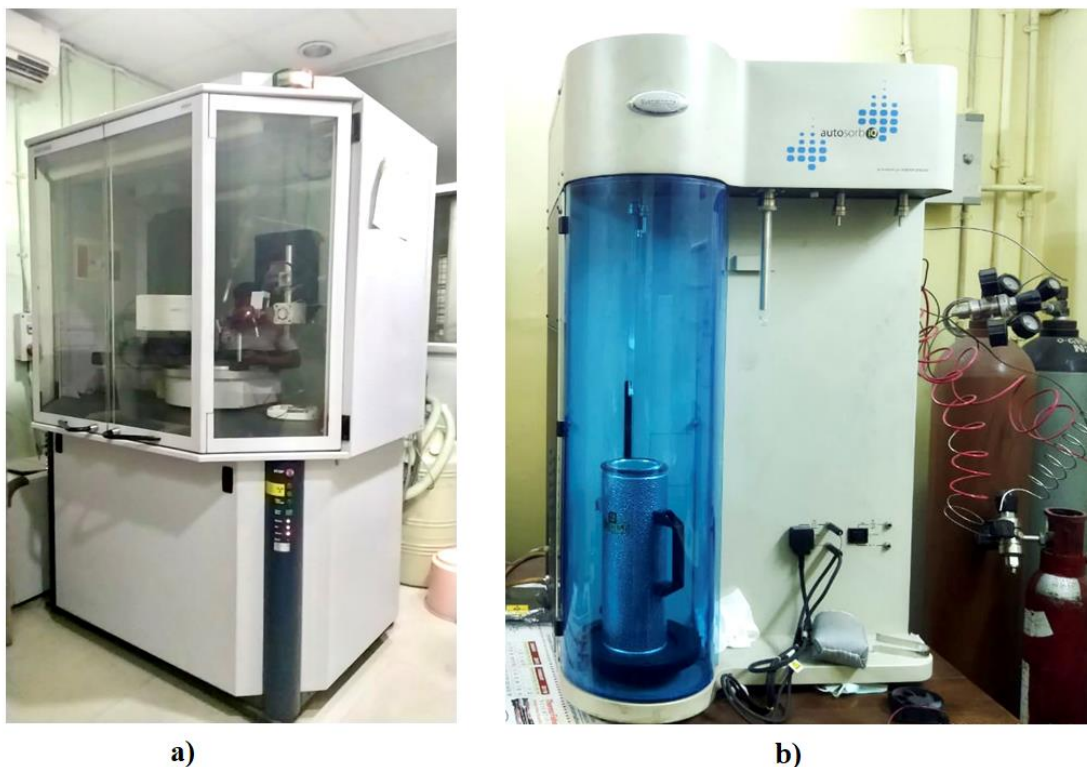
Figure 2.2.a) Bruker-AXS SMART APEX CCD diffractometer for single-crystal-X-ray diffraction; b) Quantachrome Autosorb iQ instrument for gas adsorption measurements.

2.2.4 X-ray crystallography

The crystal was positioned at 60 mm from the CCD with a Bruker-AXS SMART APEX CCD diffractometer. 360 frames were measured with a counting time of 5s. The structures were solved using Patterson method by using the SHELXS97. Subsequent difference Fourier synthesis and least-square refinement revealed the positions of the remaining non-hydrogen atoms. Non-hydrogen atoms were refined with independent anisotropic displacement parameters. Hydrogen atoms were placed in idealized positions and their displacement parameters were fixed to be 1.2 times larger than those of the attached

non-hydrogen atom. Successful convergence was indicated by the maximum shift/error of 0.001 for the last cycle of the least squares refinement. Absorption corrections were carried out using the SADABS program [13]. All calculations were carried out using SHELXS 97 [14], SHELXL 97 [15], PLATON 99 [16], ORTEP-32 [17] and WinGX system Ver-1.64 [18]. Data collection and structure refinement parameters and crystallographic data for the crystal are given in Table 2.1.

CCDC-1427294 contains the supplementary crystallographic data for compound **1**. These data can be obtained free of charge via http://www.ccdc.cam.ac.uk/conts/retrieving.html, or from the Cambridge Crystallographic Data Centre, 12 Union Road, Cambridge CB2 1EZ, UK; fax: (+44) 1223-336-033; or e-mail: deposit@ccdc.cam.ac.uk.

Table 2.1. Crystal data and structure refinement for compound 1

Compound	**1**
Mol. Formula	$C_{14}H_{10}CdN_2O_5$
Formula wt.	398.65
Space group	*P*2/c
Crystal system	Monoclinic
a / Å	14.9608(3)
b / Å	6.4121(1)
c / Å	6.9966(2)
β / deg	91.955(1)
V / Å^3	670.79(3)
Z	2
d_{cal} (g.cm^{-3})	1.974
μ (mm^{-1})	1. 654
R_{int}	0.0212
No. of unique data	2565
Data with I > 2σ(I)	2393
R1 on I>2σ(I)	0.0233
wR2 on I>2σ(I)	0.0635
GOF on F^2	1.070

$R_1 = \sum |(|F_o| - |F_c|)| / \sum |F_o|, wR_2 = \{ \sum [w (F_o^2 - F_c^2)^2] / \sum [w (F_o^2)^2] \}^{1/2}$

2.3 Results and discussion

2.3.1 Description of the crystal structure

Structure of the compound **1** is two-dimensional polymeric network and space group is *P*2/c with Z value 2 (Table 2.1). The crystal system of compound **1** is monoclinic. The 2D sheet that propagates parallel to the crystallographic *ac* plane are composed of a Cd(II) ion, a 3,3′-azobis(benzoate) (abb) and a water molecule. 2D layered structure of the compound consists of double $\mu_{1,1}$-carboxylato-bridged chains of Cd(II) ions along the crystallographic *c*-axis, which are connected by abb linker along the *a*-axis (Figure 2.3, bottom). Both carboxylate groups of the linker have same $\mu_{1,1',3}$coordination mode (1-κ^2OO':2-κO). Structure of the compound consists of one cadmium atom in the asymmetric unit on a twofold axis. The Cd(II) ion present as a hepta-coordinated distorted pentagonal bipyramidal geometry where the equatorial plane is formed by the four oxygen atoms of two abb ligands and one oxygen atom from water and two apical oxygen atoms from two different abb ligands. The coordination environment surrounding Cd(II) metal atom has shown in Figure 2.3(top) and bond parameters are summarized in Table 2.2. The equatorial plane contains five oxygen donor atoms, O1, O2, O1^a, O2^a and Ow to form the bond with cadmium ion with distances [19, 20] of 2.200(2)–2.782(1) Å (symmetry operation a= 2-x,y,3/2-z, b= x,-y,1/2+z and c= 2-x,-y,1-z). The root mean square (r.m.s.) deviations of the five basal donor atoms from their mean planes around Cd(1) is 0.406 Å, and the Cd(1) ion lies in the mean plane with oxygen atom of the water molecule. The two *trans* axial positions are occupied by two symmetrically equivalent oxygen atom (O2^b and O2^c) with the distance of 2.379(1) Å.
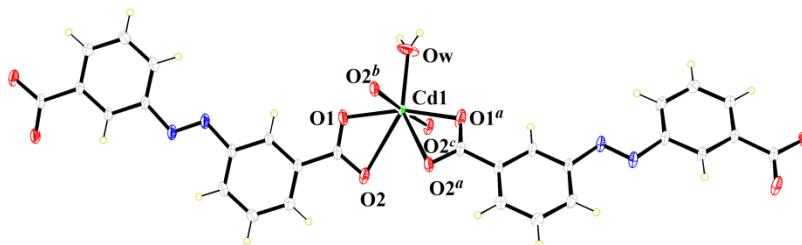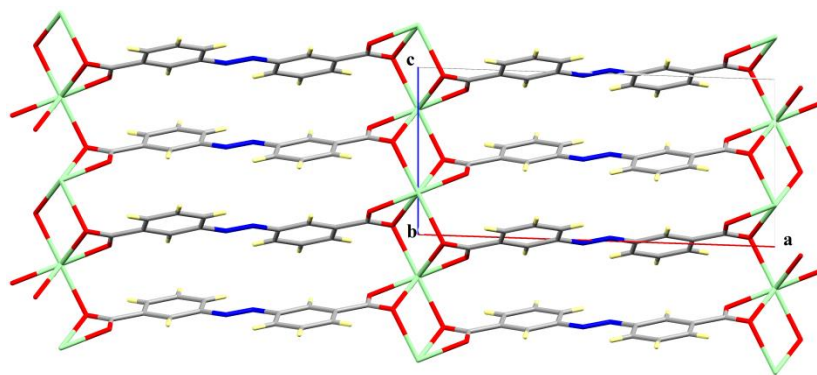
Figure 2.3. (top) Coordination environment around the central Cd(II) atom and (bottom) molecular propagation of the compound 1 viewed parallel to crystallographic *b* axis (water molecules are omitted for clarity)

Each 2D layer interacted with each other by classical hydrogen bonds and thus formed a 3D network along crystallographic *b* axis (Figure 2.4, Table 2.3). The 3D reinforcement of the compound is controlled by O-H···O hydrogen bonding. The both hydrogen atoms in the coordinated water molecule are hydrogen bonded with two different oxygen atoms from different carboxylate group (Figure 2.4, top).

Powder X-ray diffraction studies (PXRD) clearly established the phase purity of bulk materials of compound **1**. Simulated and experimental PXRD patterns of compound **1** matched well indicating reasonable phase purity of **1**. PXRD pattern of compound **1** almost similar when it is out-gassed at 90ºC for 3 h and the well-matched pattern revealed that the structural framework remains intact after out-gassed treatment. Structural integrity of the recovered sample after gas adsorption is also remained unaltered (Figure 2.5).
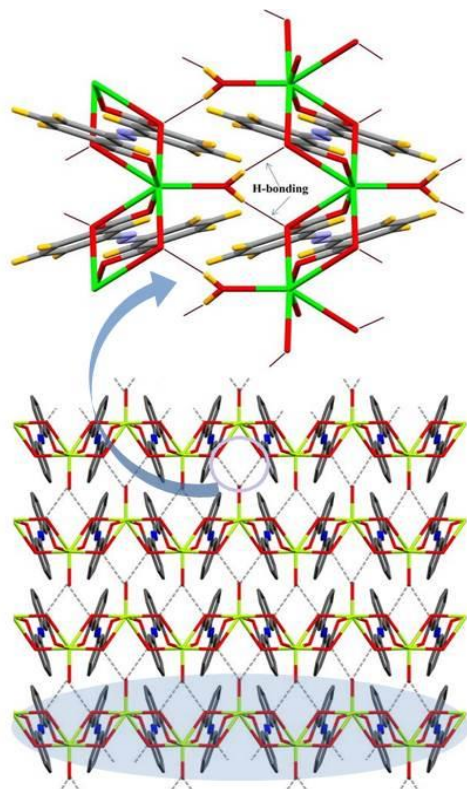
Figure 2.4. 3D supramolecular network formed via H-bonding between 2D layer, viewed along crystallographic *a*-axis (bottom) and the H-bonding unit in the compound (top)
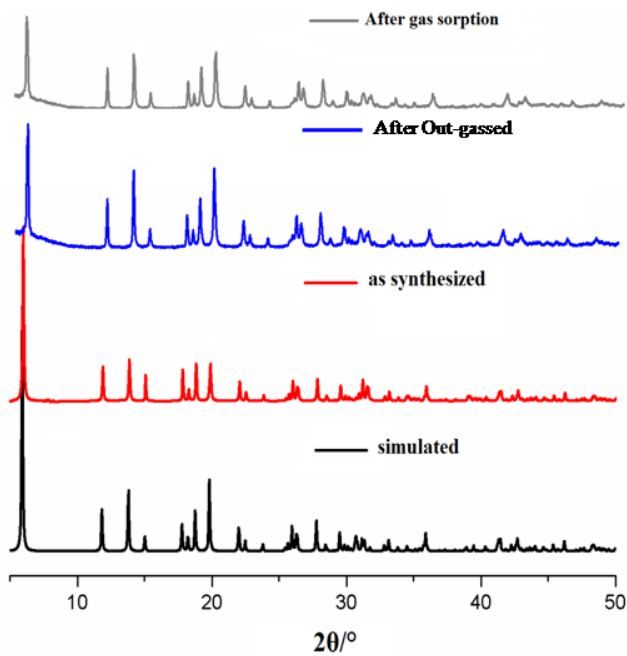
Figure 2.5. Powder X-ray diffraction patterns of compound 1

Table 2.2. Bond distances (Å) and angles (º) of the compound 1

Atoms	Distance
Cd1 - O1/O1[a]	2.200(2)
Cd1 - Ow	2.205(3)
Cd1 - O2/O2[a]	2.782(1)
Cd1 - O2[b]/O2[c]	2.379(1)
Atoms	**Angle**
O1 - Cd1 – Ow	97.60(5)
O1 - Cd1 - O1[a]	164.79(7)
O1 - Cd1 -O2[c]	95.55(6)
O1 - Cd1 - O1[b]	84.90(6)
Ow - Cd1 - O2[c]	88.32(3)
O2[c]- Cd1 - O2[b]	176.63(4)
Ow - Cd1 - O2	141.37(3)
O1 - Cd1 - O2	50.67(6)
O2 - Cd1 - O1[a]	115.28(6)
O2 - Cd1 - O2[a]	77.26(4)
O2 - Cd1 - O2[c]	75.71(4)
O2 - Cd1 - O2[b]	107.024)

Symmetry operation a= 2-x,y,3/2-z, b = x,-y,1/2+z and c = 2-x,-y,1-z

Table 2.3. Hydrogen bond dimensions of compound 1

D-H⋯A	D-H (Å)	H⋯A (Å)	D⋯A(Å)	∠D-H⋯A (°)	Symmetry
OW-H1W⋯O2	0.77(3)	1.91(3)	2.674(2)	172(3)	x,1+y,z

2.3.2 Solid state photoluminescence

Solid state absorption spectrum displayed two broad absorption bands near 245 and 320 nm for both the ligand and the compound (Figure 2.6). The peak at that 250 nm region may be attributed to π→π* transition while the other one is for ligand to metal charge transfer transition (LMCT). The emission spectral measurement (λ_{ex}=320 nm) showed for the both ligand and compound are emissive

(Figure 2.7). The intensity of $[Cd(abb)H_2O]_n$ (**1**) was observed quite higher than the ligand itself and it may be due to the complexation of the free ligand anions. Two broad emission peaks found at around 408 and 469 nm region in **1** which is shifted towards shorter wavelength region (blue shift) upon complex formation with linker H_2abb. Shifting of the emission peak in metal complex in comparison to free ligand is probably due to the deprotonation of ligand in compound **1** and ligand to ligand charge transitions (LLCT) [21-23].
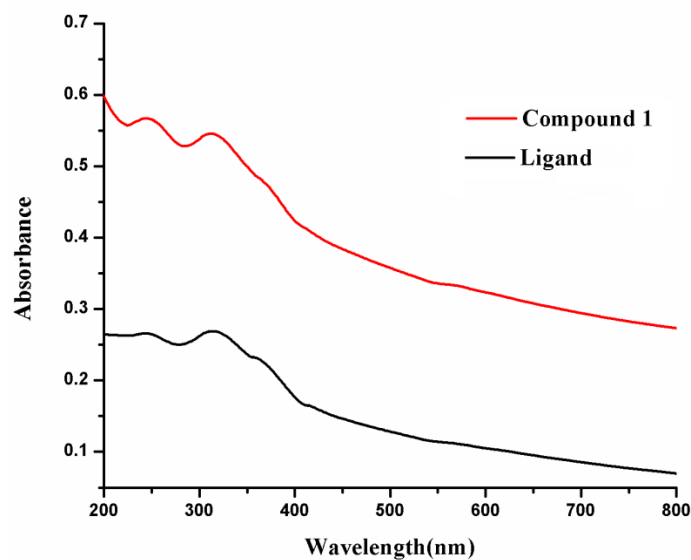
Figure 2.6. Solid-state UV-Vis absorption spectra of the ligand and compound 1
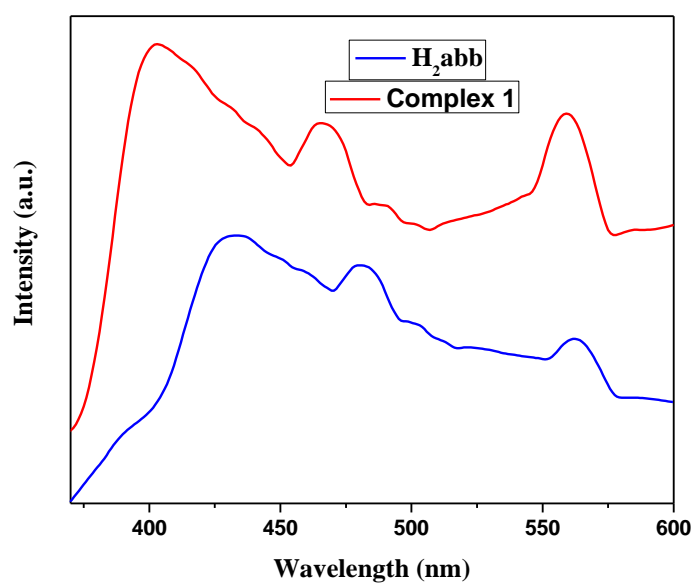
Figure 2.7. Solid-state emission spectra of the ligand and compound 1 (excitation at 320 nm)

2.3.3 Thermogravimetric analysis

The thermogravimetric analysis showed that upon heating compound **1** loses coordinated water molecule in the temperature range 90-170 °C (Figure 2.8). The observed weight loss of ~3.9% (theoretical 4.0%) corresponds to one molecule of water per formula unit. Due to the hydrogen bonding in the crystal packing, complete loss of the water molecule happened at higher temperature. The next sharp step is due to the decomposition of ligand. The observed weight loss ~58.4% (theoretical 63.3%) indicated more or less all the ligands are lost from the compound and only the cadmium oxide was left.
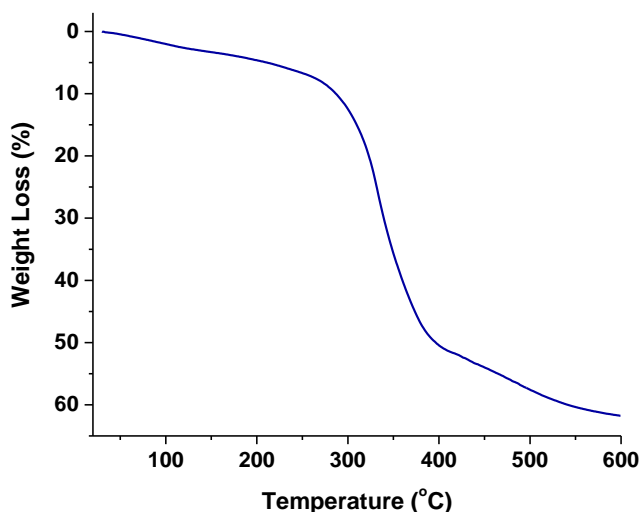
Figure 2.8. Thermogravimetric plot of compound 1

2.3.4 Gas adsorption study

Removal of CO_2 from sources of anthropogenic emission is currently a top priority, because CO_2 emission is closely associated with climate change. Due to lack of high internal surface area 2D MOFs are generally not capable of absorbing CO_2. Nevertheless, there are some reports that 2D MOFs can accommodate CO_2 molecules [7, 24].

Gas sorption measurements of the compound **1** were undertaken to verify the capability of 2D compound to adsorb small molecule of gasses like N_2, H_2, and CO_2. Before the sorption experiments, the samples were out-gassed at the desired temperature (90 °C) for 3 h under high vacuum (10^{-3} Torr). Surface area of **1** was measured by N_2 sorption at 77 K (Figure 2.9a), and the Brunauer-Emmett-Teller (BET) surface area is measured to be 47 m^2g^{-1} (Langmuir surface areas of 157 m^2g^{-1}) for **1**. The pore diameter was calculated by NLDFT method and half pore width value (22.7 Å) obtained for the

compound is very high (Figure 2.9b). Such type of materials containing low surface area and pore diameter close to 4.5 nm is comparable to nanomaterials [25, 26].
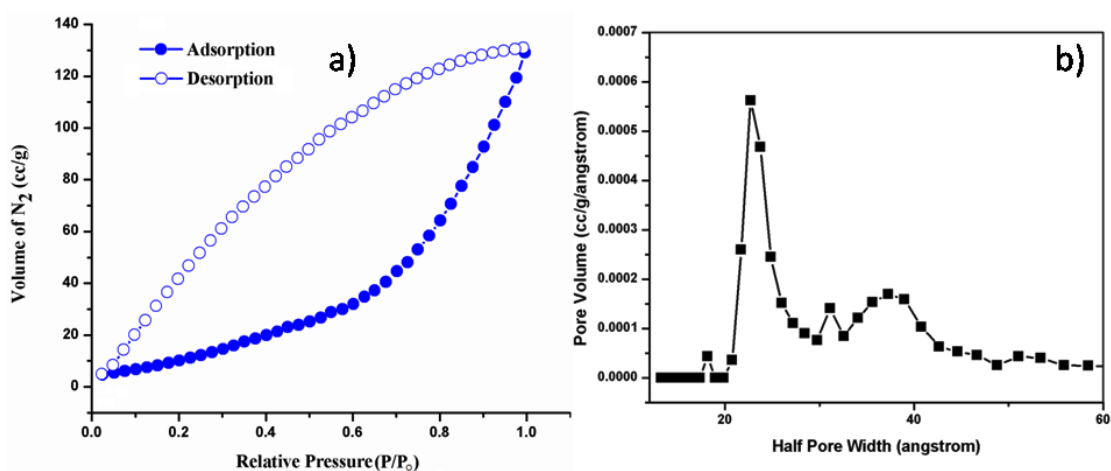
Figure 2.9. a) N$_2$ sorption isotherm at 77K and b) pore size distribution using NLDFT method

The hydrogen uptake of **1** reached about 0.99 wt.% or 111 cc g^{-1} at the adsorbate pressure of 1 bar at 77 K (Figure 2.10a), which is much higher than our previously reported Mg-based 2D MOF system [6].
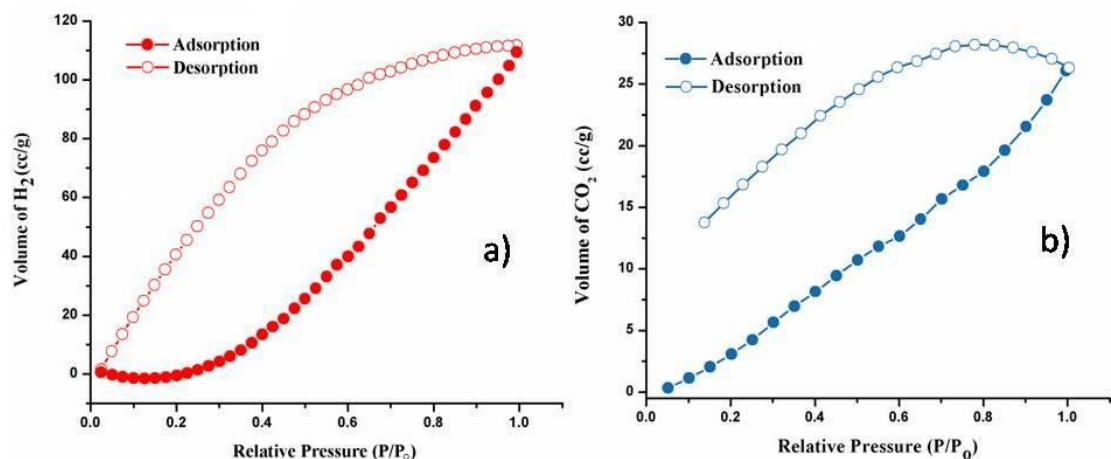
Figure 2.10. a) H$_2$ sorption isotherm at 77 K and b) CO$_2$ sorption isotherm at 298 K
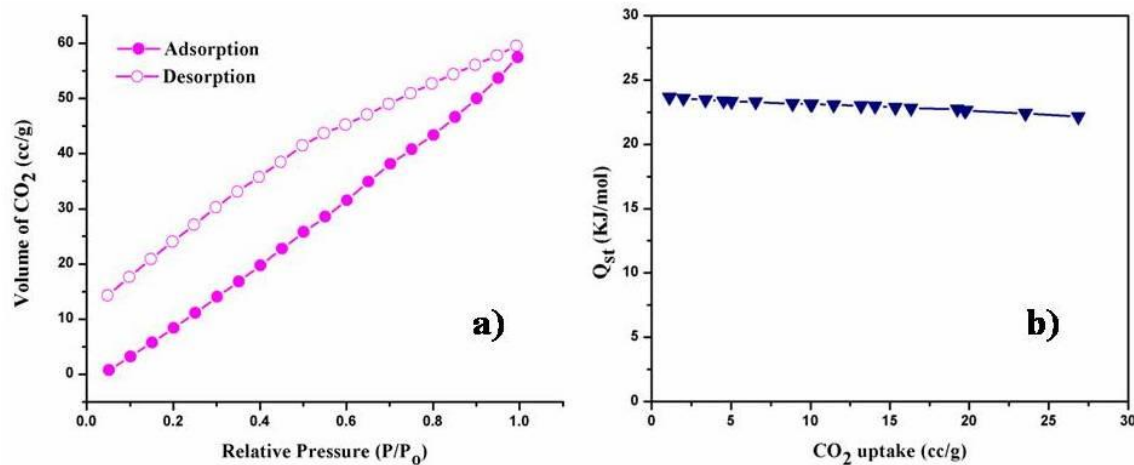
Figure 2.11. a) CO_2 sorption isotherm at 273K and b) heats of adsorption from CO_2 uptake

At 298 K, **1** showed CO_2 uptake of about 5.21 wt.% or 26.5 cc g^{-1} at 1 bar pressure (Figure 2.10b). At 273 K, it also showed CO_2 uptake of 10.36 wt.% or 58 cc g^{-1} at 1 bar pressure (Figure 2.11a), which is almost two times of CO_2 uptakes at 298 K. The compound exhibited type III isotherms (according to the IUPAC nomenclature) and a good hysteresis for all gases. The presence of hysteresis in the adsorption-desorption isotherm may be due to the strong interaction of gas molecules with the open metal sites. Particularly considering H_2 sorption, compound **1** unprecedentedly exhibited the highest gas uptake at 77 K amongst the two-dimensional MOFs. The heats of adsorption (Q_{st}) were calculated using by Clausius-Clapeyron equation [27] of CO_2 gas adsorption between two different temperatures at 273 and 298K. Compound **1** showed $Q_{st}(-\Delta H)$ value of about 24.1 kJ mole^{-1} (Figure 2.11b) which is comparable to other 2D microporous MOFs. This may be due to the presence of well decorated azo (– N=N–) functional group [28, 29] in compound **1** and may be also the reason to highest CO_2 gas uptake in this compound compare to other 2D Cd-based MOFs reported previously [6-11]. Table 2.4 displayed the comparison of uptake of different gases by compound **1** with the other reported two-dimensional MOFs.

In a previous study 2D layered MOF [Cu(BF$_4$)$_2$(bpy)$_2$] (bpy = 4,4′-bipyridine) showed expansion/shrinkage structural transformation through CO_2 gate adsorption/desorption at 273K because of weak interlayer interactions [24]. Further, a flexible 1D MOF [Cu(BF$_4$)$_2$(bpp)$_2$] (bpp = 1,3-bis(4-pyridyl)propane) also displayed expansion/shrinkage structural conversion to adsorb gas molecules [30]. However, there was no noticeable crystallographic void space in both the cases. A similar kind of mechanism may be operative in case of [Cd(abb)H$_2$O]$_n$ (**1**).

Table 2.4. Comparison gas uptake capacity of various 2D-MOFs

MOFs	Surface area from N_2 adsorption [$m^2\ g^{-1}$]		H_2 uptake [$cc\ g^{-1}$] at 1 bar at 77K	CO_2 uptake [$cc\ g^{-1}$] at 1 bar		Ref.
	Langmuir	BET		at 273k	at 298K	
Compound **1**	157	47	111	53	26.5	this study
$C_{16}H_{16}N_4O_5Zn$	–	–	14.3	26	14.5	[7]
$C_{32.3}H_{29.45}N_{9.15}O_{10}Zn_2$	–	–	6.5	53	39	[7]
$C_{41.5}H_{44.5}N_{9.5}O_{12.5}Zn_2$	–	–	56	69	43	[7]
$\{[Mg_2(HL)_2(H_2O)_4](H_2O)\}_n$		–	63	8	–	[6]
$C_{46}H_{38}CdN_8O_{10}$		–	–	49.5	–	[11]
$C_{46}H_{38}Br_2CdN_6O_4$	–	–	–	40	–	[11]
$C_{46}H_{44}Cd_2F_{12}N_4O_{12}$	–	–	26	–	–	[10]
$C_{21}H_{19}Ni_{0.5}O_7$	_	391	–	–	29	[8]
$[Zn_2(CN_5H_2)_3(H_2O)_3].6H_2O$	433	341	–	56	–	[9]

2.4 Conclusion

In summary, a two-dimensional Cd(II)-based MOF, $[Cd(abb)H_2O]_n$ was prepared by hydrothermal treatment of $Cd(NO_3)_2·4H_2O$ and H_2abb at 140 °C. Single crystal X-ray structural analysis established the hepta-coordinated pentagonal bipyramid Cd(II) center is quite unusual among the plethora of all cadmium containing coordination polymers. Carboxylate ligands have two different types of coordination modes (bridging and chelating) in the compound. Obviously, the water and temperature played an important role in the formation of these cadmium(II) coordination polymers. The supramolecular structure which is formed through H-bonding gives the framework additional space and flexibility to accommodate small gaseous molecules. Compound **1** exhibited unprecedented high uptake of H_2 amongst the two-dimensional MOFs which is expected to attract a lot of interest in this field.

2.5 References

[1]   Z.-F. Chen, Z.-L. Zhang, Y.-H. Tan, Y.-Z. Tang, H.-K. Fun, Z.-Y. Zhou, B. F. Abrahams, H. Liang, CrystEngComm 2008, **10**, 217.

[2]   L.-L. Liu, F. Zhao, ActaCryst. C 2013, **69**, 29.

[3]   L. Zhang, C.-Y. Jing, Y.-Q. Zhong, Q.-H. Meng, K.-L. Zhang, J. Coord. Chem. 2015, **68**, 3954.

[4]   L.-L. Liu, L. Liu, J.-J. Wang, Inorg. Chim. Acta 2013, **397**, 75.

[5]   Z.-F. Chen, R.-G. Xiong, B. F. Abrahams, X.-Z. You, C.-M. Che, J. Chem. Soc., Dalton Trans. 2001, 2453.

[6]   D. Saha, T. Maity, S. Das, S. Koner, Dalton Trans. 2013, **42**, 13912.

[7]   L.-W. Lee, T.-T. Luo, S.-H. Lo, G.-H. Lee, S.-M. Peng, Y.-H. Liu, S.-L. Lee, K.-L. Lu, CrystEngComm 2015, **17**, 6320.

[8]   J. R. Karra, Y.-G. Huang, K. S. Walton, Cryst. Growth Des. 2013, **13**, 1075.

[9]   Q. Yan, Y. Lin, P. Wu, L. Zhao, L. Cao, L. Peng, C. Kong, L. Chen, ChemPlusChem 2013, **78**, 86.

[10]   W. Yang, X. Lin, A. J. Blake, C. Wilson, P. Hubberstey, N. R. Champness, M. Schroder, Inorg. Chem. 2009, **48**, 11067.

[11]   U. P. Singh, S. Narang, P. Pachfule, R. Banerjee, CrystEngComm 2014, **16**, 5012.

[12]   E. B. Reid, E. C. Pritchett, J. Org. Chem. 1953, **18**, 715.

[13]   SAINT, version 6.02; SADABS, version 2.03; Bruker AXS, Inc.: Madison, WI, 2002.

[14]   Sheldrick, G.M. SHELXS97, Program for Structure Solution, University of Göttingen, Germany, 1997.

[15]   Sheldrick, G.M. SHELXL97, Program for Crystal Structure Refinement, University of Göttingen, Germany, 1997.

[16]   A. L. Spek, PLATON, Molecular Geometry Program, J. Appl. Crystallogr.2003, **36,** 7.

[17]   L. J. Farrugia, J. Appl. Crystallogr. 1997, **30**, 565.

[18]   L. J. Farrugia, J. Appl. Crystallogr. 1999, **32**, 837.

[19]   M. J. Plater, M. R. St. J. Foreman, T. Gelbrich, S. J. Coles, M. B. Hursthouse, J. Chem. Soc., Dalton Trans. 2000, 3065.

[20]   S. Banerjee, M. G. B. Drew, A. Ghosh, Polyhedron 2003, **22**, 2933.

[21]   T. Maity, D. Saha, S. Das, S. Koner, Eur. J. Inorg. Chem. 2012, 4914.

[22]   Z.-Q. Shi, Z.-J. Guo, H. G. Zheng, Chem. Commun. 2015, **51**, 8300.

[23]   Y.-N. Gong, Y.-R. Xie, D.-C. Zhong, Z.-Y. Du, T.-B. Lu, Cryst. Growth Des. 2015, **15**, 3119.

[24]   A. Kondo, H. Noguchi, S. Ohnishi, H. Kajiro, A. Tohdoh, Y. Hattori, W.-C. Xu, H. Tanaka, H.

Kanoh, K. Kaneko, Nano Lett. 2006, **6**, 2581.

[25]   A. M. Pourrahimi, D. Liu, V. Ström, M. S. Hedenqvist, R. T. Olssona, U. W. Gedde, J. Mater. Chem. A, 2015, **3**, 17190.

[26]   V. I. Markoulaki, I. T. Papadas, I. Kornarakis, G. S. Armatas, Nanomaterials 2015, **5,** 1971.

[27]   J. L. C. Rowsell, O. M. Yaghi, J. Am. Chem. Soc. 2006, **128,** 1304.

[28]   P. Kanoo, A. C. Ghosh, S. T. Cyriac, T. K. Maji, Chem. -Eur. J. 2012, **18**, 237.

[29]   N. Sikdar, A. Hazra, T. K. Maji, Inorg. Chem. 2014, **53**, 5993.

[30]   T. Suzuki, R. Kotani, A. Kondo, K. Maeda, J. Phys. Chem. C 2016, **120**, 21571.

Chapter 3
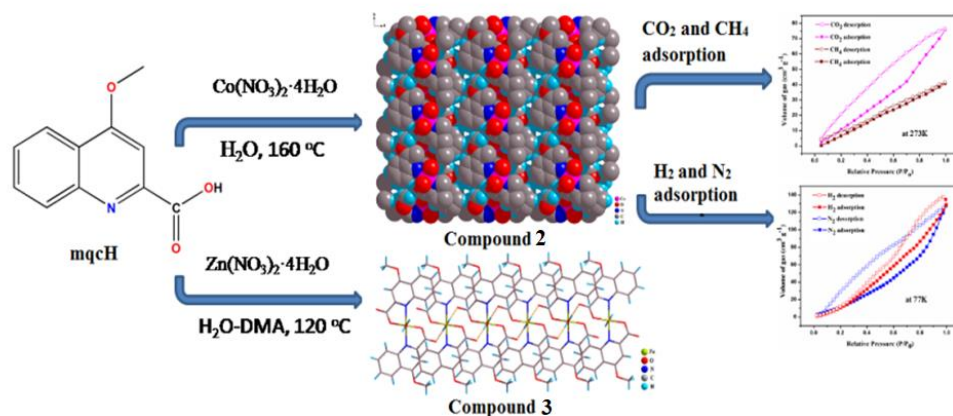
Figures shown: chemical structure labeled **mqcH**; reaction with **Co(NO$_3$)$_2$·4H$_2$O**, **H$_2$O, 160 °C** yielding **Compound 2**; reaction with **Zn(NO$_3$)$_2$·4H$_2$O**, **H$_2$O-DMA, 120 °C** yielding **Compound 3**; **CO$_2$ and CH$_4$ adsorption** and **H$_2$ and N$_2$ adsorption** plots.

Monomeric and polymeric metal carboxylates: synthesis, crystal structure and gas adsorption study over a 2D layered framework

3.1 Introduction

The attraction of MOFs is not only confined in the field of crystal engineering and molecular topologies but also covers a broad area of research due to their numerous applications in photoluminescence, magnetism, drug delivery, gas adsorption and storage etc. The coordination polymers or MOFs can be obtained as a crystalline solid, however, topology of these solids depends on the ligands and coordination geometry of metal ions. Additionally, the overall structural framework of coordination polymer can be influenced by some external stimuli like pH, temperature, pressure and also solvent of the reaction medium. All these issues have been discussed in Chapter 1. In this study, cobalt and zinc metal containing compounds have been synthesized using a prospective linker, 4-methoxy-2-quinolinecarboxylate (mqc). Till date this linker has been employed scarcely in designing of MOFs [1]. Ravi Shankar *et al.* reported two organometallic Sn(II) compounds using di-n-butyltin and 4-methoxy 2-quinolinecarboxylic acid which were isolated from acetonitrile/dichloromethane solvent [1a, 1b]. Oxorhenium(V) complexes using 4-methoxy-2-quinolinecarboxylate ligand have been successfully synthesized [1c]. *p*-Tolylimido rhenium(V) compounds containing mqc ligand have also been reported [1d]. Nevertheless, literature survey showed there was no previous report of complex of 3d metal ions containing 4-methoxy-2-quinolinecarboxylate ligand. Various metal binding coordination modes of mqc linker have shown in Scheme 3.1.

In the course of continuing investigation on uses of MOFs in gas adsorption and separation, two 4-methoxy-2-quinolinecarboxylate compounds $[Co(mqc)_2]_n$ **(2)** and $[Zn(mqc)_2(H_2O)]$ **(3)** are synthesized. The structure of both the compounds has been solved through X-ray single crystal analysis. It was revealed that structurally compounds **2** and **3** are strikingly different. While compound **2** features a 2D layered framework structure **3** is a discrete monomer. Compound **2** showed potential in sorption of H_2 and CO_2 gases.
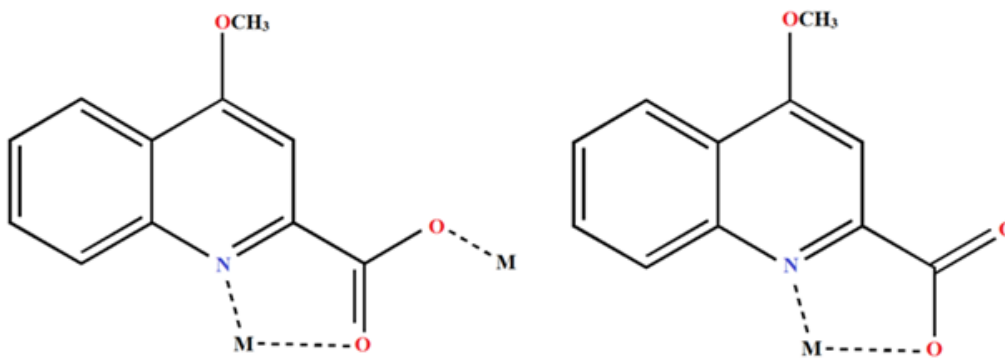
Scheme 3.1. Different coordination modes of mqc linker

3.2 Experimental

3.2.1 Materials

4-Methoxy-2-quinoline-carboxylicacid, 4,4′-bipyridine and 1,2-di(4-pyridyl)ethylene were purchased from Sigma-Aldrich. Cobalt nitrate hexahydrate $Co(NO_3)_2 \cdot 6H_2O$, Zinc nitrate hexahydrate $Zn(NO_3)_2 \cdot 6H_2O$ and N,N-dimethylacetamide (DMA) were purchased from Merck India. All the reagents were used without further purification.

3.2.2 Synthesis of [Co(mqc)₂]ₙ (2) and [Zn(mqc)₂(H₂O)] (3)

Synthesis of [Co(mqc)₂]ₙ (2)

[Co(mqc)₂]ₙ **(2)** was synthesized through hydrothermal route. The initial reaction mixture was prepared by mixing $Co(NO_3)_2 \cdot 6H_2O$ (0.073 g, 0.25 mmol), mqcH (0.05 g, 0.25 mmol) and 4,4′-bipyridine (0.039 g, 0.25 mmol) in 3-4 ml of water. Then it has been taken in a 20 ml of teflon-lined Parr acid digestion bomb. The compound was obtained as orange-colored crystals in a teflon-lined Parr acid digestion bomb, at 160 ºC for 3 days followed by slow cooling at the rate of 5 ºC/h to room temperature. As the crystal structure doesn't contain 4,4′-bipyridine moieties, therefore it performed only as a weak base in the reaction.

Yield *ca*. 0.062 g, 62% based on the metal.

Anal. for $C_{22}H_{16}N_2O_6Co$ in %: C, 57.03; H, 3.48; N, 6.05. Found: C, 56.86; H, 3.5; N 6.1. IR (KBr): $v(COO^-)$ = 1570 cm^{-1} and 1362 cm^{-1}, $v(O\text{-}CH_3)$ = 3015 cm^{-1} (Figure 3.1a).

Synthesis of [Zn(mqc)₂(H₂O)] (3)

Zn based monomer, [Zn(mqc)₂(H₂O)] **(3)** has been also prepared by solvothermal synthesis. First, $Zn(NO_3)_2 \cdot 6H_2O$ (0.074 g, 0.25 mmol), ligand mqcH (0.05 g, 0.25 mmol) and 1,2-di(4-pyridyl)ethylene (0.045 g, 0.25 mmol) were mixed well in 3-4 ml of DMA-H_2O (1:1) and then it has been taken in a 20ml of teflon-lined Parr acid digestion bomb. The white-colored block crystalline product obtained by heating at 120 ºC temperature for 3 days followed by slow cooling to room temperature at 5 ºC/h rate. No crystal were found while using of 4,4′-bipyridine in place of 1,2-di(4-pyridyl)ethylene in H_2O even also in DMA-H_2O (1:1) medium.

Yield *ca*. 0.084 g, 84% based on the metal.

Anal. for $C_{22}H_{18}N_2O_7Zn$ in %: C, 54.17; H, 3.72; N, 5.74. Found: C, 54.3; H, 3.63; N 5.71. IR (KBr): $v(COO^-)$ = 1564 cm^{-1} and 1382 cm^{-1}, $v(O\text{-}CH_3)$ = 3045 cm^{-1} (Figures 3.1b, 3.1c).
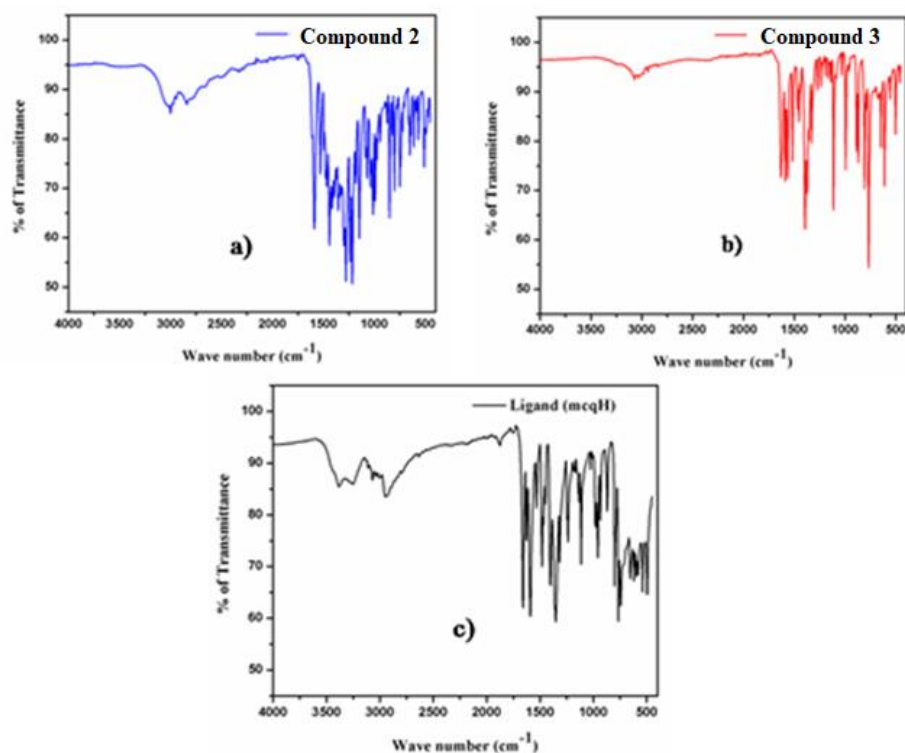
Figure 3.1. FT-IR spectra of a) compound 2, b) compound 3 and c) free ligand (mcqH).

3.2.3 Physical measurements

All the physical measurements were performed by using the same instruments already discussed in **Section 2.2.3, Chapter 2.**

3.2.4 X-ray crystallography

The X-ray diffraction data for **2** and **3** were collected at 273(2) and 296(2) K respectively, with a Bruker SMART APEX CCD X-ray diffractometer. Cell refinement and integrated intensities were determined by using SAINT software package with a narrow-frame integration algorithm [2]. The structures were solved by direct methods and refined by full-matrix least-squares technique against F2 with anisotropic displacement parameters for non-hydrogen atoms with the programs SHELXS97 and SHELXL97 [3]. An empirical absorption correction was carried out by SADABS [2]. The hydrogen atoms of compounds **2** and **3** were refined with isotropic thermal parameters. Hydrogen atoms of coordinated water molecule in compound **3** were placed at calculated positions with suitable riding models with isotropic displacement parameters derived from their carrier oxygen atom. In the final difference of Fourier map there were no remarkable peaks except the ghost peaks surrounding the metal

centers. All the other calculations were done by PLATON 99 [4], ORTEP-32 [5] and WinGX system version 1.64 [6]. All crystallographic data for two compounds are given in Table 3.1.

CCDC 1569623 and 1569622 contain the supplementary crystallographic data for compound **2** and **3** respectively. These data can be obtained free of charge via http:// www.ccdc.cam.ac.uk/conts/retrieving.html, or from the Cambridge Crystallographic Data Centre, 12 Union Road, Cambridge CB2 1EZ, UK; fax: +44 1223 336 033; or e-mail: deposit@ccdc.cam.ac.uk.

Table 3.1. Crystallographic data and structural refinement of compound 2 and 3

Compound	2	3
Mol. Formula	$C_{22}H_{16}CoN_2O_6$	$C_{22}H_{18}ZnN_2O_7$
Formula wt.	463.30	487.77
Space group	P21/c	C2/c
Crystal system	Monoclinic	Monoclinic
a / Å	12.9899(7)	16.9495(7)
b / Å	9.5945(5)	13.7167(4)
c / Å	7.1262(4)	9.5218(4)
α / deg	90	90
β / deg	94.850(4)	115.391(3)
γ / deg	90	90
V / Å^3	884.97(8)	1999.89(14)
Z	2	4
d_{cal} (g.cm^{-3})	1.739	1.620
μ (mm^{-1})	1.019	1.278
R_{int}	0.071	0.065
No. of unique data	1412	2230
Data with I > 2σ(I)	985	1670
R1 on I>2σ(I)	0.0467	0.0461
wR2 on I>2σ(I)	0.0949	0.1318
GOF on F^2	1.012	0.920
F(000)	474	1000

$$R_1 = \sum |(|F_o| - |F_c|)| / \sum |F_o|, \ wR_2 = \{ \sum [w (F_o^2 - F_c^2)^2] / \sum [w (F_o^2)^2] \}^{1/2}$$

3.3 Results and discussion

3.3.1 Crystal structure of compounds 2 and 3

Crystal structure of [Co(mqc)$_2$]$_n$ (2)

Single-crystal-X-ray crystallographic study revealed that compound **2** crystallizes in a monoclinic space group *P2$_1$/c* with *Z* = 2 (Table 3.1). There is only one type of ligand arrangement found to be surrounding the Co atoms (Co1) in compound **2**. Co1 center is arranged with six coordination sites, two axial O atoms (O3 and O3^b), two equatorial oxygen atoms (O2 and O2^b) and two equatorial N atoms N1 and N1^b (symmetry operation: a = 1-*x*, 1/2+*y*, 5/2-*z*, b = 1-*x*, 1-*y*, 2-*z* and c = *x*, 3/2-*y*, -1/2+*z*). The minimum and maximum bond-distances of Co1-O2 and Co1-O3 are 2.077(3) and 2.132(3) Å respectively. The distance of Co-N1 bond is 2.164(4) Å. In compound **2**, mqc acts as tridentate chelating ligand. In each mqc linker, both oxygen atoms of carboxylate group (O2 and O3) and one nitrogen N1 involve in metal coordination where O2 and N1 form chelate with metal center (Figure 3.2a). Two adjacent Co1 atoms are connected by $\mu_{1,3}$-*syn-anti* bridging carboxylato oxygen atom (O3) of mqc linker (Figure 3.2a). Each Co1 center is linked by four mqc ligands, two from axial and two from equatorial sites formed a distorted octahedral geometry (Figure 3.2b). Four Co1 centers again arrange to form a square shaped linkage (Figure 3.2c). Each square-shaped linkage further connected with each other to form a two-dimensional network along crystallographic *ac*-plane (Figure 3.2d). Asymmetric unit of compound **2** with atom numbering scheme has been shown by ORTEP diagram (Figure 3.2e). 2D sheets are also connected each other by weak van der Walls force of attraction and finally formed a 3D supramolecular porous framework having void space parallel to crystallographic *c*-axis in between each 2D layer. The crystallographic data and structural refinement are given in Table 3.1. Bond-length and bond-angle values are summarized in Table 3.2.

Topological analysis displayed that the compound **2** have a simple uninodal 2D net structure with Schläfli symbol {4^4.6^2} consisting of cobalt center as four-coordinated node (Figure 3.2f) [7].

Crystal structure of [Zn(mqc)$_2$(H$_2$O)] (3)

Single crystal XRD study made known that compound **3** crystallizes in a monoclinic space group *C2/c* with *Z* value 4. The structure of compound **3** is basically monomer which is further extended to one-dimensional structure by a strong intermolecular hydrogen-bonding [8]. The Zn1 metal center is coordinated in square pyramidal geometry. In compound **3,** mqc acts as bidentate chelating ligand bonded with Zn1 atom through one carboxylato oxygen atom O2 and N1 atom (Figure 3.3a). Metal center is

penta-coordinated with one axial oxygen atom, O4, of water molecule, two equatorial N atoms (N1 and N1^a) and two equatorial carboxylato O atoms (O2 and O2^a) of two mqc ligand (symmetry operation: a = -*x*, *y*, 3/2-*z*, b = -*x*, *y*, 1/2-*z* and c = -*x*, -*y*, 1-*z*) having bond-distance range from 1.966(3) to 2.203(3) Å (Figure 3.3b). There is a strong intermolecular hydrogen-bonding (O4-H1O4···O1) occurred in between hydrogen atoms of coordinated water molecule and carboxylato oxygen atom O1 (Table 3.3). Such a strong hydrogen-bonded interaction gives rise to the formation of a one-dimensional chain-like structure (Figure 3.3c) parallel to crystallographic *c*-axis. Asymmetric unit of compound **3** with atom numbering scheme is shown in ORTEP diagram (Figure 3.3d). The crystallographic data and bond-parameters are described in Table 3.1 and Table 3.2, respectively.

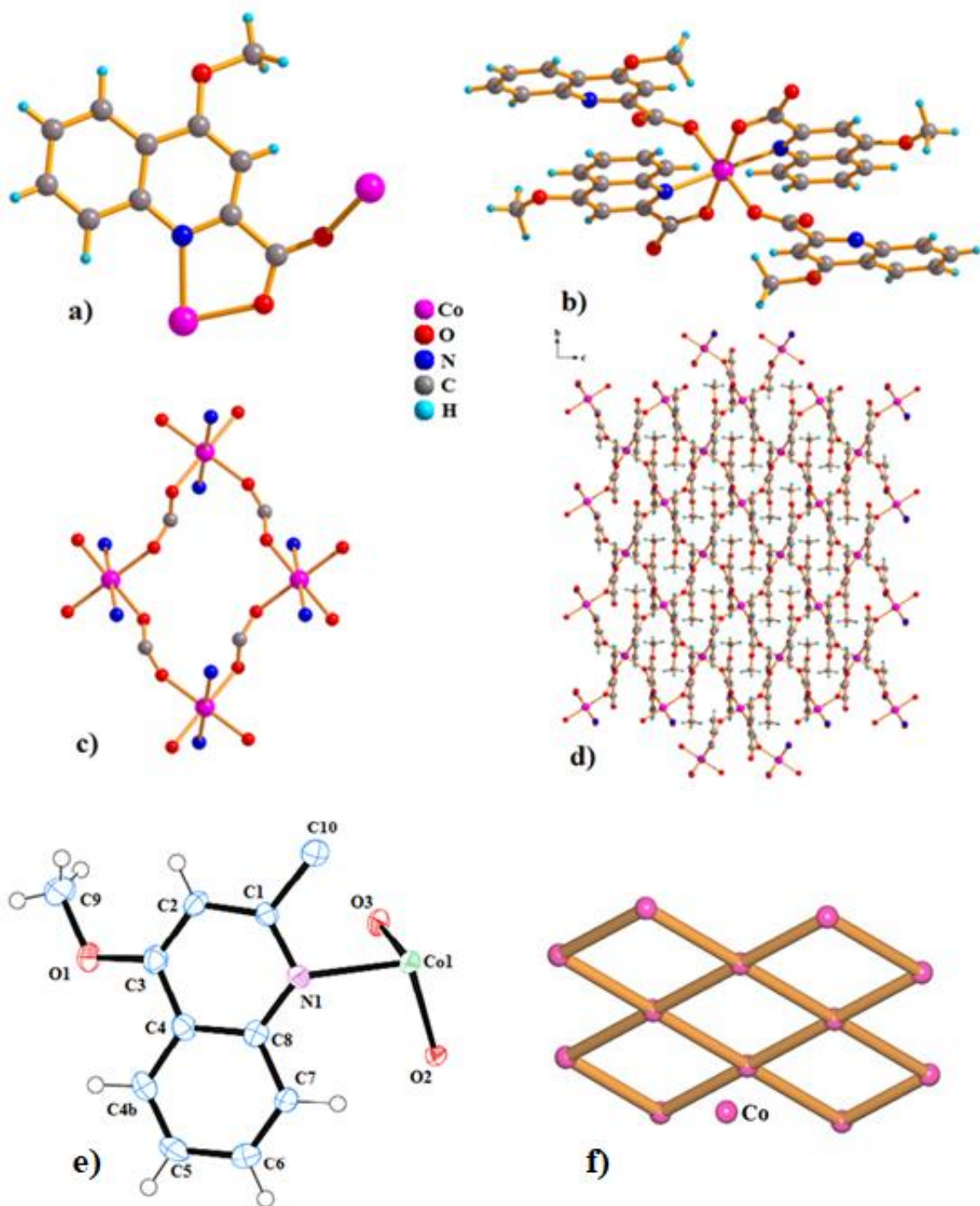**Figure 3.2. Different coordination motif in compound 2, a) ligand coordination; b) metal coordination; c) square shaped connecting unit; d) 2D network; e) ORTEP diagram of 2; f) topological view of compound 2.**
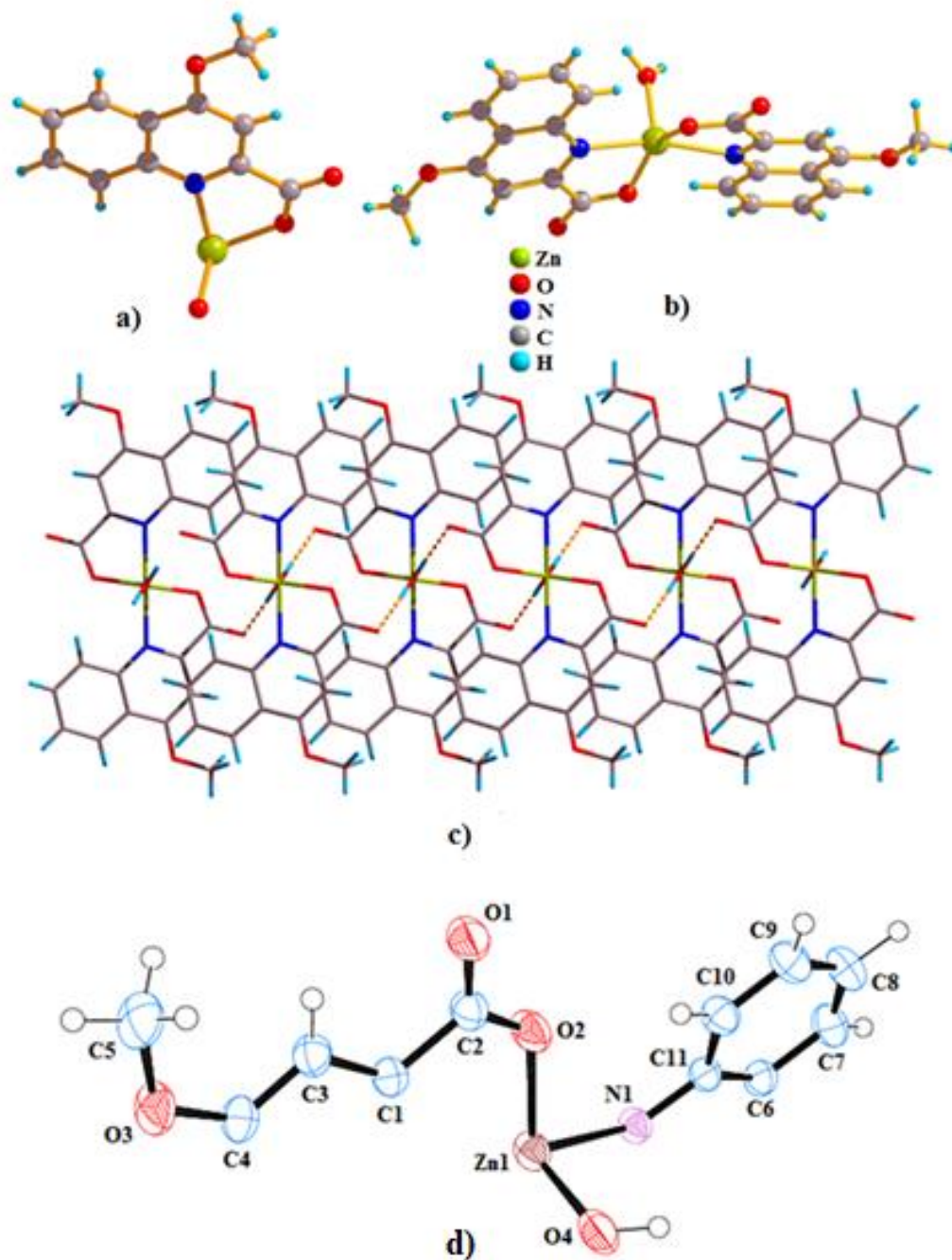
Figure 3.3.a) Asymmetric unit of compound 3, b) metal coordination of Zn(II) center in 3, c) hydrogen bonded (dotted orange lines) 1D-structure of compound 3 along to *c*-axis, d) ORTEP diagram of 3.

Table 3.2. Bond-parameters of compound 2 and 3

Bond-length (Å) of compound 2		Bond-length (Å) of compound 3	
Co1 – O2	2.077(3)	Zn1–O2	1.966(3)
Co1 – O3	2.132(3)	Zn1–O4	1.988(4)
Co1 – N1	2.163(3)	Zn1–N1	2.203(3)
Co1 – O2^b	2.077(3)	Zn1–O2^a	1.966(3)
Co1 – O3^b	2.132(3)	Zn1–N1^a	2.203(3)
Co1 – N1^b	2.163(3)		
Bond-angles (degree) of compound 2		**Bond-angles (degree) of compound 3**	
O2- Co1- O3	93.73(11)	O2 - Zn1 - O4	107.42(8)
O2- Co1- N1	102.75(2)	O2 - Zn1 - N1	95.86(11)
O2- Co1- O2^b	180.00	O2 - Zn1 - O2^a	145.17(12)
O2- Co1- O3^b	86.27(11)	O2 - Zn1 - N1^a	79.04(11)
O2- Co1- N1^b	77.25(11)	O4 - Zn1 - N1	98.46(7)
O3- Co1- N1	88.70(11)	O2^a - Zn1 - O4	107.42(8)
O2^b- Co1- O3	86.27(11)	O4 - Zn1 - N1^a	98.46(7)
O3- Co1- O3^b	180.00	O2^a - Zn1 - N1	79.04(11)
O3- Co1- N1^b	91.30(11)	N1 - Zn1 - N1^a	163.07(10)
O2^b- Co1- N1	77.25(11)	O2^a - Zn - N1^a	95.86(11)
O3^b- Co1- N1	91.30 (11)		
N1- Co1- N1^b	180.00		
O2^b- Co1- O3^b	93.73(11)		
O2^b- Co1- N1^b	102.75(11)		
O3^b- Co1- N1^b	88.70(11)		

Symmetry operation a = 1-*x*, 1/2+*y*, 5/2-*z*, b = 1-*x*, 1-*y*, 2-*z* and c = *x*, 3/2-*y*, -1/2+*z* for compound **2.**

Symmetry operation a = -*x*, *y*, 3/2-*z*, b = -*x*, *y*, 1/2-*z* and c = -*x*, -*y*, 1-*z* for compound **3.**

Table 3.3. Hydrogen bonding parameters of compound 3

D-H⋯A	D-H (Å)	H⋯A (Å)	D⋯A(Å)	∠D-H⋯A (°)	Symmetry
O4-H1O4⋯O1	0.91(4)	1.80(5)	2.71(4)	177(6)	-*x*,-*y*,1-*z*

3.3.2 PXRD study

Powder X-ray diffraction (PXRD) study of compound **2** evidently revealed the phase purity of bulk materials. Experimental and simulated PXRD patterns of compound **2** are well-matched that point out the rational phase purity of **2**. PXRD of compound **2** was performed after out-gassed at 80°C for 2 h and the well-matched PXRD pattern revealed that the structural integrity remains unaltered after out-gassed procedure. Structural framework of compound **2** after gas adsorption is also remained unchanged (Figure 3.4a). Powder X-ray diffraction study also displayed the phase purity of compound **3** by well matching simulated and experimental patterns (Figure 3.4b).
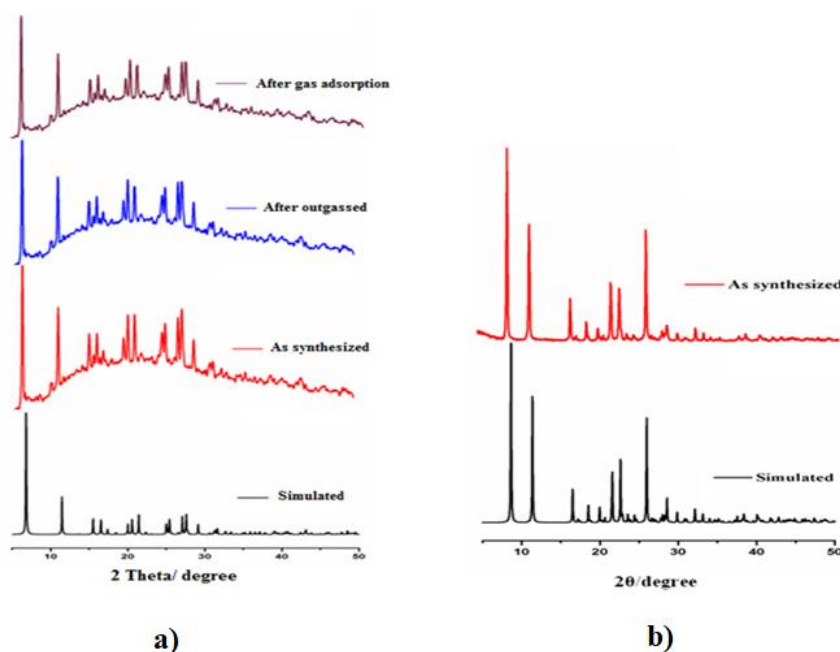
Figure 3.4. Power-X-ray-diffraction patterns of a) compound 2, b) compound 3

3.3.3 Thermogravimetric analysis

Thermogravimetric analysis (TGA) was carried out under nitrogen atmosphere in the temperature range 30-800 °C. From the thermogram, it is clear that there is no significant weight loss occurred in compound **2** up to a temperature of ~360°C. A slight weight loss was observed initially in the TGA curve, it may be due to loss of some absorbed water molecules. Then a sharp loss was observed from 360 °C due to the decomposition of the compound. One small endothermic peak at about 400 °C of corresponding DTA curve also revealed the decomposition of compound **2** (Figure 3.5a).

In case of compound **3**, first weight loss occurred due to removal of one coordinated water molecule in the temperature range 110-237°C. The observed weight loss in this range is ~3.68% (theoretical 3.7%) and then a sharp weight loss was observed after 237 °C, due to decomposition of compound **3** indicating that the metal-organic framework of compound **3** is stable thermally up to 237 °C (Figure 3.5b).
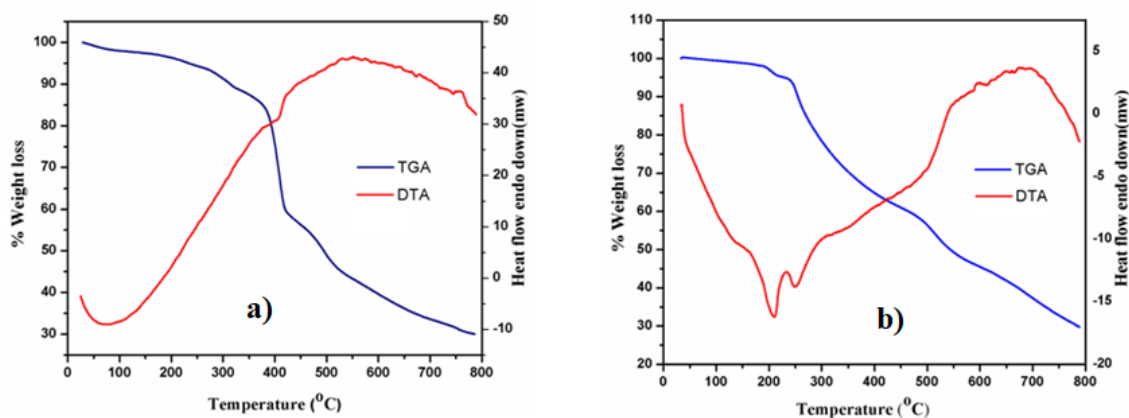
Figure 3.5. TG-DTA curve of a) compound 2, b) compound 3

3.3.4 Gas adsorption study of compound 2

N$_2$ sorption measurement is a routine work to measure surface properties of porous materials. Surface properties of compound **2** were measured with respect to adsorption of different small gas molecules. Before the gas sorption experiments, for removing the adsorbed water molecules the samples were degassed under high vacuum (10^{-3} Torr) at the preferred temperature (80 °C) for 2 hr. Brunauer–Emmett–Teller (BET) surface area of compound **2** was calculated to be 74 m^{2}g^{-1} with respect to N$_2$ adsorption isotherm at 77K (Figure 3.6a). Calculation revealed compound **2** showed a moderate nitrogen uptake of ~137 cc/g at 1 bar pressure. NLDFT method is used to calculate the half pore width value acquired for compound **2** on the basis of N$_2$ adsorption and the value is about 14.5 Å (Figure 3.6b). Hydrogen sorption on microporous or mesoporous materials is one of the most important methods which may be used to consideration for vehicle applications [9]. It is well known that the benefit of using hydrogen gas as fuel is mainly due to decrease of air pollution. Compound **2** demonstrated a significant amount of hydrogen uptake, about 135 cc/g (1.22 wt%), at 77K and 1 bar pressure (Figure 3.6a). Comparison of gas adsorption capacity into different 2D microporous MOFs are collated in Table 3.1.

Previously a 2D Cu-based MOF system showed a comparable hydrogen uptake (~1.28 wt%) as shown by compound **2** [10]**.**

Global warming is one of the major worldwide environmental issues developing from emission of greenhouse gases, mostly CO_2. Of different CO_2 capture technologies that have been envisioned so far, chemical adsorption processes are currently thought to be the most effective one for the power plants to post-combustion. Compound **2** showed type III isotherms (according to the IUPAC nomenclature). In the present study compound **2** showed a significant uptake of CO_2 gas at two different temperatures, 298 K and 273 K. The CO_2 uptake capacity was measured to be 78 cc/g (15 wt%) and 38 cc/g (7.5 wt%) at 1 bar pressure at 273 K and 298 K, respectively (Figures 3.6c, 3.6d) which is higher in comparison to many other 2D MOF systems (Table 3.4) [10-18; compound **1**, chapter **2**]. To get deeper insight, isosteric heat of adsorption (Q_{st}) of CO_2 was determined by applying the Clausius-Clapeyron equation at two different temperatures *viz.* 273 K and 298 K [19]. Q_{st}(-ΔH, adsorption enthalpy) value for compound **2** was observed about 21.6 KJ/mole (Figure 3.7a).

Measurement of CH_4 adsorption was carried out at both 298 and 273 K temperatures. Compound **2** adsorbed methane gas 13 cc/g (0.93 wt%) at 298K which increased to 42 cc/g (3 wt%) at 273K (Figures 3.6c, 3.6d). The extent of adsorption of CH_4 was lower than CO_2. This difference in adsorption behavior may be explained in terms of kinetic diameter of CH_4 (3.80 Å) which is larger than that of CO_2 (3.30 Å). Linear structure of CO_2 helps for its easy entering into the void space of compound **2.** Besides, as CO_2 possesses quadrupole moment (-1.4×10^{-35} C m), it can interact with surface of the framework more strongly than CH_4 molecule [20]. Recently Moorthy *et al.* reported 2D MOFs containing triptycene triacid that exhibited selectively high uptake of CO_2 owing to formation of highly porous 2D honeycomb layers [11]. In comparison compound **2** is not highly porous like the above said systems, however, it showed noticeable high uptake of both CO_2 and H_2. Void space available between two 2D sheets hosts the gas molecule (Figure 3.7b). As 2D layers in compound **2** are connected to each other through weak interaction, the interlayer distance can be elongated under pressure leading to high adsorption of small gas molecules.
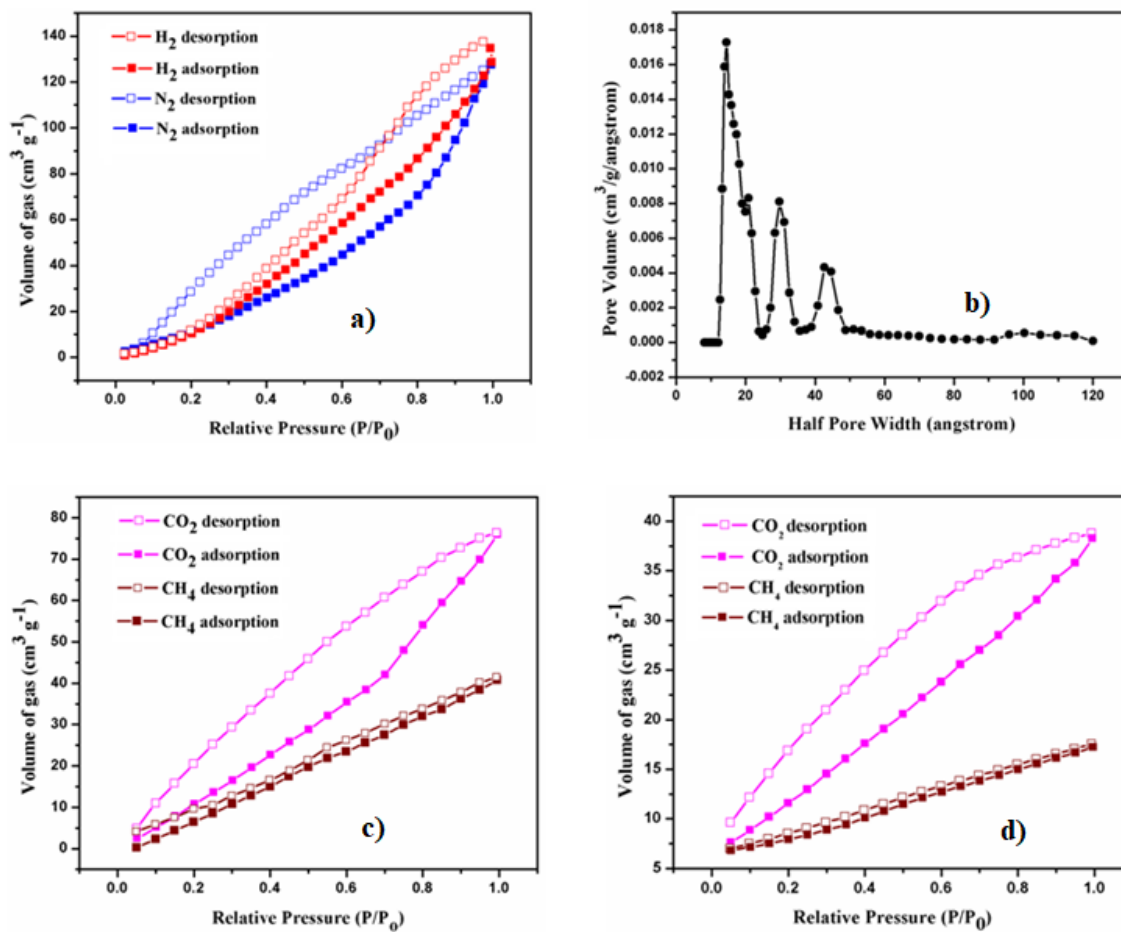
Figure 3.6. a) N$_2$ and H$_2$ sorption isotherm of compound 2 at 77 K; b) Pore size distribution using NLDFT method on basis of N$_2$ sorption; c) CO$_2$ and CH$_4$ sorption isotherm of compound 2 at 273 K; d) CO$_2$ and CH$_4$ sorption isotherm of compound 2 at 298 K.
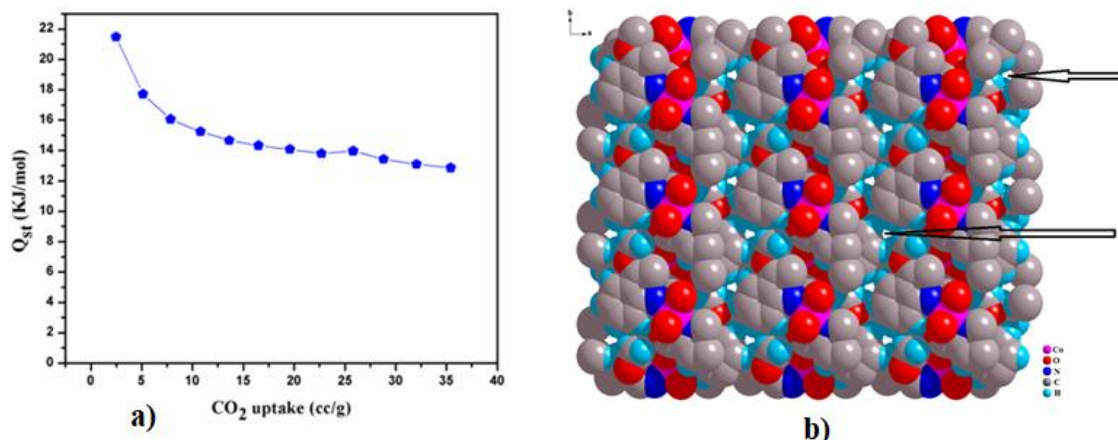
Figure 3.7. a) Isosteric heat of adsorption for CO_2 sorption; b) Void space (arrow marked) in between each 2D sheet of compound 2 along *c*-axis in space fill arrangement.

Combining all effect, partial adsorption selectivity of compound **2** towards CO_2 in comparison to CH_4 cannot be ignored. There have been few previous reports regarding selectivity of CO_2 over CH_4 on two-dimensional metal-organic frameworks which deserve mention [17]. Zhang and Su *et al.* reported a microporous 2D Zn(II)-MOF that adsorbed CO_2 65 cc/gat 273K, which about 6.5 times more than the corresponding CH_4 (10 cc/g) uptake [17a]. Two 2D layered MOF systems which displayed a moderate uptake of CO_2 (38 cc/g and 25 cc/g) at 195 K whereas no significant adsorption of CH_4 was observed by these MOFs [17c]. In this study, compound **2** exhibited uptake of CO_2 is doubled to that of CH_4 at 273K while it is 3 times to that of CH_4 at 298K (w.r.t volume). Besides, the sorption amount of both adsorbates is comparably higher than those of previously reported systems described above. Natural gas mixtures like biogas, natural gas, landfill gas etc. CH_4 often mixed with CO_2, selective adsorption of CO_2 over CH_4 played an important role to remove CO_2 from the mixtures to improve the energy content of this types of mixtures [21].

Table 3.4. Comparison of gas uptake ability of different 2D-microporous MOFs

MOFs	Surface area from N_2 adsorption [$m^2 g^{-1}$]		H_2 uptake [wt %] at 1 bar at 77K	CO_2 uptake [wt %] at 1 bar			Ref.
	Langmuir	BET		195K	273K	298K	
Compound **2**	_	74	1.22	_	15	7.5	this study
$C_{14}H_{10}CdN_2O_5$	157	47	1	_	10	5	Compound **1**, Chapter **2**
$C_{33}H_{30}Cu_2N_4O_{12}$	_	217	1.28	_	_	_	[10]
$C_{16}H_{16}N_4O_5Zn$	_	_	0.13	_	5	2.8	[14]
$C_{32.3}H_{29.45}N_{9.15}O_{10}Zn_2$	_	_	0.06	_	10.4	7.6	[14]
$C_{41.5}H_{44.5}N_{9.5}O_{12.5}Zn_2$	_	_	0.5	_	13.6	8	[14]
$\{[Mg_2(HL)_2(H_2O)_4](H_2O)\}_n$	_	_	0.57	_	1.6	_	[12]
$C_{46}H_{38}CdN_8O_{10}$	_	_	_	_	9.7	_	[13]
$C_{46}H_{38}Br_2CdN_6O_4$	_	_	_	_	8	_	[13]
Co-TPA	_	562	0.12	33	19.9	14	[11]
Mn-TPA	_	402	0.1	40	14	8	[11]
Cd-TPA	_	188	0.1	24	16	11.6	[11]
Zn-TPA	_	246	0.13	25	14	10	[11]
$C_{21}H_{19}Ni_{0.5}O_7$	_	391	_	_	_	6	[15]

$[Zn_2(CN_5H_2)_3(H_2O)_3].6H_2O$	433	341	–	–	11	–	[16]
$C_{54}H_{34}O_{20}Zn_3$	–	–	0.8	–	11.4	4.8	[17a]
$C_{50}H_{52}Cl_2N_{12}O_{20}Zn_3$	–	4.1	–	5	1	–	[17b]
$C_{22}H_{20}O_7N_2S_2Zn$	–	–	–	7.5	–	–	[17c]
$C_{22}H_{22}O_8N_2S_2Co$	–	–	–	5	–	–	[17c]
$C_{51}H_{40}Cd_2N_9O_{15}S_2$	–	–	–	8	3	2	[18]

3.4 Conclusion

Two new coordination compounds have been synthesized through solvothermal treatment of $Co(NO_3)_2 \cdot 6H_2O$ and $Zn(NO_3)_2 \cdot 6H_2O$ using 4-methoxy-2-quinolinecarboxylic acid linker at 160 °C and 120 °C respectively. While cobalt variety displayed a 2D coordination polymer structure, zinc is a simple monomer. Compound **2** showed higher uptake of H_2 and CO_2 in comparison to the many other 2D metal-organic frameworks. Interestingly, compound **2** exhibited partial selectivity of CO_2 over CH_4 which can be utilized in betterment of energy content of natural gases and separation of CO_2 from binary gas mixtures (e.g. CO_2/ CH_4) in various industrial processes.

3.5 References

[1] a) R. Shankar, M. Kumar, R. K. Chadha, G. Hundal, Inorg. Chem. 2003, **42**, 8585;

b) R. Shankar, A. P. Singh, G. Hundal, R. J. Butcher, J. Organ. Chem. 2007, **692**, 5555;

c) B. Machura, M. Wolff, E. Benoist, J. A. Schachner, N. C. Mösch-Zanetti, Dalton Trans. 2013, **42**, 8827;

d) I. Gryca, B. Machura, L. S. Shul'pina, G. B. Shul'pin, Inorg. Chim. Acta, 2017, **455**, 683.

[2] SAINT, version 6.02; SADABS, version 2.03; Bruker AXS, Inc.: Madison, WI, 2002.

[3] a) Sheldrick, G.M. SHELXS97, Program for Structure Solution, University of Göttingen, Germany, 1997;

b) Sheldrick, G.M. SHELXL97, Program for Crystal Structure Refinement, University of Göttingen, Germany, 1997.

[4] A. L. Spek, PLATON, Molecular Geometry Program, J. Appl. Crystallogr. 2003, **36**, 7.

[5] L. J. Farrugia, J. Appl. Crystallogr. 1997, **30**, 565.

[6]   L. J. Farrugia, J. Appl. Crystallogr. 1999, **32**, 837.

[7]   V. A. Blatov, A. P. Shevchenko, D. M. Proserpio, Cryst. Growth Des. 2014, **14**, 3576.

[8]   M.-Y. Li, F. Wang, J. Zhang, Inorg. Chem. Commun. 2017, **79**, 37.

[9]   D. J. Durbin, C. M. -Jugroot, Int. J. Hydrogen. Energy, 2013, **38**, 14595.

[10]   Z. Ozturk, D. A. Kose, Z. S. Sahin, G. Ozkan, A. Asan, Int. J. Hydrogen. Energy, 2016, **41**, 12167.

[11]   P. Chandrasekhar, A. Mukhopadhyay, G. Savitha, J. N. Moorthy, J. Mater. Chem. A, 2017, **5**, 5402.

[12]   D. Saha, T. Maity, S. Das, S. Koner, Dalton Trans. 2013, **42**, 13912.

[13]   U. P. Singh, S. Narang, P. Pachfule, R. Banerjee, CrystEngComm, 2014, **16**, 5012.

[14]   L.-W. Lee, T.-T. Luo, S.-H. Lo, G.-H. Lee, S.-M. Peng, Y.-H. Liu, S.-L. Lee, K.-L. Lu, CrystEngComm, 2015, **17**, 6320.

[15]   J. R. Karra, Y.-G. Huang, K. S. Walton, Cryst. Growth Des. 2013, **13**, 1075.

[16]   Q. Yan, Y. Lin, P. Wu, L. Zhao, L. Cao, L. Peng, C. Kong, L. Chen, ChemPlusChem, 2013, **78**, 86;

[17]   a) X.-M. Lin, T.-T. Li, Y.-W. Wang, L. Zhang, C.-Y. Su, Chem. Asian J. 2012, **7**, 2796;
        b) S. Parshamoni, S. Konar, CrystEngComm, 2016, **18**, 4395;
        c) S. Sanda, S. Biswas, S. Parshamoni, S. Konar, J. Solid State Chem. 2015, **229**,103.

[18]   S. Parshamoni, J. Telangae, S. Konar, Dalton Trans. 2015, **44**, 20926.

[19]   J. L. C. Rowsell, O. M. Yaghi, J. Am. Chem. Soc. 2006, **128**, 1304.

[20]   a) S. Bourrelly, P. L. Llewellyn, C. Serre, F. Millange, T. Loiseau, G. Ferey, J. Am. Chem. Soc. 2005, **127**, 13519;
        b) P. L. Llewellyn, S. Bourrelly, C. Serre, Y. Filinchuk, G. Férey, Angew. Chem. Int. Ed. 2006, **45**, 7751;
        c) K. S. Walton, A. R. Millward, D. Dubbeldam, H. Frost, J. J. Low, O. M. Yaghi, R. Q. Snurr, J. Am. Chem. Soc. 2008, **130**, 406.

[21]   Y. Li, H. Yi, X. Tang, F. Li, Q. Yuan, Chem. Eng. J. 2013, **229**, 50.

Chapter 4
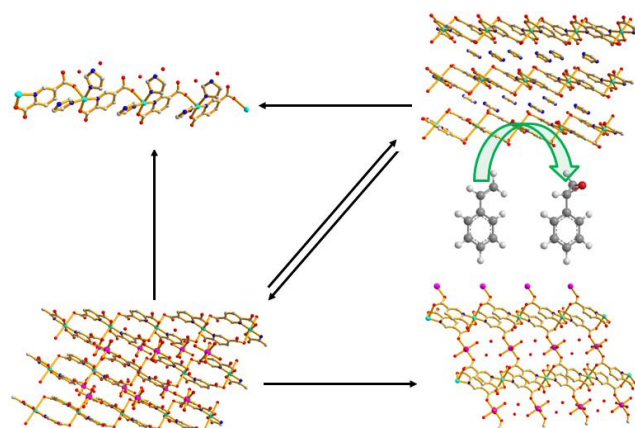
Synthesis, structural diversity, inter-conversion in Cu(II)/Cu(II)-Mg(II) containing Pyridine-2,5-dicarboxylate based MOF and heterogeneous catalytic epoxidation

4.1 Introduction

Metal-organic framework (MOF) is nothing but a symmetric arrangement of metal ions through organic linkers into extended one, two and three-dimensional networks via coordination bonding and other weak bonding interactions [1]. Designing of metal-organic framework has reached at higher level of sophistication, however, challenges remained how to control the structure of MOF employing basic knowledge of supramolecular chemistry and crystal engineering [2-3]. There are various synthesis methods to design MOFs such as diffusion-based crystallization and hydro-, solvo- and ionothermal synthesis etc. Hydrothermal process is one of the most popular methods utilized in the synthesis of MOFs [4]. However, to have control over the product formation in hydrothermal reactions is still remained elusive to chemists, since there are many factors influencing the formation and structure of the compounds, such as the reaction media (solvent), temperature, pH, molar ratio of starting materials, reaction time, and so on [5-9]. Therefore, an investigation for understanding the relationship between the structures of compounds and various stimuli is highly desirable.

Further, MOFs have been employed as catalyst in a variety of organic reactions [10]. C=C bond functionalization reaction is one of such important reactions in organic chemistry that can lead to a diverse array of derivatives. For example, simple epoxidation reaction that produces epoxide. The epoxides are active intermediate for industrial applications, which is used as feedstock for many value-added products [11]. Olefin epoxidation catalyzed by transition metal complexes has been a subject of great interest in the past few decades [12]. In this connection several copper catalyzed epoxidation reactions have been reported [13]. Usually, epoxidation is carried out in the presence of an oxidant such as hydrogen peroxide, TBHP or peracids. Hydroperoxides in combination with suitable catalysts constitute a suitable system from the viewpoint of green chemistry.

In this chapter, the structural interconversion among four metal carboxylate framework compounds, $\{[Mg(H_2O)_6][Cu(pdc)_2] \cdot 2H_2O\}_n$ (H_2Pdc = pyridine-2,5-dicarboxylic acid) (**4**), $\{[CuMg(pdc)_2(H_2O)_4] \cdot 2H_2O\}_n$ (**5**), $\{2(Him) \cdot [Cu(pdc)_2]\}_n$ (im = imidazole) (**6**), and $\{[Cu(pdc)(im)_2] \cdot 2H_2O\}_n$ (**7**) have been discussed. Synthesis, X-ray crystal structure and catalytic efficacy of the new compound **6** in olefin epoxidation reaction are also described. Synthesis, characterization and catalytic efficacy of others compounds were reported previously [14].

4.2 Experimental section

4.2.1 Materials

Pyridine-2,5-dicarboxylic acid, magnesium nitrate hexahydrate, copper nitrate trihydrate, imidazole and alkenes were purchased either from Sigma-Aldrich or Merck (India) and were used as received. Ethanol was purchased from Merck (India) and was distilled and dried before use.

4.2.2 Synthesis of the compounds 4, 5, 6 and 7

All compounds were prepared following the same procedure. Pyridine-2,5-dicarboxylic acid (0.167 g, 1 mmol) and imidazole first added in 10 ml of milli-Q water and the mixture was stirred for 0.5 h, to this mixture magnesium nitrate hexahydrate (0.128 g, 0.5 mmol) and copper nitrate trihydrate (0.120 g, 0.5 mmol) were added and the final mixture was stirred for 0.25 h. The mixture was then transferred to a 20 ml capacity teflon-lined acid digestion bomb and kept at 175 °C for 3 days followed by slow cooling at a rate of 5 °C h^{-1} to room temperature. Crystalline products were obtained from the digestion bomb. Compound **4**, **5**, **6** and **7** were obtained respectively from 1, 2, 3 and 4 mmol of imidazole (Figure 4.1). For characterization of the bulk compound, PXRD measurements (Figures 4.2-4.5), elemental analysis and IR spectroscopic study were performed. Blue block crystals of compound **6** were obtained in about 62% yield based on copper.

Anal. Calc. for $\{[Mg(H_2O)_6][Cu(pdc)_2]\cdot 2H_2O\}_n$ **4**: C, 29.88%; H, 3.94%; N, 4.98%. Found: C, 29.92%; H, 3.97%; N, 4.92%. Selected IR peaks (KBr disk, ν, cm^{-1}): 1607, 1551 [υ_{as} (CO$_2^-$)], 1358 [υ_s (CO$_2^-$)], 1287, 1268 [υ_s(C-O)], and 3472-3179 s.br [υ(O-H)].

Anal. Calc. for $\{[CuMg(pdc)_2(H_2O)_4]\cdot 2H_2O\}_n$ **5**: C, 31.96%; H, 3.45%; N, 5.32%. Found: C, 32.99%; H, 3.41%; N, 5.27%. Selected IR peaks (KBr disk, ν, cm^{-1}): 1688, 1612 [υ_{as} (CO$_2^-$)], 1395 [υ_s (CO$_2^-$)], 1357, 1287 [υ_s(C-O)], and 3477 br [υ(O-H)].

Anal. Calc. for $\{2(Him)\cdot[Cu(pdc)_2]\}_n$ **6**: C, 45.16%; H, 3.03%; N, 15.80%. Found: C, 45.22%; H, 3.05%; N, 15.73%. Selected IR peaks (KBr disk, ν, cm^{-1}): 1616, 1555 [υ_{as} (CO$_2^-$)], 1396 [υ_s (CO$_2^-$)], 1336, 1274 [υ_s(C-O)], 3112-3160 [υ_s (N-H)], and 3457 s.br [υ(O-H)].

Anal. Calc. for $\{[Cu(pdc)(im)_2]\cdot 2H_2O\}_n$ **7**: C, 38.95%; H, 3.71%; N, 17.47%. Found: C, 39.02%; H, 3.68%; N, 17.43%. Selected IR peaks (KBr disk, ν, cm^{-1}): 1652, 1616 [υ_{as} (CO$_2^-$)], 1396 [υ_s (CO$_2^-$)], 1348, 1262 [υ_s(C-O)], and 3432 br [υ(O-H)].

4.2.3 Physical measurements

The metal content of the sample was estimated on a Varian Techtron AA-ABQ atomic absorption spectrometer. The products of the catalytic reactions were identified and quantified by a Varian CP-3800 Gas Chromatograph using a CP-Sil 8 CB capillary column. Other physical measurements were undertaken by the same instruments already described in **Section 2.2.3, Chapter 2.**

4.2.4 X-ray crystallography

X-ray diffraction data for compound **6** was collected at 296(2) K on a Bruker SMART APEX CCD X-ray diffractometer using graphite-monochromated Mo-Kα radiation (λ = 0.71073Å). Determination of integrated intensities and cell refinement were performed with the SAINT software package using a narrow-frame integration algorithm [15]. An empirical absorption correction (SADABS) was applied [16]. The structure was solved by direct methods and refined using full-matrix least-squares technique against F^2 with anisotropic displacement parameters for non-hydrogen atoms with the programs SHELXS97 [17] and SHELXL2014/7 [18]. The C-bound hydrogen atoms were freely refined. In the final difference Fourier maps, there were no remarkable peaks except the ghost peaks surrounding the metal centers. A summary of crystal data and relevant refinement parameters for compound **6** is given in Table 4.1. Structural characterization of compound **4**, **5**, and **7** were reported previously [14].

CCDC 1586363 contains the supplementary crystallographic data for compound **6**. These data can be obtained free of charge via http://www.ccdc.cam.ac.uk/conts/retrieving.html, or from the Cambridge Crystallographic Data Centre, 12 Union Road, Cambridge CB2 1EZ, UK; fax: (+44) 1223-336-033; or e-mail: deposit@ccdc.cam.ac.uk.

Table 4.1. Crystallographic data and structure refinement parameters of compound 6

Chemical formula sum	$C_{20}H_{16}CuN_6O_8$
Chemical formula weight	531.94
Crystal system	Triclinic
Space group	$P\bar{1}$
a (Å)	6.6465(2)
b (Å)	7.5421(2)
c (Å)	10.4307(3)
$\alpha(°)$	108.4310(1)

$\beta(°)$	96.643(2)
$\gamma(°)$	96.7370(1)
$V\,(\text{Å}^3)$	486.11(2)
Z	1
Temperature (K)	296(2)
$D_c\,(\text{g cm}^{-3})$	1.817
$\mu\,(\text{mm}^{-1})$	1.193
$F(000)$	271
θ range (°)	2.1-26.7
Intervals of reflection indices	$-8 \leq h \geq 8,\ -9 \leq k \geq 9,\ -13 \leq l \geq 13$
Measured reflections	7758
Reflections with $[\,I > 2\sigma\,(I)]$	1971
Independent reflections	2062
Final R indices $[I > 2\sigma\,(I)]$	$R1 = 0.0278,\ wR2 = 0.0796$
R indices (all data)	$R1 = 0.0291,\ wR2 = 0.0811$
R_{int}	0.0220
$\Delta\rho_{\text{max}}(\text{e Å}^{-3})$	0.317
$\Delta\rho_{\text{min}}(\text{e Å}^{-3})$	-0.278
Goodness-of-fit on F^2	0.790

$$R_1 = \sum |(|F_o| - |F_c|)| / \sum |F_o|,\ wR_2 = \left\{ \sum [\text{w}\,(F_o^2 - F_c^2)^2] / \sum [\text{w}\,(F_o^2)^2] \right\}^{1/2}$$

4.2.5 Catalytic reaction

The catalytic reactions were carried out in a glass batch reactor according to the following procedure. Substrate (10 mmol), ethanol (5 ml) and catalyst (2 mg) were first mixed. The mixture was then equilibrated to desired temperature in an oil bath. After addition of hydrogen peroxide (14.4 mmol, 1.5 equiv.) the reaction mixture was stirred continuously. Reactions were performed in open air. The products of the reactions were collected at different time intervals and were identified and quantified by gas chromatography.

4.3 Results and discussion

4.3.1 Syntheses and imidazole dependent structural variation and transformation

Compound **4**, **5**, **6** and **7** were synthesized from an identical reaction mixture with different imidazole concentration (Figure 4.1). All compounds except for **7** are crystallized in a triclinic space group $P\bar{1}$ with $Z = 1$. Increase of the imidazole concentration led to the formation of compounds **4** to **7**. Basic structure of **4**, **5** and **6** are same. These are 1-D coordination polymer contains copper(II) ions connected by pdc-dianions forming $\{[Cu(pdc)_2]^{2-}\}_n$ ribbon like chains. Coordination geometry of copper(II) in **4**, **5** and **6** is distorted octahedron where two nitrogen atoms and two oxygen atoms from two chelating pdc-dianions formed the basal plane of the octahedron while axial positions are occupied by two oxygen atoms from two different pdc-dianions. When 1 mmol of imidazole is used, compound **4** is formed where negative charge of $\{[Cu(pdc)_2]^{2-}\}_n$ is satisfied by the $[Mg(H_2O)_6]^{2+}$ ions and ultimately formed a hydrogen bonded 2D network through hydrogen of coordinated water molecule and free carboxylato oxygen atom [14a]. Upon increasing the amount of imidazole to 2 mmol, hydrothermal treatment of the reaction mixture afforded compound **5** where $\{[Cu(pdc)_2]^{2-}\}_n$ chains are linked with Mg(II) ions through carboxylate oxygen atoms and a 2D network was formed [14b]. In compound **5**, free carboxylate oxygen atoms present in compound **4** involved in bonding with Mg(II) ions and replaced two coordinated water molecules of Mg(II) ions present in **4**. Upon adjusting the amount of imidazole to 3 mmol, magnesium ions were replaced by the imidazolium ions and compound **6** was thus formed. Structure of compound **6** is close resembles with compound **4** but only difference is that the place of hexa-aqua Mg(II) ions are occupied by uncoordinated imidazolium ions. When amount of the imidazole was adjusted to 4 mmol, imidazole is coordinated by the Cu(II) ion and compound **7** was formed [14c]. In compound **7**, each Cu(II) ion is coordinated by two nitrogen atoms from two imidazole molecules, two carboxylato oxygen atoms of two different carboxylate groups from two different pdc^{2-} ligand and one nitrogen atom of pdc^{2-} ligand. Here, pdc^{2-} ligand is connected through two copper(II) ions in a similar fashion as in other compounds, thus formed 1D chain of distorted square pyramidal Cu(II) coordination geometry. Another difference is that instead of four connecting pdc^{2-} ligands with one Cu(II) center, only two are involved here.

All structural transformations are shown in Figure 4.1. Upon increasing imidazole concentration **4** was converted to **5, 6** and **7** through hydrothermal treatment. Similarly, **6** was converted to **7**. But attempts for conversion of **5** to **6** and **5** to **7** were unsuccessful. This is important to mention that in presence of excess magnesium nitrate **6** was also converted to **4** through hydrothermal treatment.
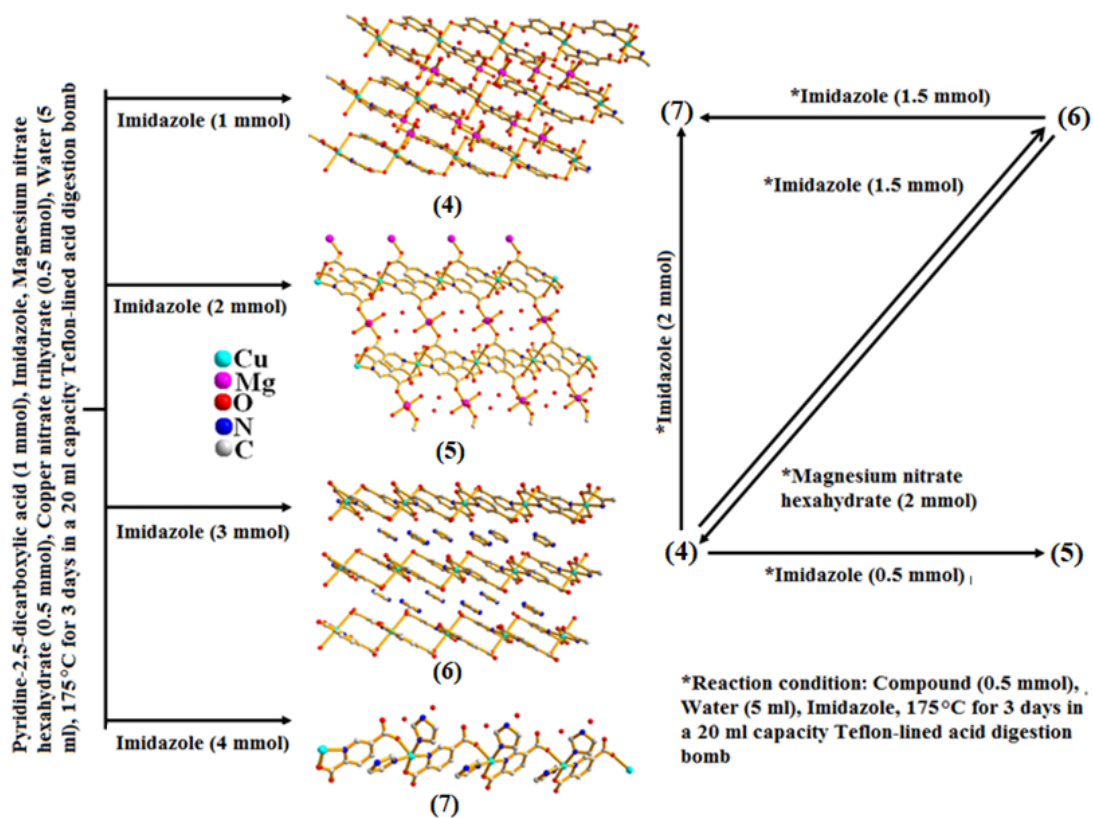
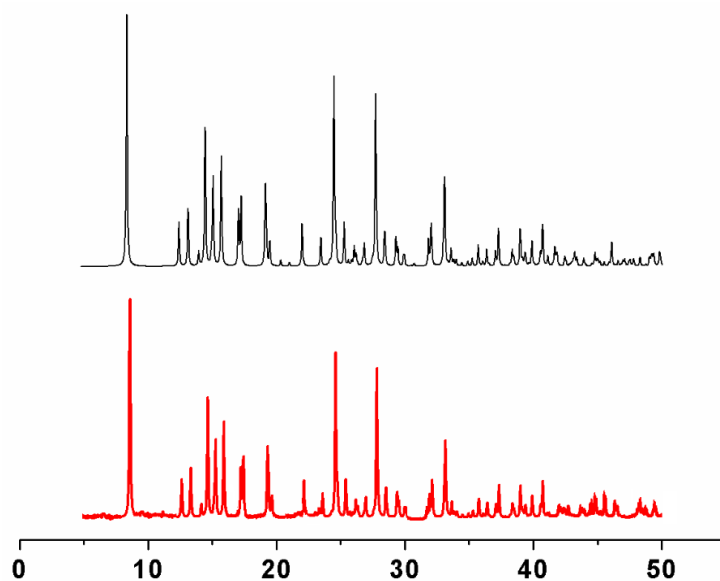**Figure 4.1. Imidazole dependent structural variation and inter-conversion**

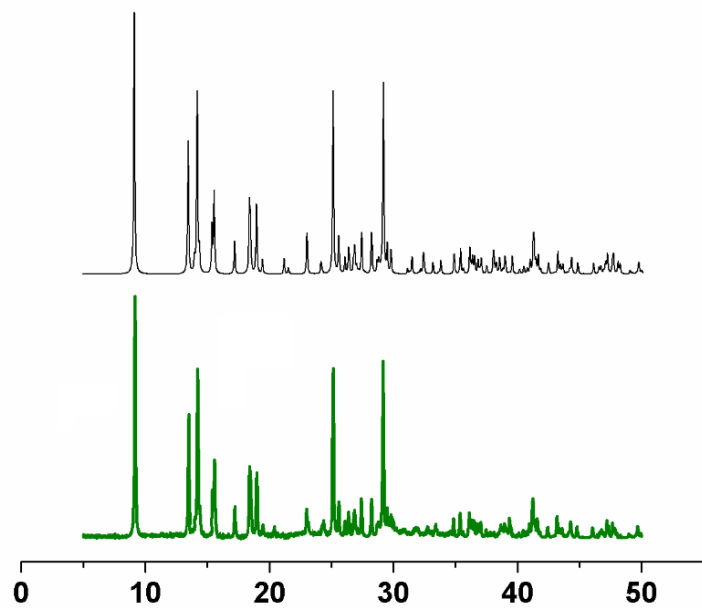**Figure 4.2. PXRD pattern of compound 4 (Black: simulated; Red: experimental)**

Figure 4.3. PXRD pattern of compound 5 (Black: simulated; Green: experimental)
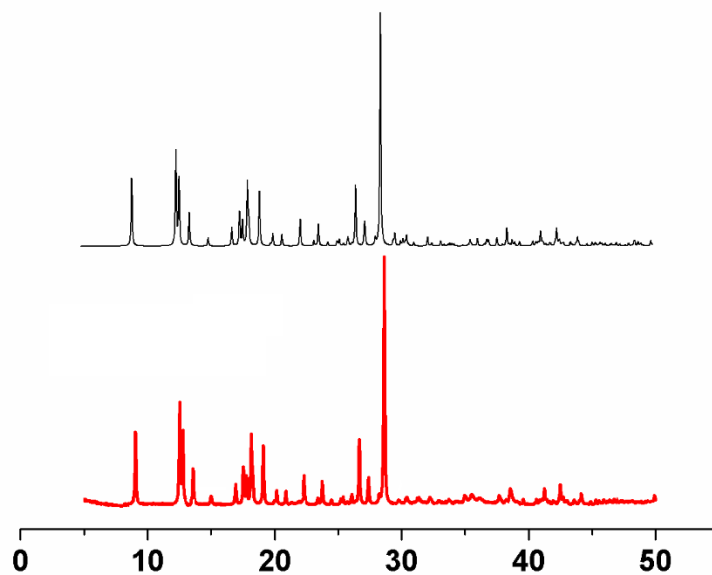

Figure 4.4. PXRD pattern of compound 6 (Black: simulated; Red: experimental)
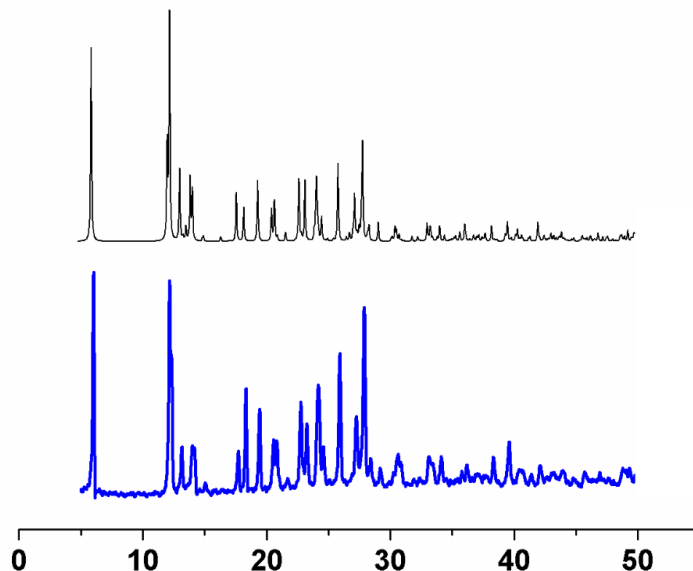
Figure 4.5. PXRD pattern of compound 7 (Black: simulated; Blue: experimental)

4.3.2 X-ray structure of {2(Him)·[Cu(pdc)$_2$]}$_n$ (6)

Compound **6** crystallized in the triclinic space group $P\bar{1}$ with $Z = 1$. Compound **6** has a polymeric ribbon like 1D chain structure consist of copper(II) ion and carboxylate linker. The chain is propagated parallel to the crystallographic *a* axis (Figure 4.6). The chain is actually anionic in nature which is balanced by uncoordinated imidazolium cations. Crystallographically unique [Cu(pdc)$_2$]$^{2-}$ units constructed the ribbon, where each Cu^{2+} adopted a tetragonally distorted octahedron geometry (Figure 4.7). An ORTEP diagram with atom-numbering scheme is shown in the Figure 4.8. Selected bond distances and the bond angles are collected in Table 4.2. Four donor atoms (N1, O1 and ^{c}N1, ^{c}O1; c = –*x*, –*y*, –*z*) from two chelating pdc^{2-} ligands occupied the equatorial positions where N1 and O1 of pdc^{2-} ligand form chelate with metal center and axial positions are occupied by two carboxylato oxygen atoms (^{a}O4 and ^{b}O4; a = 1+*x*, *y*, *z*; b = –1–*x*, –*y*, –*z*) from two different pdc^{2-} ligands. The pdc^{2-} ligand showed μ_3 connectivity mode. In one site it is formed a chelate with copper center through one heterocyclic nitrogen atom (N1) and one carboxylato oxygen (O1) atom adjacent to ring nitrogen and in another site, it is linked with another copper center through oxygen (O4) of different carboxylate group. Among the four carboxylato oxygen atoms of pdc^{2-} ligand, two (O2 and O3) remain uncoordinated. Those 1-D chains are connected through imidazolium ions by intermolecular H-bonding between hydrogen bonded with the ring nitrogen of imidazolium ion and free carboxylato oxygen atom of pdc^{2-}ligand resulted a 2D supramoleculer structure (Table 4.3 and Figure 4.6).
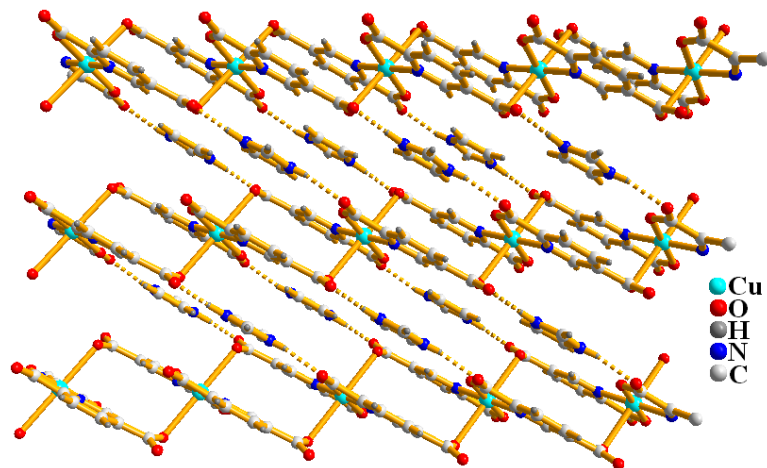
Figure 4.6. Chains of compound 6, dotted bonds are showing hydrogen bonded 2D net.
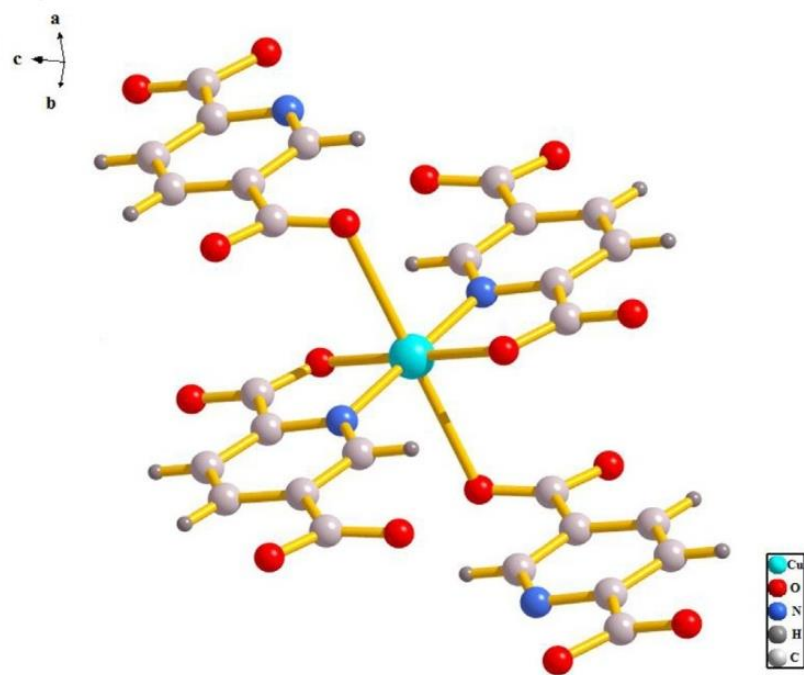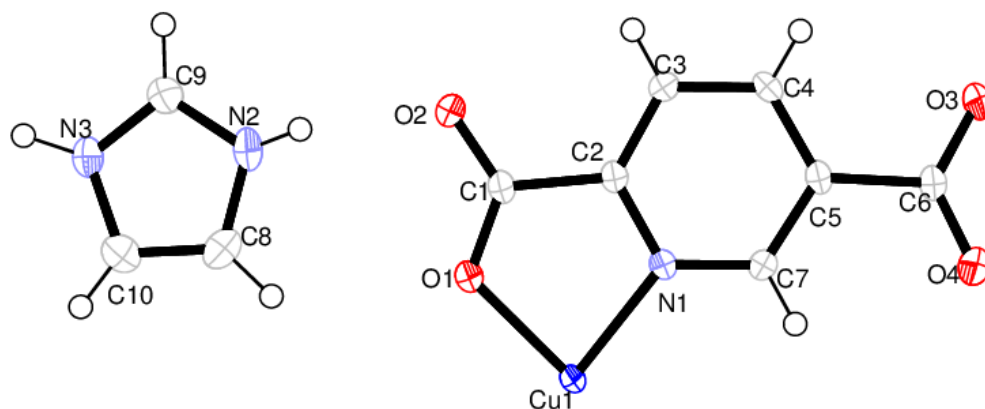

Figure 4.7. Metal-ligand coordination of compound 6

Figure 4.8. ORTEP diagram of 6 with 40% ellipsoid probability

Table 4.2. Selected bond-lengths (Å) and angles (°) of compound 6

Bond-length	
Cu1-O1	1.9678(13)
Cu1-N1	1.9655(14)
Cu1-[a]O4	2.6473(15)
Cu1-[b]O4	2.6473(15)
Cu1-[c]O1	1.9678(13)
Cu1-[c]N1	1.9655(14)
Bond-angle	
O1-Cu1-N1	82.98(6)
O1-Cu1-[a]O4	84.25(5)
O1-Cu1-[b]N4	95.75(5)
O1-Cu1-[c]O1	180.00
O1-Cu1-[c]N1	97.02(6)
[a]O4-Cu1-N1	93.78(5)
[b]O4-Cu1-N1	86.23(5)
[c]O1-Cu1-N1	97.02(6)
N1-Cu1-[c]N1	180.00

[a]O4-Cu1-[b]O4	180.00
[c]O1-Cu1-[a]O4	95.75(5)
[a]O4-Cu1-[c]N1	86.23(5)
[c]O1-Cu1-[b]O4	84.25(5)
[b]O4-Cu1-[c]N1	93.78(5)
[c]O4-Cu1-[c]N1	82.98(6)

Symmetry Code: [a] 1+*x*, *y*, *z*; [b] –1–*x*, –*y*, –*z*; [c] –*x*, –*y*, –*z*.

Table 4.3. Hydrogen bonding interactions (Å, º) in compound 6

D-H···A	d(D-H)	d(H-A)	d(D···A)	∠DHA	Symmetry Transform
			compound **3**		
N2—H2...O2	0.75(3)	2.02(3)	2.750(2)	164(3)	–
N3—H11...O3	0.91(3)	1.75(3)	2.655(2)	170(3)	2+*x*,1+*y*,z

4.3.3 Thermal analysis of compound {2(Him)·[Cu(pdc)₂]}ₙ (6)

TG measurement confirms that the compound **6** was thermally stable up to around 325 °C (Figure 4.9). Compound **6** showed a single stage mass loss. A sharp mass loss at around 325 °C observed may be due to the decomposition of the compound **6**. The corresponding DTA curve of compound **6** showed an endothermic peak centered at 353 °C. The final solid product of thermal decomposition was identified as CuO with total mass loss of 88.57 % (*ca.* 88.05 %). Being a 1D chain structure, the high thermal stability of this MOF can be explained in terms of the salt like nature, rigidity of the linkers, strong bonds between the metal ions and the organic linkers, absence of solvent molecules, etc. Thermal stability of compound **6** also verified by variable temperature PXRD study. Major experimental PXRD peaks of compound **6** are well maintained with the simulated one up to 300 °C (Figure 4.10).
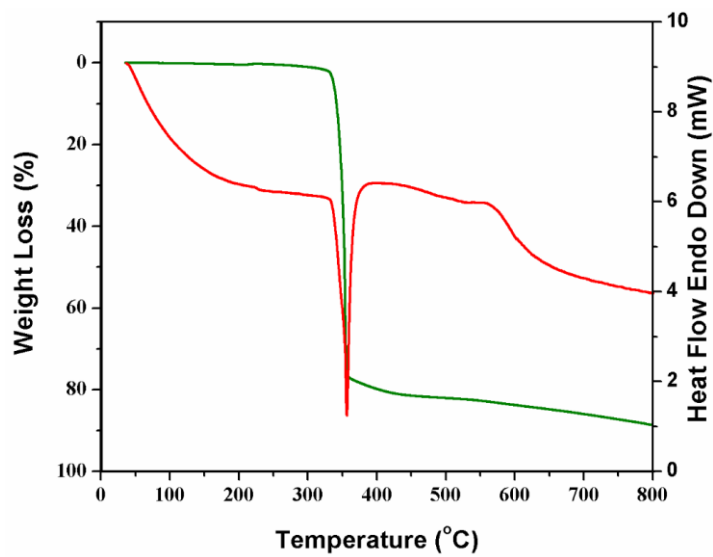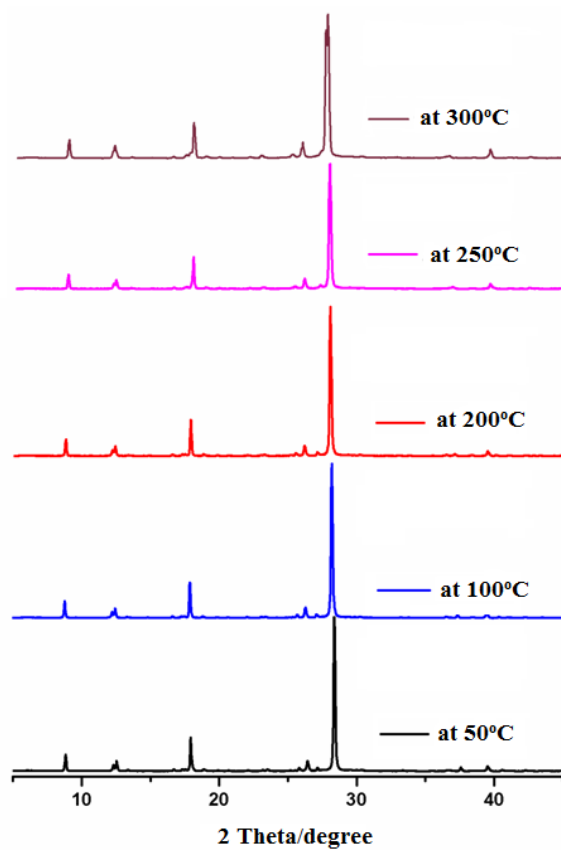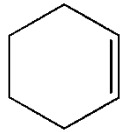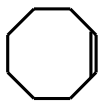
Figure 4.9. TGA and DTA curve of compound 6

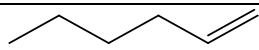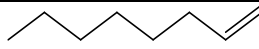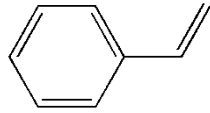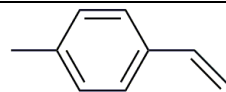**Figure 4.10. Variable temperature PXRD pattern of compound 6**

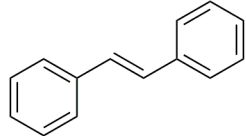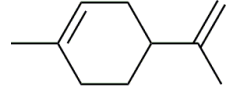**4.3.4 Catalytic activities of compound {2(Him)·[Cu(pdc)$_2$]}$_n$ (6)**

Catalytic epoxidation of alkenes using compound **6** was performed at 60 °C in heterogeneous conditions. Examination was carried out by the epoxidation of 1-hexene and cyclooctene in six different solvents to obtain the suitable solvent. The best conversion and selectivity were found in ethanol. Although acetonitrile displayed as very good solvent, but selectivity was less in case of styrene and cyclohexene epoxidation. The conversion increases in the order CH_2Cl_2>$CHCl_3$>MeOH>CH_3COCH_3>EtOH>CH_3CN (Figure 4.11). But the selectivity increases in the order CH_2Cl_2>$CHCl_3$>CH_3COCH_3>CH_3CN>MeOH>EtOH for styrene and cyclohexene (Figure 4.12). To monitor the temperature effect, reaction temperature was increased from 30–78 °C for the epoxidation of cyclooctene and 1-hexene, a good yield with good product selectivity was obtained at a moderate temperature of 60 °C (Figure 4.13) in ethanol. At higher temperatures the conversion decreased, as H_2O_2 started to degrade at higher temperatures. The epoxidation of alkenes was studied here goes smoothly, displayed an excellent conversion (80% to 100%) to form epoxides as the major product. Results of the catalytic epoxidation of different substrates are given in Table 4.4. Oxidation of cyclohexene proceeds smoothly, displayed 100% conversion after 8 h of reaction to form epoxycyclohexane with *ca.* 72% selectivity and some amount of alkenes were converted to 2-cyclohexen-1-ol and 2-cyclohexene-1-one. Cyclooctene was effectively converted to epoxycyclooctane with *ca.* 100% selectivity and conversion. In case of linear alkenes, 1-hexene showed almost complete conversion and producing epoxide as the sole product, but in case of 1-octene the conversion was not complete; the conversion is only limited to 80% after 8 h of reaction. It suggests that the catalytic activity decreases along with chain length of alkene. This may due to the larger hexyl group of 1-octene connected to double bond sterically hinders it in approaching to the active site with respect to 1-hexene in which its double bond carries a smaller butyl group. Consequently, the conversion was lowered in catalytic reaction. To study conjugated olefins, styrene, 4-methylstyrene and *trans*-stilbene were used. Styrene and 4-methylstyrene were converted with 100% efficiency, and the product selectivity remained around 78 and 70%, respectively, with benzaldehyde as the usual corresponding bi-product. The epoxidation of *trans*-stilbene with H_2O_2 gives stilbene oxide in 82% conversion but 100% selectivity. A different substrate, limonene, was also subjected to oxidation reaction; 100% conversion with a product selectivity of 86% and along with some unidentified products. A graphical representation of relative efficacy of **6** for the epoxidation of various alkenes in ethanol with time is given in Figure 4.14. The same reaction was catalyzed by compound **4** but in homogeneous condition [14a]. Therefore, it can be said that counter ion in compound **6** and also the nature of supramolecular interactions played crucial role to maintain heterogeneity of the reaction.

To ascertain the heterogeneous nature of catalyst, a hot filtration test was performed. The liquid phase of the reaction mixture was collected by filtration after *ca.* 36% of the reaction was completed for epoxycyclooctane. The supernatant solution was then kept in the reaction conditions for another 24 h. Almost no progress of the reaction was observed during this period, which excludes the presence of active species in the solution. Besides, atomic absorption spectrometric analysis (sensitivity up to 0.001 ppm) of the supernatant solution of reaction mixture thus collected by filtration confirms the absence of copper ions in the liquid phase. For the recycling study, catalyst was recovered by centrifugation, washed thoroughly with ethanol, then activated at 140 °C under vacuum for 3 h, and reused five times using epoxycyclooctane. All repeated reactions gave almost identical conversion (Figure 4.15). The IR spectra and PXRD patterns of a fresh and a used sample of the catalyst did not show any significant differences which convincingly demonstrated that its structural integrity is well maintained after several cycles of reactions (Figures 4.16, 4.17).

Table 4.4. Oxidation of selected olefins by H_2O_2 with catalyst 6[a]

Substrate	Conversion (wt %)	% yield of product		TOF[b] (h^{-1})
		Epoxide	Others	
	100	72	28[c]	332
	100	100	-	332
	92	92	-	305
	80	80	-	265
	100	78	22[d]	332
	100	70	30[e]	332

(trans-stilbene structure)	82	100	-	271
(limonene structure)	100	86[f]	14[g]	332

[a] Reaction condition: Substrate (10 mmol), ethanol (10 ml) and catalysts (2 mg); hydrogen peroxide (1.5 equiv.); temperature: 60 °C; reaction time: 8 h; The products of the reactions were collected at different time intervals and were identified and quantified by Varian CP-3800 gas chromatograph equipped with an FID detector and a CP-Sil 8 CB capillary column. [b] Turn over frequency (TOF) = moles converted per moles of active site per hour. [c] 2-cyclohexen-1-ol and 2-cyclohexene-1-one. [d] Benzaldehyde. Benzoic acid. [e] 4-Methylbenzaldehyde. [f] Limonene oxide. [g] Unidentified product.
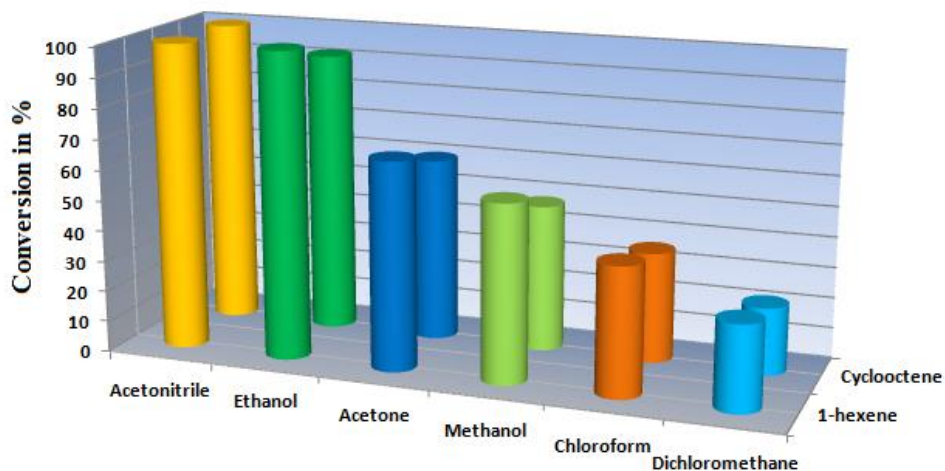
Figure 4.11. Catalytic efficacy of compound 6 in different solvents on the basis of olefin conversion. Reaction conditions were the same as given in the footnote of Table 4 (Reaction temperature is the boiling point for those solvent having boiling point below 60 °C)
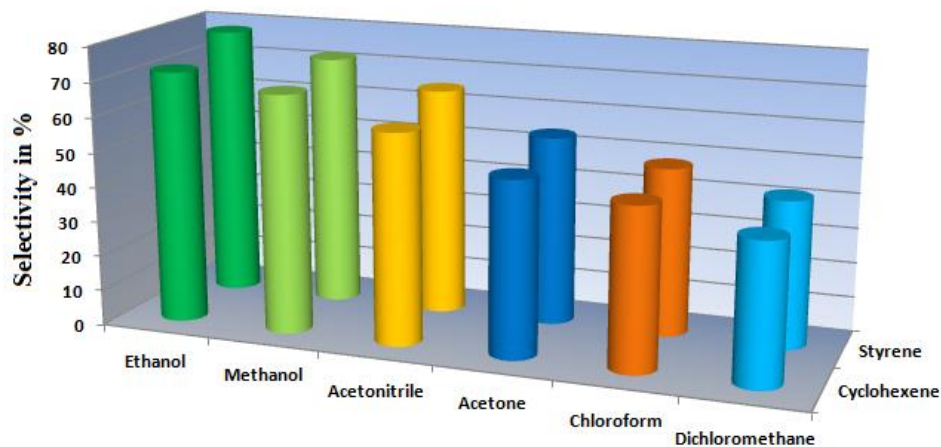
Figure 4.12. Catalytic efficacy of compound 6 in different solvents on the basis of epoxide selectivity. Reaction conditions were the same as given in the footnote of Table 4 (Reaction temperature is the boiling point for those solvent having boiling point below 60 °C)

Figure 4.13. Catalytic efficacy of compound 6 in different temperature. Reaction conditions were the same as given in the footnote of Table 4.

Figure 4.14. Kinetic plots for the epoxidation of alkenes catalyzed by 6

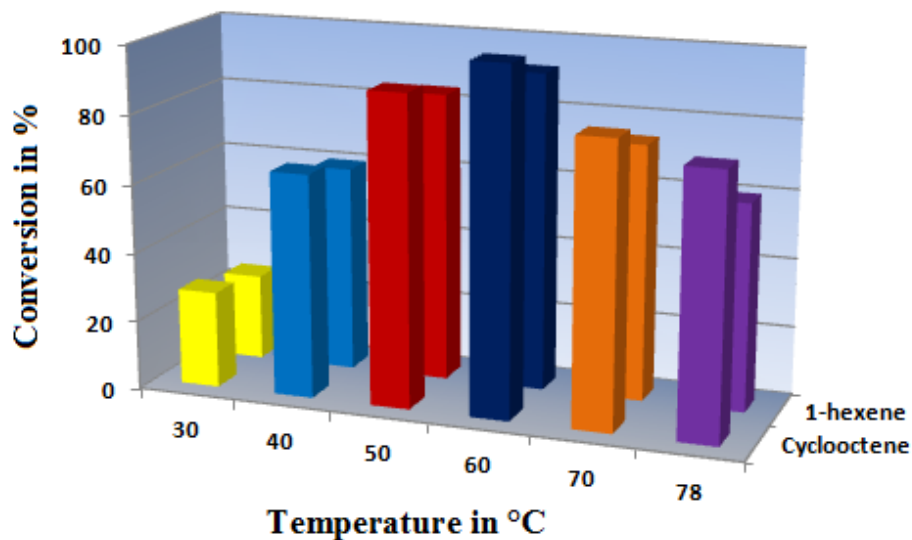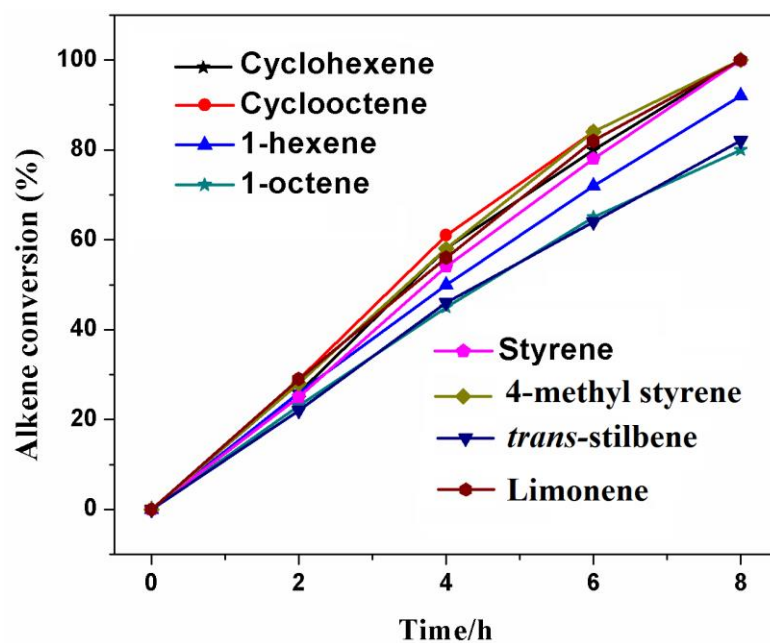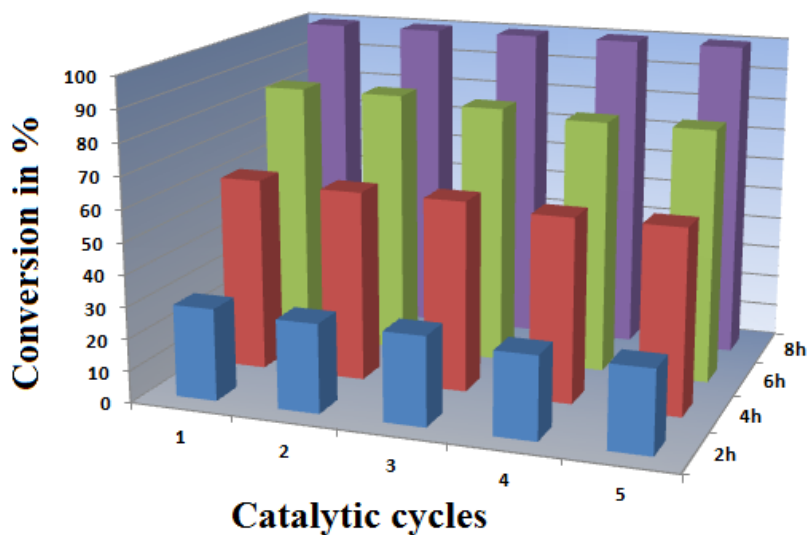**Figure 4.15. Catalytic activity of 6 in different catalytic cycles. Reaction conditions were the same as given in the footnote of Table 4.**
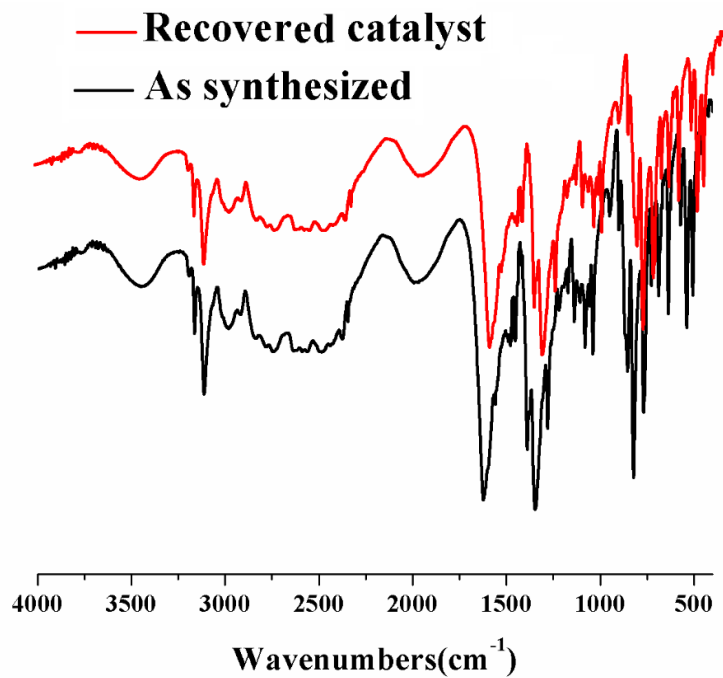
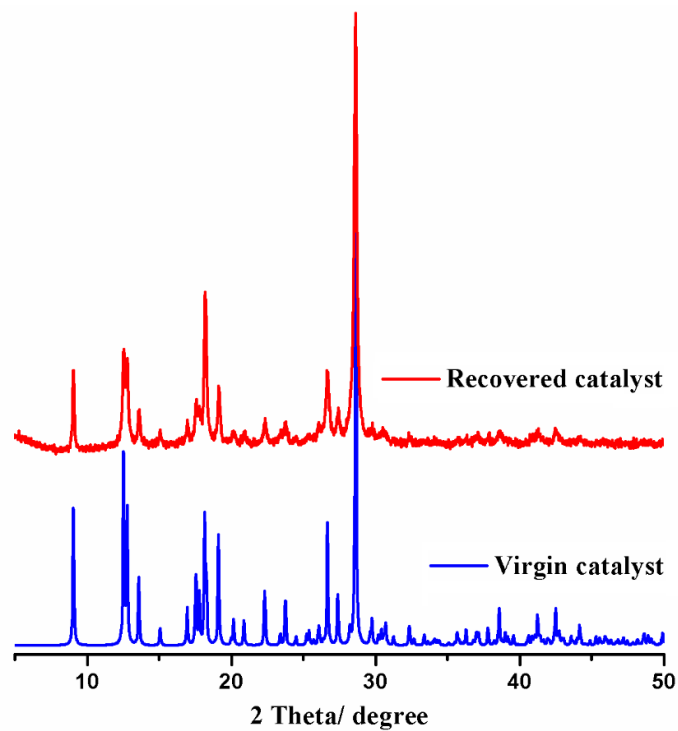**Figure 4.16. IR spectra of virgin and recovered catalyst**

Figure 4.17. PXRD patterns of virgin and recovered catalyst

4.4 Conclusion

In essence, structural inter-conversion of four metal carboxylate compounds, $\{[Mg(H_2O)_6][Cu(pdc)_2]\cdot 2H_2O\}_n$ (**4**), $\{[CuMg(pdc)_2(H_2O)_4]\cdot 2H_2O\}_n$ (**5**), $\{2(Him)\cdot[Cu(pdc)_2]\}_n$ (**6**), and $\{[Cu(pdc)(im)_2]\cdot 2H_2O\}_n$ (**7**) (H$_2$pdc = pyridine-2,5-dicarboxylic acid and im = imidazole) through hydrothermal reaction have been investigated. The new compound, **6**, has been synthesized hydrothermally and characterized by single-crystal-X-ray diffraction. High thermal stability of compound **6** was established by variable temperature PXRD study. Olefin epoxidation reactions in heterogeneous condition were catalyzed by compound **6** where H$_2$O$_2$ displayed the role of oxidizing agent. Catalytic activities were tested in different temperature and solvent medium. The best catalytic activity of the compound was observed in ethanol at 60 °C. This demonstrates the choice of an appropriate solvent and temperature is important in catalytic reactions.

4.5 References

[1]   (a) B. Moulton, M. J. Zaworotko, Chem. Rev. 2001, **101**, 1629; (b) D. Bradshaw, J. B. Claridge, E. J. Cussen, T. J. Prior, M. J. Rosseinsky, Acc. Chem. Res. 2005, **38**, 273; (c) F. Gándara, E.G. Puebla, M. Iglesias, D.M. Proserpio, N. Snejko, M. A. Monge, Chem. Mater. 2009, **21**, 655; (d) P. J. Saines, B. C. Melot, R. Seshadri, A. K. Cheetham, Chem. Eur. J. 2010, **16**, 7579; (e) C.-H. Huang, J. R. Morrow, Inorg. Chem. 2009, **48**, 7237; (f) J. Luo, H. Xu, Y. Liu, Y. Zhao, L. L. Daemen, C. Brown, T. V. Timofeeva, S. Ma, H.-C. Zhou, J. Am. Chem. Soc. 2008, **130**, 9626; (g) R. Chakrabarty, P. S. Mukherjee, P. J. Stang, Chem. Rev. 2011, **111**, 6810; (h) G. K. Kolea, J. J. Vittal, Chem. Soc. Rev. 2013, **42**, 1755.

[2]   (a) J.-M. Lehn, Supramolecular Chemistry, VCH, Weinheim, 1995; (b) Transition Metals in Supramolecular Chemistry, (Eds: L. Fabbrizzi, A. Poggi), ASI Kluwer Academic Publishers: Dordrecht, 1994.

[3]   (a) G. R. Desiraju, Crystal Engineering, The Design of Organic Solids, ELSEVIER, Amsterdam, 1989; (b) O. Kahn, Molecular Magnetism, VCH, Weinheim, 1993; (c) B. F. Abrahams, B. F. Hoskins, D. M. Michail, R. Robson, Nature 1994, **369**, 727; (d) S. Kawata, S. Kitagawa, H. Kumagai, C. Kudo, H. Kamesaki, T. Ishiyama, R. Suzuki, M. Kondo, M. Katada, Inorg. Chem. 1996, **35**, 4449; (e) H. Li, M. Eddaoudi, M. O'Keeffe, O. M. Yaghi, Nature, 1999, **402,** 276; (f) J. Seo, H. Sakamoto, R. Matsuda, S. Kitagawa, J. Nanosci. Nanotechnol. 2010, **10**, 3; (g) S. Horike,

S. Shimomura, S. Kitagawa, Nat. Chem. 2009, **1**, 695; (h) W. Xuan, C. Zhu, Y. Liu, Y. Cui, Chem. Soc. Rev. 2012, **41**, 1677; (i) T. R. Cook, Y.-R. Zheng, P. J. Stang, Chem. Rev. 2013, **113**, 734; (j) P. Müller, V. Bon, I. Senkovska, J. Getzschmann, M. S. Weiss, S. Kaskel, Cryst. Growth Des. 2017, **17**, 3221.

[4]   A. Qiu, G. Zhu, Coord. Chem. Rev. 2009, **253**, 2891.

[5]   (a) X.-Y. Wang, L. Wang, Z.-M. Wang, S. Gao, J. Am. Chem. Soc. 2006, **128,** 674; (b) P.-X. Yin, J. Zhang, Y.-Y. Qin, J.-K. Cheng, Z.-J. Li, Y.-G. Yao, CrystEngComm, 2011, **13**, 3536; (c) X. Qu, L. Zhai, B. Wang, Q. Wei, G. Xie, S. Chen, S. Gao, Dalton Trans. 2016, **45**, 17304; (d) C. K. Brozek, L. Bellarosa, T. Soejima, T. V. Clark, N. Lopez, M. Dinca, Chem. Eur. J. 2014, **40**, 6871.

[6]   (a) M. L. Tong, S. Kitagawa, H. C. Chang, M. Ohba, Chem. Commun. 2004, 418; (b) J. Chen, M. Ohba, D. Zhao, W. Kaneko, S. Kitagawa, Cryst. Growth Des. 2006, **6**, 664; (c) J. Zhang, X. Bu, Chem. Commun. 2008, 444.

[7]   (a) R. Sen, D. Saha, S. Koner, Chem. Eur. J. 2012, **18**, 5979; (b) H. Yang, S. Gao, J. Leu, B. Xu, J. Lin, R. Cao, Inorg. Chem. 2010, **49**, 736; (c) S. Shishido, T. Ozeki, J. Am. Chem. Soc. 2008, **130**, 10588; (d) J.-W. Dai, X. Dong, Z.-H. Zhou, Inorg. Chim. Acta 2016, **453**, 463; (e) X.-Y. Xu, B. Yan, Dalton Trans. 2016, **45**, 7078.

[8]   (a) P. M. Forster, A. R. Burbank, C. Livage, G. Férey, A. K. Cheetham, Chem. Commun. 2004, 368; (b) K. L. Gurunatha, K. Uemura, T. K. Maji, Inorg. Chem. 2008, **47**, 6578.

[9]   P. Mahata, M. Prabu, S. Natarajan, Inorg. Chem. 2008, **47**, 8451.

[10]   (a) M. Ranocchiari, J. A. van Bokhoven, Phys. Chem. Chem. Phys. 2011, **13**, 6388; (b) A. Corma, H. García, F. X. L. Xamena, Chem. Rev. 2010, **110**, 4606; (c) Y. Liu, A. J. Howarth, N. A. Vermeulen, S.-Y. Moon, J. T. Hupp, O. K. Farha, Coord. Chem. Rev. 2017, **346**, 101; (d) B. Rungtaweevoranit, J. Baek, J. R. Araujo, B. S. Archanjo, K. M. Choi, O. M. Yaghi, G. A. Somorjai, Nano Lett. 2016, **16**, 7645.

[11]   (a) B. S. Lane, K. Burgess, Chem. Rev. 2003, **103**, 2457; (b) R. Noyori, M. Aoki, K. Sato, Chem. Commun. 2003, 1977; (c) T. Katsuki, Chem. Soc. Rev. 2004, **33**, 437; (d) T. Punniyamurthy, S. Velusamy, J. Iqbal, Chem. Rev. 2005, **105**, 2329.

[12]   (a) A. Dhakshinamoorthy, M. Alvaro, H. Garcia, J. Catal. 2012, **289**, 259; (b) R. Luo, R. Tan , Z. Peng, W. Zheng, Y. Kong, D. Yin, J. Catal. 2012, **287**, 170; (c) M. J. Beier, W. Kleist, M. T.

Wharmby, R. Kissner, B. Kimmerle, P. A. Wright, J.-D. Grunwaldt, A. Baiker, Chem. Eur. J. 2012, **18**, 887; (d) R. Sen, R. Bera, A. Bhattacharjee, P. Gütlich, S. Ghosh, A. K. Mukherjee, S. Koner, Langmuir, 2008, **24**, 5970; (e) R. Sen, S. Bhunia, D. Mal, S. Koner, Y. Miyashita, K.-I. Okamoto, Langmuir, 2009, **25**, 13667; (f) J. Zhang, A. V. Biradar, S. Pramanik, T. J. Emge, T. Asefa, J. Li. Chem. Commun. 2012, **48**, 6541; (g) Y.-Y. Liu, K. Leus, M. Grzywa, D. Weinberger, K. Strubbe, H. Vrielinck, R. V. Deun, D. Volkmer, V. Van Speybroeck, P. V. Der Voort, Eur. J. Inorg. Chem. 2012, 2819; (h) J. S. Lee, S. B. Halligudi, N. H. Jang, D. W. Hwang, J.-S. Chang, Y. K. Hwang, Bull. Korean Chem. Soc. 2010, **31**, 1489; (i) A. M. Shultz, O. K. Farha, J. T. Hupp, S. T. Nguyen, Chem. Sci. 2011, **2**, 686; (j) S. Bhattacharjee, D.-A. Yang, W.-S. Ahn, Chem. Commun. 2011, **47**, 3637; (k) K. Leus, G. Vanhaelewyn, T. Bogaerts, Y.-Y. Liu, D. Esquivel, F. Callens, G. B. Marin, V. V. Speybroeck, H. Vrielinck, P. V. D. Voort, Catal. Today 2013, **208**, 97; (l) A. P. Zhang, L. Q. Li, J. Li, Y. Zhang, S. Gao, Catal. Commun. 2011, **12**, 1183; (m) M. J. Beier, W. Kleist, M. T. Wharmby, R. Kissner, B. Kimmerle, P. A. Wright, J. D. Grunwaldt, A. Baiker, Chem. Eur. J. 2012, **18**, 887.

[13]   (a) P. Karandikar, M. Agashe, K. Vijayamohanan, A. J. Chandwadkar, Appl. Catal. A: Gen. 2004, **257**, 133; (b) S. Jana, B. Dutta, R. Bera, S. Koner, Langmuir 2007, **23**, 2492; (c) S. Jana, S. Bhunia, B. Dutta, S. Koner, Appl. Catal. A: Gen. 2011, **392**, 225; (d) S. Rayati, S. Zakavi, M. Koliaei, A. Wojtczak, A. Kozakiewicz, Inorg. Chem. Commun. 2010, **13**, 203; (e) D. Torres, N. Lopez, F. Illas, R. M. Lambert, J. Am. Chem. Soc. 2005, **127**, 10774; (f) M. B. Andrus, Z, Zhou, J. Am. Chem. Soc. 2002, **124**, 8806; (g) T. Ohta, T. Tachiyama, K. Yoshizawa, T. Yamabe, T. Uchida, T. Kitagawa, Inorg. Chem. 2000, **39**, 4358; (h) K. Brown, S. Zolezzi, P. Aguirre, D. Venegas-Yazigi, V. Paredes-Garcia, R. Baggio, M. A. Novak, E. Spodine, Dalton Trans. 2009, 1422; (i) S. Parshamoni, J. Telangae, S. Sanda, S. Konar, Chem. Asian J. 2016, **11**, 540; (j) C. Chen, P. Shen, M. Wan, N. Ding, X. Shi, X. Wang, N. Zhang, Microporous and Mesoporous Mater. 2016, **232**, 167.

[14]   (a) D. Saha, T. Maity, T. Dey, S. Koner, Polyhedron 2012, **35**, 55; (b) D. Saha, D. K. Hazra, T. Maity, S. Koner, Inorg. Chem. 2016, **55**, 5729; (c) A. T. Çolak, F. Çolak, D. Akduman, O. Zafer Yeşilel, O. Büyükgüngor, Solid State Sci. 2009, **11**, 1908.

[15]   APEX 2, SAINT, XPREP, Bruker AXS Inc., Madison, WI, USA, 2007.

[16]   SADABS, Bruker AXS Inc., Madison, WI, USA, 2001.

[17]   SHELXS97: G. M. Sheldrick, Acta Crystallogr. Sect. A 2008, **64**, 112.

[18]   SHELXL-2014/7: G. M. Sheldrick, Acta Crystallogr. Sect. C71, 2015, 3.

Chapter 5
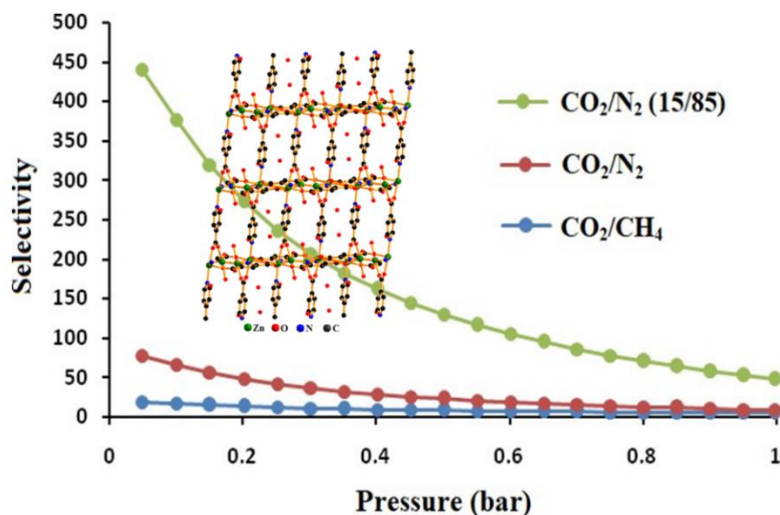
Mixed linker Zn(II)-carboxylate framework compound: synthesis, X-ray structure, preferential CO_2 adsorption, and computational study

5.1 Introduction

Massive emission of anthropogenic carbon dioxide (CO_2) into the atmosphere has become a greatest environmental concern because it is the primary source of greenhouse gas causing climate change and other environmental problems [1-3]. Separation of CO_2 from methane (CH_4) also plays very crucial for upgradation and treatment of biogas to improve purity [4]. In addition, pre-combustion CO_2 capture is essential to separate it from hydrogen (H_2), which is produced by the reaction of primary fuel with oxygen or air [5]. Selective trapping of CO_2 using carbon capture and sequestration (CCS) technologies play a vital role in these issues [6, 7]. Presently, along with traditional CCS methods, use of metal-organic frameworks (MOFs), which is also known as porous coordination polymers (PCPs), have been rapidly emerging as a new type of functional materials for the selective CO_2 adsorption due to the presence of highly ordered pores, large surface areas, and high thermal stability [8-11]. The advantage of PCPs with adjustable pore shape and size, and controllable pore surface properties for specific applications is based on their design strategy, which can be elegantly tuned by judicious selection of metal ions and linkers [12-18]. Selective CO_2 adsorption by the MOF can be achieved by (a) control of pore aperture [19], (b) presence of open metal sites within the pore [20-25], (c) decoration of pore wall by polar functional group [26-29], or by the (d) immobilization of alkali metal ions within the pore [30-32]. The first criterion to make a MOF suitable for selective CO_2 sequestration is to have its pore size and pore aperture commensurate with the kinetic diameters of CO_2 [33, 34]. Nonetheless, it is difficult to achieve the selectivity of CO_2 over N_2 and CH_4 only by the fine control of the pore aperture as their kinetic diameters are very close to each other (CO_2 = 3.30 Å, N_2= 3.65 Å, CH_4 = 3.76 Å). There are only few reported MOFs where selectivity is achieved by merely controlling the pore size. In most of the cases pore size as well as environment together helped in achieving selectivity. Because of having quadrupole moment, CO_2 can efficiently interact with the coordinately unsaturated metal sites present in any MOF. CO_2 uptake capacity of MOFs may be enhanced upon modification of the surface structure of framework by inducting local dipoles which can interact more strongly through non-bonding interaction. Hence, inclusion of electronegative atoms like N, O, or F in the pore structure is an effective means to increase adsorption energies for the molecules like H_2 and CO_2 [35-42]. The potential of fluorine or amine groups to interact with CO_2 has been reasonably exploited in the industry. Chemisorption of CO_2 over amines is being applied as an effective tool for removal of CO_2 from flue gases. It has been suggested that amending of pore surface by decorating Lewis base centers (-amino, -pyrimidine, -hydroxo) enhance low pressure CO_2 uptake as well as isosteric heat of adsorption [36-42]. Studies on synthesis and characterization of MOF were prolific in recent years, however, porous MOF of mixed ligand systems for selective CO_2 adsorption are still scanty in the literature. In this study, adsorption

and storage of small gas molecules in the porous MOF medium have been emphasized. Particularly, designing of MOFs with ability of selective CO_2 adsorption.

To this end, a mixed ligand 3D metal carboxylate framework compound, $[Zn_2(H_2O)(nic)(pzdc)]_n \cdot nH_2O$ (**8**), (H_2pzdc = pyrazole-3,5-dicarboxylic acid and Hnic = isonicotinic acid) (Figure 5.1) has been synthesized. Compound **8** showed very selective CO_2 adsorption with respect to small gas molecules like H_2, N_2, CH_4 at low partial pressure. To get deeper insight into the selective CO_2 adsorption capability of MOF compared to other small gas molecules, Molecular Dynamics and Monte Carlo simulations have been undertaken vis-à-vis consideration of experimental results.

A   B
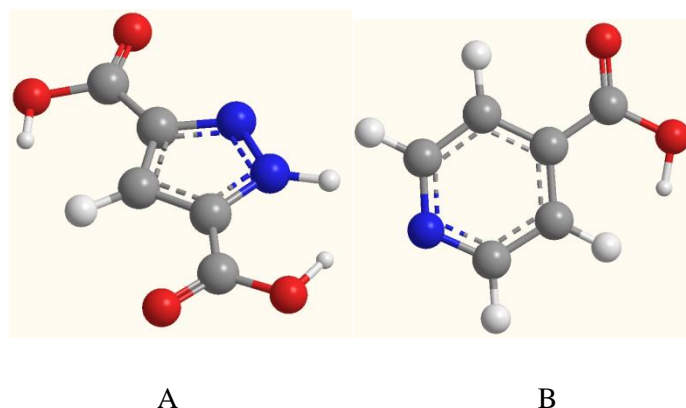
Figure 5.1. Figure shown structure of pyrazole-3,5-dicarboxylic acid (A) and isonicotinic acid (B). Atoms colour code: Nitrogen (blue), Oxygen (red), Carbon (grey) and Hydrogen (white).

5.2 Experimental section

5.2.1 Materials

Zinc(II) nitrate hexahydrate, pyrazole-3,5-dicarboxylic acid and 1,2-bis(4-pyridyl)ethane were purchased either from Sigma-Aldrich or from Merck (India) and were used as received without further purification.

5.2.2 Synthesis of $[Zn_2(H_2O)(nic)(pzdc)]_n \cdot nH_2O$ (8)

Equimolar (0.5 mmol) amount of $Zn(NO_3)_2.4H_2O$, pyrazole-3,5-dicarboxylic acid and 1,2-bis(4-pyridyl)ethane were mixed in milliQ water (8 mL) and stirred for 1 h and it was transferred into a 25 mL teflon-lined autoclave and kept in an oven at 170 °C for 3 days. After slow cooling to room temperature over a period of 8 h, rod-shaped, light-yellow crystals were obtained (84% yield based on metal ion).

Elemental analysis (%) *ca.* for $[Zn_2(H_2O)(nic)(pzdc)]_n \cdot nH_2O$: C 29.89, H 2.05, N 9.51, O 28.96; found: C 29.9, H 2.0, N 9.5, O 28.9. Selected IR peaks (KBr disk, ν, cm^{-1}): 1594, 1559 [ν_{as} (CO_2^-)], 1501 [ν_s (CO_2^-)], 1388, 1343 [ν_s (C–O)], and 3019-3505 s.br [ν_s (O–H)] (Figure 5.2).
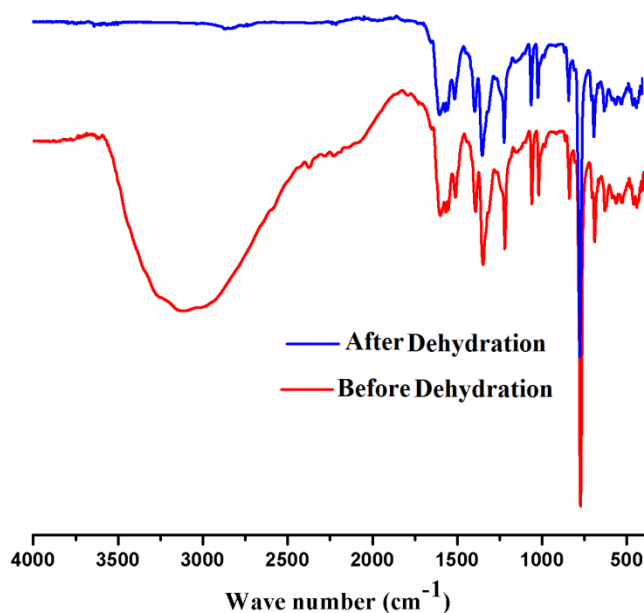
Figure 5.2. IR spectra of the compound 8 before and after dehydration

5.2.3 Physical measurements

All the physical measurements were undertaken by the same instruments as described previously in **Section 2.2.3, Chapter 2.**

5.2.4 X-ray crystallography

X-ray diffraction data for $[Zn_2(H_2O)(nic)(pzdc)]_n \cdot nH_2O$ (**8**) was collected at 180(2) K on a Bruker SMART APEX CCD X-ray single crystal diffractometer using graphite-monochromated Mo-Kα radiation ($\lambda = 0.71073$Å). Determination of integrated intensities and cell refinement were performed with the SAINT [43] software package using a narrow-frame integration algorithm. An empirical absorption correction SADABS [44] was applied. The structure was solved by direct methods and refined using full-matrix least-squares technique against F^2 with anisotropic displacement parameters for non-hydrogen atoms with the programs SHELXS2018 and SHELXL2018 [45]. Two water solvent molecules (O100 and O200) were found to be disordered, and their occupancies were fixed at 0.5 before final refinement. All the hydrogen atoms except the hydrogen at the disordered atom were placed at calculated positions using suitable riding

models with isotropic displacement parameters derived from their carrier atoms. The hydrogen atoms of the water molecules with half occupancy as well as the lattice water (O21) were not taken into account in the structure refinement. In the final difference Fourier maps there were no remarkable peaks except the ghost peaks surrounding the metal centers. A summary of crystal data and relevant refinement parameters for compound $[Zn_2(H_2O)(nic)(pzdc)]_n \cdot nH_2O$ has given in Table 5.1.

CCDC 1006963 contain the supplementary crystallographic data for compound **8**. These data can be obtained free of charge via http:// www.ccdc.cam.ac.uk/conts/retrieving.html, or from the Cambridge Crystallographic Data Centre, 12 Union Road, Cambridge CB2 1EZ, UK; fax: +44 1223 336 033; or e-mail: deposit@ccdc.cam.ac.uk.

Table 5.1. Crystal data and refinement details of $[Zn_2(H_2O)(nic)(pzdc)]_n \cdot nH_2O$

Formula	$C_{11}H_9N_3O_8Zn_2$
Formula Weight	441.95
Crystal System	Monoclinic
Space Group	C2/c
a (Å)	22.8941(17)
b (Å)	11.2210(7)
c (Å)	16.7025(11)
α (°)	90.00
β (°)	127.370(3)
γ (°)	90.00
V (Å^3)	3410.0(4)
Z	8
D_{calc} (gcm^{-3})	1.722
μ (mm^{-1})	2.855
R_{int}	0.0895
Unique data	4204
Data with $I > 2(I)$	3045
R_1 $(I > 2(I))$	0.0632

wR_2 $(I > 2(I))$	0.1962
(GOF) on F^2	1.080

$$R_1 = \sum |(|F_o| - |F_c|)| \,/\, \sum |F_o|, \; wR_2 = \left\{ \sum [w\,(F_o{}^2 - F_c{}^2)^2] \,/\, \sum [w\,(F_o{}^2)^2] \right\}^{1/2}$$

5.2.5 Computational details

Molecular dynamics (MD) and Monte Carlo (MC) simulations of the monoclinic *C2/c* MOF crystal structure (cell formula of $C_{88}H_{72}N_{24}O_{64}Zn_{16}$) was calculated with the GULP and SORPTION program codes of Accelrys, Inc. [46]. The starting experimental crystal optimization, MD and MC simulations were calculated with the Dreiding force-field [47]. It is a diagonal force-field with harmonic potentials terms and a cosine-Fourier expansion torsion term. The umbrella functional form is used for inversions, which were defined according to the Wilson out-of-plane definition. The Lennard-Jones potential described the Van-der Waals interactions. Electrostatic interactions were characterized by atomic monopoles and a screened Coulombic term. An explicit Lennard-Jones 12-10 potential described hydrogen bonding. Materials Studio provides the QEq method for calculating approximate atomic point charges [48]. The CO_2, H_2, N_2, and CH_4 molecules were treated with the same force field and charges method that the MOF structure. The potential parameters and charges used are reported in Table 5.2.

Four MD simulations of 10 ns with CO_2, H_2, N_2, and CH_4 molecules within the MOF structure were simulated with the microcanonical ensemble, respectively. The Verlet leapfrog algorithm was used to integrate the equations of motion with a time step of 1fs. The first 50 ps of the simulation time were spent in equilibrating the kinetic and potential energy distribution before the production phase. Figure 5.3 showed the models, which were fully balanced after 1 ns of the simulation time.

The Metropolis Monte Carlo simulations were carried out with grand canonical ensemble [49]. In this ensemble, the fugacities of all components, volume, as well as the temperature, are fixed. The MOF was in open contact with an infinite sorbate reservoir with a fixed temperature. In this method, the sorbate structure is treated as rigid and only rigid body translations and reorientations are incorporated. Sorbate molecules are allowed to flow in and out the framework to accommodate the fixed fugacity of the reservoir. A fixed pressure simulation closely mimics experimental conditions and allows to calculate the average loading of a sorbate component at a given fugacity and temperature. Adsorption isotherm calculation is essentially performed by using a series of fixed pressure simulations with the grand canonical ensemble where the fugacity is steadily ramped up over the series. Simulations were carried out for a total of 10^6 cycles, in which the first 10^5 cycles were used for equilibration.

Table 5.2. Calculated parameters of MOF-CO_2 (lengths in Å, angles in degrees) from 0 to 100 bars of pressure

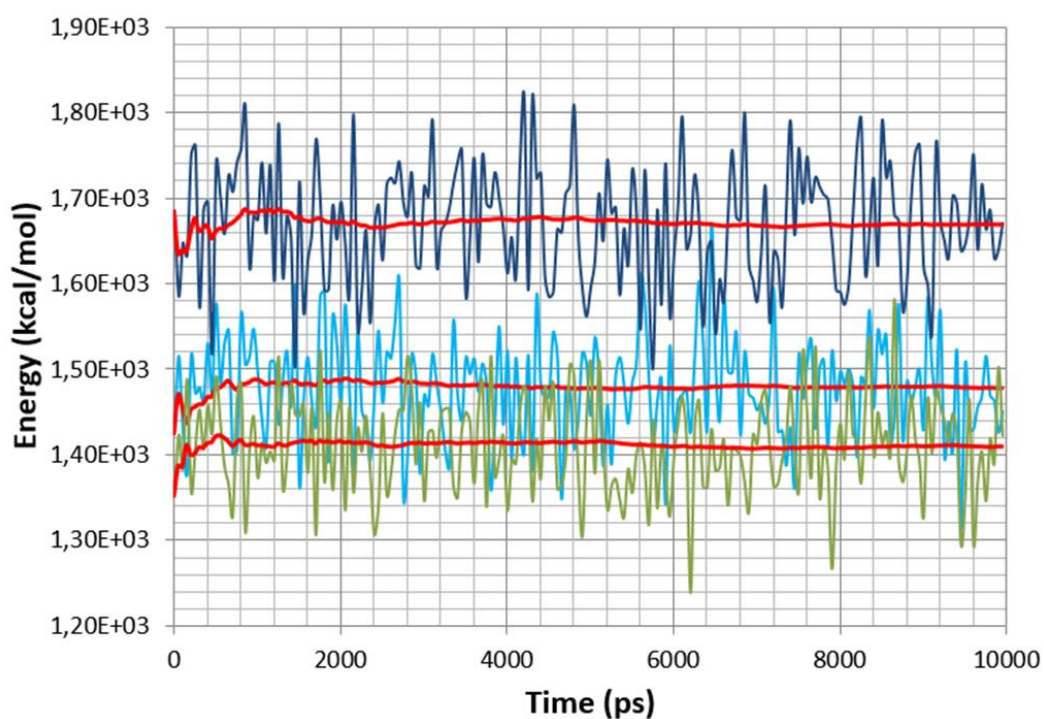| P (bar)	1	50	100
a (Å)	22.89	22.24	22.04
b (Å)	11.22	10.88	10.79
c (Å)	16.70	16.36	16.33
α (°)	90.0	90.2	90.2
β (°)	127.4	127.6	127.8
γ (°)	90.0	90.3	88.0

Figure 5.3. Total internal energies of the MOF-H_2 (green), MOF-N_2 (purple) and MOF-CO_2 (blue) during 10 ns of MD simulations. The red lines are the average of the series showed in colours.

5.3 Results and discussion

5.3.1 Synthesis and characterization

The compound have been designed based on pillar-layer technique where pyrazole-3,5-dicarboxylic acid have been chosen to achieve metal-carboxylate layers and 1,2-bis(4-pyridyl)ethane as N,N'-donor auxiliary ligand or spacer to extend the layers into 3D porous framework. Pyrazole-3,5-dicarboxylic acid has multiple donor sites with both oxygen and nitrogen donor atoms and it also has versatile binding modes which makes it very useful to get a 2D layered network in presence of another ligand having two donor sites at opposite direction. But the problem of use of very long spacer is the interpenetration which makes the framework unsuitable for gas adsorption. In this case 1,2-bis(4-pyridyl)ethane oxidised to isonicotinate in the reaction medium. This conversion from 1,2-bis(4-pyridyl)ethane to isonicotinate helped to get a desired porous 3D framework without any interpenetration. Mere use of isonicotinate instead of 1,2-bis(4-pyridyl)ethane does not afford any stable framework compound.

5.3.2 Crystal structure of $[Zn_2(H_2O)(nic)(pzdc)]_n \cdot nH_2O$ (8)

Compound **8** crystallized in a monoclinic space group *C2/c* with *Z* = 8. Selected bond distances and angles are collated in Table 5.3. The asymmetric unit of $[Zn_2(H_2O)(nic)(pzdc)]_n \cdot nH_2O$ contains two Zn(II) ion, one pyrazole-3,5-dicarboxylate linker (pzdc), one isonicotinate linker (nic), one coordinated water molecule and one crystalline water molecule. The ORTEP diagram is given in Figure 5.4. Both metal centers (Zn1 and Zn2) of compound **8** are hexa-coordinated with distorted octahedral geometry (Figure 5.5). Zn1 center is surrounded by four carboxylato oxygen atoms, three (O1, O11[a] and O11[b]; a = x, -y, -1/2+z; b = 1/2-x, 1/2+y, 1/2-z) from three different pyrazole-3,5-dicarboxylate (pzdc) linker and one (O12) from isonicotinate (nic) linker and other two positions are occupied by two nitrogen atoms, N6 and N18 from pzdc and nic linker respectively. Whereas, Zn2 center contains four carboxylato oxygen atoms (O1, O2, O10 and O13) linked in same fashion as in Zn1 center and one nitrogen atom (N5) from pzdc linker along with a water molecule. Here two carboxylate group of two different pzdc molecules and one carboxylate group of nic molecule connect two Zn(II) centers in $\mu_{1,3}$, $\mu_{1,1}$, and $\mu_{1,3}$ fashion respectively, forming a dinuclear secondary building unit (SBU), and each dinuclear core connected by the pyrazole-3,5-dicarboxylate to form 2D sheet arrangements (Figure 5.6) along the crystallographic *ac* plane. Each 2D sheet is further pillared by isonicotinate linker resulting in 3D pillared networks (Figure 5.7). The three-dimensional structure of compound **8** contained water filled channels parallel to crystallographic *b*-axis. Coordinated water molecules are pointed towards the interior of the channels. Upon removal of the water molecules the framework featureed channels along *c*-axis of dimension about 8.5×4.5 Å^2 and along *b*-axis

of dimension about 9×7 Å^2, with the open metal sites exposed to the pores. After the removal of the lattice water molecules void space enhanced from 15.9% to 30.2% with respect to the total crystal volume as estimated by PLATON and further removal of coordinated water molecules the value again enhanced to 34.1% with the open metal sites exposed to the pores [50].

To understand the structure of compound **8** further, a topological analysis was performed by reducing the multidimensional structure to a simple node-and-linker net. Topological analysis by TOPOS revealed that the compound possessed a simple 3-nadal 2,4,6-c 3D net structure (Figure 5.8) consisting of nic linker as two-coordinated node, pzdc linker as four-coordinated node and Zn dimers as six-coordinated node [51].
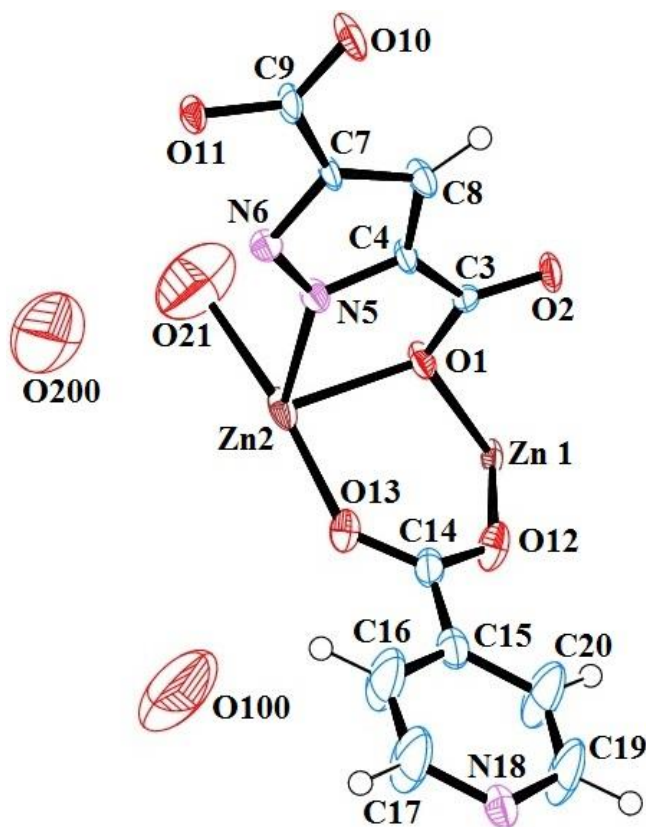
Figure 5.4. ORTEP diagram of [Zn₂(pzdc)(nic)]ₙ·nH₂O with 40% ellipsoid probability
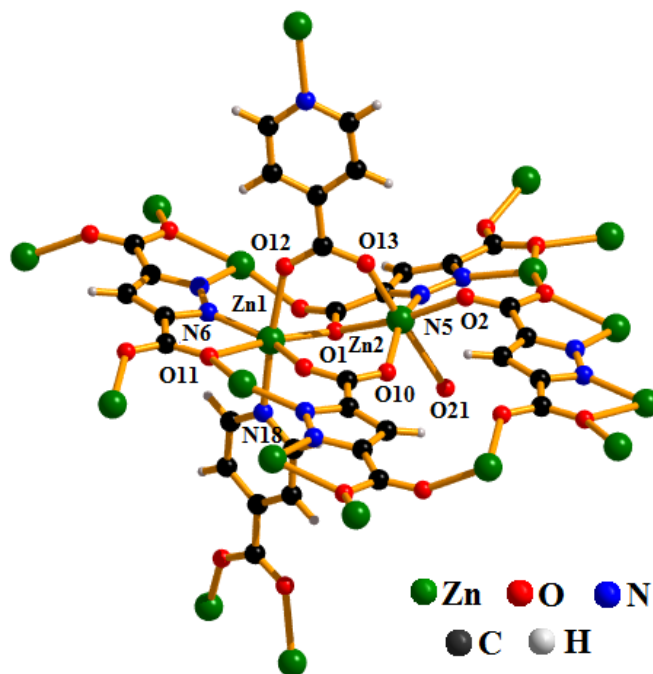
Figure 5.5. Network connectivity of [Zn₂(H₂O)(nic)(pzdc)]ₙ·nH₂O.
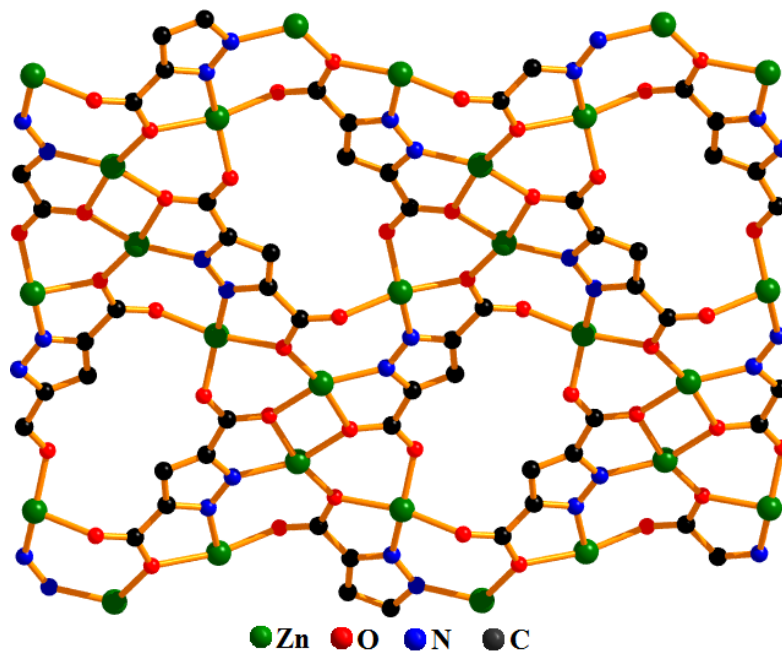
Figure 5.6. 2D arrangement in [Zn₂(H₂O)(nic)(pzdc)]ₙ·nH₂O along crystallographic *ac* plane.
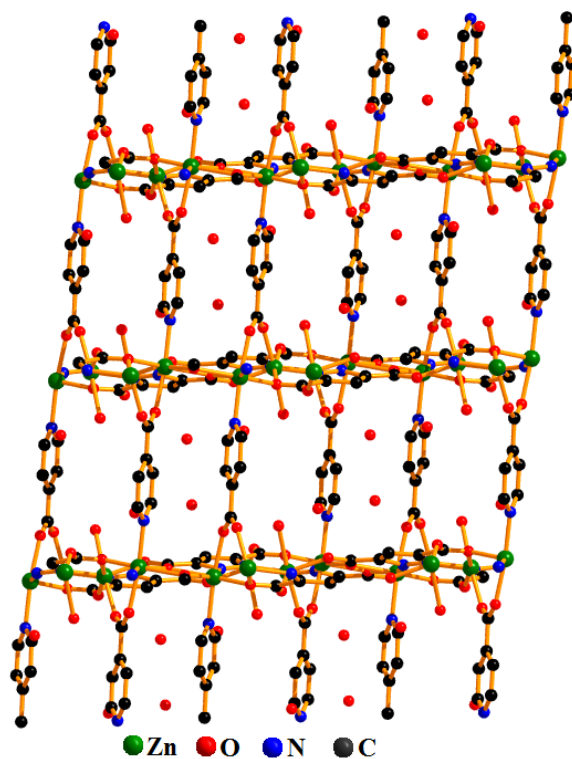
Figure 5.7. 3D network in [Zn$_2$(H$_2$O)(nic)(pzdc)]$_n$·nH$_2$O with water filled 1D channels along crystallographic *b*-axis.
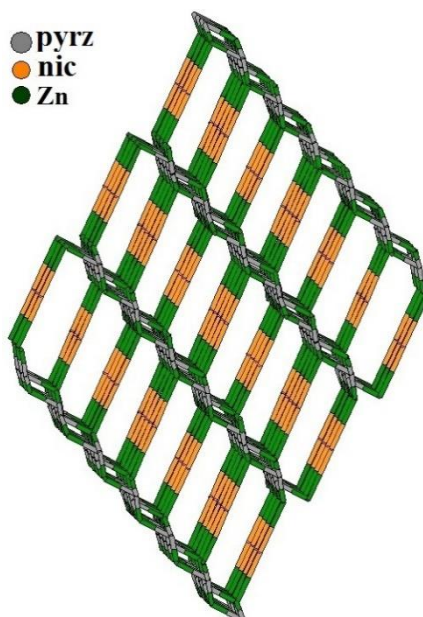
Figure 5.8. Topological view of the 3D nets of [Zn$_2$(H$_2$O)(nic)(pzdc)]$_n$·nH$_2$O along crystallographic *b*-axis.

Table 5.3. Selected bond lengths (Å) and angles (°) of [Zn$_2$(H$_2$O)(nic)(pzdc)]$_n$·nH$_2$O

Zn1–O1	2.057(6)	Zn2–O1	2.185(5)
Zn1–O12	2.150(7)	Zn2–O13	2.035(7)
Zn1– O11^a	2.069(5)	Zn2–O21	2.388(15)
Zn1– O11^b	2.296(6)	Zn2–N5	2.014(7)
Zn1– N6^b	2.047(6)	Zn2–O10^a	1.994(6)
Zn1– N18^c	2.155(7)	Zn2–O2^d	2.074(5)
O1–Zn1–O12	84.9(2)	O1–Zn2–O13	89.8(2)
O1–Zn1–O11^a	95.7(2)	O1–Zn2–O21	95.7(4)
O1–Zn1–O11^b	168.56(18)	O1–Zn2–N5	76.0(2)
O1–Zn1–N6^b	116.6(2)	O1–Zn2–O10^a	97.23(18)
O1–Zn1–N18^c	88.7(2)	O1–Zn2–O2^d	168.3(2)
O11^a–Zn1–O12	88.9(2)	O13–Zn2–O21	173.1(4)
O11^b–Zn1–O12	95.2(2)	O13–Zn2–N5	107.5(3)
O12–Zn1–N6^b	86.7(2)	O10^a–Zn2–O13	97.3(3)
O12–Zn1–N18^c	173.5(3)	O2^d–Zn2–O13	88.2(2)
O11^a –Zn1–O11^b	72.9(2)	O21–Zn2–N5	78.0(4)
O11^a–Zn1–N6^b	146.8(3)	O10^a–Zn2–O21	78.0(4)
O11^a–Zn1–N18^c	93.1(2)	O2^d–Zn2–O21	87.3(4)
O11^b–Zn1–N6^b	74.8(2)	O10^a–Zn2–N5	154.1(3)

O11^b–Zn1–N18^c	91.4(2)	O2^d–Zn2–N5	93.6(2)
N6^b–Zn1–N18^c	95.0(2)	O2^d–Zn2–O10^a	94.5(2)

a = x, -y, -1/2+z; b = 1/2-x, 1/2+y, 1/2-z;

c = -1/2+x, 1/2-y, -1/2+z; d = 1/2-x, -1/2+y, 1/2-z.

5.3.3 TG-DTA analysis

Thermogravimetric analysis (TGA) and differential thermal analysis (DTA) were carried out to study the stability of the framework. Thermal analysis of compound **8** was performed using powdered sample from room temperature to 800 °C under nitrogen atmosphere (Figure 5.9). Compound **8** showed a two-stage mass loss. At the first step, upon heating a sharp mass loss of 7.8% from 28–68 °C was observed with the theoretical value of 8.15% owing to loss of one lattice and one coordinated water molecule. Desolvated framework is then thermally stable up to 270 ℃. On further heating compound decomposed steadily. The corresponding DTA curve showed two endothermic peaks at *ca.* 55 and 490 ℃ for the loss of water molecules and for decomposition of the compound, respectively.
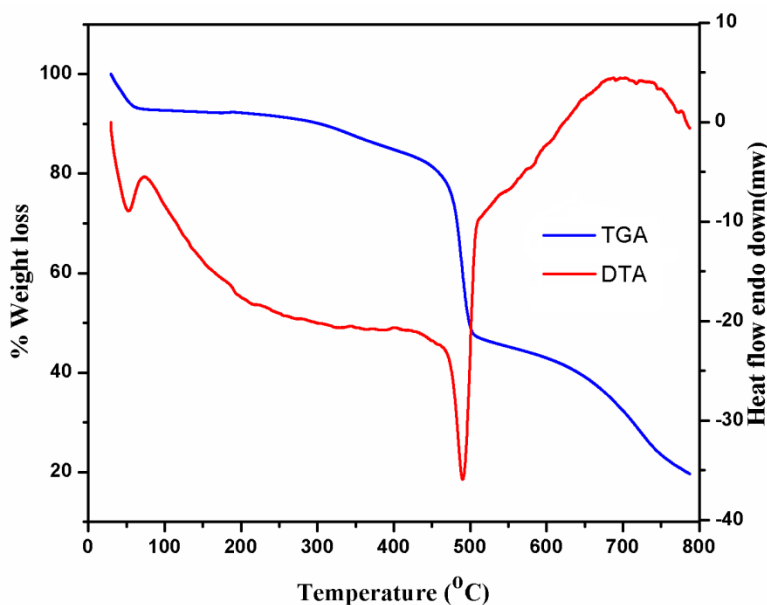

Figure 5.9. TG-DTA plots of [Zn₂(H₂O)(nic)(pzdc)]ₙ·nH₂O.

5.3.4 PXRD study

To confirm the phase purity of the bulk material of compound **8**, powder X-ray diffraction (PXRD) measurements were carried out. The PXRD patterns of the compound are shown in Figure 5.10. X-ray powder diffraction patterns of compound **8** were simulated using their single crystal data. Comparison of experimental and simulated PXRD patterns showed that all the major peaks of experimental PXRD of compound **8** matched well with those of simulated ones, indicating their reasonable crystalline phase purity. TG analysis clearly indicated that upon heating compound **8** lost all water molecules to produce a dehydrated product which is stable up to 270 °C. For PXRD measurement of dehydrated variety, required amount of dehydrated product of compound **8** has been collected from the TG analyzer in several batches after heating up to 270 °C. Dehydration can also be performed by heating compound **8** at 100 °C under vacuum (10^{-3} Torr) for 1 h (conditions used for activation to gas adsorption experiments). Dehydration of compound **8** was further confirmed by IR spectral analysis and elemental analysis (Figure 5.2) (Anal. for dehydrated product of compound **8**; C = 32.55, H = 1.24, N = 10.35, O = 23.65 found C = 32.58, H = 1.26, N = 10.31, O = 23.69). PXRD patterns of the calcined species is slightly shifted to a lower *2θ* angle, indicating a slight elongation of the unit cell, but is largely unchanged, suggesting the robustness of the framework, after dehydration. PXRD patterns of the as-synthesized and dehydrated compound are retained upon prolonged storage (at least 6 months). No significant changes of the PXRD patterns of the as-synthesized and dehydrated compounds are observed upon exposure to water. Variable temperature PXRD patterns were also measured for compound **8** up to 250 °C (Figure 5.10). In-situ variable temperature PXRD measurement also revealed that framework structure of the compound is stable enough up to 250 °C. The framework structure also retained after gas adsorption study.
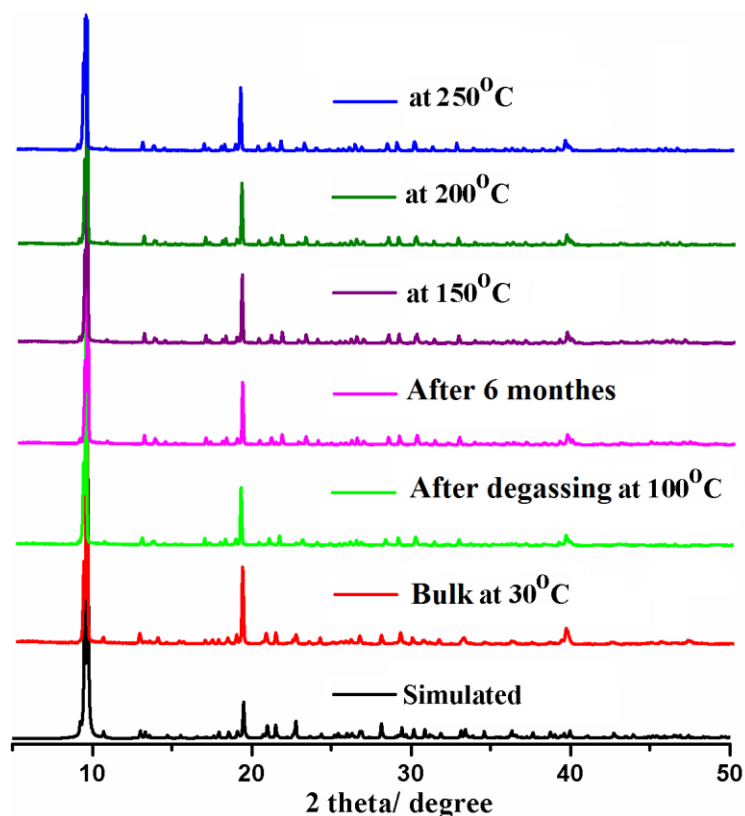
Figure 5.10. PXRD patterns of compound 8.

5.3.5 Gas sorption studies

Gas sorption isotherms for N_2 (77 K), H_2 (77 K), CO_2 (273 K and 298 K) and CH_4 (273 K and 298 K) in the pressures range 0–1 bar was measured with an Autosorb iQ (Quantachrome Inc., USA) gas sorption system with an ultrahigh pure (99.999% purity) gas source. Samples were evacuated under a dynamic vacuum (10^{-3} Torr) at the desired temperature (100 °C). For all isotherms, warm and cold free-space correction measurements were performed with ultrahigh pure He gas (99.999% purity). Prior to all the measurements, the samples (~150 mg) were activated under vacuum for 3h at 90°C.

$[Zn_2(H_2O)(nic)(pzdc)]_n \cdot nH_2O$ as well as its dehydrated analogue contain solvent accessible voids. Their pore sizes are bigger than the kinetic diameter of N_2, CO_2, CH_4 and H_2. Thus, to evaluate the porosity and the adsorption capability of compound **8**, N_2, H_2, and CO_2 adsorption measurements of the compound were carried out. Compound **8** was found to be very selective towards CO_2 capture compared to N_2, CH_4 and H_2. Even the dehydrated compound adsorbed very small amount of N_2, CH_4 and H_2 at low partial pressure (~1 bar) (Figure 5.11).

Figure 5.11. Gas adsorption (filled) and desorption (open) curve by the dehydrated compound.
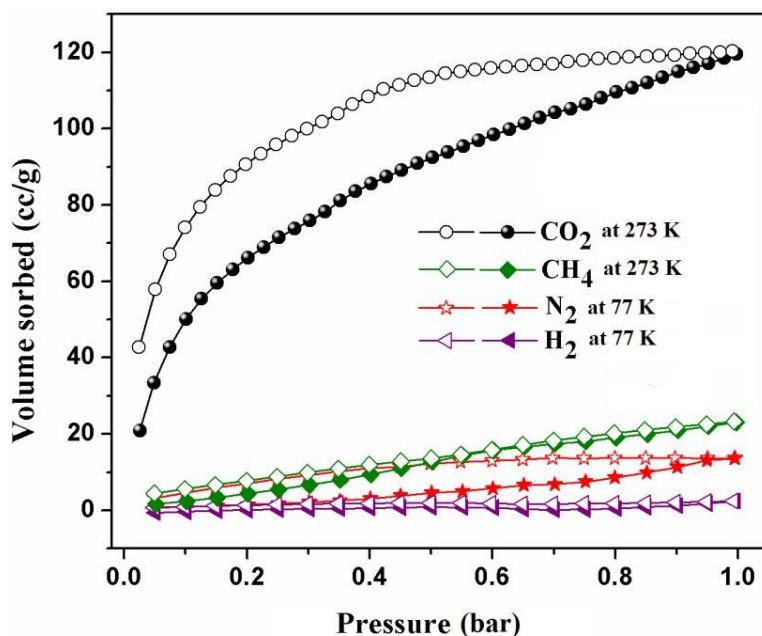
For post-combustion CO_2 capture, the pressure of the flue gas (~1 bar) and the low partial pressure of CO_2 (0.15 bar) thereof leads to the lower-pressure region of the CO_2 adsorption isotherm being the area of interest [52]. CO_2 adsorption isotherms for the as-synthesized (without any activation) and dehydrated compound were measured at 273 K and 298 K up to 1 bar pressure (Figure 5.12). CO_2 adsorption of compound **8** showed type I isotherms. Gas uptake of the as-synthesized (without usual activation) and dehydrated compound was 5.6 and 11.7 wt% at 0.15 bar and 10.2 and 23.6 wt% at 1 bar respectively, at 273 K. At 298 K, the as-synthesized and dehydrated compound showed an uptake of 2.2 and 5.7 wt% at 0.15 bar and 5.3 and 12.2 wt% at 1 bar, respectively. Steepness of the slope in the low-pressure part of the isotherms indicates strong adsorption. The presence of hysteresis in adsorption-desorption isotherm also indicated the presence of strong interaction of CO_2 with the surface of compound **8**. The selective CO_2 adsorption capacity of the activated compound was measured with respect to N_2, H_2 and CH_4, compared (Table 5.4) with other reported 3D-porous MOFs [53-67]. The selective CO_2 uptake capacity of activated compound was higher than that observed in some of the other MOFs [53-61]. There are few recent reported MOFs in which the values are higher than that of compound **8** [62-66]. It is noteworthy that Zn-MOF was highly selective towards CO_2 adsorption over all three small gas molecules (H_2, N_2, CH_4) at low partial pressure. High selectivity of CO_2 by the PCPs over multiple gas molecules are scanty in literature [67, 68].

The stable three-dimensional magnesium(II) and calcium(II) PCPs synthesized using a neutral ligand are very selective in carbon dioxide adsorption and separation of small gas molecules [67]. Preferential CO_2 adsorption by the 2D Cu(II) PCP have been achieved due to the strong interaction of CO_2 with the pore wall decorated by the fluorinated anions [68]. Selectivity of activated compound **8** was calculated using the ratio of the initial slopes in the Henry region of the CO_2 and CH_4 adsorption isotherms at 273 K. Selectivity of CO_2 with respect to CH_4 at 273 K is calculated to be 22.4 (Figure 5.13). IAST selectivity also has been simulated on the basis of pure gas sorption data (Figure 5.14). Heat of adsorption calculated for deactivated and dehydrated compound using DFT model with respect to the CO_2 isotherms of 298 K and 273 K was 23.40 kJ/mol and 50.57 kJ/mol, respectively at 0.84 mmol/g and 0.51 mmol/g loading (Figure 5.15). At higher loading these values fall slightly as the highest affinity sites are filled. The isosteric heat of adsorption for CO_2 reported in this work is compared with the literature values (Table 5.5) [63-69].
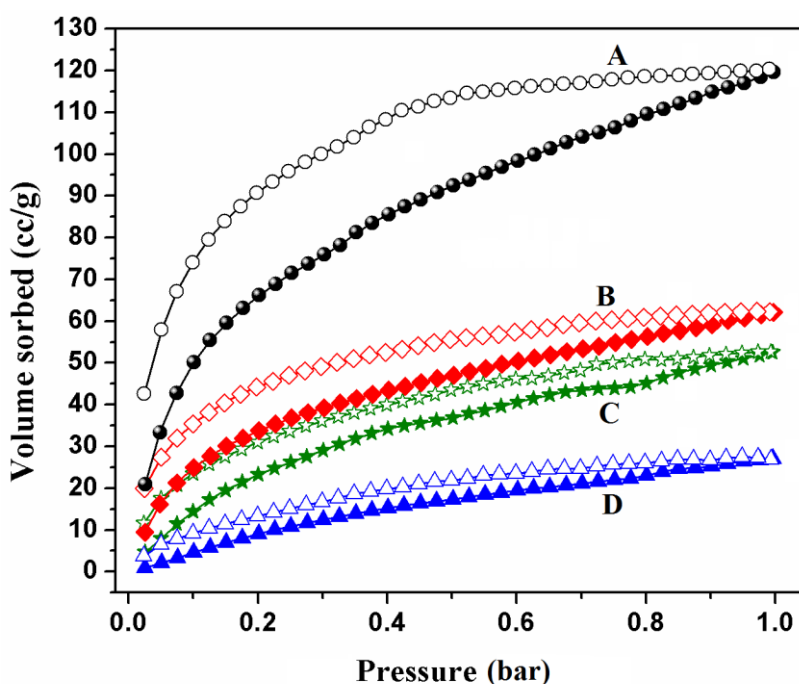

Figure 5.12. CO_2 adsorption (filled) and desorption (open) curve of dehydrated compound at (A) 273 K and (B) 298 K and compound 8 without any activation at (C) 273 K and (D) 298 K.
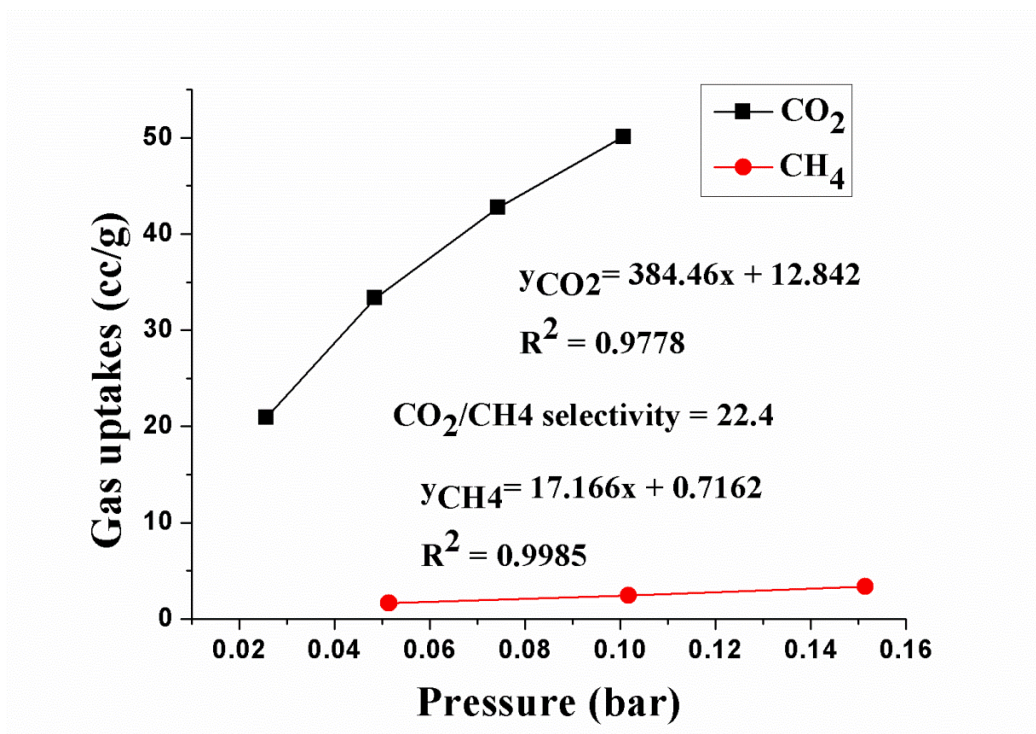
Figure 5.13. CO2/CH4 selectivity of activated compound at 273 K.
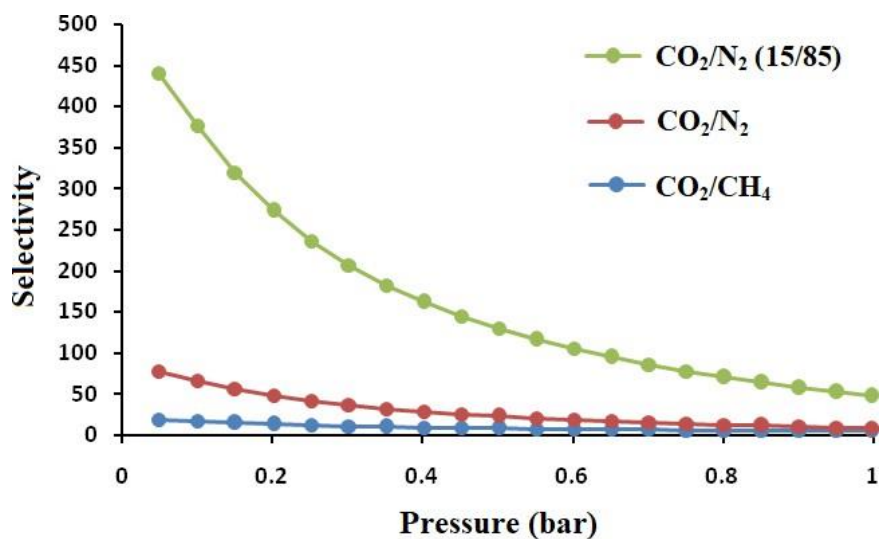
Figure 5.14. Simulated IAST selectivity based on gas sorption.
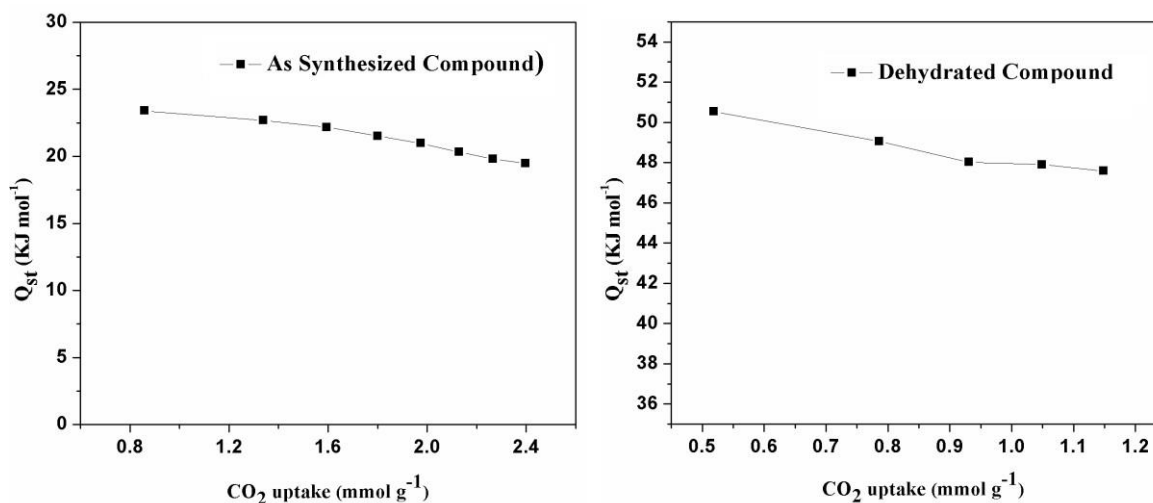
Figure 5.15. Isosteric heat of adsorption for CO2 adsorption calculated using DFT model for compound without any activation (left) and activated (right) compound.

Table 5.4. Comparison of gas uptake ability of different 3D-microporous MOFs*

MOFs	Surface area from N_2 adsorption [$m^2 g^{-1}$] BET	H_2 uptake [wt %] at 1 bar at 77K	CH_4 uptake [wt %] at 1 bar at 298 K	CO_2 uptake [wt %] at 1 bar			Ref.
				195K	273K	298K	
Compound **8** (activated)	_	_	0.5	_	23.6	12.2	this study
[Zn₂(NH₂PDC)₂(dpNDI)]ₙ	89.7	_		_	6.6	5.6	53
[Cu(bcppm)H₂O]	_	_		_	8.14	7.62	54
{[Zn₃(bpy)₃(H₂O)₂][Fe(CN)₆]₂·2(bpy)·3H₂O}ₙ	_	0.47		_	5.89	4.71	55
{[Zn₃(azpy)₂(H₂O)₂][Fe(CN)₆]₂·4H₂O}ₙ	_	0.7		_	7.46	5.89	55
{[Cd₂(sdb)₂(3-bpmh)₂]}ₙ·3n(H₂O)·n(C₆H₅NO)	_	_		11.96	7.5	5.7	56
[{Co(muco)(bpa)(2H₂O)}·2H₂O]ₙ	_	_		_	7	4.9	57
[Zn₂(imtha)₂]·2DMA·3H₂O	_	1.18		41	10.29	5.36	58

[Mg$_{16}$(PTCA)$_8$(μ$_2$-H$_2$O)$_8$(H$_2$O)$_{16}$(dioxane)$_8$].(H$_2$O)$_{13}$.(DMF)$_{26}$	438.1	0.83		31.52	8.68	4.63	59
[Zn$_2$(3,3′-PDBA)$_2$(DABCO)$_{1.5}$]·2DMF·H$_2$O	-	0.07		8.21	3.87	2.3	60
{[Cd(BIPA)(HIPA)]·DMF}n	-	-		-	21.7	-	61
PCN-124-stu(Cu)	2153	_		_	31.42	16.85	62
IISERP-MOF20, 2D Cu based ultramicroporous MOF	945	-		39.6	-	15.4	63
[Zn$_2$(tdc)$_2$dabco]	-	2.23		-	30	13.2	64
SIFSIX-2-Cu-i	-	-	0.75	-	-	23.8	65
Mgdobdc	-	-	1.78	-	-	35.2	66
{[Mg$_2$(BDC)$_2$(bpdo)]·2DMF}$_n$	-	-	1.50	-	-	12.99	67[#]

*Ligand used: [53] 2-aminoterephthalic acid (NH$_2$PDC) and N,N′-di(4-pyridyl)-1,4,5,8-naphthalenediimide (dpNDI), [54] Bis(4-(4-carboxyphenyl)-1H-pyrazolyl)methane (H$_2$bcppm), [55] 4,4′-bipyridyl (bpy), 4,4′-azobipyridyl (azpy) and [Fe(CN)$_6$]$^{3-}$, [56] 4,4′-sulfonyl dibenzoic acid (sdb), N,N-bis-pyridin-3-ylmethylene-hydrazine (3-bpmh) and 3-pyridinecarboxaldehyde (C$_6$H$_5$NO), [57] Trans, trans-muconatedianion (muco) and 1,2-bis(4-pyridyl)ethane (bpa), [58] 2-(imidazol-1-yl)terephthalic acid (H$_2$imtha), [59] Pyrene-1,3,6,8-tetracarboxylic acid (H$_4$PTCA), [60] 3,3′-(pyrazine-2,5-diyl)dibenzoic acid (3,3′-PDBA) and 1,4-diazabicyclo[2.2.2]octane (DABCO), [61] bis(4-(1H-imidazol-1-yl)phenyl)amine) (BIPA) and 5-hydroxyisophthalic acid (H$_2$HIPA), [62] 5,5′-(pyridine-3,5-dicarbonyl)bis(azanediyl)di-isophthalic acid, [63] 2-(4-carboxyphenyl)-1H-benzo-[*d*]imidazole-5-carboxylate, [64] Thiophene-2,5-dicarboxylic acid (H$_2$tdc) and 1,4-diazabicyclooctane (dabco), [65] SIFSIX-2-Cu-i is composed of doubly interpenetrated nets that are isostructural to the nets in SIFSIX-2-Cu where SIFSIX-2-Cu refer to [Cu(dpa)$_2$(SiF$_6$)]$_n$ (4,4′-dipyridylacetylene (dpa)), [66] 2,5-dihydroxyterephthalic acid (H$_4$dobdc). [67] 1,4-benzenedicarboxylic acid (H$_2$BDC) and 4,4′-bipyridine-N,N′-dioxide (bpdo). [#]The values are given at a pressure near to 1 bar.

Table 5.5. Comparison of isosteric heat of adsorption (Q$_{st}$) for CO$_2$ in different MOFs at low CO$_2$ loading

MOFs	Q$_{st}$ (kJ/mol)	Ref.
Compound **8** without any activation	23.40	this study
Compound **8** (activated)	50.57	this study

IISERP-MOF20, 2D Cu based ultramicroporous MOF	26	63
SIFSIX-2-Cu	22	65
SIFSIX-2-Cu-i	31.9	65
SIFSIX-2-Zn	45	65
Mgdobdc	47	66
Nidobdc	41	66
Codobdc	37	66
$\{[Mg_2(1,4\text{-bdc})_2(bpdo)]\cdot 2DMF\}_n$	34.9	67
$[Cu(PF_6)_2(4,4'\text{-bpy})_2]_n$	31	68
$[Cu_3(BTC)_2]_n$	35	69

Ligand used: [68] 4,4′-bipyridine (bpy), [69] 1,3,5-benzenetricarboxylate (BTC). Other ligands are same as in Table 5.4.

5.3.6 Computational studies

A previous geometric optimization for each of the models studied (MOF-CO$_2$, MOF-H$_2$, MOF-N$_2$ and MOF-CH$_4$) was performed starting from the experimental crystal structure and including a CO$_2$, H$_2$, N$_2$ or CH$_4$ molecule. Figure 5.16 showed the isonicotinic acid bridges disposition between Zn layers in each crystal MOF channel (Figure 5.16A-C). Red arrows in Figure 5.16D showed that the possible diffusion ways of the gas molecule, through the 001 and 010 faces of the crystal. Later molecular dynamics simulations have been used to investigate the MOF modifications during a certain time. At that time, the presence of rotations of the aromatic plane formed by the isonicotinic acid bridged between the Zn layers have been observed. In Table 5.6, a polar diagram of the changes undergone by each molecule bridge (A-D) has shown throughout the time of the simulation. Each dot represented the dihedral angle formed by the aromatic ring with respect to the layers of Zn to which they are attached. These rotations are performed synchronously with the rest of the bridge molecules found in the MOF. The arrangement of the four-bridge molecules averaged over the entire time of the MD can be seen schematically in Figure 5.17B.
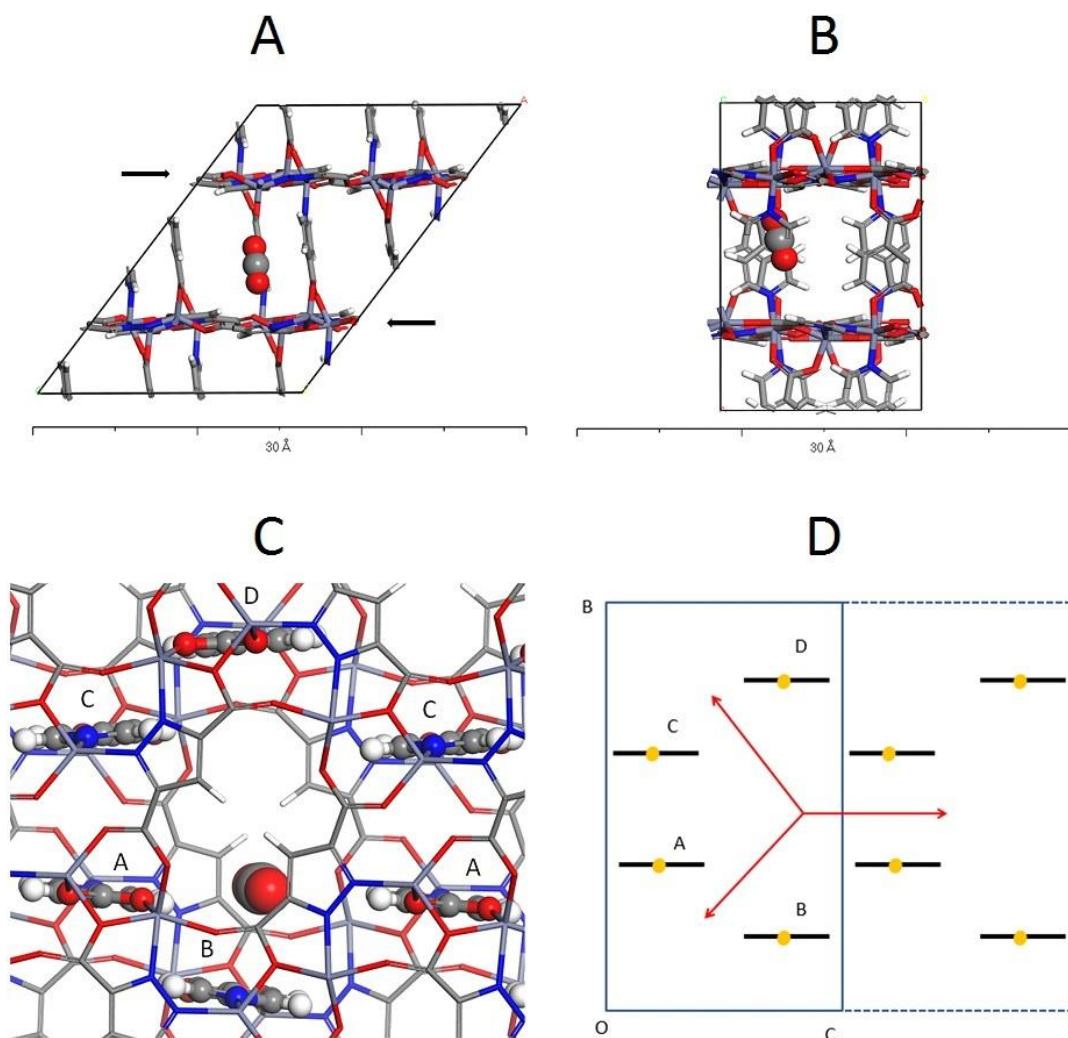
Figure 5.16. A) and B) Snapshots of the 010 and 001 miller planes of MOF-CO₂. The CO₂ is represented with CPK balls. Black arrows shows the Zn layers into the crystal structure. C) Snapshots of the 100 miller plane of the MOF-CO₂. Only the atoms between the layers of Zn are showed. The aromatic parts of the A, B, C and D isonicotinic acid are represented in ball and sticks, the Zn layers are only sticks and CO₂ is only CPK balls. D) Schematic representation of the Figure C. The aromatic rings of the isonicotinic acid molecules are represented as black lines. The yellow dot represents the rotation axis of each molecules represented (A, B, C or D) within each unit cell. The contiguous cell is represented by dotted lines. The red arrows represent the possible routes of diffusion of water molecules or gases within the MOF. Atoms colour code: Nitrogen (blue), Oxygen (red), Carbon (grey), Hidrogen (white) and Zn (purple).

Table 5.6. Evolution of the dihedral angle in the molecular dynamics simulations. Each point of each diagram represents the dihedral angle of the aromatic part of each isonicotinic acid molecule (A-D, see Figure 5.16) with the layer of Zn where it is bound in a simulation time. The time is a picosecond.

	CO_2	H_2	N_2	CH_4
A				
B				
C				
D				
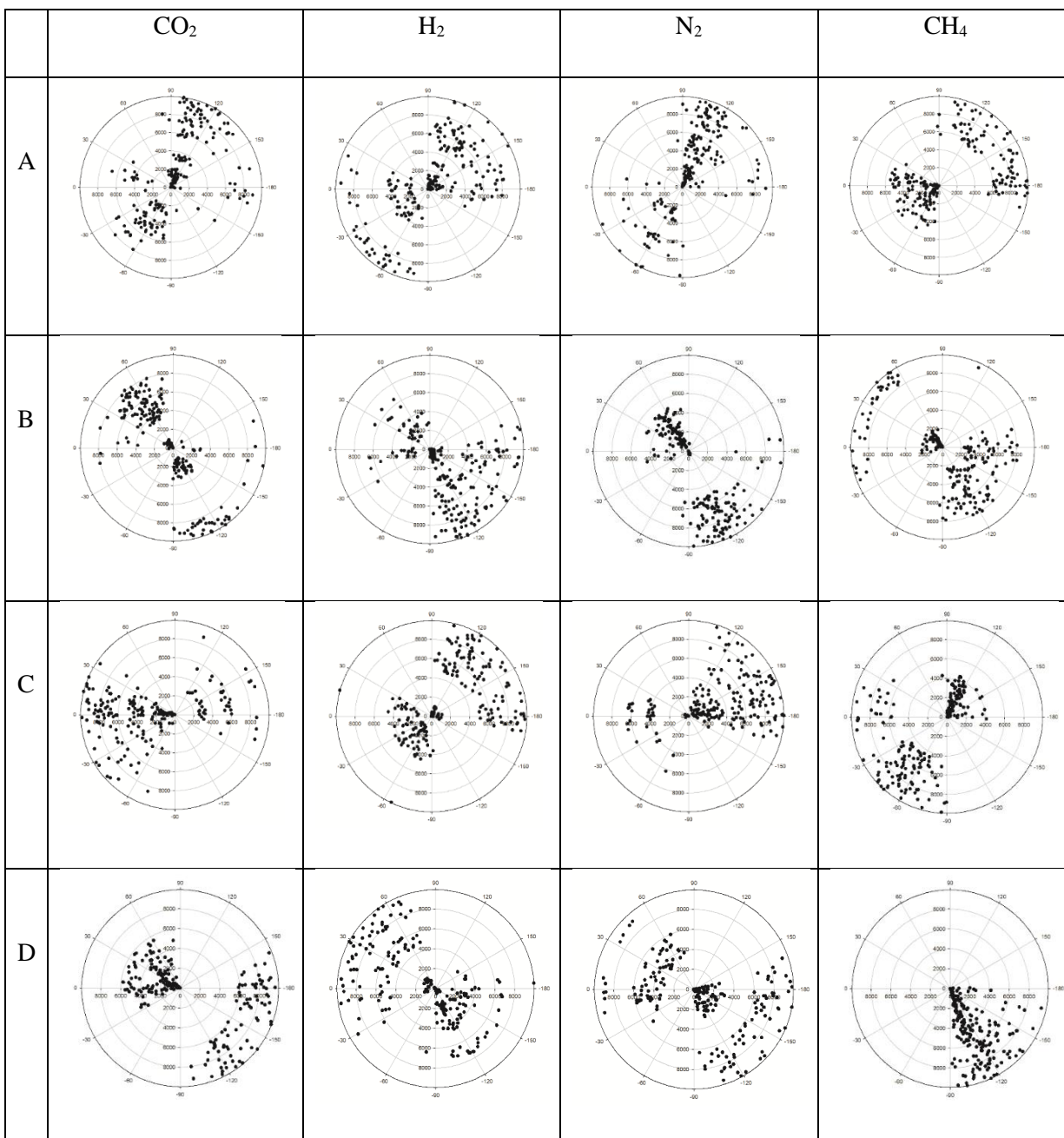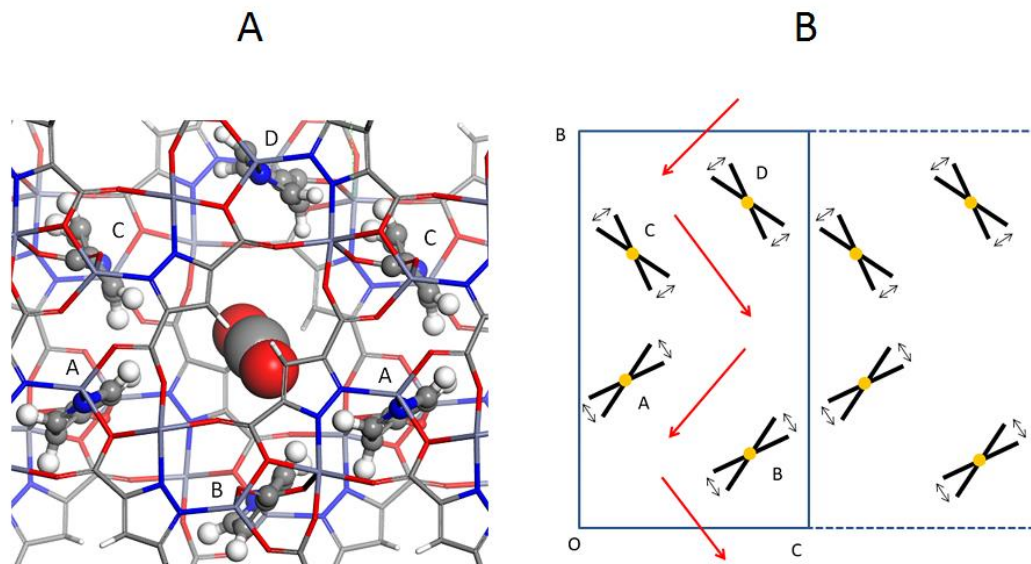
Figure 5.17. A) Snapshots of the 100 miller plane of the MOF-CO$_2$. Only the atoms between the layers of Zn are showed. The aromatic parts of the A, B, C and D isonicotinic acid are represented in ball and sticks, the Zn layers are only sticks and CO$_2$ is only CPK balls. B) Schematic representation of the Figure B. The aromatic rings of the isonicotinic acid molecules are represented as black lines. The yellow dot represents the rotation axis of each molecules represented (A, B, C or D) within each unit cell. Black arrows show the angle range in the MD simulations. The contiguous cell is represented by dotted lines. The red arrows represent the possible routes of diffusion of water molecules or gases within the MOF. Atoms colour code: Nitrogen (blue), Oxygen (red), Carbon (grey), Hydrogen (white) and Zn (purple)

Figure 5.18. Adsorption isotherms obtained using Grand Canonical Monte Carlo simulation for the MOF-CO_2 (black line), MOF-CH_4 (red line), MOF-N_2 (green line) and MOF-H_2 (blue line) systems at 273 K.
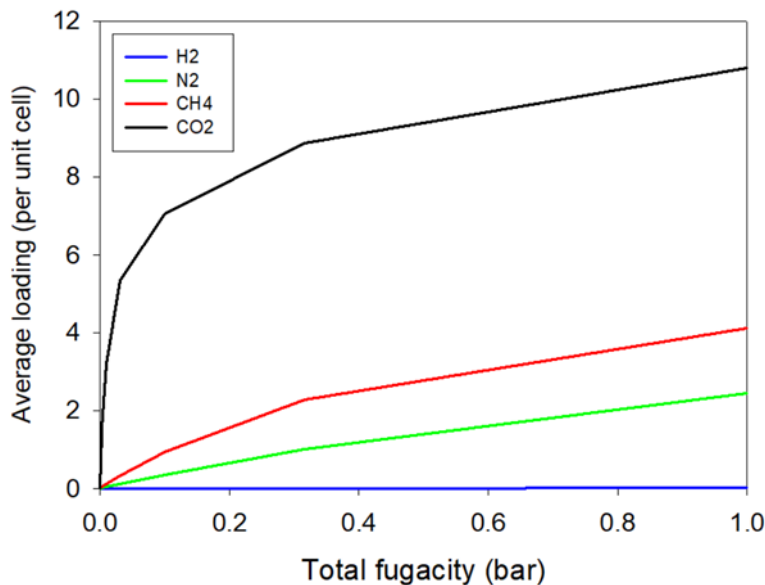
As can be seen in Table 5.6 and Figure 5.17 the spatial arrangement of the four bridges per unit cell of the MOF is common and independent of the introduced gas. The synchronized rotations of the aromatic part of the organic bridges were able to form a hexagonal encapsulation within the Zn layers (Figure 5.17B).

Starting from a repressive snapshot of the full molecular dynamics, the calculation of the adsorption isotherm with grand canonical Monte Carlo simulation for the MOF-CO_2, MOF-H_2, MOF-N_2 and MOF-CH_4 systems was performed. This type of calculation allowed to characterize the affinity of a specific sorbate component toward a framework and can be directly compared with experimental results. In this case and as shown in Figure 5.18 a great concordance has been found between the theoretical and experimental results. As can be observed, the MOF-CO_2 system is the one that presented higher adsorption even at low pressures (~ 10.7 molecules average loading per unit cell at 1 bar of pressure) being the MOF-H_2 system (~ 0.0 molecules loading per unit cell at 1 bar pressure) the worst. The adsorption capacity between compounds was also correctly characterized, being the same as that found experimentally (MOF-CO_2 > MOF-CH_4 > MOF-N_2 > MOF-H_2).

These results are qualitatively similar to those found by MD, where a comparison of the MD showed that in the case of MOF-CO_2, the CO_2 is retained in the whole time of the simulation in the formed packaging. However, the molecules of H_2, N_2 and CH_4 can move freely through the channel formed between layers of Zn without being retained. Differences between MOF-H_2 and MOF-N_2 or MOF-CO_2 MD models

have also been observed. Just as the N_2 and CH_4 are only able to move freely through the formed zig-zag path (001 face of the MOF) (red arrows in Figure 5.17B), the H_2 molecule mostly moves through the face 001 but can also do so by the 010 face of the crystal due to its reduced size.

5.4 Conclusion

In essence, a new mixed ligand porous 3D metal carboxylate framework compound, $[Zn_2(H_2O)(nic)(pzdc)]_n \cdot nH_2O$ (H_2pzdc = pyrazole-3,5-dicarboxylic acid, Hnic = isonicotinicacid) was synthesized hydrothermally, and characterized by single crystal X-ray diffraction and other physicochemical methods. As synthesized compound had large solvent accessible void space (15.9%) which enhanced to 34.1% upon removal of water molecules led to creation of open metal sites that are exposed to the pores. $[Zn_2(H_2O)(nic)(pzdc)]_n \cdot nH_2O$ and its dehydrated product were highly selective towards CO_2 adsorption over all three small gas molecules *viz*. H_2, N_2 and CH_4. Molecular Dynamics and Monte Carlo simulations afforded a possible rationalization of the fact found in experiments.

5.5 References

(1)   M. Z. Jacobson, Energy Environ. Sci. 2009, **2**, 148.

(2)   K. S. Lackner, S. Brennan, J. M. Matter, A. -H. A. Park, A. Wright, B. van der Zwaan, Proc. Natl. Acad. Sci. U. S. A., 2012, **109**, 13156.

(3)   M. R. Allen, D. J. Frame, C. Huntingford, C. D. Jones, J. A. Lowe, M. Meinshausen, N. Meinshausen, Nature, 2009, **458**, 1163.

(4)   S. Chaemchuen, N. A. Kabir, K. Zhou, F. Verpoort, Chem. Soc. Rev. 2013, **42**, 9304.

(5)   J.-R. Li, Y. Ma, M. C. McCarthy, J. Sculley, J. Yu, H.-K. Jeong, P. B. Balbuena, H.-C. Zhou, Coord. Chem. Rev. 2011, **255**, 1791.

(6)   M. G. Plaza, C. Pevida, B. Arias, M. D. Casal, C. F. Martin, J. Fermoso, F. Rubiera, J. J. Pis, J. Environ. Eng. 2009, **135**, 426.

(7)   IPCC, IPCC Special Report on Carbon Dioxide Capture and Storage, Cambridge University Press, 2005.

(8)   B. Zheng, J. Bai, J. Duan, L. Wojtas, M. J. Zaworotko, J. Am. Chem. Soc. 2011, **133**, 748.

(9)   L. Du, Z. Lu, K. Zheng, J. Wang, X. Zheng, Y. Pan, X. You, J. Bai, J. Am. Chem. Soc. 2013, **135**, 562.

(10)   J. Liu, P. K. Thallapally, B. P. McGrail, D. R. Brown, J. Liu, Chem. Soc. Rev. 2012, **41**, 2308.

(11) K. Adil, Y. Belmabkhout, R. S. Pillai, A. Cadiau, P. M. Bhatt, A. H. Assen, G. Maurin, M. Eddaoudi, Chem. Soc. Rev. 2017, **46**, 3402.

(12) S. Kitagawa, S.-I. Noro, R. Kitaura, Angew. Chem. Int. Ed. 2004, **43**, 2334.

(13) R. Banerjee, A. Phan, B. Wang, C. Knobler, H. Furukawa, M. O'Keeffe, O. M. Yaghi, Science, 2008, **319**, 939.

(14) R. Singh, P. K. Bharadwaj, Cryst. Growth Des. 2013, **13**, 3722.

(15) R. Haldar, R. Matsuda, S. Kitagawa, S. J. George, T. K. Maji, Angew. Chem. Int. Ed. 2014, **53**, 11772.

(16) J. F. Van Humbeck, T. M. McDonald, X. Jing, B. M. Wiers, G. Zhu, J. R. Long, J. Am. Chem. Soc. 2014, **136**, 2432.

(17) S. Yuan, W. Lu, Y.-P. Chen, Q. Zhang, T.-F. Liu, D. Feng, X. Wang, J. Qin, H.-C. Zhou, J. Am. Chem. Soc. 2015, **137**, 3177.

(18) Y.-B. Zhang, H. Furukawa, N. Ko, W. Nie, H. J. Park, S. Okajima, K. E. Cordova, H. Deng, J. Kim, O. M. Yaghi, J. Am. Chem. Soc. 2015, **137**, 2641.

(19) B. Chen, S. Ma, F. Zapata, F. R. Fronczek, E. B. Lobkovsky, H.-C. Zhou, Inorg. Chem. 2007, **46**, 1233.

(20) O. K. Farha, A. M. Spokoyny, K. L. Mulfort, M. F. Hawthorne, C. A. Mirkin, J. T. Hupp, J. Am. Chem. Soc. 2007, **129**, 12680.

(21) Y.-S. Bae, O. K. Farha, A. M. Spokoyny, C. A. Mirkin, J. T. Hupp, R. Q. Snurr, Chem. Commun. 2008, 4135.

(22) H. Sakamoto, R. Matsuda, S. Bureekaew, D. Tanaka, S. Kitagawa, Chem. –Eur. J. 2009, **15**, 4985.

(23) Z. Zhang, S. Xiang, K. Hong, M. C. Das, H. D. Arman, M. Garcia, J. U. Mondal, K. M. Thomas, B. Chen, Inorg. Chem. 2012, **51**, 4947.

(24) P. Kanoo, A. C. Ghosh, S. T. Cyriac, T. K. Maji, Chem.–Eur. J. 2012, **18**, 237.

(25) S. D. Burd, S. Ma, J. A. Perman, B. J. Sikora, R. Q. Snurr, P. K. Thallapally, J. Tian, L. Wojtas, M. J. Zaworotko, J. Am. Chem. Soc. 2012, **134**, 3663.

(26) R. Vaidhyanathan, S. S. Iremonger, K. W. Dawson, G. K. H. Shimizu, Chem. Commun. 2009, 5230.

(27) P. Pachfule, Y. Chen, J. Jiang and R. Banerjee, J. Mater. Chem. 2011, **21**, 17737.

(28) S. A. Sapchenko, D. N. Dybtsev, D. G. Samsonenko, R. V. Belosludov, V. R. Belosludov, T. Kawazoe, M. Schröder, V. P. Fedin, Chem. Commun. 2015, **51**, 13918.

(29) Y.-W. Li, J. Xu, D.-C. Li, J.-M. Dou, H. Yan, T.-L. Hu, X.-H. Bu, Chem. Commun. 2015, **51**, 14211.

(30)   S. Horike, R. Matsuda, D. Tanaka, M. Mizuno, K. Endo, S. Kitagawa, J. Am. Chem. Soc. 2006, **128**, 4222.

(31)   Y.-S. Bae, B. G. Hauser, O. K. Farha, J. T. Hupp, R. Q. Snurr, MicroporousMesoporous Mater. 2011, **141**, 231.

(32)   C. F. Leong, T. B. Faust, P. Turner, P. M. Usov, C. J. Kepert, R. Babarao, A. W. Thornton, D. M. D'Alessandro, Dalton Trans. 2013, **42**, 9831.

(33)   J.-R. Li, R. J. Kuppler, H.-C. Zhou, Chem. Soc. Rev. 2009, **38,** 1477.

(34)   Y. Hijikata, S. Horike, M. Sugimoto, M. Inukai, T. Fukushima, S. Kitagawa, Inorg. Chem. 2013, **52**, 3634.

(35)   Z, Hulvey, D. A. Sava, J. Eckert, A. K. Cheetham, Inorg. Chem. 2011, **50**, 403.

(36)   Feréy, M. Latroche, C. Serre, F. Millange, T. Loiseau, A. P. G. Gan, Chem. Commun. 2003, 2976.

(37)   J. L. C. Rowsell, O. M. Yaghi, J. Am. Chem. Soc. 2006, **128**, 1304.

(38)   M. Dincã, A. Dailly, C. Tsay, J. R. Long, Inorg. Chem. 2008, **47**, 11.

(39)   R. Vaidhyanathan, S. S. Iremonger, G. K. H. Shimizu, P. G. Boyd, S. Alavi, T. K. Woo, Science, 2010, **330**, 650.

(40)   A. Demessence, D. M. D'Alessandro, M. L. Foo, J. R. Long, J. Am. Chem. Soc. 2009, **131**, 8784.

(41)   S. M. Chen, J. Zhang, T. Wu, P. Y. Feng, X. H. Bu, J. Am. Chem. Soc. 2009, **131**, 16027.

(42)   J. An, N. L. Rosi, J. Am. Chem. Soc. 2010, **132**, 5578.

(43)   Bruker (**2007**). APEX 2, SAINT, XPREP, Bruker AXS Inc., Madison, Wisconsin, USA.

(44)   Bruker (**2001**). SADABS, Bruker AXS Inc., Madison, Wisconsin, USA.

(45)   G. M. Sheldrick, Crystal structure refinement with SHELXL. SHELXS2018 and SHELXL2018: Acta Cryst. 2015, **C71**, 3.

(46)   J. D. Gale, A. L. Rohl, Mol. Simul. 2003, **29**, 291.

(47)   S. L. Mayo, B. D. Olafson, W. A. Goddard III, J. Phys. Chem. 1990, **94**, 8897.

(48)   N. Metropolis, A. W. Rosenbluth, M. N. Rosenbluth, A. H. Teller, E. Teller, J. Chem. Phys. 1953, **21**, 1087.

(49)   A. K. Rappe, W. A. Goddard, J. Phys. Chem. 1991, **95,** 3358.

(50)   A. L. Spek, Acta Crystallogr., Sect. D, 2009, **65**, 148.

(51)   V. A. Blatov, A. P. Shevchenko, D. M. Proserpio, Cryst. Growth Des. 2014, **14**, 3576.

(52)   K. Sumida, D. L. Rogow, J. A. Mason, T. M. McDonald, E. D. Bloch, Z. R. Herm, T.-H. Bae, J. R. Long, Chem. Rev. 2012, **112***, 724.

(53)   S. S. Dhankhar, N. Sharma, S. Kumar, T. J. Dhilip Kumar, C. M. Nagaraja, Chem. –Eur. J. 2017, **23**, 16204.

(54)   W. M. Bloch, R. Babarao, M. R. Hill, C. J. Doonan, C. J. Sumby, J. Am. Chem. Soc. 2013, **135**, 10441.

(55)   A. Hazra, S. Bonakala, S. K. Reddy, S. Balasubramanian, T. K. Maji, Inorg. Chem. 2013, **52**, 11385.

(56)   S. Parshamoni, J. Telangae, S. Konar, Dalton Trans. 2015, **44**, 20926.

(57)   B. Ugale, S. S. Dhankhar, C. M. Nagaraja, Cryst. Growth Des. 2017, **17**, 3295.

(58)   J. Liu, G.-P. Yang, Y. Wu, Y. Deng, Q. Tan, W.-Y. Zhang, Y.-Y. Wang, Cryst. Growth Des. 2017, **17**, 2059.

(59)   Y.-L. Huang, Y.-N. Gong, L. Jiang, T.-B. Lu, Chem. Commun. 2013, **49**, 1753.

(60)   H.-C. Kim, S. Huh, S.-J. Kim,Y. Kim, Sci. Rep. 2017, **7**, 17185.

(61)   Z.-J. Wang, L.-J. Han, X.-J. Gao, H.-G. Zheng, Inorg. Chem. 2018, **57**, 5232.

(62)   W.-G. Jin, W. Chen, P.-H. Xu, X.-W. Lin, X.-C. Huang, G.-H. Chen, F. Lu, X.-M. Chen, Chem. –Eur. J. 2017, **23**, 13058.

(63)   S. Nandi, R. Maity, D. Chakraborty, H. Ballav, R. Vaidhyanathan, Inorg. Chem. 2018, **57**, 5267.

(64)   V. A. Bolotov, K. A. Kovalenko, D. G. Samsonenko, X. Han, X. Zhang, G. L. Smith, L. J. McCormick, S. J. Teat, S. Yang, M. J. Lennox, A. Henley, E. Besley, V. P. Fedin, D. N. Dybtsev, M. Schröder, Inorg. Chem. 2018, **57**, 5074.

(65)   P. Nugent, Y. Belmabkhout, S. D. Burd, A. J. Cairns, R. Luebke, K. Forrest, T. Pham, S. Ma, B. Space, L. Wojtas, M. Eddaoudi, M. J. Zaworotko, Nature, 2013, **495**, 80.

(66)   S. R. Caskey, A. G. Wong Foy, A. J. Matzger, J. Am. Chem. Soc. 2018, **130**, 10870.

(67)   S.-i. Noro, J. Mizutani, Y. Hijikata, R. Matsuda, H. Sato, S. Kitagawa, K. Sugimoto, Y. Inubushi, K. Kubo, T. Nakamura, Nature Commun. 2015, **6**, 5851.

(68)   S.-i. Noro, Y. Hijikata, M. Inukai, T. Fukushima, S. Horike, M. Higuchu, S. Kitagawa, T. Akutagawa, T. Nakamura, Inorg. Chem. 2013, **52**, 280.

(69)   Q. M. Wang, D. Shen, M. Bülow, M. L. Lau, S. Deng, F. R. Fitch, N. O. Lemcoff, L. Semanscin, Microporous Mesoporous Mater. 2002, **55**, 217.

Chapter 6
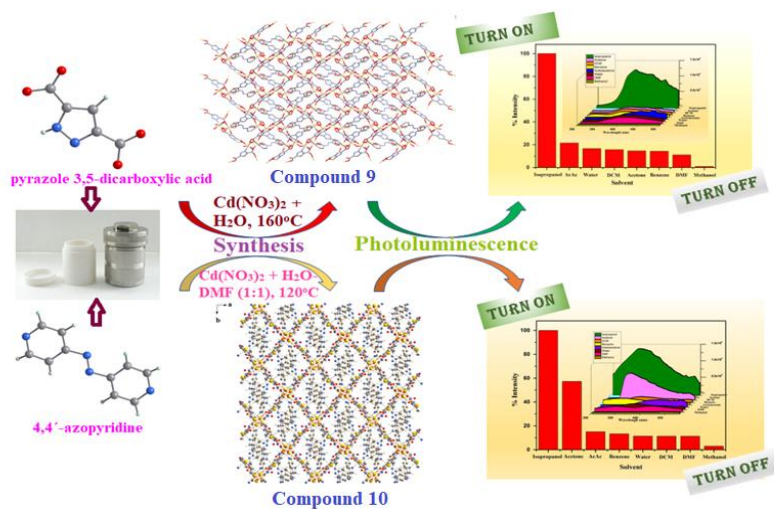
Cd(II) containing mixed linker based metal-organic framework: synthesis, X-ray crystallography and solvent mediated photoluminescence response

6.1 Introduction

MOFs can be built with single linker or more than one linker to assemble metal ions in the framework. Single ligand derived MOFs are commonplace and their synthetic methodologies are, generally, straight-forward. As a result, reports of single linker-based MOFs are prolific in the literature, however, mixed-linker MOFs are still limited [1]. Hence further exploration is desirable in search of facile synthetic route for mixed-linker MOFs with required stability and functionality. As regards the application of MOFs, luminescent MOFs (LMOFs) have witnessed significant progress along with other applications like catalysis, gas sorption, proton conduction etc. Various molecular processes like ligand-based emission, metal-based emission, emission due to excimer or exciplex formation, guest induced emission etc. play crucial role in photoluminescence response in LMOFs [2]. Sensing of neutral molecule such as organic compounds, gases, vapors etc. entails a large part of luminescence studies of MOFs [3]. Neutral species tends to undergo host-guest type interaction with MOFs and in suitable cases that manifests in the change of emission profile of MOF. It is well known that sensing of various species with probes can be realized through two types of responses *viz.* "turn-on" and "turn-off" [2]. Kitagawa *et al.* in their pioneering report showed that $[Zn_2(BDC)_2(DABCO)] \cdot DSB$ (BDC= 1,4-benzenedicarboxylate, DABCO= 1,4-diazabicyclo-[2.2.2]octane, DSB= distyrylbenzene) selectively enhanced the fluorescence response in presence of CO_2 and C_2H_2 over other gases like N_2, O_2 and Ar [4]. Upon exposure to C_2H_2 or CO_2 the luminophore, DSB undergone conformational changes. Porous MOF, $[Cd(CVBA)(H_2O)] \cdot 4DMF \cdot 2H_2O$ (CVBA= (E)-4-(2-carboxyvinyl)-benzoic acid) on absorbing rhodamine B dye impartedtuneable luminescence in presence of a variety of organic molecules like benzene, toluene, phenol, acetophenonone, 4-methylphenol etc. [5]. Dong *et al.* showed copper (I) based MOF can be utilized for sensing of volatile alcohols, ketones and halocarbons [6]. $[Mg(dhtp)(H_2O)_2] \cdot DMA$ (H_2dhtp: 2,5-dihydroxy-terepthalic acid; DMA: N,N-dimethylacetamide) exhibited an enhanced fluorescence associated with a red shift of the fluorescence maxima upon addition of water to dispersed phase of the MOF in THF, ethanol and acetonitrile [7]. Ming-Sun *et al.* reported an LMOF, $\{Cd_3(hcpo)(bipy)_2.4DMA\}_n$ (H_6hcpo = (hexa[4-(carboxyphenyl)oxamethyl]-3-oxapentane acid), bipy = 2,2′-bipyridine) displayed a selective turn-on behaviour for benzene. MOF being capable of withstanding wide range of pH variation along with possibility of its reuse led the authors to conclude the MOF supposed to be a prospective material for practical usage, particularly, in environmental applications [8]. In addition, MOFs have been demonstrated to be fluorescent sensors for selective detection and identification of various cations, anions and metal ions based on their fluorescence response [9-12]. MOFs have also been used for the detection of DNA or biomolecules [13]. In this chapter, studies of luminescent MOFs especially its response towards small organic molecules have been discussed.

Application of temperature and solvent dependent hydrothermal synthetic routes led to afford a pair of Cd(II) based mixed linker 3D MOFs *viz.*, $[Cd_2(pzdc)_2(azpy)_{0.5}(H_2O)]_n$ **(9)** and $\{[Cd_3(pzedc)_2(azpy)_2] \cdot H_2O\}_n$ **(10)** (pzdc = pyrazole-3,5-dicarboxylate, pzedc = pyrazolate-3,5-dicarboxylate and azpy = 4,4′-azopyridine) (Scheme 6.1). Both the framework compounds featured interesting photoluminescence property in the solid state as well as in dispersed medium. Interestingly, solvent specific turn-on/turn-off photoluminescence responses have been observed for both the compounds **9** and **10.**
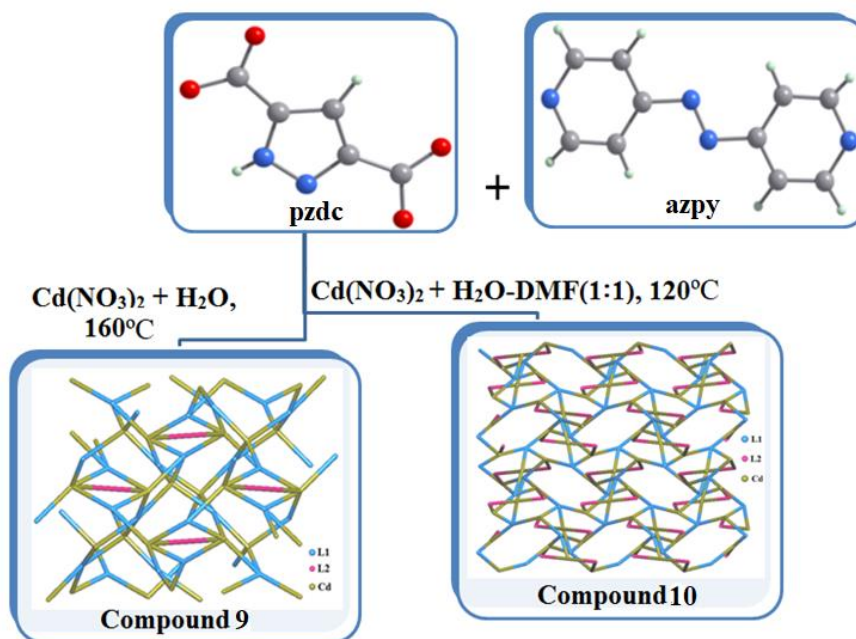
Scheme 6.1. Schematic representation of synthetic route of two 3D Cd-based MOFs, 9-10

6.2 Experimental Section

6.2.1 Materials

Pyrazole-3,5-dicarboxylic acid, 4,4′-azopyridine and cadmium nitrate tetrahydrate $Cd(NO_3)_2 \cdot 4H_2O$ were purchased from Sigma-Aldrich. All other reagents were purchased from Merck India. Solvents were distilled and dried before use.

6.2.2 Syntheses of MOF

Synthesis of compound $[Cd_2(pzdc)_2(azpy)_{0.5}(H_2O)]_n$ (9)

$[Cd_2(pzdc)_2(azpy)_{0.5}(H_2O)]_n$ **(9)** was synthesized by mixing $Cd(NO_3)_2 \cdot 4H_2O$ (0.077 g, 0.25 mmol), pyrazole-3,5-dicarboxylic acid (0.043 g, 0.25 mmol) and 4,4′-azopyridine (0.046 g, 0.25 mmol) in 3-4 ml

of water. Then the mixture was transferred to a 20 ml of teflon-lined Parr type acid digestion bomb for hydrothermal treatment. The desired compound was obtained as orange-colored crystals in a teflon-lined Parr acid digestion bomb, at 160 °C for 3 days followed by slow cooling at the rate of 5 °C/h to room temperature.

Yield *ca*. 0.086 g, 86% based on the metal.

Anal Calc. for $C_{15}H_8Cd_2N_6O_9$ in %: C, 28.07; H, 1.25; N, 13.10; Found: C, 28.09; H, 1.31; N, 13.06. IR (KBr disk, v, cm^{-1}): 1593 and 1518 [$v_{as}(COO^-)$], 1411 [$v_s(COO^-)$], 1345 [$v_s(C-O)$], 3248 [$v(N-H)$],3400 [$v(N=N)$], 3069–3498 s.br [$v_s(O–H)$] (Figures 6.1, 6.2).

Experimentally measured powder X-ray diffraction patterns matched well with the simulated ones indicating excellent phase purity of the bulk compound **9** (Figure 6.3).
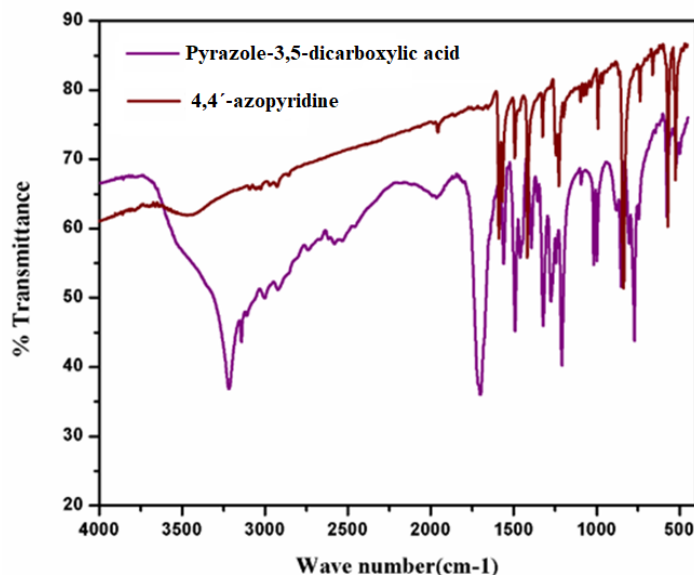

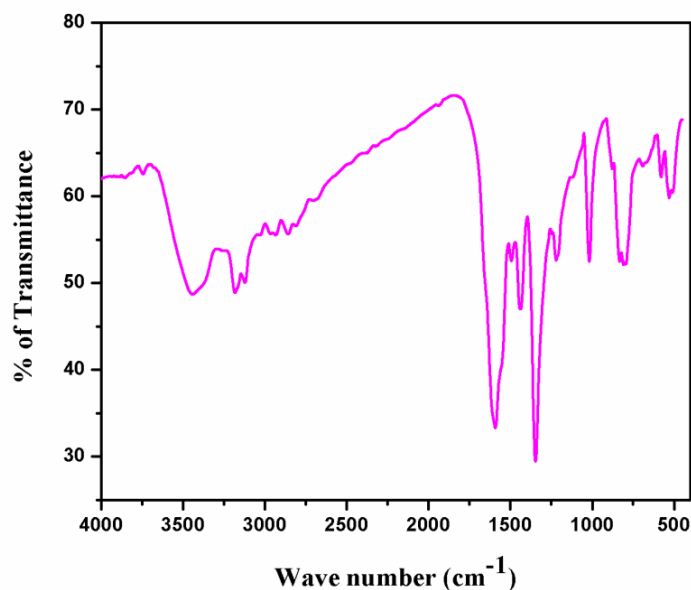**Figure 6.1. IR spectroscopy of linkers**

Figure 6.2. **IR spectroscopy of compound 9**
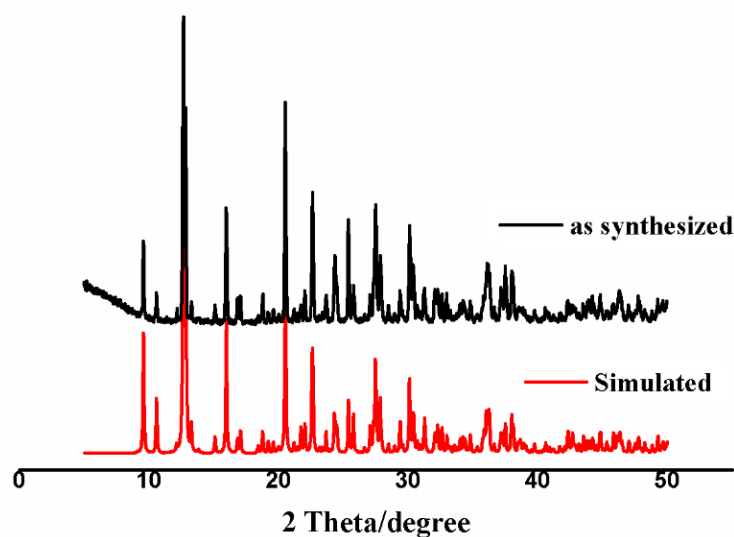
Figure 6.3. **PXRD patterns of compound 9**

Synthesis of compound $\{[Cd_3(pzedc)_2(azpy)_2]\cdot H_2O\}_n$ (10)

Another Cd-based compound $\{[Cd_3(pzedc)_2(azpy)_2]\cdot H_2O\}_n$ (**10**) has also been synthesized by solvothermal synthesis. First, $Cd(NO_3)_2\cdot 4H_2O$ (0.077g, 0.25 mmol), pyrazole-3,5-dicarboxylic acid (0.043 g, 0.25 mmol) and 4,4′-azopyridine (0.046g, 0.25 mmol) were mixed well in ~4 mL of DMF-H_2O (1:1) and then the mixture was transferred to a 20 mL of teflon-lined Parr type acid digestion bomb.

Yellowish white block crystalline product was obtained by heating the mixture at 120 ℃ temperature for 3 days followed by slow cooling to room temperature at 5 ℃/h rate.

Yield *ca*. 0.082 g, 82% based on the metal.

Anal. Calc. for $C_{30}H_{18}Cd_3N_{12}O_9$ in %: C, 34.95; H, 1.94; N, 16.31; Found: C, 34.91; H, 1.92; N 16.41. IR (KBr disk, *v*, cm^{-1}): 1606 and 1523 [$v_{as}(COO^-)$], 1411 [$v_s(COO^-)$], 1360 [$v_s(C\text{-}O)$], 3269 [$v(N=N)$], 3103–3524 s.br [$v_s(O–H)$] (Figure 6.4).

Experimentally measured powder X-ray diffraction patterns matched well with the simulated ones indicating excellent phase purity of the bulk compound **10** (Figure 6.5).

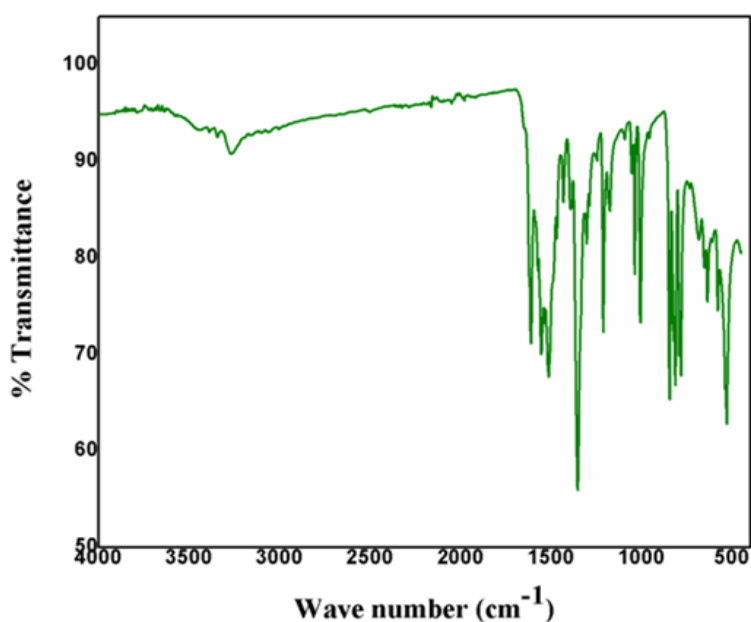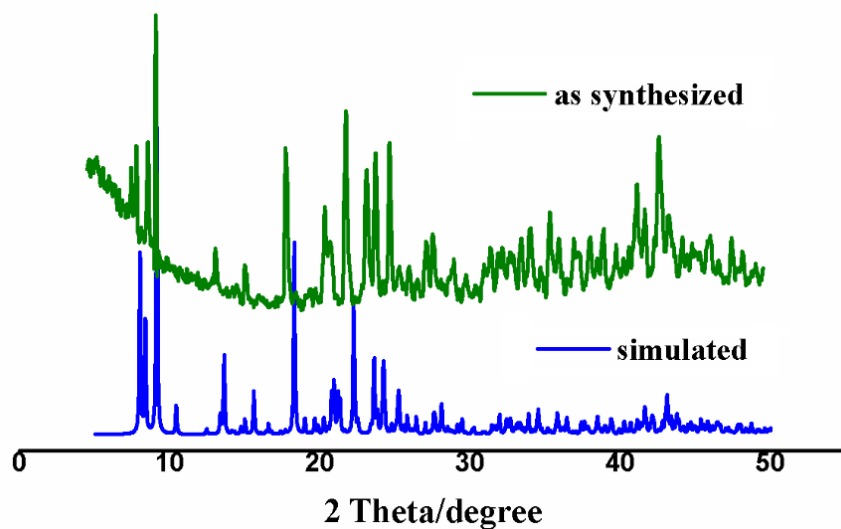**Figure 6.4**. **IR spectroscopy of compound 10**

Figure 6.5. PXRD patterns of compound 10

6.2.3 Physical measurements

The solid-state ^{113}Cd NMR spectra of MOFs were measured with the single crystals collected for crystallography, in a finely ground powder form. The spectra were obtained using the ^{113}Cd CP/MAS NMR techniques on a Bruker Advance 600 MHz spectrometer (14.10 T) operating at a frequency 133.11 MHz. The contact time was 1 ms, the delay time 10 s and the rotor speed set at 5 and 7 kHz. The solid-state NMR spectra chemical shifts are quoted relative to $Cd(NO_3)_2·4H_2O$ with positive chemical shifts downfield. The solid-state photoluminescence experiments were performed by using finely ground samples (5 mg) of both compounds **9** and **10** on a Horiba FluroMax-4 fluorescence spectrometer. The luminescence experiments in dispersed media were performed as follows: finely powdered samples (2 mg) were first taken in desired solvents (2 mL) and sonicated for 30 min in an ultrasonic bath, then the mixture was allowed to stand for some time. The resultant dispersed medium was used for luminescence measurement. The instruments used for other physical measurements have already been described in **Section 2.2.3, Chapter 2.**

6.2.4 X-ray crystallography

Single crystals suitable for X-ray diffraction were selected from bulk under a microscope and carefully glued to thin glass fiber. Single crystal X-ray diffraction data for **9** and **10** were collected at 298(2) K, on a Bruker-AXS SMART APEX CCD diffractometer with graphite-monochromated Mo-Kα radiation (λ = 0.71073 Å). CCD data were integrated and scaled by SAINT software package through a narrow-frame integration algorithm [14]. The structures were solved by direct methods and refined by

full-matrix least-squares technique against F2 with anisotropic displacement parameters for non-hydrogen atoms with the programs SHELXL-2014 package [15], SHELXL 2018 [16]. An empirical absorption correction was determined by SADABS [17]. All other hydrogen atoms of compounds **9** and **10** were refined by isotropic thermal parameters and placed in their geometrically idealized positions, except for the one hydrogen atom (H7) of the azopyridine ring of compound **9**, which could not be treated isotopically in the Fourier map. All calculation and molecular graphics were performed with WinGX [18], Diamond [19], Mercury [20] and PLATON [21]. A summary of crystal data and related refinement parameters for two compounds are given in Table 6.1.

CCDC-1986604 and CCDC-1986605 contains the supplementary crystallographic data for compound **9** and **10** respectively. These data can be obtained free of charge via http://www.ccdc.cam.ac.uk/conts/retrieving.html, or from the Cambridge Crystallographic Data Centre, 12 Union Road, Cambridge CB2 1EZ, UK; fax: (+44) 1223-336-033; or e-mail: deposit@ccdc.cam.ac.uk.

Table 6.1. Crystal data and structure refinement for compound 9 and 10

Compound	9	10
Mol. Formula	$C_{15}H_8Cd_2N_6O_9$	$C_{30}H_{20}Cd_3N_{12}O_9$
Formula wt.	641.09	1029.78
Space group	*P2$_1$/c*	*P2$_1$2$_1$2$_1$*
Crystal system	Monoclinic	Orthorhombic
a / Å	9.8244(10)	13.2642(8)
b / Å	11.1092(9)	14.2476(8)
c / Å	16.9659(14)	17.5525(10)
α / deg	90	90
β / deg	99.361(7)	90
γ / deg	90	90
V / Å^3	1827(3)	3317.1(3)
Z	4	4
d$_{cal}$ (g.cm^{-3})	2.331	2.062
μ (mm^{-1})	2.397	1.981
R$_{int}$	0.112	0.055
No. of unique data	3743	7349
Data with I > 2σ(I)	2275	7240

R1 on I>2σ(I)	0.0598	0.0608
wR2 on I>2σ(I)	0.1407	0.1296
GOF on F^2	0.99	1.37
F(000)	1232	2000

$$R_1 = \sum |(|F_o| - |F_c|)| / \sum |F_o|, \; wR_2 = \{ \sum [\text{w} \, (F_o{}^2 - F_c{}^2)^2] / \sum [\text{w} \, (F_o{}^2)^2] \}^{1/2}$$

6.3 Results and discussion

6.3.1 X-ray structure

X-ray structure of compound [Cd$_2$(pzdc)$_2$(azpy)$_{0.5}$(H$_2$O)]$_n$ (9)

Single-crystal X-ray crystallographic study revealed that compound **9** crystallizes in the space group *P2$_1$/c* with Z = 4 (Table 6.1) and possessed a 3D polymeric structure consists of Cd(II) with pyrazole-3,5-dicarboxylate and 4,4′-azopyridine linkers (Figure 6.6). The asymmetric unit of **9** with an atom numbering scheme is shown by ORTEP diagram (Figure 6.7). In compound **9**, two crystallographically different types of Cd metal centers (Cd1 and Cd2) with different coordination numbers, *viz.* six and seven respectively, are connected through the ligand pyrazole-3,5-dicarboxylate with μ_4- and μ_5- connectivity (Figure 6.6a). Coordination geometry of Cd1 in compound **9** is distorted octahedral (Figure 6.6b) while Cd2 featured a distorted pentagonal bipyramidal geometry (Figure 6.6c). Of two types of binding modes of pyrazole-3,5-dicarboxylate, one binds with four Cd-centers through carboxylate oxygen atoms in which one carboxylate group connected Cd1 and Cd2 centers through O7 and O8 atoms adopted μ_3-η^1:η^2 bridging coordination mode and while other carboxylate group connected with Cd1 center through O5 oxygen atom in monodentate fashion (Figure 6.6d). In another binding mode, carboxylate groups of pyrazole-3,5-dicarboxylate coordinated to four Cd metal centers where one carboxylate group linked through μ_2-η^2 binding with Cd2 center (through O2 carboxylato oxygen atom) and another carboxylate group adopted μ_3-η^1:η^2 bridging coordination mode between Cd1 and Cd2 centers through O4 and O3 carboxylato oxygen atom (Figure 6.6e). The Cd2 centers formed two types of five membered chelate rings; while one through N1 nitrogen atom of pyrazole moiety and O8 carboxylato oxygen atom another through N3 atom of pyrazole and O2 carboxylato oxygen atom (Figures 6.6d, 6.6e). On the other hand, two pyridyl nitrogen atoms (N5) of 4,4′-azopyridine displayed as a spacer that connected two Cd1 centers (Figure 6.6f). On the other hand, two pyridyl nitrogen atoms connected with two Cd1 centers (Figure 6.6f). The Cd-O and Cd-N bond-lengths are in the range of 2.197(7) Å– 2.629(7)

Å for both cadmium centers have shown in Table 6.2. Cd-O and Cd-N bond lengths are agreement with reported values [8, 22]. Selected bond lengths and angles of **9** are given in Table 6.2.
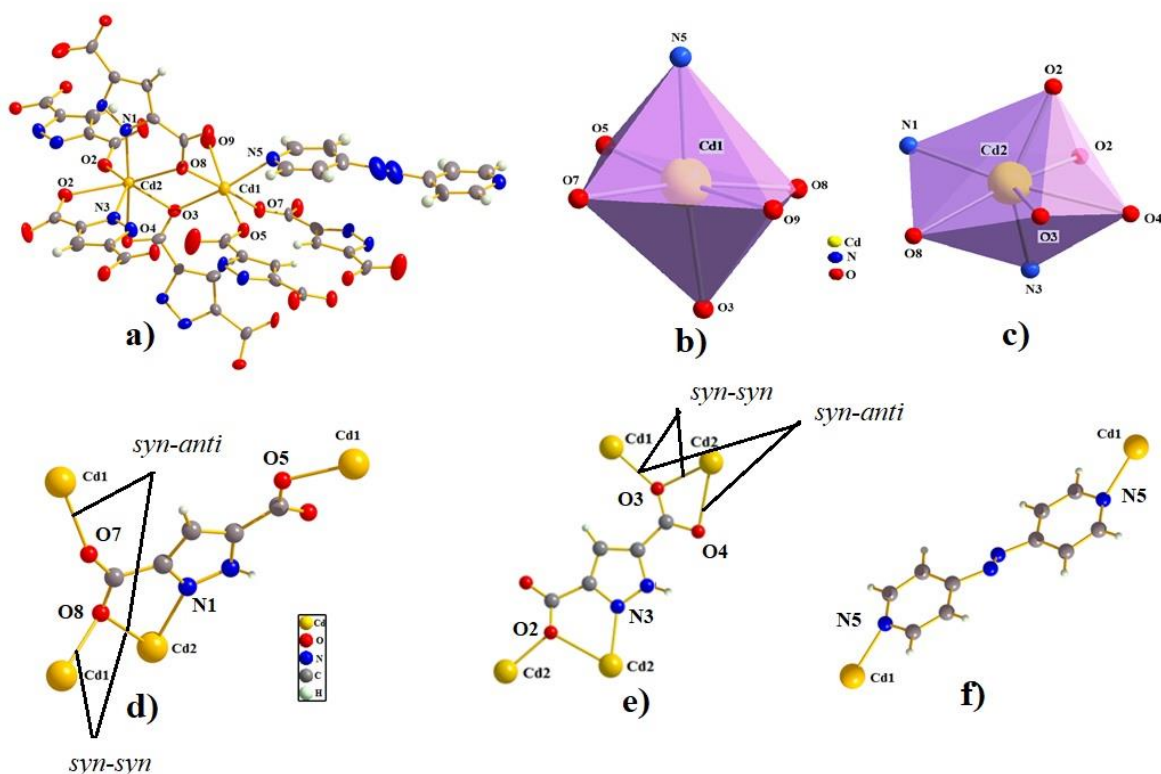

Figure 6.6. Coordination environment of Cd(II) in compound 9: a) metal coordination of two different Cd(II) centers; b) polyhedral drawing of hexa-coordinated Cd1; c) polyhedral drawing of hepta-coordinated Cd2; d), e), f) various coordination modes of linkers.

In MOF **9** pyrazole-3,5-dicarboxylate connected two crystallographically different Cd metal centers (Cd1 and Cd2) through *syn-syn* and *syn-anti* bridging mode of carboxylato oxygens (O8, O7; O3, O4 respectively) (Figures 6.6d, 6.6e). Such Cd-carboxylate moieties are stacked through bis-chelated mode of two –COO$^-$ and one N-atom (N3) parallel to crystallographic *b* axis (Figure 6.8a) and which are further pillared by N,N´-donor 4,4´-azopyridine (Figure 6.8b). Finally, a zigzag 3D framework is formed on further connection of Cd1 centers of the above sub-structure via carboxylato oxygen (O5, O7) of pyrazole-3,5-dicarboxylate (Figure 6.8c).
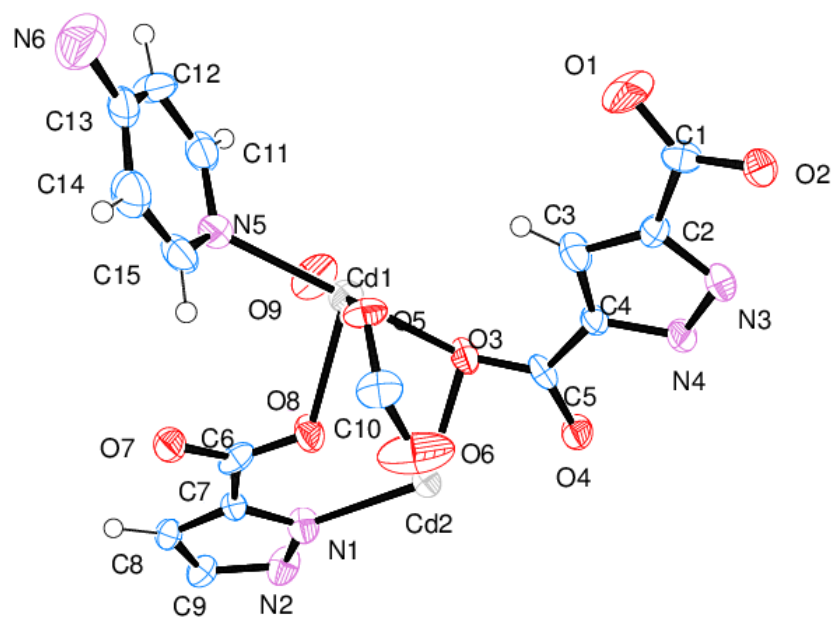
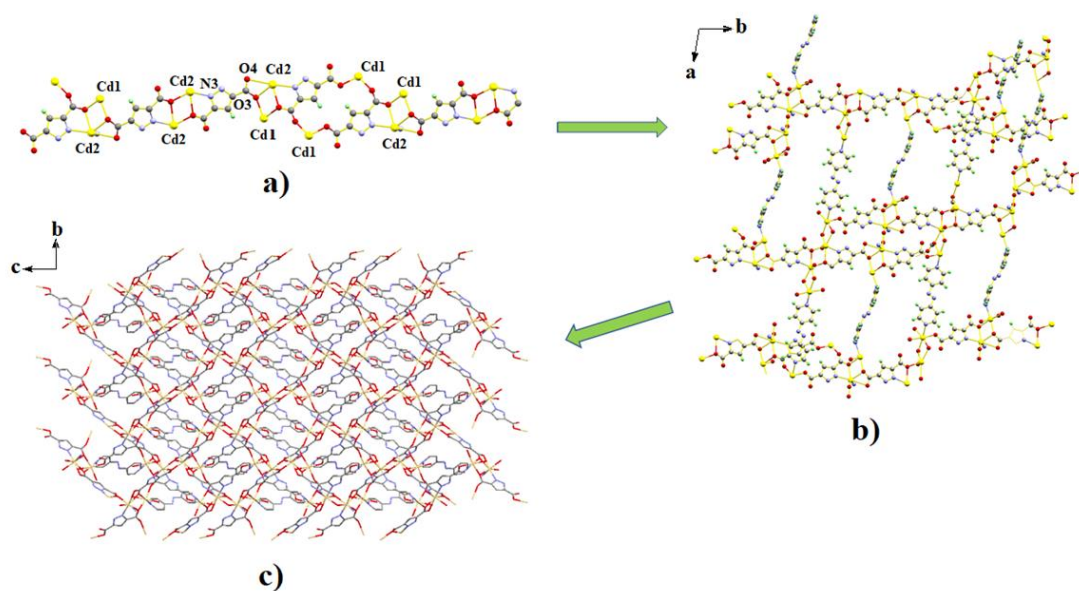**Figure 6.7. Ortep diagram of compound 9**

Figure 6.8. a) Stacking of Cd carboxylate moieties; b) pillaring through 4,4′-azopyridine; c) 3D zigzag framework.

To understand the structure of compound **9** further, a topological analysis was performed by reducing the multidimensional structure to a simple node-and-linker net. Topological analysis by TOPOS [23] revealed that the compound **9** has a 5-nodal 2,4,4,4,5-c 3D net structure with the Schläfli symbol $\{4^2.8^4\}6\{4^2.8^6.10^2\}2\{8\}$ consisting of 4,4′-azopyridine as two-coordinated node, pyrazole-3,5-dicarboxylate as four-coordinated node with two different types of binding mode, Cd1 center as four-coordinated node and Cd2 center as five-coordinated node (Figure 6.9).
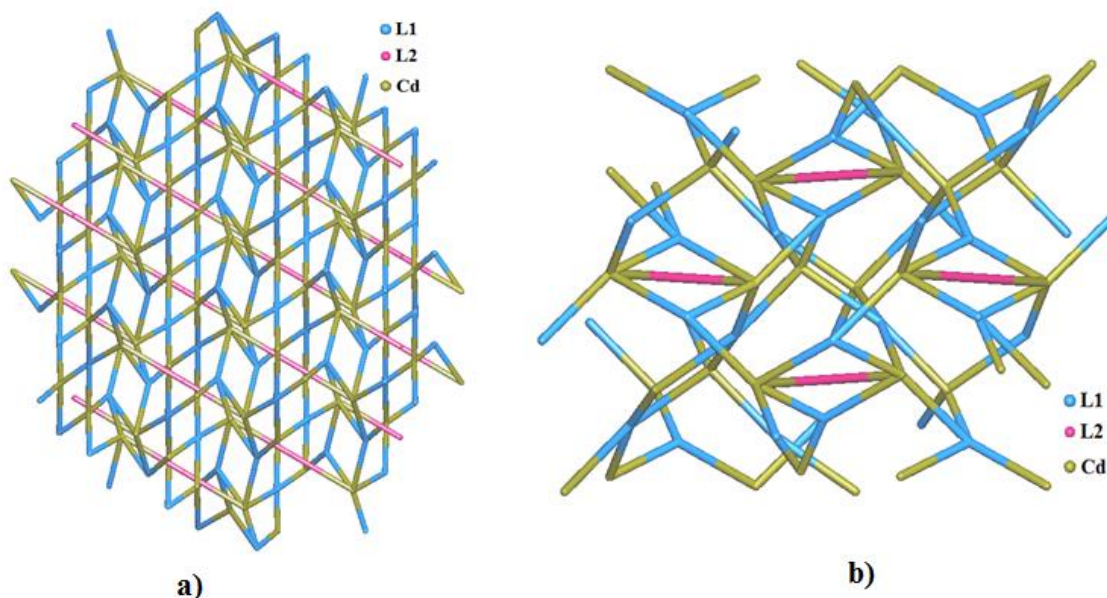

Figure 6.9. Topological view of compound 9: a) view along crystallographic *b* axis, b) view along crystallographic *c* axis.

X-ray structure of compound $\{[Cd_3(pzedc)_2(azpy)_2]\cdot H_2O\}_n$ (10)

Structure of compound **10** also exhibited a three-dimensional polymeric network consisting of Cd(II) coordinated by pyrazolate-3,5-dicarboxylate and 4,4′-azopyridine linkers, which crystallized in the orthorhombic space group *P2₁2₁2₁* with Z = 4 (Table 6.1). The asymmetric unit of $\{[Cd_3(pzedc)_2(azpy)_2]\cdot H_2O\}_n$ contains three different Cd(II) ions, two pyrazolate-3,5-dicarboxylate linker (pzedc), two 4,4′-azopyridine linker (azpy) and one uncoordinated water molecule. The ORTEP diagram of compound **10** with an atom numbering scheme is shown in the Figure 6.10. Three crystallographically different types of Cd atoms are present in compound **10** (Figure 6.11a). The coordination around three Cd centers; Cd1, Cd2, Cd3 is shown in Figures 6.11b, 6.11c, 6.11d, respectively. Cd1 center featured a distorted octahedral geometry (Figure 6.11e) and is surrounded by four donor nitrogen atoms (N2, N6, N20, N21) and two carboxylato oxygen atoms (O3, O12). Cd2 and Cd3 centers are hepta-coordinated having distorted pentagonal bi-pyramidal geometry (Figures 6.11f, 6.11g). Cd2 is surrounded by five

donor oxygen atoms (O3, O5, O7, O11, O13[c]) and two nitrogen atoms (N23[g], N30[h]). Cd3 also featured a similar coordination environment like Cd2. In case of MOF **10**, one carboxylate group from a pyrazolate-3,5-dicaboxylate linker (pzedc) connected two Cd(II) centers (Cd1 and Cd2) through O3 and O11 atom in a bridging chelate mode while Cd1 and Cd3 are connected through N21 and N22 of another pzedc ligand (Figures 6.12a, 6.12b). Cd2 and Cd3 are interconnected by O7 and O13 in a bridging chelate mode (Figure 6.12a) of pzedc ligand. Pyrazolate-3,5-dicaboxylate linker bound three Cd centers through carboxylate groups in bridging chelate fashion forming square like channel that leads to square grid (Figures 6.13a, 6.13b). These channels are further connected through pyrazolate-3,5-dicaroxylate by sharing the corners resulted a fascinating 3D framework structure (Figure 6.13c). Additional reinforcement to the network is provided by 4,4′-azopyridine linker by connecting Cd1, Cd2 and Cd1, Cd3 through N2, N30 and N6, N9, respectively (Figure 6.12c). Interestingly, 4,4′azopyridine linked two opposite face of the square and featured a wavy structure that propagates throughout the grid (Figures 6.13c, 6.13d). Cd-O and Cd-N bond-lengths are in the range of 2.304(14) Å– 2.568(11) Å for three Cd centers in MOF **10** are collated in Table 6.2. To represent the square grid of **10** in the simplest way a figure has been drawn where 3D cube (green) represents as a square (magenta) (Figures 6.13e, 6.13f). The square units further connected through sharing of corners resulted in a square grid network structure (Figure 6.13g).

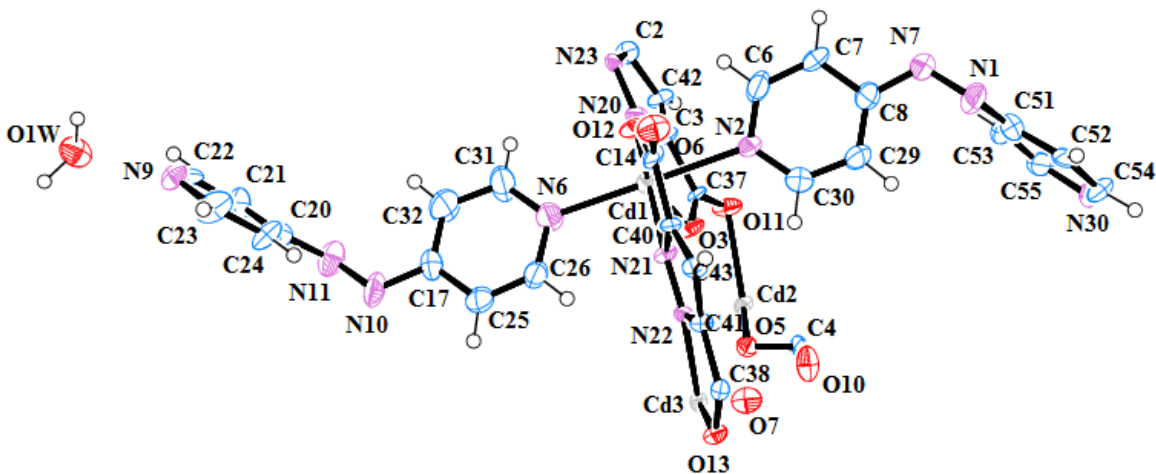**Figure 6.10. Ortep diagram of compound 10**
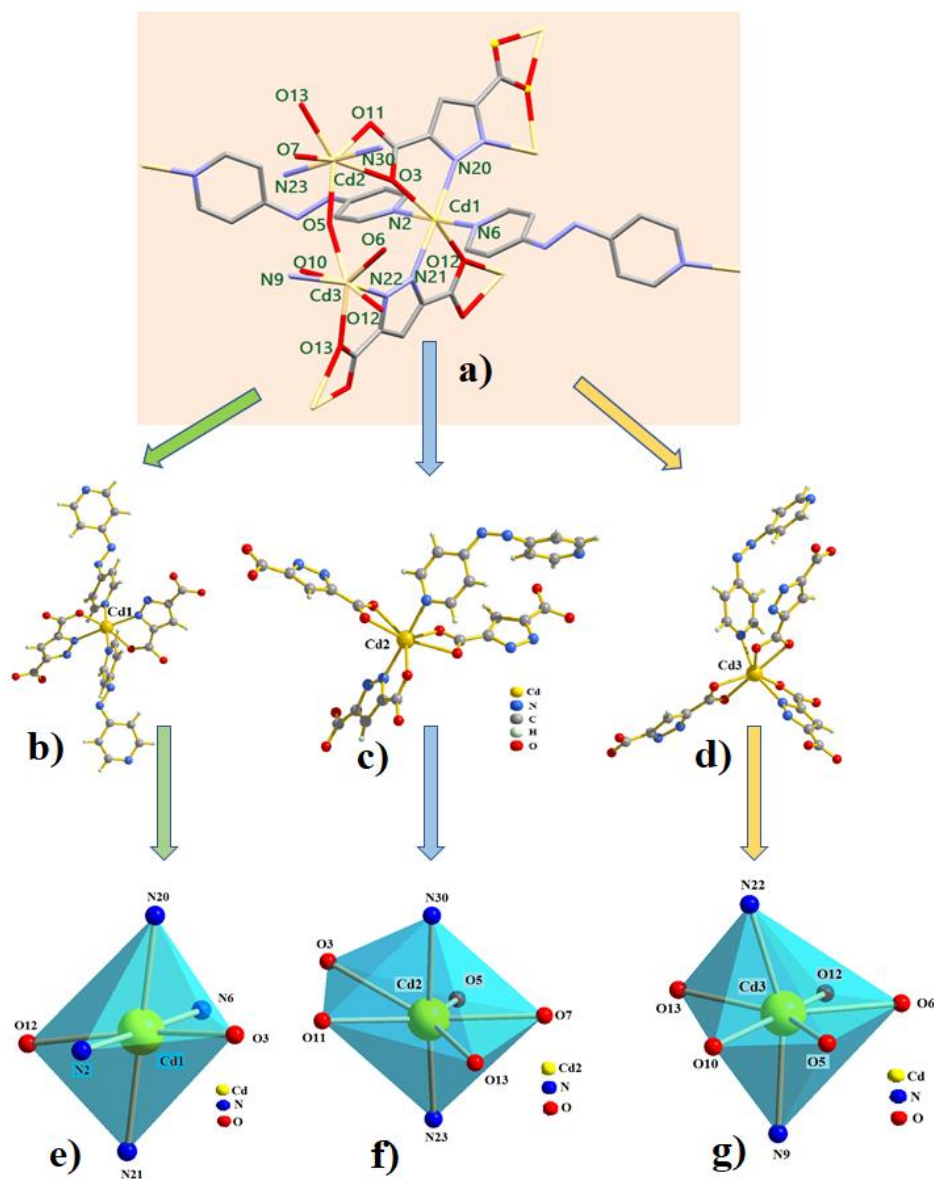
Figure 6.11. a) Part of the molecular structure of 10 (hydrogens are omitted for clarity); coordination environment of b) Cd1, c) Cd2, d) Cd3 metal center; polyhedral drawing of e) Cd1; f) Cd2; g) Cd3 coordination environment.
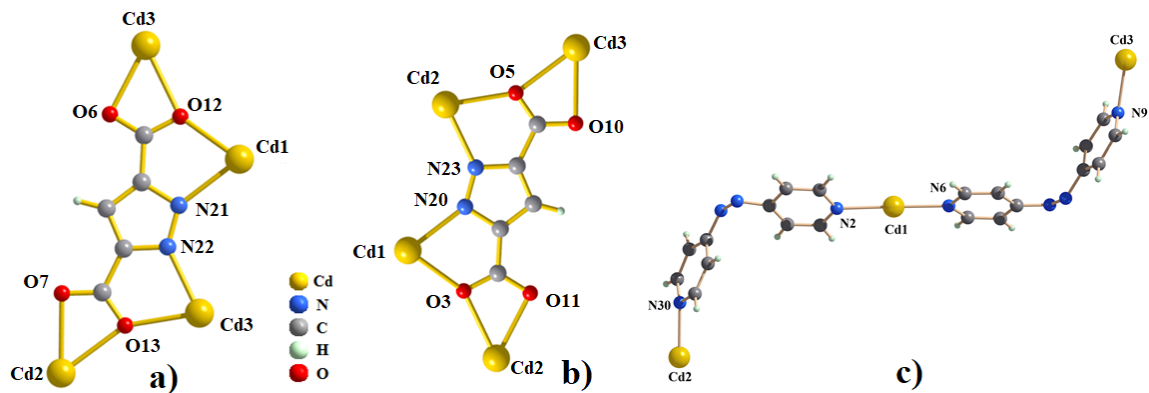
Figure 6.12. a) and b) Coordination modes of pyrazolate-3,5-dicarboxylate; c) coordination modes of 4,4′-azopyridine in 10.
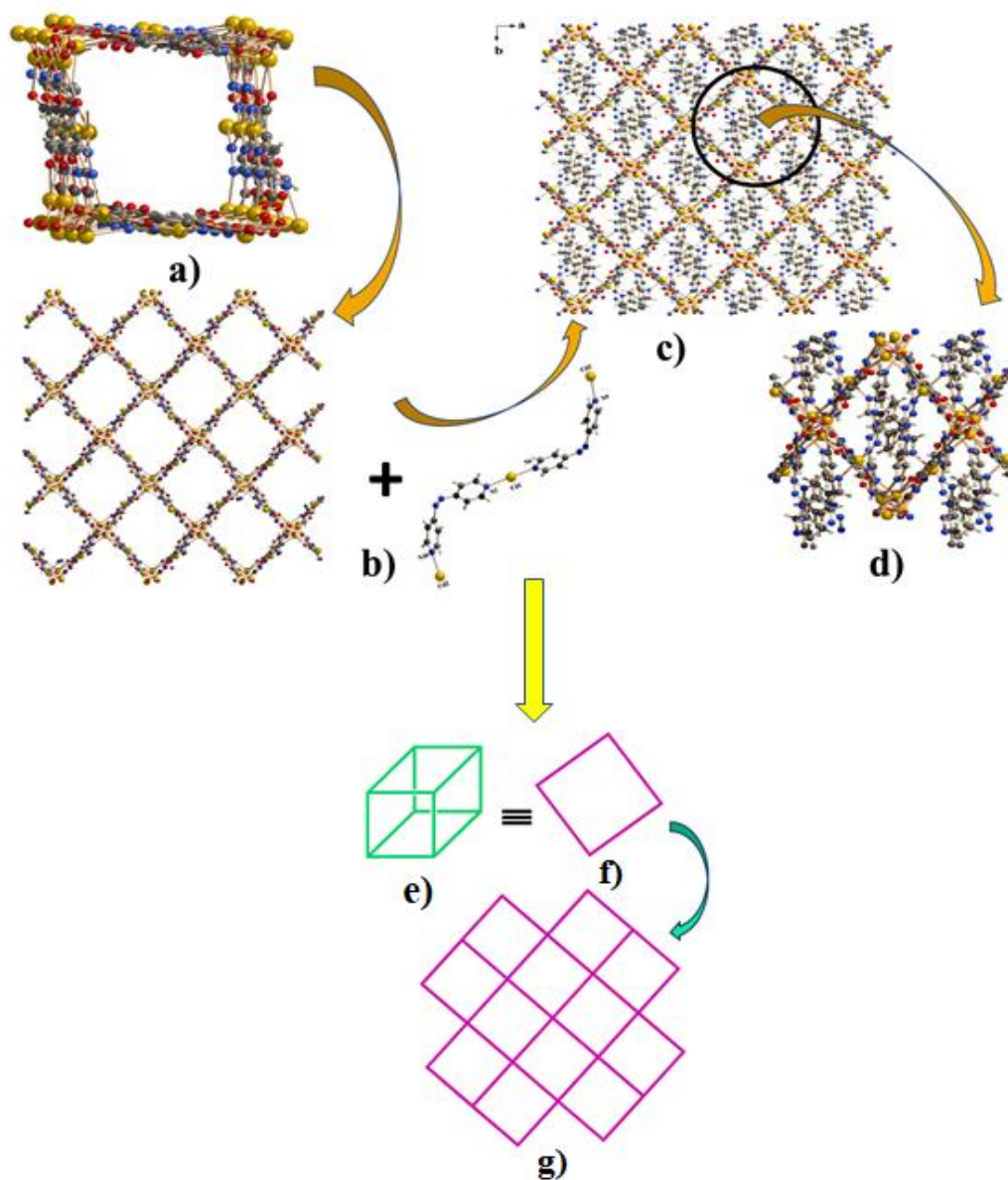
Figure 6.13. a) Representative Cd-carboxylate 3D square channel and propagation of square grid network; b) wavy nature of 4,4′-azopyridine linker; c) 4,4′-azopyridine reinforced grid structure d) close up picture of part of the square grid; e) cube represent the 3D square shaped channel; f) cube is represented by two-dimensional square shaped unit (magenta colour); g) representative square grid architecture.

Topological analysis of compound **10** revealed that the compound has a 7-nodal 2,2,4,4,4,4,4-c 3D net structure with the Schläfli symbol $\{6^3.8.10.12\}\{6^3.8.10^2\}\{6^3.8^2.10\}\{6^4.8.10\}\{6^5.8\}\{6\}2$ consisting of 4,4′-azopyridine as two-coordinated node with two different types of binding mode, pyrazolate-3,5-dicarboxylate as four-coordinated node with two different types of binding mode, Cd1, Cd2 and Cd3 center as four-coordinated (Figure 6.14).
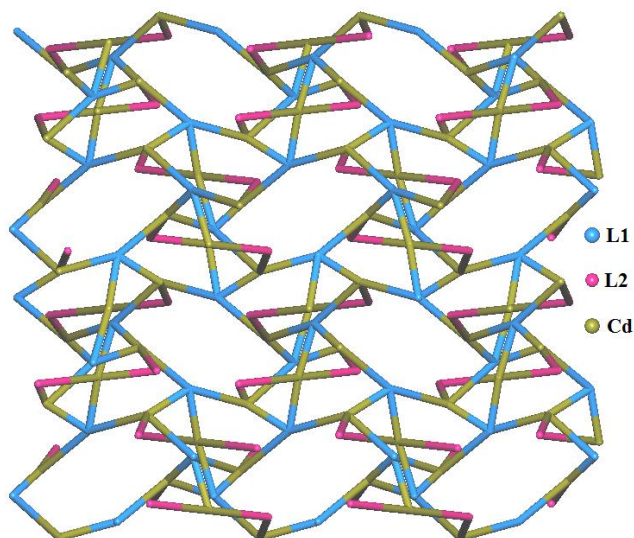
**Figure 6.14. Topological view of compound 10: view along crystallographic *b* axis.**

Table 6.2. Selected bond lengths (Å) and angles (°) of compounds 9 and 10

Bond-length (Å) of 9		Bond-length (Å) of 10	
Cd1 - O3	2.286(6)	Cd1 – O3	2.312(11)
Cd1 - O5	2.244(7)	Cd1 – O12	2.342(12)
Cd1 - O8	2.296(7)	Cd1 – N2	2.357(12)
Cd1 - O9	2.399(7)	Cd1 – N6	2.304(14)
Cd1-N5	2.324(8)	Cd1 – N20	2.328(12)
Cd1 - O7[a]	2.350(7)	Cd1 – N21	2.365(11)
Cd2 - O3	2.349 (7)	Cd2 – O3	2.568(11)
Cd2 - O4	2.629(7)	Cd2 – O5	2.317(9)
Cd2 - O8	2.455(7)	Cd2 – O7	2.467(11)
Cd2 - N1	2.301(9)	Cd2 – O11	2.337(11)

Cd2 - O2^d	2.530(6)	Cd2 – O13^c	2.472(9)
Cd2 - N3^d	2.257(8)	Cd2 – N23^g	2.317(10)
Cd2 - O2^g	2.194(7)	Cd2 – N30^h	2.361(12)
		Cd3 – O5	2.391(9)
		Cd3 – O10	2.503(11)
		Cd3 – O13	2.351(9)
		Cd3 – N22	2.319(10)
		Cd3 – N9^a	2.357(13)
		Cd3 – O6^e	2.400(11)
		Cd3 – O12^e	2.463(12)
Bond-angles (degree) of 9		**Bond-angles (degree) of 10**	
O3 - Cd1- O5	102.9(2)	O3 - Cd1 -O12	161.9(4)
O3 -Cd1- O8	74.8(2)	O3 - Cd1 -N2	78.5(4)
O3 -Cd1- O9	82.6(2)	O3 - Cd1 -N6	100.3(5)
O3 -Cd1- N5	171.5(3)	O3 - Cd1 -N20	74.4(4)
O3 -Cd1- O7^a	96.3(2)	O3 - Cd1 -N21	103.9(4)
O5 -Cd1- O8	98.2(2)	O12 - Cd1 -N2	84.0(4)
O5 -Cd1- O9	174.4(2)	O12 - Cd1 -N6	97.3(5)
O5 -Cd1- N5	85.6(3)	O12 - Cd1 - N20	108.9(4)
O5 -Cd1- O7^a	89.0(2)	O12 - Cd1 -N21	72.2(4)
O8 -Cd1- O9	82.2(3)	N2 - Cd1 -N6	178.2(5)
O8 -Cd1- N5	103.8(3)	N2 - Cd1 -N20	85.3(4)
O7^a-Cd1- O8	169.6(2)	N2 - Cd1 -N21	92.4(4)
O9 -Cd1- N5	88.9(3)	N6 - Cd1 -N20	93.0(5)
O8 - Cd2- N1	67.8(3)	N6 -Cd1 -N21	89.2(5)
O8 - Cd2- N3^d	91.9(3)	N20 - Cd1 - N21	177.4(4)
O2^d- Cd2- N1	97.2(3)	O3 - Cd2 -O5	75.8(3)
O2^d- Cd2- N3^d	67.2(3)	O3 - Cd2 -O7	149.8(4)

O2^g- Cd2- N3^d	135.2(3)	O3 - Cd2 -O11	53.3(4)
Cd2^c- O2- Cd2^f	110.4(3)	O3 - Cd2 - O13^c	143.1(3)
Cd2 - N1- N2	133.9(6)	O3 - Cd2 - N23^g	105.3(4)
Cd2^c - N3- N4	131.5(6)	O3 - Cd2 - N30^h	77.1(4)
O7^a-Cd1- O9	91.4(3)	O5 - Cd2 -O7	91.9(3)
O7^a-Cd1- N5	84.2(3)	O5 - Cd2 -O11	125.7(3)
O3 -Cd2- O4	52.4(2)	O5 - Cd2 - O13^c	140.9(3)
O3 -Cd2- O8	70.7(2)	O5 - Cd2 - N23^g	72.9(3)
O3 -Cd2- N1	130.3(3)	O5 - Cd2 - N30^h	104.5(4)
O2^d-Cd2- O3	131.6(2)	O7 - Cd2 -O11	141.6(3)
O3 -Cd2- N3^d	104.4(3)	O7 - Cd2 - O13^c	52.9(3)
O2^g-Cd2- O3	95.0(2)	O7 - Cd2 - N23^g	96.9(4)
O4 -Cd2- O8	117.3(2)	O7 - Cd2 - N30^h	79.6(4)
O4 -Cd2- N1	174.1(3)	O11 - Cd2 - O13^c	92.4(3)
O2^d-Cd2- O4	79.4(2)	O11 - Cd2 - N23g	101.2(4)
O4 -Cd2- N3^d	80.3(3)	O11 - Cd2 - N30^h	83.1(4)
O2^g-Cd2- O4	80.5(2)	O13^c- Cd2 - N23^g	93.1(3)
O2^d- Cd2- O8	151.5(2)	O13^c- Cd2 – N30^h	86.8(4)
O2^g- Cd2- O8	132.9(2)	N23^g- Cd2 -N30^h	175.7(4)
O2^g- Cd2- N1	93.8(3)	O5 - Cd3 -O10	53.9(3)
O2^d- Cd2- O2^g	69.6(2)	O5 - Cd3 -O13	140.4(3)
N1 - Cd2- N3^d	103.0(3)	O5 - Cd3 -N22	94.2(3)
Cd1 - O3- Cd2	108.3(3)	O5 - Cd3 - N9^a	81.2(4)
Cd1 - O8- Cd2	104.5(3)	O5 - Cd3 - O6^e	86.3(3)
		O5 - Cd3 - O12^e	139.3(4)

		O10 - Cd3 - O13	86.8(3)
		O10 - Cd3 - N22	82.0(3)
		O10 - Cd3 - N9^a	77.6(4)
		O6^e- Cd3 - O10	140.2(3)
		O10 - Cd3 - O12^e	164.6(4)
		O13 - Cd3 - N22	72.7(3)
		O13 - Cd3 - N9^a	96.9(4)
		O6^e- Cd3 - O13	133.0(3)
		O12^e- Cd3 - O13	80.3(3)
		N9^a - Cd3 - N22	157.6(4)
		O6^e- Cd3 - N22	105.9(4)
		O12^e - Cd3 - N22	101.9(4)
		O6^e- Cd3 - N9^a	95.8(4)
		O12^e- Cd3 - N9^a	95.6(4)
		O6^e - Cd3 - O12^e	53.4(4)
		Cd1 – O3 – Cd2	159.1(5)
		Cd2– O5 – Cd3	150.3(4)

Symmetry operation of compound **9**: a = 1-*x*, -1/2+*y*, 3/2-*z;* b = 1-*x*, 1/2+*y*, 3/2-*z*; c = 2-*x*, -1/2+*y*, 3/2-*z*; d = 2-*x*, 1/2+*y*, 3/2-*z*; f = *x*, 3/2-*y*, -1/2+*z*; g = *x*, 3/2-*y*, 1/2+*z*.

Symmetry operation of compound **10**: a = *x*, -1+*y*, *z*; b = *x*, 1+*y*, *z*; c = 1/2-*x*, -*y*, -1/2+*z*; d = 1/2-*x*, -*y*, 1/2+*z*; e = -1/2+*x*, 1/2-*y*, 2-*z*; f =1/2+*x*, 1/2-*y*, 2-*z*; g = 1-*x*, -1/2+*y*, 3/2-*z;* h = 1-*x*, 1/2+*y*, 3/2-*z*.

6.3.2 Thermal analysis

Thermogravimetric (TG) analyses were carried out to study the thermal stability of the framework in the solid state. Thermal analysis of compound $[Cd_2(pzdc)_2(azpy)_{0.5}(H_2O)]_n$ **(9)** and $\{[Cd_3(pzedc)_2(azpy)_2]·H_2O\}_n$ **(10)** was performed using powdered sample from room temperature to 800

°C under nitrogen atmosphere (Figure 6.15). Upon heating compound **9** showed slow mass loss up to a temperature of *ca.* 330 °C which may be attributed to loss of water molecule. On further heating a continuous weight loss till 800 °C indicated the decomposition of framework compound. Whereas compound **10** upon heating exhibited a noticeable mass loss up to a temperature of *ca.* 80 °C that corroborates with the loss of water of crystallization. Dehydrated framework is then thermally stable up to ~160 °C. On further heating dehydrated compound decomposed steadily showing further weight loss which completes at *ca.* 500 °C (Figure 6.15).
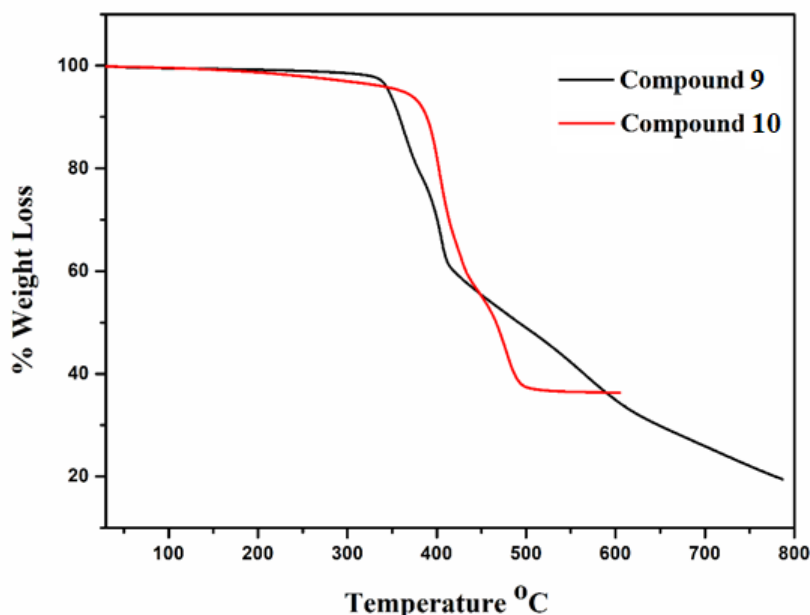

Figure 6.15. TG-DT of compound 9 and 10

6.3.3 ^{113}Cd solid state NMR

^{113}Cd solid state NMR being sensitive probe for understanding local environment of the Cd(II) ions both the samples were investigated using CP-MAS NMR experiments at 14 T (Figure 6.16). The sharp signals are obtained both for **9** and **10** indicating the well-formed crystalline nature of the Cd-MOFs. ^{113}Cd chemical shifts are strongly affected by the identity of atoms involved in coordination. In general, ^{113}Cd nuclei coordinated exclusively by oxygen-donor ligands showed chemical shift value in the range −100 to 150 ppm, while for exclusive N-donor ligands resonance lines appeared in the range 200–380 ppm. In case of mixed donor (O,N) coordination environment, isotropic shift may appear in the intermediate range [22, 24, 25]. Relaxation time (T_1) of samples was long (~100s), which may be ascribed to rigid structure of framework compounds. ^{113}Cd NMR spectra of both compound **9** and **10** featured

central resonance line; while for compound **9** a relatively sharp resonance line appeared at 13.5 ppm, for compound **9** resonance line centered at *ca.* 20 ppm. Compound **9** exhibited an additional resonance line in the downfield region centered at 103 ppm. It is established that various donor groups (triazole, pyridine, pyrimidine, carboxylate, and water etc.) can have significant influence on [113]Cd isotropic chemical shifts [24]. Therefore, role of coordinated water molecule in affecting [113]Cd chemical shift of compound **9** could not be ruled out.
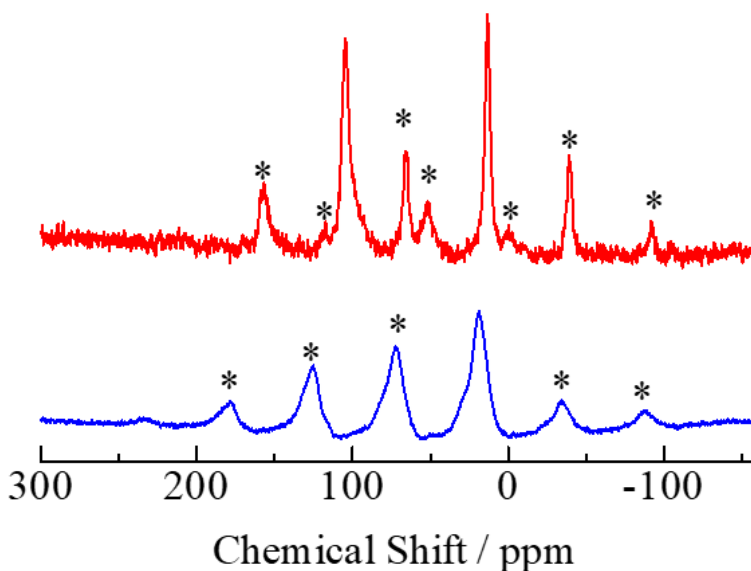

Figure 6.16. Solid state [113]Cd NMR of compound 9 (red) and compound 10 (blue) (asterisk marked peaks are spinning side bands).

6.3.4 Photoluminescence properties and sensing

The π-conjugated organic ligand containing metal-organic frameworks constructed from d^{10} metal centers (Cd, Zn etc.) have been employed as luminescent sensing materials [26-28]. Luminescence properties of such MOFs demonstrated their use in potential application of chemical sensing through host–guest chemistry. To examine the photoluminescence behavior of $[Cd_2(pzdc)_2(azpy)_{0.5}(H_2O)]_n$ **(9)** and $\{[Cd_3(pzedc)_2(azpy)_2] \cdot H_2O\}_n$ **(10)** emission spectral measurements have been carried out. Emission spectra of linkers along with compounds **9** and **10** were measured in the solid state at room temperature (Figure 6.17). It is noteworthy that while pyrazole-3,5-dicarboxylic acid is emissive in nature, 4,4´-azopyridine is not under the experimental condition. Pyrazole-3,5-dicarboxylic acid exhibited an intense

fluorescence band centered at 388 nm upon excitation at 233 nm in the solid-state (Figure 6.18). This emission may be attributed to to $\pi^*\rightarrow n$ or $\pi^*\rightarrow\pi$ transition. Two MOFs have shown 1-4 nm red shift in their emission maxima in comparison to neat pyrazole-3,5-dicarboxylic acid upon excitation at 233 nm (Figure 6.17). Therefore, solid state luminescence responses of **9** and **10** are due to ligand-based emission. It is well known that for d^{10} metal compounds, no emission originated from the metal-to-ligand (MLCT) or ligand-to-metal charge transfer (LMCT) excited states, since the d^{10} metal ions are normally difficult to be oxidized or reduced [29-32]. Thus, the fluorescent emission of compounds **9** and **10** may be assigned primarily to the intra-ligand and inter-ligand charge transition (ILCT) [33]. Interestingly, the luminescence intensity of both **9** and **10** is remarkably dependent on the organic solvent. The photoluminescence spectra of the powder samples of compounds **9** and **10** dispersed in various organic solvents were recorded (Figure 6.19). Intensity of the luminescence spectrum of MOF **9** dispersed in solvents like acetone, dichloromethane, benzene, acetylacetone, water and DMF did not show much difference from each other. However, such spectrum measured in methanol exhibits remarkable quenching of the luminescence intensity. In contrast, a significant increase in luminescence intensity was observed in isopropanol medium. Around six-fold increase in luminescence intensity was recorded in isopropanol in comparison to the other solvents like acetone, dichloromethane, benzene, acetylacetone, water etc. (Figure 6.20). Both **9** and **10** are stable in common organic solvents and can easily be dispersed in solvents without changing their framework structure (Figures 6.21, 6.22). Compound **10** has also showed the similar type of photoluminescence property. In case of **10** little over five-fold increase in luminescence intensity was observed in isopropanol in comparison to the other solvents like acetone, dichloromethane, benzene, acetylacetone, water etc. It is noteworthy that the luminescence can be regenerated upon removal of methanol from compound **9** and **10**. These results suggest that both **9** and **10** could be promising luminescent probes for detecting methanol and isopropanol. Interestingly, solvent dependent "turn-on" and "turn-off" photoluminescence responses have been observed for both the compounds **9** and **10**. Solvent specific both type of responses ("turn-on" and "turn-off") displayed by a single MOF are rarely reported previously. Nevertheless, selective responses (turn-on or turn-off) towards organic small molecules by luminescent MOF due to host-guest interaction are well documented in the literature [34]. Considering the intricacy of the structure of the MOFs possibility of similar kind of host-guest interaction in the framework compounds **9** and **10** is highly expected.
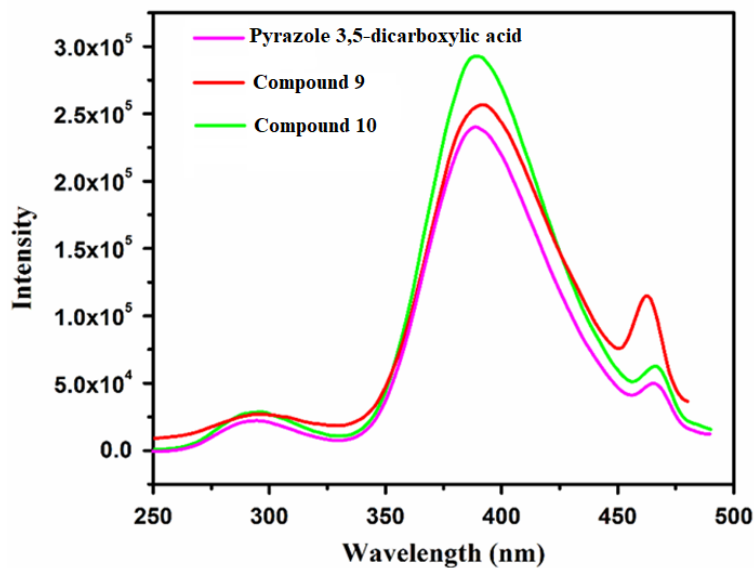
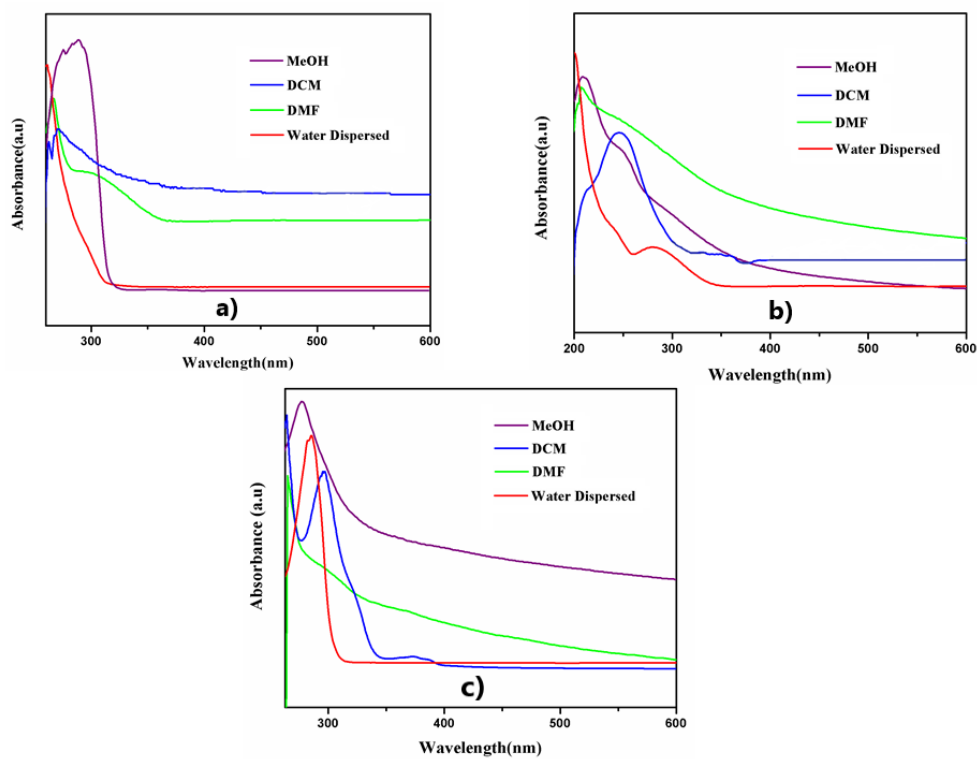**Figure 6.17. Photoluminescence spectra of compounds 9, 10 and ligand in solid state (λ_{ex}= 233 nm).**

Figure 6.18. UV-vis spectra of a) free ligand pyrazole 3,5-dicarboxylic acid; b) compound 9 and c)
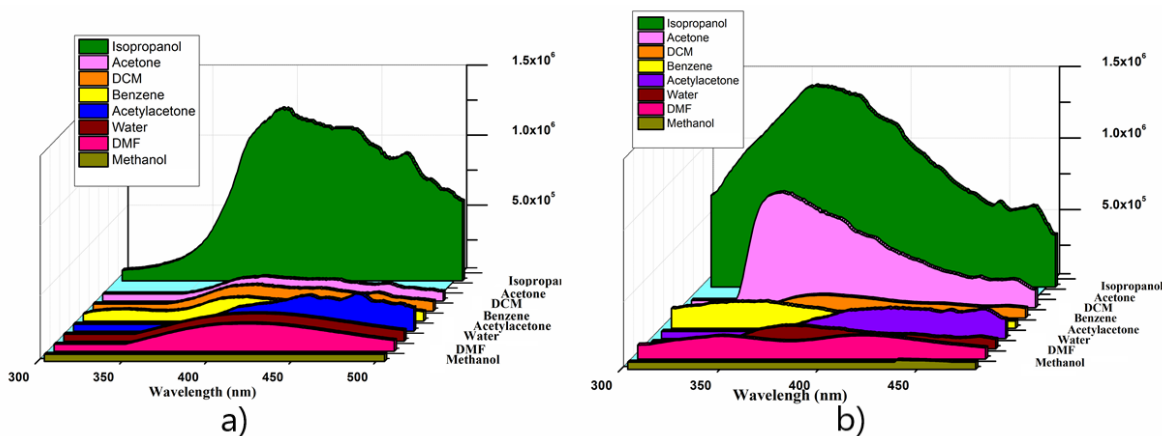
compound 10.

Figure 6.19. Comparative photoluminescence responses of compounds 9 (a) and 10 (b) towards a variety of solvents (λ_{ex}= 277 nm for compound 9 and λ_{ex}= 292 nm for compound 10).
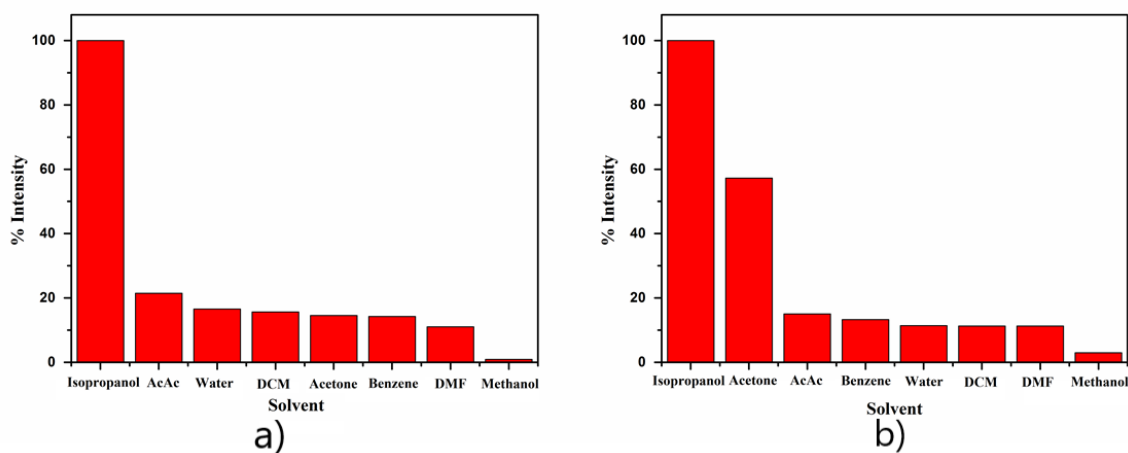

Figure 6.20. Comparison of emission intensity (in %) among various solvents for compound 9 (a) and compound 10 (b).
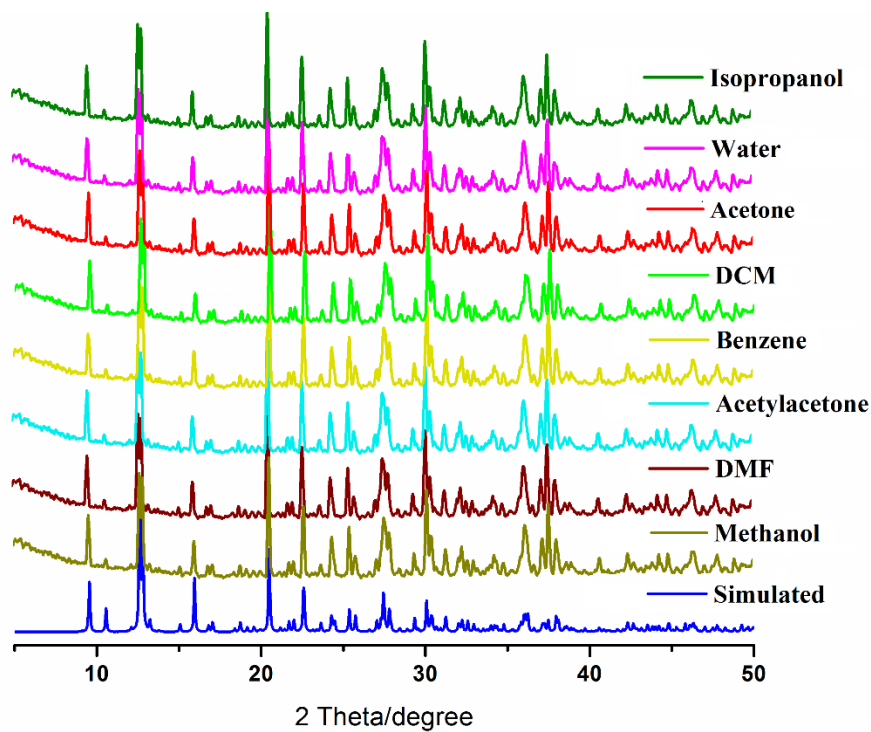
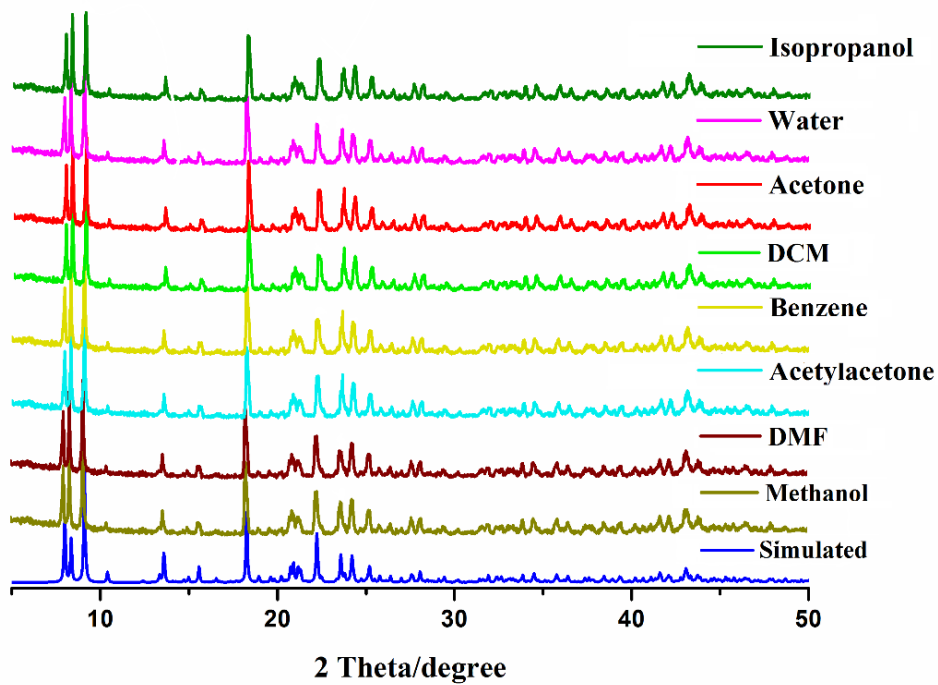**Figure 6.21. PXRD of 9 in different solvent-soaked condition**

Figure 6.22. PXRD of 10 in different solvent-soaked condition

6.4 Conclusion

In brief, two structurally diverse 3D mixed-linker cadmium based metal-organic framework (MOF), $[Cd_2(pzdc)_2(azpy)_{0.5}(H_2O)]_n$ **(9)** and $\{[Cd_3(pzedc)_2(azpy)_2] \cdot H_2O\}_n$ **(10)** have been synthesized through solvothermal route by mere subtle change in reaction conditions. Both compounds **9** and **10** have been structurally characterized by X-ray single crystal analysis. Photoluminescence properties of the framework compounds have been thoroughly investigated. Notably, each of the MOF system displayed both "turn on" and turn off" type of photoluminescence responses selectively towards specific solvent. Hence, MOF supposed to be a prospective material for practical usage, particularly, in sensing applications.

6.5 References

[1]   J-S. Qin, S. Yuan, Q. Wang, A. Alsalme, H-C. Zhou, J. Mater. Chem. A 2017, **5**, 4280.

[2]   J. R. Lakowicz, Principles of Fluorescence Spectroscopy, 3rd Edition, Springer, 2006.

[3]   M. R. Tchalala, P. M. Bhatt, K. N. Chappanda, S. R. Tavares, K. Adil, Y. Belmabkhout, A. Shkurenko, A. Cadiau, N. Heymans, G. De Weireld, G. Maurin, K. N. Salama, M. Eddaoudi, Nat. Commun. 2019, **10**, 1328.

[4]   N. Yanai, K. Kitayama, Y. Hijikata, H. Sato, R. Matsuda, Y. Kubota, M. Takata, M. Mizuno, T. Uemura, S. Kitagawa, Nat. Mater. 2011, **10**, 787.

[5]   M. J. Dong, M. Zhao, S. Ou, C. Zou, C. D. Wu, Angew. Chem. Int. Ed. 2014, **53**, 1575.

[6]   Y. Yu, J. P. Ma, C. W. Zhao, J. Yang, X. M. Zhang, Q. K. Liu, Y. B. Dong, Inorg. Chem. 2015, **54**, 11590.

[7]   A. Douvali, A. C. Tsipis, S. V. Eliseeva, S. Petoud, G. S. Papaefstathiou, C. D. Malliakas, I. Papadas, G. S. Armatas, I. Margiolaki, M. G. Kanatzidis, T. Lazarides, M. J. Manos, Angew. Chem. Int. Ed. 2015, **54**, 1651.

[8]   F. Y. Yi, Y. Wang, J. P. Li, D. Wu, Y. Q. Lan, Z. M. Sun, Mater. Horiz. 2015, **2**, 245.

[9]   B. L. Chen, S. C. Xiang, G. D. Qian, Acc. Chem. Res. 2010, **43**, 1115.

[10]   Y. Takashima, V. M. Martinez, S. Furukawa, M. Kondo, S. Shimomura, H. Uehara, M. Nakahama, K. Sugimoto, S. Kitagawa, Nat. Commun. 2011, **2**, 168.

[11]   L. E. Kreno, K. Leong, O. K. Farha, M. Allendorf, R. P. Van Duyne, J. T. Hupp, Chem. Rev. 2012, **112**, 1105.

[12]   S.-R. Zhang, D.-Y. Du, J.-S. Qin, S.-J. Bao, S.-L. Li, W.-W. He, Y.-Q. Lan, P. Shen, Z.-M. Su, Chem. –Eur. J. 2014, **20**, 3589.

[13]   H.-T. Zhang, J.-W. Zhang, G. Huang, Z.-Y. Du, H.-L. Jiang, Chem. Commun. 2014, **50**, 12069.

[14]   Bruker (2007). APEX 2, SAINT, XPREP, Bruker AXS Inc., Madison, Wisconsin, USA.

[15]   G. M. Sheldrick, A short history of SHELX. ActaCrystallogr. Sect. A: Found. Crystallogr. 2008, **64**, 112.

[16]   I. Usón, G.M. Sheldrick, ActaCrystallogr. Sect. D 2018, **74**, 106.

[17]   SAINT and SADABS, version 6.02 and version 2.03; BrukerAXS, Inc.: Madison, WI 2002.

[18]   L. Farrugia, J. Appl. Crystallogr. 1999, **32**,837.

[19]   K. Brandenburg, DIAMOND, version 3.1 e; Crystal Impact Gbr: Bonn, Germany 2007.

[20]   C. F. Macrae, I. J. Bruno, J. A. Chisholm, P. R. Edgington, P. McCabe, E. Pidcock, L. Rodriguez-Monge, R. Taylor, J. van de Streek, P. A. Wood, J. Appl. Crystallogr. 2008, **41**, 466.

[21]   A. L. Spek, J. Appl. Crystallogr. 2003, **36**, 7.

[22]   T. C. Stamatatos, E. Katsoulakou, V. Nastopoulos, C. P. Raptopoulou, E. Manessi-Zoupa, S. P. Perlepes, Z. Naturforsch., B: J. Chem. Sci. 2003, **58b**, 1045.

[23]   V. A. Blatov, A. P. Shevchenko, D. M. Proserpio, Cryst. Growth Des. 2014, **14**, 3576.

[24]   A. V. Kuttatheyil, M. Handke, J. Bergmann, D. Lässig, J. Lincke, J. Haase, M. Bertmer, H. Krautscheid, Chem. –Eur. J. 2015, **21**, 1118.

[25]   M. F. Summers, Coord. Chem. Rev. 1988, **86**, 43.

[26]   S. S. Nagarkar, B. Joarder, A. K. Chaudhari, S. Mukherjee, S. K. Ghosh, Angew. Chem. Int. Ed. 2013, **52**, 2881.

[27]   V. Stavila, A. A. Talin, M. D. Allendorf, Chem. Soc. Rev. 2014, **43**, 5994.

[28]   J. Zhang, Y. Huang, D. Yue, Y. Cui, Y. Yang, G. Qian, J. Mater. Chem. B 2018, **6**, 5174.

[29]   L.-P. Zhang, J.-F. Ma, J. Yang, Y.-Y. Pang, J.-C. Ma, Inorg. Chem. 2010, **49**, 1535.

[30]   B. Roy, S. Mukherjee, P. S. Mukherjee, CrystEngComm, 2013, **15**, 9596.

[31]   J. Zhang, J. Wu, G. Tang, J. Feng, F. Luo, B. Xu, C. Zhang, Sens Actuators B, 2018, **272**, 66.

[32]   J. Zhang, Y. Huang, D. Yue, Y. Cui, Y. Yang, G. Qian, J. Mater. Chem. B 2018, **6**, 5174.

[33]   Z.-Q. Shi, Z.-J. Guo and H. G. Zheng, Chem. Commun, 2015, **51**, 8300.

[34]   W. P. Lustig, S. Mukherjee, N. D. Rudd, A. V. Desai, J. Li, S. K. Ghosh, Chem. Soc. Rev. 2017, **46**, 3242.

Chapter 7

Highlights and summary

7.1 Highlights

The main findings of the present investigation are collated in these chapters. The thesis presents a glimpse of recent advances in the field of gas adsorption, heterogeneous catalysis and luminescence properties of metal-organic frameworks vis-à-vis their synthesis and structural diversity. The major emphasis given in on the synthesis, structural characterization, gas uptake capacity of small gas molecules like CO_2, H_2, CH_4, N_2 etc. especially selective CO_2 adsorption over N_2, CH_4 and theoretical interpretation and photoluminescence behaviors.

The importance of framework compounds in industrial and fundamental research led us to develop various metal-based systems mostly d^{10} metals (Cd, Zn etc.) and transition metals (Cu, Co etc.) that have potential application in luminescence properties, heterogeneous catalysis and gas adsorption studies. To develop porous MOFs, various types of carboxylate linkers and spacers have been used in various reaction conditions. Solvothermal and hydrothermal both techniques have been used for synthesis of MOFs. Depending on the nature of framework these have been appropriately employed in different studies.

A new cadmium(II) containing 2D metal-organic framework compound, $[Cd(abb)H_2O]_n$ (abb = 3,3′-azobis(benzoate)) have been synthesized by hydrothermal process and characterized by single-crystal X-ray diffraction method. The supramolecular structure which is formed through H-bonding in 2D framework gives the framework additional space and flexibility to accommodate small gaseous molecules. Notably, $[Cd(abb)H_2O]_n$ exhibited unprecedented high uptake of hydrogen and also displayed moderate uptake capacity of CO_2.

Two new quinoline derivative linker based polymeric and monomeric metal carboxylates, *viz.*, $[Co(mqc)_2]_n$, and $[Zn(mqc)_2(H_2O)]$ (mqc = 4-methoxy-2-quinolinecarboxylate) have been synthesized solvothermally and characterized by single-crystal X-ray diffraction measurement. $[Co(mqc)_2]_n$ is a 2D coordination polymer, which further extended to a 3D porous supramolecular network having void space in between each 2D layers. $[Co(mqc)_2]_n$ displayed high uptake of H_2 and CO_2 comparison to the many other 2D metal-organic frameworks reported so far. While $[Zn(mqc)_2(H_2O)]$ is a simple monomer.

Structural diversity and inter-conversion among four Cu(II)/Cu(II)-Mg(II) containing pyridine-2,5-dicarboxylate based hydrothermally synthesized metal carboxylate compounds have been investigated. Compounds $\{[Mg(H_2O)_6][Cu(pdc)_2]\cdot 2H_2O\}_n$, $\{[CuMg(pdc)_2(H_2O)_4]\cdot 2H_2O\}_n$, $\{2(Him)\cdot[Cu(pdc)_2]\}_n$, and $\{[Cu(pdc)(im)_2]\cdot 2H_2O\}_n$ (pdc = pyridine-2,5-dicarboxylate and im = imidazole) were synthesized respectively from 1, 2, 3 and 4 mmol of imidazole. Framework compounds have been characterized by single-crystal X-ray diffraction and powder X-ray diffraction analysis. $\{2(Him)\cdot[Cu(pdc)_2]\}_n$ revealed a

polymeric ribbon like 1D chain structure that catalyzes olefin epoxidation reaction in heterogeneous condition. Remarkably, cyclooctene was fully converted to epoxy-cyclooctane with *ca.* 100% selectivity.

Further a new mixed ligand porous 3D metal carboxylate framework compound, $[Zn_2(H_2O)(nic)(pzdc)]_n.nH_2O$ (pzdc = pyrazole-3,5-dicarboxylate, Hnic = isonicotinic acid) was synthesized hydrothermally and characterized. The compound has large solvent accessible void space (15.9%) which was significantly enhanced to 34.1% upon dehydration, leading to creation of open metal sites that are exposed to the pores. The framework compound and its dehydrated product show highly selective CO_2 adsorption compared to other small gas molecules like H_2, N_2, and CH_4 at low partial pressure. The selectivity of CO_2 with respect to CH_4 at 273 K is calculated to be 22.4. The low-pressure selective CO_2 adsorption is quite impressive with respect to other reported framework systems. $[Zn_2(H_2O)(nic)(pzdc)]_n.nH_2O$ exhibited fairly strong CO_2-framework interactions as evidenced from the measured heat of adsorption, ~50 kJ mol^{-1} at low loading. Molecular dynamics and Monte Carlo simulations explain the selective CO_2 adsorption over other small gas molecules (H_2, N_2 and CH_4) in the framework compound.

Furthermore a pair of novel 3D mixed-linker cadmium based metal-organic frameworks, $[Cd_2(pzdc)_2(azpy)_{0.5}(H_2O)]_n$ and $\{[Cd_3(pzedc)_2(azpy)_2]\cdot H_2O\}_n$ (pzdc = pyrazole-3,5-dicarboxylate, pzedc = pyrazolate-3,5-dicarboxylate and azpy = 4,4´-azopyridine) have been synthesized by solvothermal methods. Interestingly, subtle change in reaction conditions afforded two strikingly different MOFs. Compounds have been characterized structurally by single-crystal X-ray analysis. Both the compounds feature a pillared-layer framework structure. Photoluminescence properties of the framework compounds have been investigated in the solid state as well as in solvent dispersed medium. Notably, solvent specific turn-on/turn-off photo-luminescence responses have been observed for both the compounds.

Therefore, MOF is class of compounds that received ever increasing attention in recent time. It can be realized that these compounds especially porous MOFs will be continuing to become more interdisciplinary in future with features of their fundamental and practical applications in field of catalysis, gas storage and separations, sensing etc. may lead to offer better system having prospect in technological use in industry or elsewhere.

Appendix

List of Publications

[1] Saptarshi Biswas, **Saikat Gayen**, Tanmoy Maity and Subratanath Koner, Inorganica Chimica Acta, 2017, **461**, 21. Small gas molecules access into void space of H-bonded 3D network consist of 2D cadmium(II) layer.

[2] **Saikat Gayen**, Debraj Saha and Subratanath Koner, Journal of Molecular Structure, 2018, **1162**, 10. Quinoline derivative containing monomeric and polymeric metal carboxylates: Synthesis, crystal structure and gas adsorption study over a 2D layered framework.

[3] Debraj Saha, **Saikat Gayen** and Subratanath Koner, Polyhedron, 2018, **146**, 93. Cu(II)/Cu(II)-Mg(II) containing pyridine-2,5-dicarboxylate frameworks: Synthesis, structural diversity, inter-conversion and heterogeneous catalytic epoxidation.

[4] Debraj Saha, **Saikat Gayen**, Tanmoy Maity, Antonio Frontera, Joaquin Ortega-Castro, Karen Leus, Guangbo Wang, Pascal Van Der Voort, Paula Brandao and Subratanath Koner, New J. Chem., 2020, **44**, 1806. Combined experimental and computational studies on preferential CO_2 adsorption over a zinc-based porous framework solid.

[5] **Saikat Gayen**, Pameli Ghosh, Hisashi Honda, Debraj Saha, Saptarshi Biswas, Rakesh Debnath and Subratanath Koner, Polyhedron, 2021, **208**, 15444. Solvent mediated photoluminescence responses over mixed-linker cadmium (II) based metal-organic frameworks.

[6] Birendra Nath Patra, Pameli Ghosh, Nayim Sepay, **Saikat Gayen**, Subratanath Koner, Paula Brandao, Zhi Lin, Rakesh Debnath, Jahar Lal Pratihar, Tanmay Maity and Dasarath Mal, Applied Organometallic Chemistry, 2022, **36**, e6552. Aerobic epoxidation of olefins by carboxylate ligand-based cobalt (II) compound: synthesis, X-ray crystallography, and catalytic exploration.